UNIVERSITÀ DEGLI STUDI DI MILANO

Ph.D. School in Molecular and Cellular Biology – XXXII cycle

Department of Pharmacological and Biomolecular Sciences (DiSFeB)

Role of peptidoglycan remodeling in overcoming LPS biogenesis defects in *Escherichia coli*

(BIO/19)

Carlos Karan GURNANI SERRANO

Supervisor: Prof.ssa Alessandra POLISSI

Co-supervisors: Waldemar VOLLMER, Jean-Pierre SIMORRE

PhD Programme Coordinator: Martin KATER

A.A.
(2019/2020)

This project has received funding from the European Union's Horizon 2020 research and innovation programme under the Marie Skłodowska-Curie grant agreement No 721484.

"***Messieurs, c'est les microbes qui auront le dernier mot***."
(Gentlemen, it is the microbes who will have the last word)

-Louis Pasteur

Acknowledgements

What a long journey to get to where I am today! None of this would have been possible without all of you.

*I am very thankful to my supervisor **Alessandra Polissi**. It has been a pleasure to pursue the PhD at your research group. Many thanks for your support and for always watching over my welfare. A big thank you for giving me this valuable opportunity.*

*To **Waldemar's group**, thanks for all the support and welcome you provided me during my stay in Newcastle upon Tyne. **Waldemar**, thanks a lot for promoting my creativity.*

***Train2Target** fellows, you were the best colleagues one can think of. Thanks for sharing experiences together, I wish you the best of success.*

***Ale and Paola**, thank you for sweetening my experience there in the lab during all these three years. **Ale**, thank you so much for providing me continued guidance and support when I need them most.*

*Dear **Elisabete**, my PhD and life in Milan cannot be imagined without you. Thank you for all the company and good times you have given to me. Never change that cheerful mood you always have, thanks for passing it on me.*

*Impossibile dimenticarmi di te **Luca**, sei sempre stato lì ad ascoltarmi con il meglio dei tuoi sorrisi e buon umore. Siamo passati dall'essere coinquilini all'essere fratelli, grazie di tutto cuore.*

*To all the **italian and expats friends** I met throughout this "esperienza milanese", thanks all for being my partners in crime in all my adventures.*

*Thank you to all my **friends from Madrid** and those who I met in **Groningen**. You have been always there, and I am glad I have shared all this experience with all of you. Me siento orgulloso de tener unos amigos como vosotros, ¡Gracias por estar siempre ahí!*

*A mi **familia**, y especialmente a vosotros **Papa**, **Mama**, **Ana** y **Lucas**. Muchas gracias por apoyarme en mis decisiones. Nada de esto podria ser posible sin el cariño que me brindais dia tras dia. Sois la causa de mis éxitos. Os quiero.*

Table of Contents

ABBREVIATIONS **6**

ABSTRACT **7**

1. INTRODUCTION **8**

1.1 The bacterial cell envelope **9**

1.2 The Gram-negative bacterial envelope **10**

1.2.1 Inner membrane 10

1.2.2 Periplasm: peptidoglycan layer 10

1.2.3 Outer membrane 11

1.3 PG synthesis **13**

1.3.1 Peptidoglycan synthases 15

1.3.2 Peptidoglycan transpeptidases 17

1.3.3 Peptidoglycan hydrolases 19

1.4 LPS synthesis **22**

1.4.1 Kdo_2-lipid A 23

1.4.2 Core oligosaccharide 24

1.4.3 O-antigen 25

1.5 Envelope molecular machineries **27**

1.5.1 Outer membrane assembly 28

1.5.2 Divisome and elongasome complexes 33

1.6 Envelope stress response systems **37**

1.6.1 The two-component stress response system Cpx 38

1.6.2 Envelope stress sigma factor (σ^E) 40

1.6.3 Rcs phosphorelay 41

1.7 References **43**

2. AIM OF THE PROJECT 59

3. RESULTS 60

3.1 Peptidoglycan Remodeling Enables *Escherichia coli* To Survive Severe Outer Membrane Assembly Defect 61

3.2 Characterisation of YgeR, a novel amidase regulator in *Escherichia coli* 106

4. CONCLUSION 147

Abbreviations

anhMurNAc	anhydro-N-acetylmuramic acid	**LPS**	Lipopolysaccharide
BAM	β-barrel Assembly Machinery	**LT**	Lytic transglycosylase
CPase	Carboxypeptidase	**LWP**	Low Molecular Weight
DNA	Deoxyribonucleic acid	**mDAP**	meso-Diaminopimelic acid
EPase	Endopeptidases	**MurNAc**	N-acetylmuramic acid
ESRs	Envelope Stress Response Systems	**OM**	Outer Membrane
GlcNAc	N-acetylglucosamine	**OMPs**	Outer Membrane Proteins
GTase	Glycosyltransferase	**PBP**	Penicillin-Binding Protein
HMW	High Molecular Weight	**PG**	Peptidoglycan
IM	Inner Membrane	**RNA**	Ribonucleic acid
IMPs	Integral Membrane Proteins	**sRNA**	small RNA
LDTs	LD-TPases	**TPase**	Transpeptidase
Lol	Localization of Lipoproteins	**UDP**	Uridine Diphosphate
Lpp	Braun's Lipoprotein		

Abstract

The three layered Gram-negative bacteria envelope consists of an inner membrane (IM), the periplasm-containing peptidoglycan (PG), and an asymmetric outer membrane (OM) decorated with lipopolysaccharide (LPS) in the outer leaflet. Growth and assembly of cell envelope is orchestrated by action of dedicated protein machineries which span the entire envelope and whose coordinated activity guarantees proper envelope stiffness. Defects in biogenesis in any of these layers compromise the whole cell integrity and lead to cell death. In this thesis we show that *Escherichia coli* remodels the PG structure by increasing the level of 3-3 crosslinks produced by LD – Transpeptidases (LDTs), to avoid cell lysis when the LPS transport to the OM is disrupted. *E. coli* codes for six LDTs (LdtA-F): LdtA, LdtB, and LdtC covalently attach Lpp to PG while LdtD and LdtE introduce 3-3crosslinks. LdtF has no LD-Transpeptidase (LD-Tpase) activity but enhances the enzymatic activity of LdtD and LdtE. Our data outlines a major contribution of LdtD in PG remodelling and suggest that LdtD works in concert with the PG synthase PBP1B, its activator LpoB and the DD-CPase PBP6a to form a dedicated PG repair machine that runs a PG remodeling program to counteract damages to the OM. We also show that the lysis phenotype and morphological defects seen in mutants with an impaired LPS transport and lacking *ldtF*, are rescued and suppressed, respectively, by the loss of YgeR an uncharacterized lipoprotein predicted to be OM anchored. YgeR belongs to the family of LytM-domain factors which are hydrolases or hydrolase regulators implicated in PG remodeling/turnover. Important PG hydrolases are amidases which promote PG septal splitting and daughter cell separation. Our biochemical data reveal that YgeR is an amidase regulator able to activate AmiA, AmiB and AmiC the three amidases encoded by *E. coli*. We also show that YgeR binds purified PG and physically interacts with the amidase AmiC. Our biochemical analyses are complemented by *in vivo* data showing that YgeR preferentially activates AmiC and that it does it through its LytM domain. Altogether, our results point out an unexplored protective role of the 3-3 crosslinks in PG to overcome severe OM biogenesis defects and propose YgeR as a novel amidase activator whose action seems required upon envelope stress.

1. Introduction

1.1 The bacterial cell envelope

Bacteria are surrounded by a complex and protective structure, the cell envelope, that constitutes the main barrier between the bacterial cell and the environment. Based on their envelope structure and composition, bacteria can be divided into two main groups. In the so-called Gram-positive bacteria, the envelope is mainly composed of a thick peptidoglycan (PG) layer surrounding a single cytoplasmic membrane. Instead, the so-called Gram-negative bacteria possess two membranes, an outer (OM) and an inner membrane (IM), delimiting a periplasmic space in which a thin peptidoglycan layer is embedded (**Fig. 1**). Because of the presence of a second membrane Gram-negative organisms are defined "diderm" as opposed to the Gram-positive "monoderm". The multi-layered structure of the Gram-negative envelope has several consequences impacting on growth and physiology of this group of microorganisms as discussed in the following chapters of this thesis.

The model organism for Gram-negative bacteria is rod-shaped *Escherichia coli*. *E. coli*, is a facultative anaerobic organism, that can live as a commensal in the gut of vertebrates. However, pathogenic strains also exist causing severe gastrointestinal and urinary tract infections (Tenaillon et al., 2010).

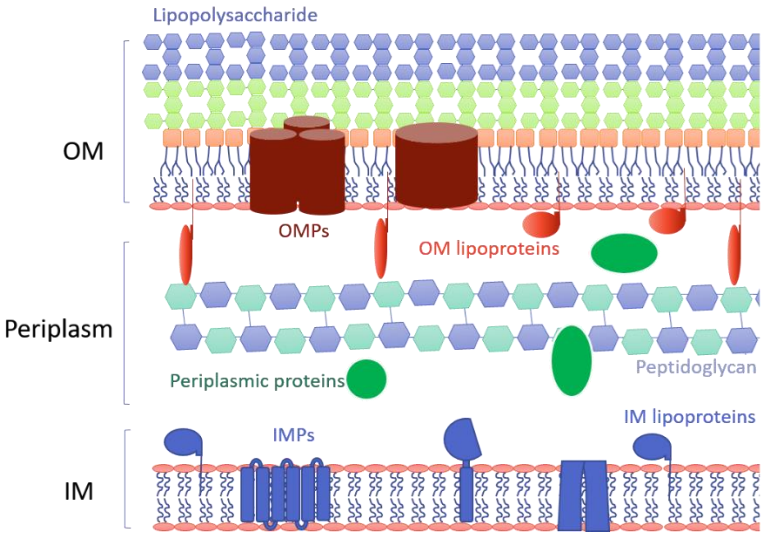

Figure 1. Cell envelope of Gram-negative bacteria. See text for details (Modified from Sperandeo et al., 2019a).

1.2 The Gram-negative bacterial envelope

1.2.1 Inner membrane

The IM, which surrounds the cytoplasm is a phospholipid bilayer. As a typical phospholipid bilayer, the IM acts as a semipermeable barrier, regulating the trafficking of molecules in and out the different compartments of the bacterial envelope. Integral membrane proteins (IMPs), lipoproteins and peripheral proteins are embedded or associated to the IM (Luirink et al., 2012). In contrast to the outer membrane proteins (OMPs), most IMPs span the IM with α-helical transmembrane domains mainly composed of hydrophobic residues (Cymer et al., 2015; Dalbey et al., 2011), whereas lipoproteins localize in the periplasmic side of the of IM linked through the N-terminal moiety (Sankaran and Wu, 1994). IMPs are often part of complexes implicated in fundamental bacterial processes such as signal transduction, protein secretion and transport, energy production and cell division (Weiner and Rothery, 2007).

1.2.2 Periplasm: peptidoglycan layer

In Gram-negative bacteria IM and OM delimit a compartment named periplasm. The periplasm is crucial to the bacteria as encloses enzymes and cellular machineries implicated in lipopolysaccharide (LPS) transport to the OM, cell division, envelope stress response, environmental sensing, osmoregulation and peptidoglycan synthesis, among others (Miller and Salama, 2018). In addition, the periplasm contributes to the resistance of the turgor pressure by comprising structural systems that act concertedly with the OM, such as the PG sacculus, lipoproteins, multidrug efflux pumps, surface appendages, and solutes that contribute to the ionic potential across the OM (Cayley et al., 2000).

PG, also termed murein, is an essential component of the bacterial cell wall, forming a continuous, mesh-like structure, the sacculus, that surrounds the IM (Höltje, 1998). In Gram-negative bacteria, the PG sacculus is located in the periplasm and is anchored to the OM through the Braun's lipoprotein (Hantke and Braun, 1973). PG is made up of linear glycan strands made up of alternating N-acetylglucosamine (GlcNAc) and N-acetylmuramic acid (MurNAc) residues linked by β-1,4 glycosidic bonds, with a stem pentapeptides attached to the MurNAc moiety. The amino acid composition of the stem pentapeptide can vary from species to species. In *E. coli*, the pentapeptide consists of L-Ala-D-Glu-mDAP-D-Ala-D-Ala (mDAP: meso-Diaminopimelic acid; Ala: Alanine;

Glu: Glutamic acid) (**Fig. 2**), this pentapeptide is cross-linked to the respective stem pentapeptides of parallel glycan strands. PG contributes cell shape maintenance during cell growth and division, provides mechanical strength to counteract the osmotic pressure in the cell, and serves as a scaffold for anchoring proteins and polymers (Vollmer et al., 2008a). Modifications in PG can alter substantially the bacterial fitness and virulence, making the bacteria more resistant to environmental stresses and toxic compounds (Pazos and Peters, 2019).

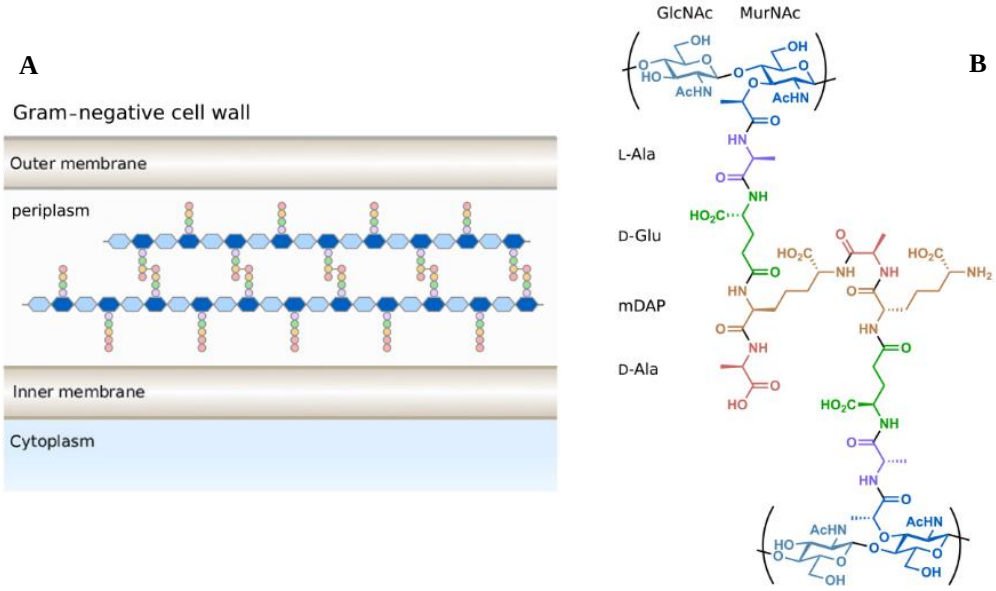

Figure 2. Structure of Gram-negative peptidoglycan. (A) Gram-negative bacteria such as *E. coli* contain a thin layer of peptidoglycan within their periplasm. (B) Gram-negative bacteria generally use D-Glutamic acid (D-Glu) and meso-Diaminopimelic acid (mDAP) at the second and third positions of peptide stem, respectively, although this pattern may be distinct amid different species (Adapted from Griffin et al., 2019).

1.2.3 Outer membrane

One of the distinguishing characteristics of Gram-negative bacteria is the presence of an additional membrane, the OM. The OM is an asymmetric lipid bilayer, with phospholipids in the inner leaflet and a peculiar glycolipid, LPS, in the outer leaflet. LPS is the most abundant component of the OM outer leaflet and is essential in most Gram-negative bacteria (Zhang et al., 2013; Silhavy et al., 2010). LPS is a complex molecule made of three structural domains: a hydrophobic moiety anchored to the OM known as lipid A, a conserved core oligosaccharide and a highly variable O-antigen made of

repeating oligosaccharide units (Raetz and Whitfield, 2002) (**Fig. 3**). LPS outer layer has a significant impact on OM properties. LPS molecules are negatively charged and the LPS outer layer is stabilized by the presence of Mg^{++} divalent cations. Tightly packed LPS molecules largely contribute to the peculiar permeability barrier properties of the OM making Gram-negative bacteria impermeable to many toxic molecules such as hydrophobic toxic molecules, detergents, cationic antimicrobial compounds and antibiotics (Nikaido, 2003). Because of the barrier function of the OM, Gram-negative bacteria can survive in harsh environments. This property is further enahnced by modulating the LPS synthesis and structure upon envelope stress (Maldonado et al., 2016).

Like biological membranes, the OM contains numerous integral membrane proteins, (outer membrane proteins, OMPs), that consist of amphipathic β-strands which adopt a β-barrel structure (Fairman et al., 2011). OMPs embrace receptors, enzymes, transporters and porins (Yamashita and Buchanan, 2010). Many lipoproteins are associated to the OM via lipid modification at their N-terminal end (Okuda and Tokuda, 2011). The *E. coli* genome codes for at least 90 lipoproteins, comprising 1-3 % of all proteins, the majority of which are anchored at the periplasmic face of the OM. (Tokuda et al., 2007; Mathelié-Guinlet et al., 2020). Lipoproteins fulfil several important different functions in the cell ranging from structural or signalling roles to sorting other lipoproteins, LPS and β-barrels proteins to the OM (Tokuda, 2009).

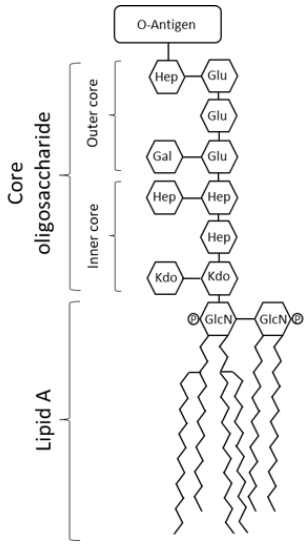

Figure 3. LPS structure in *E. coli*. General chemical structure of LPS (Modified from Sperandeo et al., 2019a).

1.3 PG synthesis

The cell wall is the first line of defence against external stressors, and the guarantor for maintaining the cell shape during growth. The relationship between the PG synthesis and bacterial growth and shape it is well known, as the lack or the fact of having defective enzymes involved in PG synthesis lead to aberrant cell morphology and growth or even lysis (Nelson et al., 2001; Denome et al., 1999., Benson et al., 1996).

The synthesis of the PG sacculus in Gram-negative bacteria is a complex process that requires numerous enzymatic reactions that take place in three different compartments of the cell namely cytoplasm, IM and periplasm (**Fig. 4**).

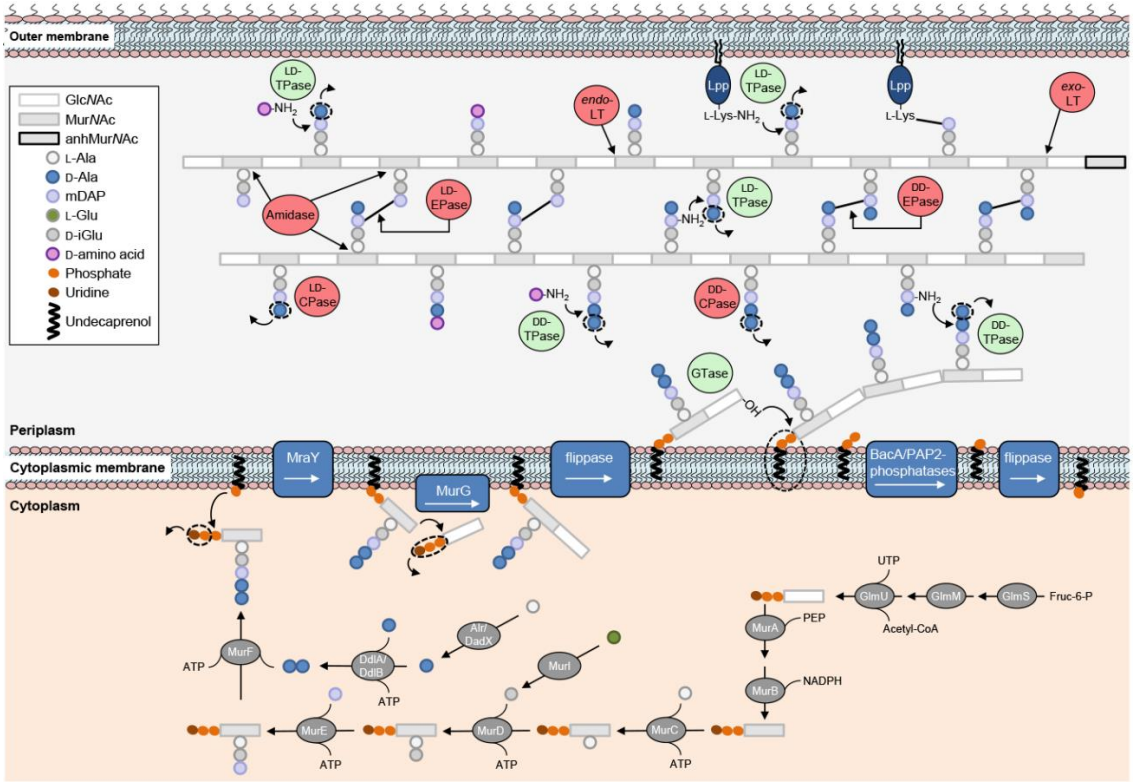

Figure 4. **Peptidoglycan synthesis in *E. coli***. PG precursors are synthesized in the cytoplasm, linked to the lipid carrier (undecaprenyl phosphate) and flipped across the IM. Then, a nascent PG chain is polymerized through a glycosyltransferase (GTase) from the lipid II precursor at the IM and inserted in the sacculus by a DD-Transpeptidase (DD-TPase). Peptides are trimmed by DD and LD-carboxypeptidases (DD- and LD-CPases) and crosslinked by DD- and LD-Transpeptidases (DD- and LD-TPases). Crosslinked peptides are cleaved by the DD and LD-endopeptidases (DD- and LD-EPases), and specific LD-TPases anchor the major outer-membrane lipoprotein (Lpp) to the glycan strands. Amidases remove peptides from glycan chains, and exo-or endo-specific lytic transglycosylases (LTs) cleave in the glycan chain producing 1,6-anhydro-N-acetylmuramic acid (anhMurNAc) residues (Text adapted from Typas et al., 2011; Figure modified from Pazos and Peters, 2019).

The synthesis of PG starts in the cytoplasm with the biosynthesis of the UDP-GlcNAc precursor from fructose-6-phosphate. It requires four successive enzymatic reactions catalysed by the GlmS, GlmM and GlmU enzymes. Then, MurA and MurB enzymes convert UDP-Gl*N*ac into UDP-Mur*N*Ac. MurA catalyzes the transfer of the enolpyruvyl moiety of phosphoenol pyruvate (PEP) to the 3' hydroxyl group of UDP-GlcNAc and the product of this reaction is then reduced by MurB (Zoeiby et al., 2003).

After the synthesis of UDP-MurNAc precursor, the amino acids that constitute the pentapeptide chain are sequentially added to the MurNAc precursor by a series of ATP-dependent ligases: (i) MurC links L-Alanine to UDP-MurNAc, (ii) MurD catalyses the insertion of D-glutamic acid (D-iGlu), (iii) MurE adds the meso-Diaminopimelic acid (mDAP) residue, and (iv) MurF inserts the D-Ala-D-Ala dipeptide, previously synthesised by the DdlA and DdlB ligases (Kouidmi et al., 2014; Barreteau et al., 2008). The resulting disaccharide pentapeptide (UDP-MurNAc-L-Ala-D-iGlu-mDAP-D-Ala-D-Ala) is transferred onto the lipid carrier undecaprenyl-phosphate, at the cytoplasmic side of the IM.

The IMP MraY catalyses the attachment of the phospho-MurNAc-pentapeptide to the undecaprenyl phosphate forming lipid I (Liu et al., 2016). Then, the translocase MurG transfers the GlcNAc moiety from UDP-GlcNAc to the lipid I, resulting in undecaprenyl-pyrophospate-MurNAc-pentapeptide-GlcNAc, also named lipid II. Lastly, lipid II is flipped from the cytoplasmic to the periplasmic side of the IM, where it is processed as substrate for the last steps of PG synthesis (Bouhss et al., 2008). The identity of the lipid II flippase is not completely determined, but two IMPs have been proposed as candidates, FtsW and MurJ. Several studies support the role of MurJ as lipid II-flippase (Ruiz, 2008; Sham et al., 2014; Zheng et al., 2018; Kumar et al., 2018), although it is not fully understood how MurJ performs this process, whereas FtsW activity is required for MurJ midcell localization in septal PG synthesis (Liu et al., 2018).

Once the lipid II reaches the periplasm, successive enzyme reactions take place to process the disaccharide pentapeptide moiety of lipid II. The synthesis of new PG proceeds with the polymerization of lipid II by glycosyltransferases (GTases) forming a linear glycan chain of alternating β-1,4-linked GlcNAc and MurNAc residues and releasing the undecaprenyl-pyrophosphate carrier (Galley et al., 2014). These carbohydrate chains are incorporated into pre-existing chains through crosslinkage of the stem peptides by

transpeptidases (TPases) (**Fig. 5**). The growth of the sacculus is a dynamic process that requires synthases to make peptidoglycan and hydrolases to cleave the PG to allow insertion of the newly synthesized material (Typas et al., 2011). Besides, several of these PG synthesis enzymes are the targets for clinically useful antibiotics, constituting an entire class of molecules named β-lactams (Frère and Page, 2014).

β-lactams are characterized by the presence of a four-membered, nitrogen-containing β-lactam ring in their chemical structure. β-lactams target the PBPs, by a specific binding of the β-lactam ring to these different PBPs, impeding their vital activity in the cell wall formation (Zapun et al., 2008).

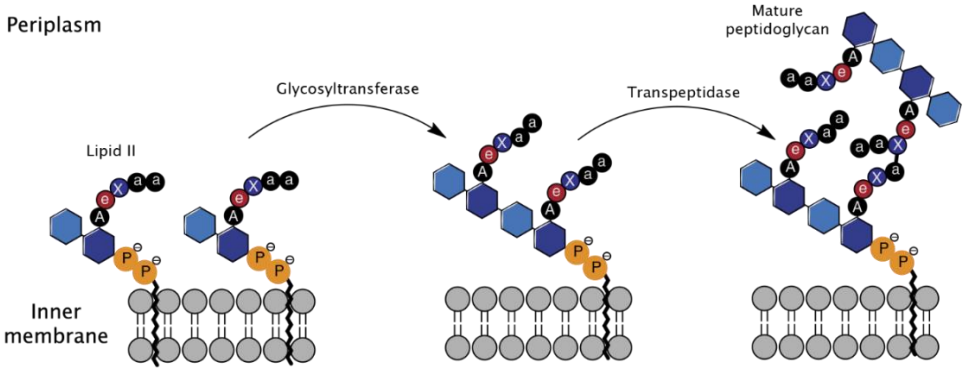

Figure 5. Lipid II polymerization. PG synthesis from lipid II disaccharide units with subsequent glycosyltransferase and transpeptidase catalysis. A: L-Ala, a: D-Ala, e: D-iGln, X: mDAP. (Modified from Zuegg et al., 2015).

1.3.1 Peptidoglycan synthases

Growth of the sacculus demands a concerted action between PG hydrolytic and synthetic enzymes. Among the former, penicillin-binding proteins (PBPs) are of special interest as the major enzymes that polymerize and crosslink new and pre-existing PG. PBPs are present in all bacteria, with some exceptions (Otten et al., 2018), in variable number. These PG synthases are typically classified based on their molecular weight: high molecular weight (HMW) and low molecular weight (LMW) PBPs.

HMW PBPs are multimodular enzymes located at the periplasmic side of the IM and anchored to the IM through their N-terminal domain. Their topology consists of a cytoplasmic tail, a transmembrane anchor, and two domains joined by a β-rich linker exposed to the periplasmic side of the IM where peptidoglycan synthesis takes place

(Miyachiro et al., 2019; Sauvage and Terrak, 2016). Depending to structure and catalytic activity of their N-terminal domain, PBPs can be grouped in class A or class B. The C-terminal domain of both classes is the so-called penicillin-binding domain, which has a transpeptidase activity. In class A HMW PBPs, the N-terminal domain carries glycosyltransferase activity (elongation of glycan chains) whereas in class B HMW PBPs, the N-terminal domain contribution to PG synthesis remains unknown, it is thought to have a role in cell morphogenesis (Haenni et al., 2006; Den Blaauwen., 2008).

LMW PBPs, usually referred as class C PBPs can exhibit transpeptidase or endopeptidase activity, but mostly DD-carboxypeptidase activity (DD-CPases). LMW PBPs play a role in regulating the extent of crosslinks in PG, and in cell division (Scheffers and Pinho, 2005; Potluri et al., 2012).

The transglycosylation reaction can also be carried out by monofunctional GTase represented by MgtA, that catalyzes glycan chain elongation, with a putative role in PG assembly during the cell cycle (Derouaux et al., 2008).

To date, 12 PBPs have been identified in *E. coli* (Sauvage et al., 2008; Denome et al., 1999). *E. coli* possesses three class A HMW PBPs (PBP1A, PBP1B and PBP1C), and two class B HMW PBPs (PBP2 and PBP3). PBP1A and PBP1B are the major bifunctional synthases carrying transpeptidase and transglycosylase activity, and the presence of at least one of them is required for cell viability, since the deletion of both genes is lethal (Sauvage et al., 2008; Yousif et al., 1985). Importantly, the activity of PBP1A and PBP1B is regulated by the OM lipoproteins LpoA and LpoB, respectively (Typas et al., 2010). On the contrary, PBP1C is not essential and its role has not been clarified yet (Schiffer and Höltje, 1999), although some data suggest that it could be involved in a PG repair mechanism (Budd et al., 2004).

Regarding the class B HMW PBPs (monofunctional transpeptidases), PBP2 is implicated in the maintenance of the cell shape and one of the key players of the elongasome, a dynamic protein complex implicated in the cell wall elongation (Philippe et al., 2009; Spratt, 1975). PBP3, also named FtsI, is an essential component of the divisome, the cell division complex (Sauvage et al., 2014).

In addition to the HMW PBPs, there are seven LMW PBPs in *E. coli*: PBP4, PBP4B, PBP5, PBP6, PBP6b, PBP7 and AmpH. These type of PBPs are involved in cell division,

maintenance of cell morphology and PG recycling or maturation (Ghosh et al., 2008), and the lack of any of them does not compromise cell integrity (Edwards and Donachie, 1993) although their combined deletion causes morphological cell defects (Pazos and Peters, 2019). Most of LMW PBPs are CPases, although PBP4 and AmpH show DD-endopeptidase (DD-EPase) activity, while PBP7 is a strict DD-EPase (Meberg et al., 2004) (see **chapter 1.3.3**).

Besides PBPs, *E. col*i contains the IMPs RodA and FtsW, which belong to the SEDS family of proteins (Taguchi et al., 2019; Cho et al., 2016). RodA possesses GTase activity and it is involved in the lateral cell wall elongation whereas FtsW carries PG polymerase activity with commitment in the cell division.

1.3.2 Peptidoglycan transpeptidases

The final step in PG biosynthesis is the peptide crosslinking (transpeptidation) of the glycan strands. This reaction provides rigidity and structure to the PG layer necessary for its protective function. There are different TPase reactions based on the donor muropeptide (**Fig. 6**). In *E. coli*, the majority (90% to 98%) of crosslinks in PG are of the DD or 4-3 type, which are formed between D-Ala at position 4 of a pentapeptide (donor) and the mDAP at position 3 of another muropeptide (acceptor). The DD-transpeptidation is made at the expense of the terminal D-Ala-D-Ala bond of the pentapeptides. The reaction begins via the formation of a serine ester-linked peptidyl enzyme followed by the release of the carboxy-terminal D-Ala of the donor pentapeptide and resumes by the transfer of the peptide moiety to the side chain amino-group mDAP residue of the acceptor muropeptide (Goffin and Ghuysen, 1998). This abundant type of crosslinks is catalysed by the DD-TPase activity of bifunctional PBP1A and PBP1B, with some studies showing that their transpeptidation activity is dependent on the transglycosylase activity of the respective enzymes (Barrett et al., 2005).

β-lactam antibiotics mimic the D-Ala-Ala terminal residues of the stem peptide of PG precursors and inactivate DD-TPase by acting as suicide substrates. Upon β-lactam treatment PG synthesis declines whereas activity of PG hydrolases remains. The resulting destabilization of the PG sacculus leads to cell lysis and cell death (Drawz et al., 2010).

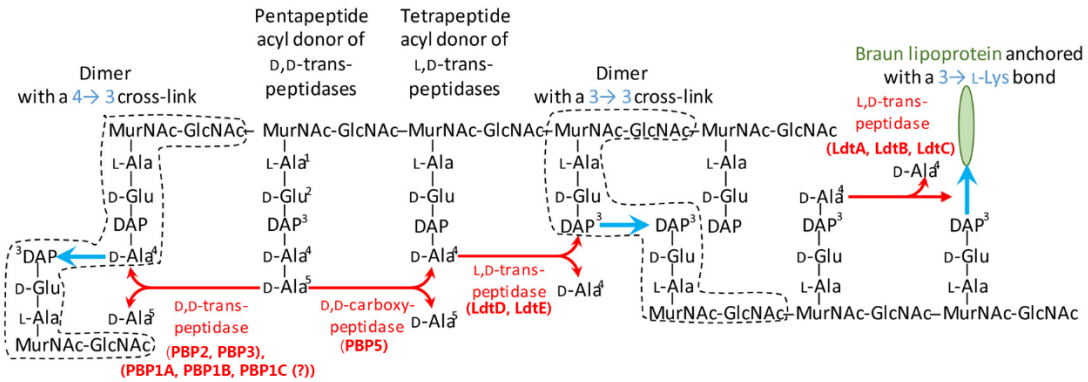

Figure 6. **Overview of the TPase reactions in *E. coli***. DD-TPases cleave the D-Ala-D-Ala peptide bond of a pentapeptide acyl donor stem to catalyse 4,3-crosslinks with an acyl acceptor. DD-CPase hydrolyse the D-Ala-D-Ala bond of pentapeptide stems, generating a tetrapeptide acyl donor that is used as substrate for LD-transpeptidation (3,3-crosslinks) by LD-TPases. Specific LD-TPases anchor the Braun lipoprotein (Lpp) to PG. (?): refers to enzymes (PBP1C) with predicted TPase activity but not determined yet (Modified from Hugonnet, et al., 2016).

Besides DD-transpeptidation, stem peptides can be crosslinked in a LD-type or 3-3 configuration. 3-3 crosslinks are formed between mDAP at position 3 of a tetrapeptide donor and the mDAP residue of the acceptor muropeptide **(Fig. 6)**. The relative abundance of LD and DD crosslinks differs across bacterial species, being highly abundant in some pathogenic bacteria (Lavollay et al., 2008). In *E. coli* the proportion of 3-3 crosslinks is very low (2-10%) and growth phase dependent (Glauner et al., 1988) The 3-3 crosslinks are catalysed by LD-TPases (LDTs) of the YkuD family of proteins (PF03734). In *E. coli* five LDTs were known until now that are divided in two class: i) LdtA, LdtB and LdtC (formerly ErfK, YcfS, YbiS) that covalently attach the abundant OM-anchoredBraun's lipoprotein (Lpp) to mDAP residues in PG (Magnet et al., 2007), ii) LdtD and LdtE (formerly YcbB, YnhG) which form 3-3 crosslinks between two mDAP residues (Magnet et al., 2008). An additional LDT, LdtF (formerly YafK) has been recently identified. LdtF has no LD-TPase activity but seems able to stimulate the activity of LdtD and LdtE (Morè et al., 2019; see **chapter 3.1**). All the six *ldt* genes can be simultaneously deleted indicating the non-essentiality of these enzymes for bacterial growth under standard laboratory conditions (Sanders et al., 2013).

LDTs are structurally unrelated to PBPs, indeed, they contain a cysteine residue in the catalytic site instead of the serine residue typical of PBPs. Introduction of 3-3 crosslinks in PG has been proposed as mechanismto bypass PBPs therefore granting resistance to β-lactam antibiotics, except for carbapenem (Mainardi et al., 2007). In fact, β-lactam-

resistant *Enterococcus faecalis* mutants remodel their PG by replacing 4-3 crosslinks with 3-3 crosslinks catalysed by the β-lactam insensitive Ldt_{fm} (Biarrotte-Sorin et al., 2006). Moreover, *E. coli* mutants with an elevated synthesis of (p)ppGpp alarmone, which up-regulates genes involved in stress response, and increased expression of LdtD, can fully bypass DD-TPase activity of PBPs thus leading to β-lactam resistance (Hugonnet et al., 2016).

1.3.3 Peptidoglycan hydrolases

Bacterial growth requires a dynamic PG remodelling to accommodate cell wall elongation and division, thus PG synthesis and degradation must be tightly coordinated. PG degradation is made by hydrolytic enzymes known as PG hydrolases. Bacterial PG hydrolases cleave the bonds in PG chain and side-chain peptides, allowing the incorporation of new PG into the sacculus. PG hydrolases are implicated in autolysis, maturation, turnover and recycling of PG (Pazos and Peters, 2019). Based on the cleavage site on PG they can be categorised as amidases, carboxypeptidases (CPases), endopeptidases (EPases) and lytic transglycosylases (LTs) (**Fig. 7**).

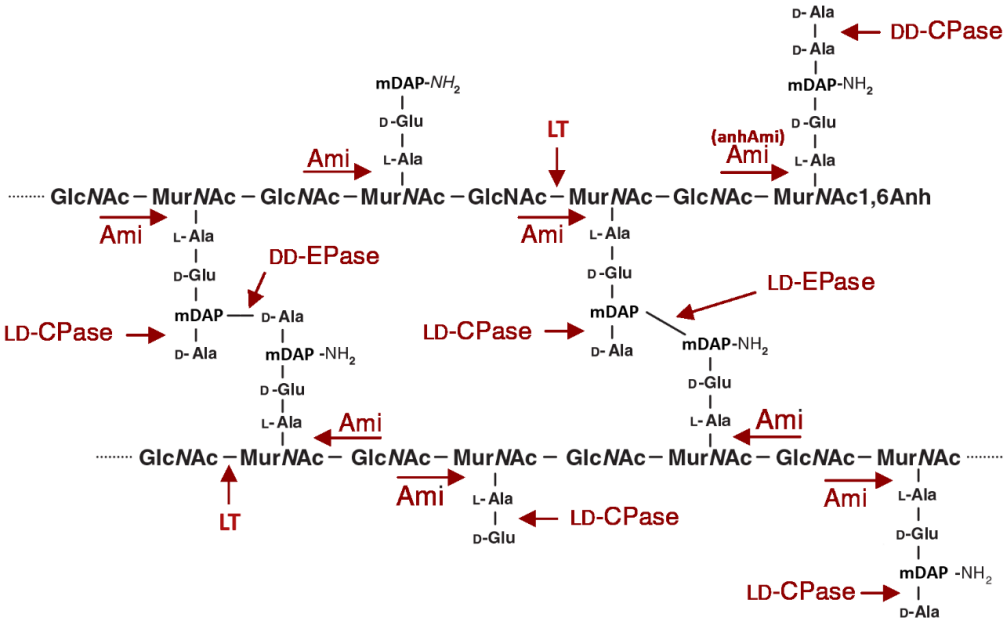

Figure 7. Cleavages sites of PG hydrolases. Amidases (Ami) cleave the amide bonds between MurNAc and the L-alanine of the stem peptide. Specific amidases (anhAmi) cleave at 1,6-anhydroMurNAc residues. DD-EPase cleave D-Ala-mDAP bonds and LD-EPases cleave mDAP-mDAP bonds. DD-CPase hydrolyse terminal D-amino acids of pentapetides whereas LD-CPase have specificity for tetrapeptides. LTs hydrolyse the β1,4-glycosidic bond between MurNAc and GlcNAc residues (Modified from Vollmer et al., 2008b).

- **Amidases**

Amidases, or N-acetylmuramyl-L-Alanine amidases, hydrolyse the amide bond between the L-Ala residue of the stem peptide and the MurNAc subunit of the glycan chain. *E. coli* encodes five amidases, which, based on amino acid sequence similarity, are subdivided into two groups: (i) AmiA, AmiB, AmiC, and (ii) AmiD and AmpD. AmiA, AmiB and AmiC have specificity for MurNAc substrates, AmpD for 1,6-anhydro-MurNAc, and AmiD breaks off both MurNAc and 1,6-anhydro-MurNAc substrates. AmiA, AmiB and AmiC play the crucial role of splitting the septum in cell division, since the lack of all three results in massive cell chaining. AmiA localises throughout the periplasm whereas AmiB and AmiC localises to the septum during cell division. Interestingly, they have semi-redundant functions as they can replace each other function (Heidrich et al., 2001; Priyadarshini et al., 2007).

Besides becoming key players during cell division, the amidases have been proposed as targets for antimicrobials (Vermassen et al., 2019). Regarding AmiD and AmpD, they have been proposed to have a role in the PG recycling pathway (Uehara et al., 2007; Hesek et al., 2009).

The AmiA, AmiB and AmiC activity is regulated by the LytM-domain factors, EnvC and NlpD, as the phenotype of mutants lacking both regulators shows the same cell chaining phenotype than a mutant missing the three amidases (Uehara et al., 2010). Proteins with LytM (Lysostaphin/ Peptidase_M23) domains are widely distributed in bacteria and participate in essential processes such as cell division and cell morphogenesis. Most of the LytM-like proteins already identified are metallo-endopeptidases that cleave crosslinks in PG (Sabala et al., 2012). *E. coli* contains four LytM-domain factors in *E. coli*: EnvC, NlpD, MepM and YgeR. Of the four, only MepM exibits hydrolytic activity on PG. MepM is a PG metallo-endopeptidase, having DD-EPase activity with specificity for 4-3 crosslinks (Singh et al., 2012). EnvC and NlpD have no activity on PG since they show a degenerated LytM domain missing important catalytic residues required for function (Uehara et al., 2010, Peters et al., 2013), consistent with their role as hydrolases regulators. EnvC has been shown to activate AmiA and AmiB, whereas NlpD activates AmiC (Tsang et al., 2017). YgeR is a predicted OM lipoprotein with an unknown function although its deletion exacerbates the cell chaining phenotype of the double *envC nlpD* mutant (Uehara et al., 2009). A characterisation of this protein is reported in **chapter 3.2**.

- **Carboxypeptidases (CPases)**

CPases remove the terminal residues from the stem peptides. *E. coli* contains seven CPases. Six of them are non-essential LMW PBPs (PBP4, PBP4B, PBP5, PBP6, PBP6B and AmpH) and one is a cytoplasmic LD-CPase (LdcA). The PBPs CPase have DD-CPase activity, cleaving the D-Ala residue from the pentapeptides, and LdcA cleaves D-Ala residue from tetrapeptides. As above-mentioned, PBP4 and AmpH can work as well as EPase. PBP5 is the most abundant CPase and removes the terminal D-Ala-D-Ala bond from disaccharide pentapeptide side-chains. Despite its dispensability, the loss of PBP5 causes morphological defects (Nelson and Young, 2001). PBP6 and PBP6b are DD-CPases that share a high sequence identity with PBP5, although their role in the cell is unknown. It has been shown that PBP6 has a weaker CPase activity compared with PBP5, whereas PBP6B has increased activity at low pH (Sarkar et al., 2011; Peters et al., 2016). PBP4B has a low DD-CPase activity and its physiological role is still unknown (Vega and Ayala, 2006), whereas AmpH is implicated in PG recycling, showing both DD-CPase and DD-EPase activity (González-Leiza, et al., 2011). Finally, LdcA is an LD-CPase that appears to be implicated in PG recycling (Templin et al., 1999).

- **Endopeptidases (EPases)**

EPases cleave the amide bonds between amino acids from different stem peptides namely, the crosslinks. According to the crosslink specificity, they are classified as DD-EPase and LD-EPase. DD-EPases cleave 4-4 crosslinks (D-Ala-mDAP bonds), *E. coli* contains three β-lactams sensitive (PBP4, PBP7, and AmpH), and four to β-lactams insensitive (MepA, MepH, MepM and MepS) EPases. It has been suggested a role of PBP4 and PBP7 in maintenance of cell morphology and biofilm formation (Meberg et al., 2004; Miyamoto et al., 2020). MepA belongs to LAS family, and MepH, MepM and MepS are members of the NlpC/P60 family. MepA and MepM require the presence of divalent metal ion for activity (Marcyjaniak et al., 2004).

The insensitive β-lactam DD-EPases are required for new PG incorporation since mutants lacking all three EPases MepH, MepS and MepM display aberrant cell shape and extensive lysis. MepA and MepS possess also a weak LD-EPase activity (Singh et al., 2012). LD-EPases cleave 3-3 crosslinks, (mDAP-mDAP bonds). *E. coli* encodes a specific LD-EPase, MepK. MepK seems to play a role in PG extension by regulating the

degree of 3-3 crosslinkage in PG. The combined activity of MepK with MepS and and MepM is required for an optimal PG enlargement (Chodisetti and Reddy, 2019).

- **Lytic Transglycosylases (LTs)**

Lytic transglycosylases cleave the β1,4-glycosidic bond between MurNAc and GlcNAc, forming a 1,6-anhydro ring at the MurNAc residue. LTs cleave at the end of the glycan chains (exolytic activity, exo-LTs) or within them (endolytic activity, endo-LTs). *E. coli* encodes eight LTs, which are grouped in four families based on their domain structure: family 1 (Slt70, MltC, MltD, MltE), family 2 (MltA), family 3 (MltB) and YceG-family (MltG). LTs are redundant although the loss of some (MltA-E and Slt) leads to cell chaining phenotype (Vollmer et al., 2008b). Slt70 is a periplasmic exo-LT of interest since it is known that it may form a multienzyme complex with PBP3 and PBP7(Romeis and Höltje, J.V, 1994). Loss of Slt70 increases sensitivity to specific β-lactams, as mecillinam (Templin et al., 1992).

A role of Slt in PG remodeling upon β-lactams attack has been inferred, as it prevents the accumulation of uncrosslinked glycan strands so that they are not aberrantly incorporated into the sacculus. This PG "quality control" mechanism might facilitate the replacement of impaired PG synthetic machineries by functional ones (Cho et al.,2014a).

1.4 LPS synthesis

The peculiar structure of the OM of Gram-negative bacteria prevents not only the entry of large polar molecules, but also that of small hydrophobic molecules. Lipopolysaccharides (LPS) are the major contributors of the OM permeability barrier properties. The LPS molecules are the main lipid components of the OM, representing approximately three quarters of the bacterial surface. LPS is composed of a lipid A moiety, inner and outer core oligosaccharides, and the O-antigen (**Fig. 3**). The biogenesis of LPS is a complex process that starts in the cytoplasm with the synthesis of the core oligosaccharide-Lipid A moiety and the O antigen, which are independently synthesised and translocated across the IM.

1.4.1 Kdo_2-lipid A

The synthesis of Kdo_2-lipid A moiety requires the action of several conserved enzymes and occurs first in the cytoplasm, and subsequently in the cytoplasmic face of the IM (**Fig. 8**) (Raetz and Whitfield, 2002). Lipid A biosynthesis begins with the acylation of UDP-GlcNAc, catalysed by the cytoplasm acyltransferase LpxA which adds β-hydroxymyristoyl chain (Anderson and Raetz, 1987; Wyckoff *et al.*, 1998). The next step involves the deacetylation of UDP-3-O-acyl-GlcNAc catalysed by LpxC, a Zn2+-dependent enzyme (Jackman *et al.*, 1999). The reaction catalysed by LpxA has an unfavourable equilibrium which makes the deacetylation catalysed by LpxC the first committed step of Kdo2-lipid A synthesis (Anderson et al., 1993). Indeed, LpxC represents a key point of control of LPS biosynthesis whose levels are controlled by the FtsH protease in response to growth rate (Ogura et al., 1999; Schäkermann et al., 2013). The next step is the transfer of a second β-hydroxymyristoyl chain catalysed by the acyltransferase LpxD to form UDP-2,3-diacyl-GlcN (Raetz et al., 2009). Following acylation, the pyrophosphate bond of the UDP-2,3-diacyl-GlcN is hydrolysed by the pyrophosphatase LpxH, resulting in UMP and 2,3-diacyl-GlcN-1-phosphate (lipid X) (Babinski et al., 2002). The biosynthesis continues with the generation of the characteristic β,1′-6 linked disaccharide by LpxB that catalyses the condensation of UDP-2,3-diacyl-GlcN with one molecule of lipid X, releasing UDP. The successive steps are catalysed by the IM proteins LpxK, KdtA, LpxL and LpxM. LpxK phosphorylates the 4' position of the disaccharide 1-phosphate to produce the intermediate lipid IV_A, requiring ATP hydrolysis in the process. Next, the bifunctional enzyme KdtA (formerly WaaA) catalyse the incorporation of two Kdo residues. Contrary to what was once believed, the presence of Kdo residues in the LPS molecule is not required for cell viability, although their absence yields to a larger cell wall permeability and a decline in antibiotic tolerance (Meredith et al., 2006). LpxL and LpxM, also named "late" acyltransferases, share strong amino acid sequence similarity and requires Kdo to function (Opiyo et al., 2010). LpxL transfers a lauroyl group which is followed by the catalysed-addition of myristoyl by LpxM, completing the formation of Kdo_2-lipid A moiety (Raetz et al., 2007). In case of growth at low temperatures, *E. coli* expresses LpxP that incorporates a palmitoleate into lipid A in place of a laurate (Carty et al., 1999).

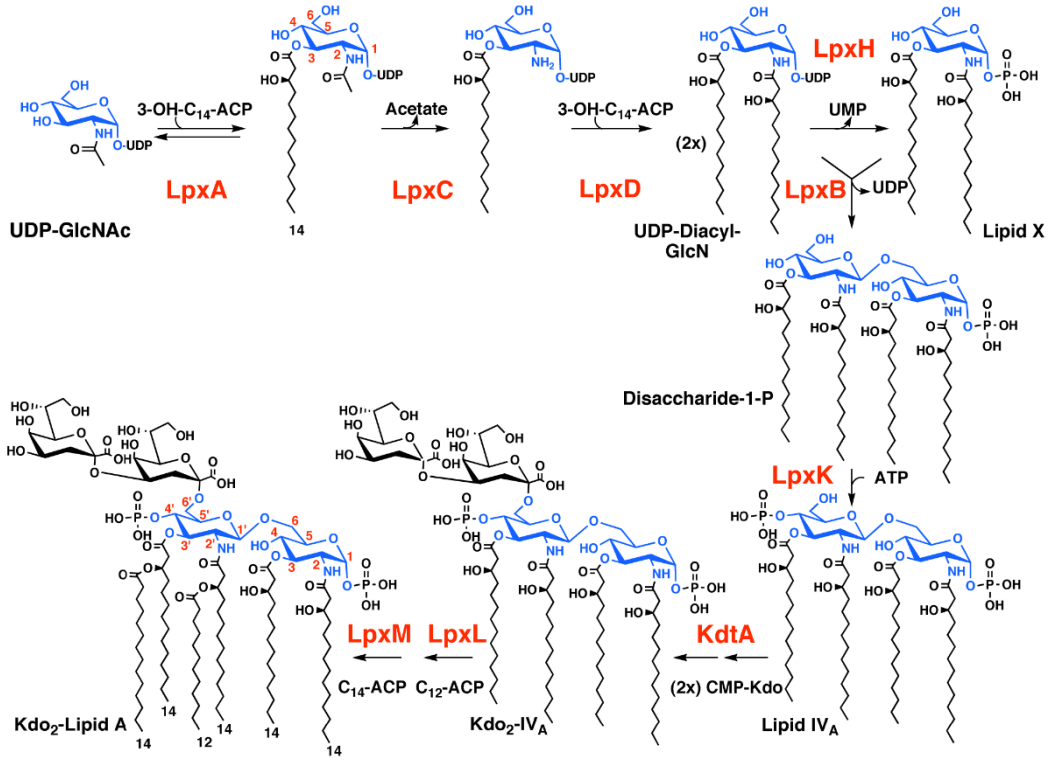

Figure 8. Biosynthesis pathway of Kdo$_2$-lipid A in E. coli. UDP-GlcNAc sugars and derivatives are highlighted in blue and enzymes in red. (Adapted from Raetz et al., 2007).

1.4.2 Core oligosaccharide

Core oligosaccharide region, or core-OS contains 8 to 15 sugars that includes heptoses (Hep), glucoses (Glc) and Kdo residues. The proximal region to the lipid A is known as 'inner' core containing Hep and Kdo residues whereas the "outer" core corresponds to rest of the core where the O-antigen is attached and is composed of Glc and Hep residues decorated with phosphates. Biosynthesis of core-OS involves several IM-glycosyltransferases which enlarge the Kdo$_2$-lipid A using nucleotide sugars donors. The *waa* locus on the chromosome of *E. coli* encodes enzymes involved in the assembly of the Core-OS (**Fig. 9**). The *waa* locus is divided into three distinct operons. The *waaA* operon contains the gene *waaA* encoding the bifunctional transferase KdtA that catalyse the attachment of two Kdo residues to the Kdo$_2$-lipid A acceptor, which is the first committed step of the inner core synthesis (see previous paragraph). The *gmhD* operon comprises *gmhD*, *waaC* and *waaF*. The GmhD enzyme catalyses the synthesis of the activated sugar nucleotide substrate for Hep addition to the inner core and WaaC and WaaF, incorporate a first (Hep$_I$) and a second (Hep$_{II}$) heptose, respectively. The *waaQ* operon encodes genes necessary for outer core-OS assembly. WaaP and WaaY add

phosphate groups to the inner core heptoses. Heptosyltransferase WaaQ attaches a third heptose (Hep_{III}) to Hep_{II}. Then, WaaG inserts the first Glc residue, on which WaaB catalyse the addition of a Galactose (Gal). Then, a second (Glc_{II}) and a third (Glc_{III}) glucoses are subsequently incorporated by WaaO and WaaR, respectively. The last step of core-OS synthesis is the attachment of the fourth heptose (Hep_{IV}) to Glc_{III} by WaaU (Wang et al., 2015; Frirdich and Whitfield, 2005).

Once the synthesis of core-lipid A moiety is completed at the inner leaflet of the IM the essential ABC transporter MsbA catalyses the flipping of core lipidA across the IM (Borbat et al., 2007; Polissi and Georgopuolos 1996; Zhou et al., 1998). The final steps of LPS synthesis occur at the periplasmic face of the IM as discussed in the next paragraph.

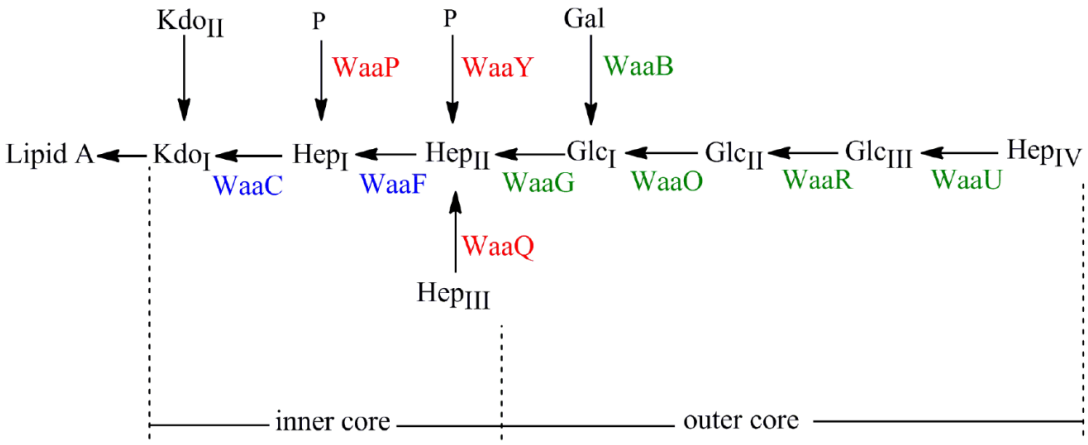

Figure 9. General structure and biosynthesis pathway of the *E. coli* core-OS. Same colour in the Waa proteins indicate that the corresponding genes belong to the same operon. (Adapted from Wang et al., 2015).

1.4.3 O-antigen

The O-antigen is the distal, surface exposed LPS moiety and responsible of the immunogenic properties of this macromolecule. The O-antigen consists of a variable number of repeating sequences of three to six sugar residues (O unit). O-antigen structures are highly variable components of LPS, a feature used as a tool for strains classification based on the different serological properties (Raetz and Whitfield, 2002). As an example, around 200 different serogroups in *E. coli* alone have been recognised (DebRoy et al., 2016). In many pathogens O-antigen is a virulent factor employed to survive host defence mechanisms (Lerouge and Vanderleyden, 2002; Reeves, 1995). It is important to note

that E. *coli* K-12 and derivative strains lack O-antigen as a result of mutations in the O-antigen synthesis gene cluster (Stevenson et al., 1994).

The O-antigen synthesis initiates with the transfer of a sugar monophosphate to the lipid carrier Und-P at the inner leaflet of the IM. The resulting saccharide-Und-PP becomes an acceptor for additional glycosylation reactions to complete the O-antigen units. In *E. coli* the polymerization of the O units into O-antigen falls into two different pathways: Wzy polymerase-dependent and ABC transporter-dependent mechanisms (**Fig. 10**) (Kalynych et al., 2014).

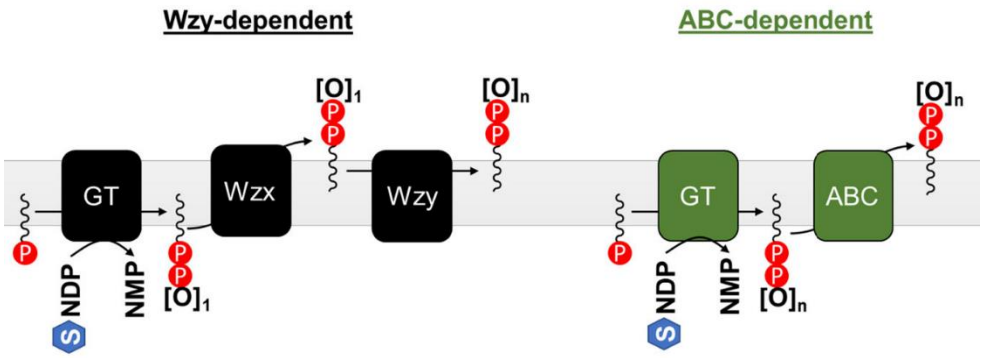

Figure 10. Summary of the two O-Antigen synthesis pathways in *E. coli*. GT: glycosyltransferases required to generate the O-antigen. [O]: O-unit, while the subscript "n" represents the number of repeats present. (S inside hexagon): Individual sugar units, which are bind to an arbitrary nucleotide carrier NDP. The lipid carrier is Und-P. (Modified from Bertani and Ruiz, 2018).

The Wzy-dependent pathway implies the synthesis of single O-units on Und-P and further translocation of these Und-P-linked-O units to the periplasmic leaflet of the IM by the Wzx flippase. The glycosyl polymerase Wzy catalyses the polymerization of these O units on a single Und-P carrier molecule, whose polymer length is controlled by Wzz. Finally, the polymerised O-antigen is linked to the core-lipid A by the WaaL ligase, and the Und-PP carrier is recycled (Kalynych et al., 2014; Bertani and Ruiz, 2018). Disruption of certain steps in this pathway results in sequestration of Und-P, leading to important growth defects as Und-P is utilised in the PG synthesis (Jorgenson and Young, 2016).

In the ABC-dependent pathway, the entire polymerised O-antigen is assembled in the cytoplasm. Dedicated GTases polymerise the complete O-antigen on a single Und-P molecule in the inner leaflet of the IM. An ABC transporter translocates the completed O-antigen-Und-PP molecule to the periplasm, where WaaL attaches the O-antigen moiety to the core-OS-lipid A (Greenfield and Whitfield, 2012; Han et al., 2012).

Full length LPS or core-lipid A moiety (in O-antigen non-producing strains) are then transported from the IM to the outer leaflet of the OM by the dedicated lipopolysaccharide transport (Lpt) machinery as illustrated in **chapter 1.5**.

1.5 Envelope molecular machineries

Most OM and PG components are synthetized in the cytoplasm or at the IM and subsequently exported to the periplasm or OM for their final assembly in the cell envelope. This is not an easy task, since both the periplasm and the OM are not energised and envelope building blocks need to cross compartments with different physico-chemical characteristics. To overcome these issues, bacteria have evolved multiprotein envelope machineries. The LPS molecules are transported across the periplasm and assembled at the OM by the multiprotein Lpt machinery (Sperandeo et al., 2019a). After synthesis in the cytoplasm, OMPs cross the IM thanks to the Sec system and then are escorted by chaperones across the periplasm to the OM, where they are folded, assembled and positioned by the β-barrel assembly machinery (BAM) complex (Bakelar et al., 2017; Knowles et al., 2009). OM Lipoproteins, which cross the IM thanks to the Sec system as well, contain a specific sorting signal which is recognised by the Lol (lipoprotein OM localization) protein complex that mediates their transport from the IM to their final location at the OM (Tokuda and Matsuyama, 2004). Very little is known on the systems that transport phospholipids to the OM inner leaflet and these will not be discussed in this thesis.

Besides the machineries required to build the OM, Gram-negative bacteria employ dynamic multiprotein complexes to ensure a tightly regulated growth of the PG sacculus during the cell cycle. These complexes are known as the elongasome (cell elongation machinery) for cell growth, and the divisome (division machinery) for cell division (Egan et al., 2017).

Since the envelope is a crucial structure for bacterial survival it is not surprising that bacteria have evolved sophisticated sensory systems that sense internal or external perturbations and counteract them to restore envelope homeostasis. These so-called envelope stress response systems (ESRs), are discussed at the end of this chapter focusing on the Cpx two-component system, the σE stress response, and the Rcs phosphorelay of *E. coli*.

1.5.1 Outer membrane assembly

As mentioned in the previous paragraph, structural constituents of the OM as lipoproteins, LPS or OMPs have different pathways in their transit routes to the OM which are discussed in the following paragraphs.

- **LPS transport and assembly: Lpt machinery**

The Lpt machinery is a multiprotein complex composed, in *E. coli*, of seven essential proteins (LptABCDEFG) that span all compartments of the cell envelope. These proteins physically interact with each other forming a protein bridge connecting IM and OM. The Lpt machinery works as a single device as depletion of any component results in accumulation of the LPS at the IM outer leaflet (Sperandeo et al., 2008). The multiprotein machinery is organized in two sub-complexes, the ABC transporter $LptB_2CFG$ at the IM and the OM LptDE translocon, connected by LptA in the periplasm (**Fig. 11**).

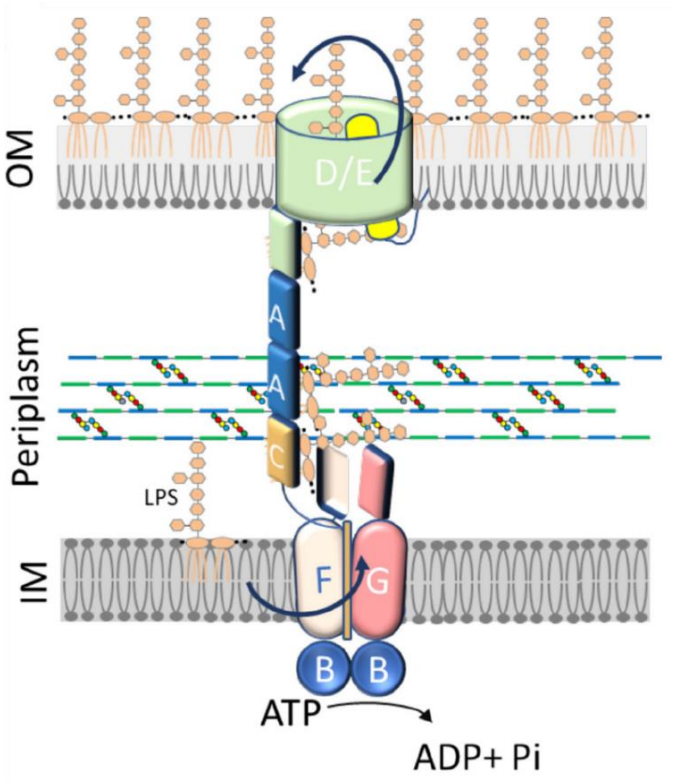

Figure 11. The LPS export pathway. Flipped LPS molecule is extracted from the IM, escorted across the periplasm and assembled at the OM outer leaflet by the Lpt machinery. The IM complex LptB2FG is an ABC transporter which provides the energy for the transport (Adapted from Moura et al., 2020).

After its translocation through the IM by MsbA, LPS is detached from the IM in an energy-demanding process that requires the ATPase activity of the $LptB_2CFG$ complex. Unlike classical ABC transporters (such as MsbA), $LptB_2CFG$ is an unusual transporter in that it does not translocate its substrate across the IM, but it rather extracts LPS molecules from the IM outer leaflet and delivers them to the proteins in the periplasmic bridge (Sperandeo et al., 2019b). Similar to the ABC importers, $LptB_2CFG$ comprises four subunits (Davidson, 2008). In the cytoplasm, the dimeric $LptB_2$ constitutes the nucleotide-binding domain (NBD) of the transporter, which binds ATP and catalyses its hydrolysis. At the cytoplasmic side of the IM, LptB2 interacts to LptF and LptG, which constitute the transmembrane domains (TMD) of the transporter. $LptB_2FG$ core transporter is tightly associated with the IM bitopic protein LptC (Narita and Tokuda, 2009), which has been recently shown to represent an unconventional fifth subunit of the transporter endowed with a regulative function (Owens, 2019; Li, 2019). Structural analyses of the $LptB_2CFG$ transporter have revealed that LptFG domains form a hydrophobic cavity that accommodates LPS; the energy provided by the ATPase LptB2 is used to funnel LPS from the IM towards the periplasmic domain of LptC (Owens, 2019, Tang et al., 2019). LptC interacts with the periplasmic domains of LptF and its N-terminal transmembrane helix is wedged between the transmembrane helices of LptF and LptG (Li et al., 2019; Owens et al., 2019). Although essential, the lack of LptC can be compensated by specific mutations in LptF (Benedet et al., 2016). According to the current model, LptC accepts the LPS from LptB2FG and transfers it through its C-terminal domain to the N-terminal domain of the periplasmic protein LptA (Sperandeo et al., 2011). It is known that LptA can form homo-oligomeric complexes in vitro (Suits et al., 2008; Merten et al., 2012; Santambrogio et al., 2013). Therefore, the periplasmic bridge could be constituted of more than one LptA monomer interacting each other in a head-to-tail fashion. At the OM, LptA interacts with the N-terminal periplasmic domain of LptD (Freinkman et al., 2012). Notably, Lpt proteins with a periplasmic domain (LptA, LptC, LptF, LptG, LptD) share a β-jellyroll fold structure, characterized by a hydrophobic interior (Suits et al., 2008), which is supposed to determine the formation of the hydrophobic channel that connects the IM and the OM. Several residues laying the interior of the β-jellyroll of LptA and LptC, as well as the interaction interface among them, have been shown to interact with LPS, suggesting that periplasmic bridge formation might allow for LPS translocation across the periplasm (Hicks and Jia, 2018; Laguri et al., 2017; Villa et al., 2013). The final step of LPS assembly at the OM surface is mediated

by the two-protein translocon constituted by the β-barrel protein LptD and the lipoprotein LptE, which is embedded in the lumen of LptD (Freinkman et al., 2011; Dong et al., 2014; Gu et al., 2015). The LptDE complex receives the LPS molecules from LptA and translocates them into the outer leaflet of the OM. A proper functionality of this OM complex and its interaction with the periplasmic LptA bridge are essential to avoid LPS mistargeting, with LptE assisting LptD in its folding and its assembly into the Lpt machinery (Chimalakonda et al., 2011; Freinkman et al., 2012). Even though some aspects of the LPS transport are still unclear, a large body of evidence supports the so-called PEZ-model (in analogy with the homonymous candy dispenser), in which ATP hydrolysis provided by the $LptB_2$ dimer boost LPS detachment from the IM and generate a continuous stream of LPS molecules across the periplasm. Each power stroke pushes the LPS molecules from LptF to LptC (Owens et al., 2019) and across the LptA bridge towards the LptDE complex at the OM (Okuda et al., 2012; Xie et al., 2018), to be eventually translocated to the bacterial surface (Okuda et al., 2016).

- **Lipoproteins transport and assembly at the OM - Lol system**

Following the Sec-mediated translocation to the periplasm, the lipoprotein precursors remain anchored to the IM through their N-terminal signal peptide, exposing the C-terminal domain to the periplasm. The signal peptides of lipoproteins in addition to the canonical positively charged amino acid residues in the N-terminal region and uncharged amino acids in the central hydrophobic region, have a characteristic consensus sequence called the "lipobox" in the C-terminal region. The "lipobox" sequence is Leu-(Ala/Ser) -(Gly/Ala)-Cys (Ser: Serine; Cys: Cysteine), where the first three residues are present in the C-terminus of the signal peptide, and the last Cys is located at the N-terminus of mature lipoprotein and modified with diacylglycerol and fatty acyl chains (Narita and Tokuda, 2017). Lipoprotein maturation at the IM involves three IMPs (Lgt, Signal peptidase II or LspA and Lnt). Lgt diacylates the conserved Cys residues at the N-terminal, and subsequently LspA recognises and cleaves the "lipobox" motif. Lastly, these modifications performed in the N-terminal allow Lnt to incorporate a third acyl chain (Zückert, 2014).

Lipoproteins are localized to either the IM or the OM depending on the sorting signals. It has been shown that the amino acid residue next to N-terminal Cys (+2 position) of mature lipoproteins determines the membrane specificity (IM or OM).

In *E. coli*, lipoproteins targeted to the IM show a strong preference for Asp residue at position 2, which works as Lol avoidance signal as it interferes with the recognition by the Lol system (Hara et al., 2003). Conversely, lipoproteins lacking this IM retention signal are committed to the Lol pathway (Tokuda et al., 2007). The Lol system is composed of the IM ABC transporter LolCDE, the periplasmic chaperone LolA, and the OM lipoprotein LolB. At the IM, the LolCDE complex catalyses the extraction of mature OM lipoproteins using energy provided by ATP hydrolysis in the cytoplasm, with a mechanism that resembles that of the $LptB_2FG$ complex. LolCDE delivers the lipoprotein to the chaperone LolA that transport it across the periplasm to LolB. At the OM, LolA transfers the lipoprotein to LolB, which catalyses its insertion into the OM (Narita and Tokuda, 2017) (**Fig. 12- left side**).

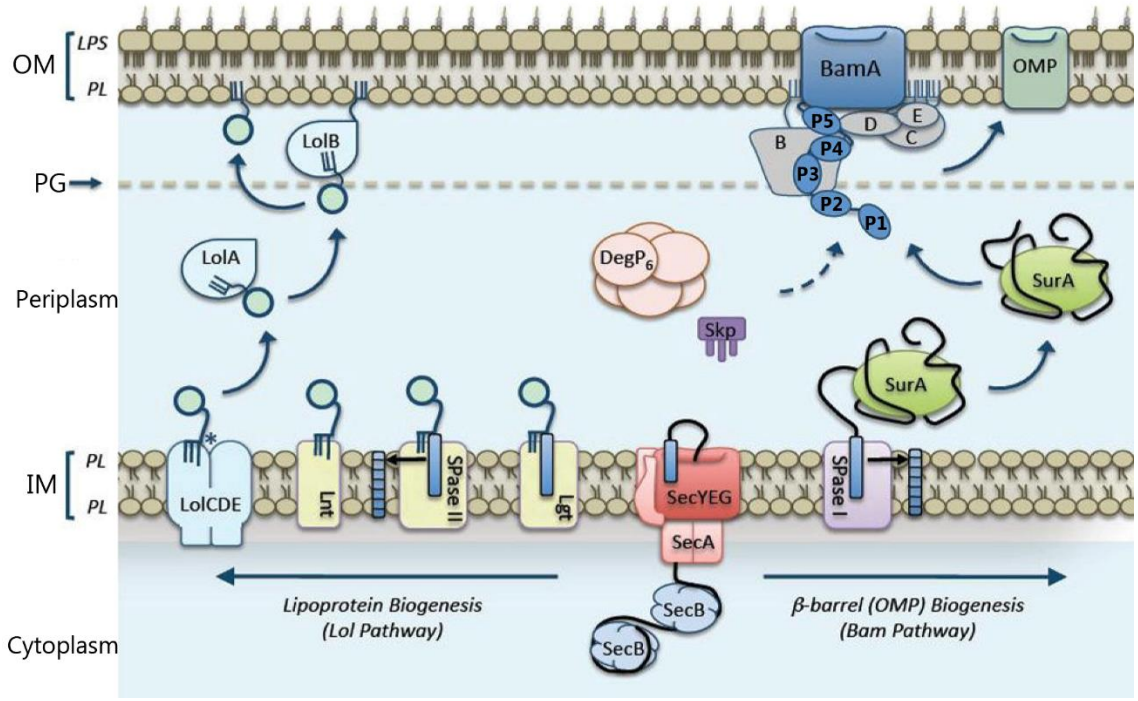

Figure 12. OM lipoprotein and OMP biogenesis. Precursor OM proteins bind to the cytoplasm SecB chaperon, which delivers them to the SecA ATPase and the SecYEG translocase at the IM. After translocation across the IM, precursor OM proteins are sorted for processing by separate pathways. OM lipoprotein synthesis pathway – Lol pathway (left of the IM Sec system): The asterisk (*) refers to a lipoprotein with a OM sorting signal (Seydel et al., 1999). OMP synthesis pathway – BAM pathway: (right of the IM Sec system) P1-P5: POTRA domains; LPS: Lipopolysaccharide; PL: Phospholipid (Modified from Malinverni and Silhavy, 2011).

- **OMPs assembly at the OM- BAM complex**

Precursors of β-barrel proteins (pre-OMPs) are synthetized in the cytoplasm and translocated from the cytoplasm to the periplasmic face of the IM by the Sec translocon. The Signal peptidase I (Spase I) or LepB cleaves the N-terminal signal sequence and the pre-OMPs are then released into the periplasm. To transit across the periplasm in an unfolded condition, OMPs must bind to specific periplasmic chaperones. This carrier function is performed by three periplasmic proteins in *E. coli*: SurA, Skp and DegP (Hagan et al., 2011; Allen et al., 2009). Most OMPs have more affinity for the periplasmic chaperone SurA whereas Skp is required to assembly certain OMPs, for instance LptD (Schwalm et al., 2013). The periplasmic protein DegP exhibits dual function as it works primarily as protease, but it has also chaperone activity. It has been proposed that DegP, via its protease activity, prevents OMP accumulation upon stress conditions (Costello et al., 2016), and that upon such unfavourable conditions it works along with Skp to rescue misplaced OMPs that did not follow the canonical SurA pathway (Sklar et al., 2007).
Once OMPs are transported across the periplasm, they are assembled and inserted into the OM by the β-barrel assembly machinery (BAM). The BAM complex is composed of the OM β-barrel protein BamA, which is the core component of the machinery, and four associated OM lipoproteins (BamB, BamC, BamD, and BamE). BamA and BamD are essential for cell survival whereas loss of BamB, BamC or BamE results in cells with OMP assembly defects. The BAM complex is organized in two sub-complexes, BamA-BamB and BamA-BamCDE. The essential integral OM protein BamA comprises a C-terminal β-barrel domain and a periplasmic N-terminal composed of five polypeptide transport-associated (POTRA) domains that contribute to the interaction among Bam complex members and to the assembly of the OMP (including BamA) (Tommassen, 2010) as its absence leads to lower OMP levels and impaired binding between BamA and the rest of the components of the machinery (Hagan et al., 2011). The POTRA domains may start the assembly process in the periplasm, with β-barrel domain involved in the OM insertion of the OMP precursors (Malinverni and Silhavy, 2011). In addition to BamA, the essential lipoprotein BamD plays also an important role in OMP assembly in *E. coli*; indeed, mutations in *bamD* compromise cell growth and OM integrity (Hagan et al., 2015). The binding activity of BamD to unfolded OMP in the periplasm appears to trigger BamA activity (Lee et al., 2018). BamB interacts directly with BamA and seems to increase the efficiency of substrate assembly for several OMPs. Furthermore, BamC

and BamE interact indirectly with BamA, and they are important for the complex as they stabilize the interaction between BamA and BamD (Ricci and Silhavy, 2019). The current model postulates that BamA and BamD catalyse the substrate recognition and assembly while BamB, BamC and BamE enhance the efficiency of the system, although the molecular mechanisms in charge of the OMP folding into β-barrel remain unclear (Kim et al., 2012) (**Fig. 12- right side**).

1.5.2 Divisome and elongasome complexes

During bacteria life cycle, the cell wall is subjected to conformational changes entailing cell wall enlargement, septum ring formation and lastly daughter cell separation. To go through these cell cycle stages, the semi-rigid PG sacculus requires to be continuously remodelled to maintain cell shape and morphology without impairing cell integrity. To overcome this challenge, *E. coli* utilizes two highly dynamic IM-associated multienzymatic complexes named elongasome and divisome, which are responsible of cell elongation and cell division, respectively. The assembly and disassembly of these complexes is coupled with cell cycle, and their composition is highly variable and includes many diverse proteins, ranging from PG synthases, hydrolases and their regulators to cytoskeletal proteins (Pazos and Peters, 2019) (Szwedziak and Löwe, 2013).

- **Elongasome**

In rod-shaped bacteria, as *E. coli*, the elongasome complex drives the lateral PG insertion, thus allowing the elongation of the PG sacculus (**Fig. 13**). The elongation process is driven by the cytoskeletal actin homologue MreB, which guides the orientation of the glycan strands to the long-axis of the cell. In an ATP-dependent process, MreB polymerizes as short helical filaments that are attached to the IM, and dynamically rotate evenly around the entire cell. These filaments appear to be implicated in promoting chromosome segregation, and to maintain the rod-shape morphology under stress conditions (Morgenstein et al., 2015; Kruse et al., 2003). Indeed, disruption of the filaments or of MreB causes cell to stop elongating, producing an unusual spherical cell shape (Nilsen et al., 2005). MreB and the associated cell shape IM proteins MreC, MreD and RodZ regulate the synthesis of PG in the lateral wall with the PG synthases PBP1A, PBP2, PBP5 and RodA. It has been shown that MreB and MreD organize the spatial positioning of the enzymes implicated in the cytosolic PG precursor synthesis (White et

al., 2010). Furthermore, MreC interacts through its periplasmic domain with PG synthases, including PBP2, and PG hydrolases, thus suggesting that MreC may play a role in positioning a PG synthetic complex in the periplasm (White et al., 2010).

RodZ is a transmembrane protein that mediates MreB rotation by coupling MreB to PB1A, PBP2 and RodA (Morgenstein et al., 2015). Likewise, RodZ plays a role in cell-shape maintenance since mutations that impair its interaction with MreB result in loss of rod-shape (Ago and Shiomi, 2019; van den Ent et al., 2010). The overall idea is that IM-cytoskeletal proteins, with MreB as the major player, serve as scaffold recruiting and positioning the cell wall biosynthetic enzymes of the complex. Following on this model, the OM lipoprotein LpoA controls the activity of the bifunctional PBP1A (Typas et al., 2010; Jean et al., 2014) which synthesises PG through a direct interaction with PBP2 and RodA. The GTase activity of PBP1A poylmerises new glycan strands while its TPase activity along with the TPase PBP2 crosslink the nascent glycan chains (Banzhaf et al., 2012), although it has been proposed another model in which PBP1A works regardless from PBP2 and RodA (Cho et al., 2016). This alternative model proposes that the monofunctional TPase PBP2 forms a relevant association with the SEDS family protein RodA, which has GTase activity (Meeske et al., 2016), thus coupling PG polymerization and crosslinking. Moreover, PBP2 plays a crucial role in the elongasome by leading the localization and activity of the PG synthetic machineries (Özbaykal et al, 2020; Rohs et al., 2018). Consequently, the resulting PG may be processed by the DD-CPase PBP5 (Potluri et al., 2010).

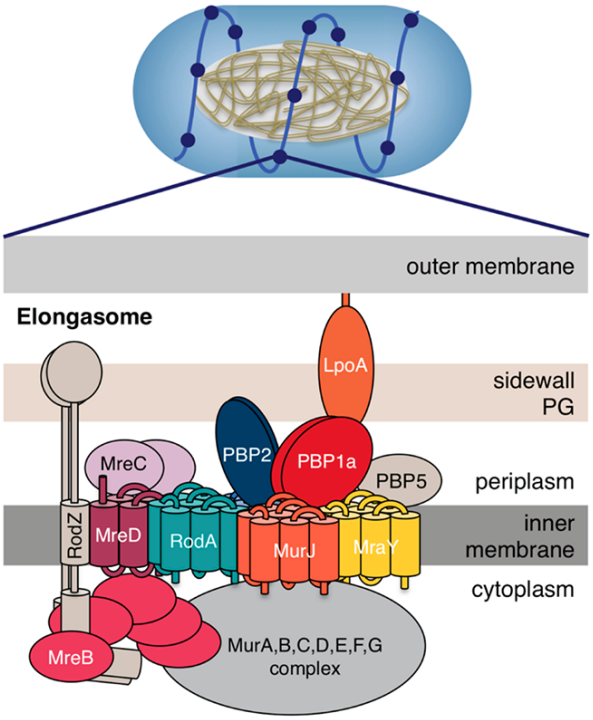

Figure 13. Elongasome complex in *E. coli*. The lateral elongation of the cell wall is mediated by the protein components of the elongasome, which moves along the lateral sidewall (blue line). (Adapted from Dik et al., 2018).

- **Divisome**

The divisome is a multiprotein complex that directs the cell division in *E. coli*, namely septation and separation of the two daughter cells. This specific-cell division machinery comprises a large dynamic network of proteins that localise in all three compartments of the cell (**Fig. 14A**) (Blaauwen and Luirink, 2019). The divisome consists of more than 30 proteins with a dozen of them required for initial steps of assembly of the complex (FtsZ, FtsA, ZipA, FtsE, FtsX, FtsK, FtsQ, FtsL, FtsB, FtsW, PBP3 and FtsN) (Du and Lutkenhaus, 2017). As in the elongasome, the core component of the complex is the cytoskeletal protein FtsZ. Notably, the direct interaction between the elongasome master regulator MreB and FtsZ dictates the transition from cell wall elongation to cell division (Fenton and Gerdes, 2013). The tubulin homologue FtsZ polymerises into filaments forming the essential Z-ring at midcell, where the progressive constriction of this helical ring structure leads to the formation of the septum. The Z-ring serves as scaffold to recruit all other proteins of the complex. (Xiao and Goley, 2016). Midcell location of the FtsZ ring is mediated by the Min system (**Fig. 14B**) (Lutkenhaus et al., 2012). The polymerised Z-ring is anchored at the inner leaflet of the IM by the FtsA and ZipA proteins, thus

keeping it from floating further into the cytoplasm. In addition, FtsA recruits late divisome protein via FtsEX (Pichoff et al., 2018; Du et al., 2016). The FtsEX pair forms an ABC transporter and uses its ATPase activity to govern PG hydrolysis at the septum through direct regulation of the amidase regulator EnvC, which activate the PG amidase AmiB (Yang et al., 2011). In addition, the other regulator NlpD spurs septal PG cleavage by activating AmiC (Bernhardt and de Boer, 2003; Tsang et al., 2017). FtsK is a DNA translocase implicated in division and segregation of the chromosome (Besprozvannaya and Burton, 2014).

It has been recently shown that FtsQ, FtsL and FtsB form a complex that regulates the activity of the termed septal PG synthase subcomplex (FtsW-PBP3-PBP1B) by keeping it repressed until placement of FtsN (Boes et al., 2019). The cell division protein FtsN is the last essential division protein to be recruited and it plays a key role in triggering the cell constriction at the division site (Liu et al., 2015; Gerding et al., 2009). Concerning the septal PG synthase subcomplex, it resembles that of the lateral PG synthesis of the elongasome. The SEDS family protein FtsW is specific for cell division with a PG polymerase activity that requires to be associated with the TPase PBP3 to be functional (Taguchi et al., 2019). Furthermore, the bifunctional PBP1B, that interacts with FtsN and PBP3, is enriched at the septum and its dual activity is regulated by the OM lipoprotein LpoB and the periplasmic protein CpoB (Gray et al., 2015; Bertsche et al., 2006). It has been proposed that PBP2 may play a role in a preparative phase of the cell division, by facilitating the transition from elongasome to divisome proteins at midcell (Ploeg et al., 2013), while the function of PBP5 is to orientate the Z-ring at midcell with its absence leading to abnormal septation (Potluri et al., 2012). To complete the cell division, the OM must be invaginated and septum correctly cleaved. The Tol-Pal system, which links the OM and the PG, promotes the constriction OM by stimulating the cleavage of septal PG chains via PG hydrolases (Yakhnina and Bernhardt, 2020; Gerding et al., 2007).

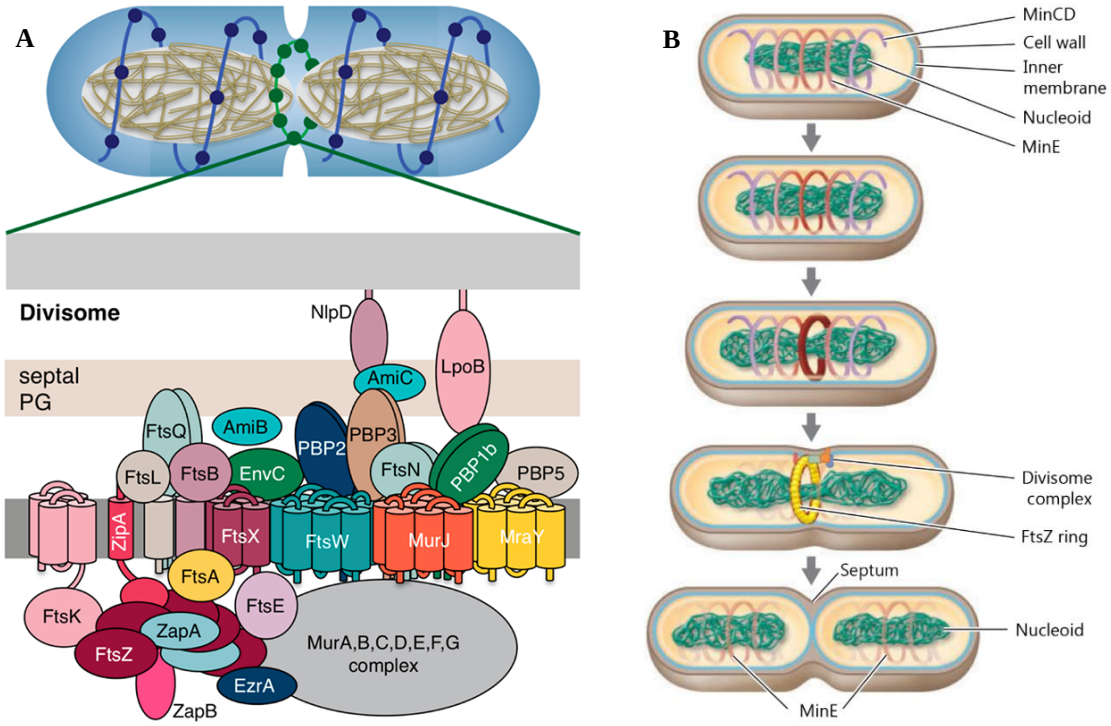

Figure 14. Divisome complex (A) and general outlook of the division site formation (B) in *E. coli*. (A) The divisome localises at the midcell (green line) where it facilitates the cell division (Figure adapted from Dik et al., 2018). (B) The Min system proteins antagonise the FtsZ ring assembly. MinCDE proteins assist in the Z-ring midcell position by preventing its formation near the poles of the cell. MinCDE oscillates between pole-to-pole across the cell. Thus, when the cell is elongated enough the Min proteins do pass through the centre and the Z-ring polymerisation at the cell centre can occur (Modified from Madigan, 2009).

1.6 Envelope stress response systems

Bearing in mind the structural importance of the cell envelope and the numerous essential processes that take place on it, it is imperative for the cell to have mechanisms for safeguarding the cell envelope integrity against potential stresses. To achieve this, bacteria rely on the envelope stress response systems (ESRs) that monitor cell wall perturbations and develop appropriate cellular responses to mitigate the stresses and restore cell envelope homeostasis (Cho et al., 2014b; Raivio, 2005). *E. coli* have several ESRs with each one presumably specialised in addressing different set of internal/external stresses. Among the different ESRs, the two-component system Cpx, the σE-dependent cell envelope stress, and the Rcs phosphorelay are discussed in the next paragraphs as they are mostly relevant in the envelope biogenesis context. It appears that these three ESRs are interconnected with small RNAs (sRNAs), acting as coordinators of this stress response network (Grabowicz and Silhavy, 2017).

1.6.1 The two-component stress response system Cpx

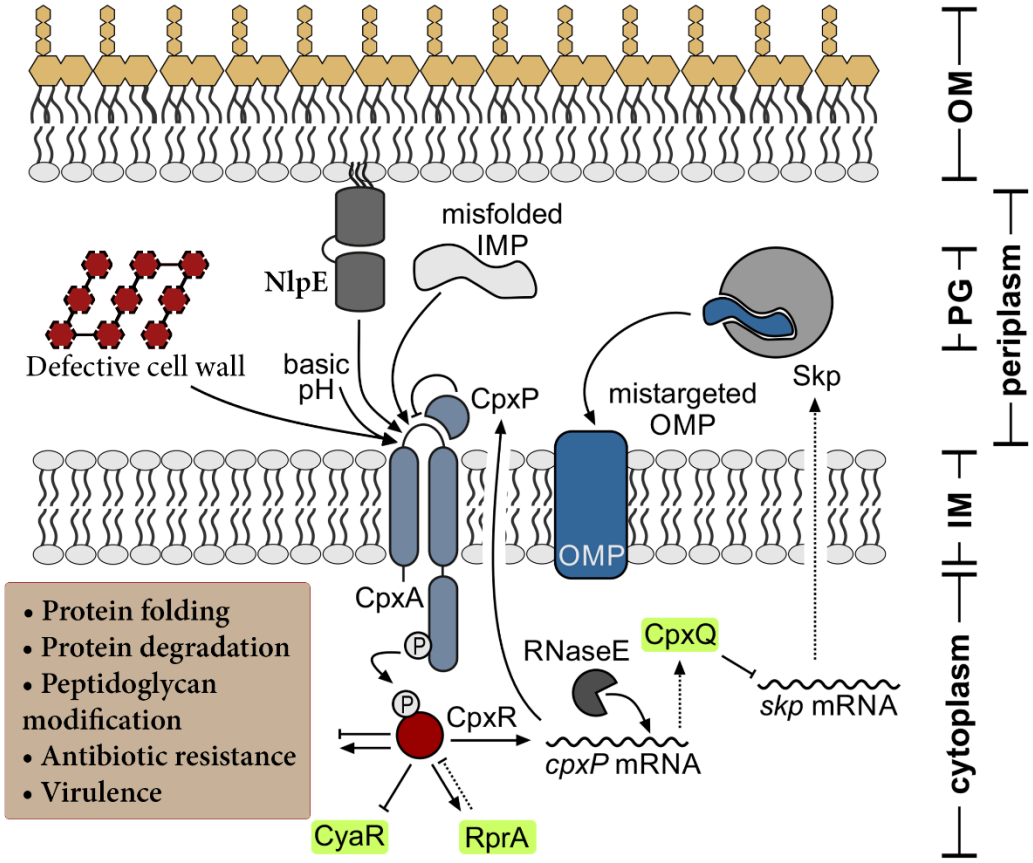

Figure 15. The Cpx stress response system. The Cpx ESRs is activated upon different perturbations in the periplasm and IM. The core of the pathway is a canonical two-component system with CpxA as the histidine kinase, and CpxR the response regulator. The Cpx system attempts to restore the envelope homeostasis through the regulation of an extensive transcriptome by CpxR, including non-coding RNA molecules (highlighted in green) with regulatory functions (Modified from Fröhlich and Gottesman, 2018).

The Cpx ESRs is a canonical two-component system (TCS) comprising the CpxA sensor protein and the cognate response regulator CpxR. Cpx responds to a broad array of stresses, such as elevated pH, changes in the osmolarity, changes in the IM lipid composition, defects in the PG layer, and exposure to copper and ethanol, among other stresses (Mitchell and Silhavy, 2019; Evans et al., 2013). The cell adhesion to hydrophobic surfaces has been also proposed to be an inducer of the Cpx ESRs but a recent study has challenged this view (Kimkes and Heinemann, 2018). The induction of the Cpx pathway is thought to involve the sensing of misfolded IM and periplasmic proteins and defective protein translocation across the IM.

Stress-signaling in the Cpx ESRs relies on the IM sensor histidine-kinase CpxA and the cytoplasmic response regulator CpxR **(Fig. 15)**. Inducing conditions lead to autophosphorylation of cytoplasmatic histidine-kinase domain of CpxA, followed by the transfer of the phosphate group to CpxR. Phosphorylated CpxR becomes activated and regulates the expression of numerous genes. Proper activation of the Cpx two-component system is crucial; indeed, mutations in *cpxA* result in overactivation of the Cpx pathway with deleterious consequence for the cell (Delhaye et al., 2016). The activity of CpxA is modulated by the accessory proteins NlpE and CpxP. NlpE is an OM lipoprotein that activates the Cpx pathway through direct interaction with CpxA at the IM upon cell adhesion to abiotic surfaces and impaired trafficking of lipoproteins to the OM (Delhaye et al., 2019; May et al., 2019). On the contrary, the periplasmic protein CpxP represses the Cpx signalling by binding to the periplasmic domain of CpxA, thus blocking its sensor function under non-stress conditions. Current evidence shows that high salt concentrations, and misfolded pilus subunits and proteins displace CpxP from CpxA, and subsequently are degraded by chaperone DegP in the periplasm (Tschauner et al., 2014). Nevertheless, other stresses such alkaline pH activates Cpx response in a CpxP non-dependent manner (Fleischer et al., 2007). The CpxP transcript encodes for a sRNA termed CpxQ, which negatively regulates the levels of CpxP and prevents toxic OMP folding into the IM by curbing the production of the periplasmic chaperone Skp (Grabowicz et al., 2016). It is known that the Cpx ESRs downregulates the σ^E ESRs and stifles the OMP synthesis; Cpx also induces the Rcs ESRs response through the sRNA RprA which in turn controls the levels of CpxR (Grabowicz and Silhavy, 2017). The Cpx regulon comprises genes involved in peptidoglycan modification (notably *ldtD* (Bernal-Cabas et al., 2015), antimicrobial resistance, envelope protein folding and degradation, virulence, and catabolite repression through the sRNA CyaR (Vogt et al., 2014).

1.6.2 Envelope stress sigma factor (σ^E)

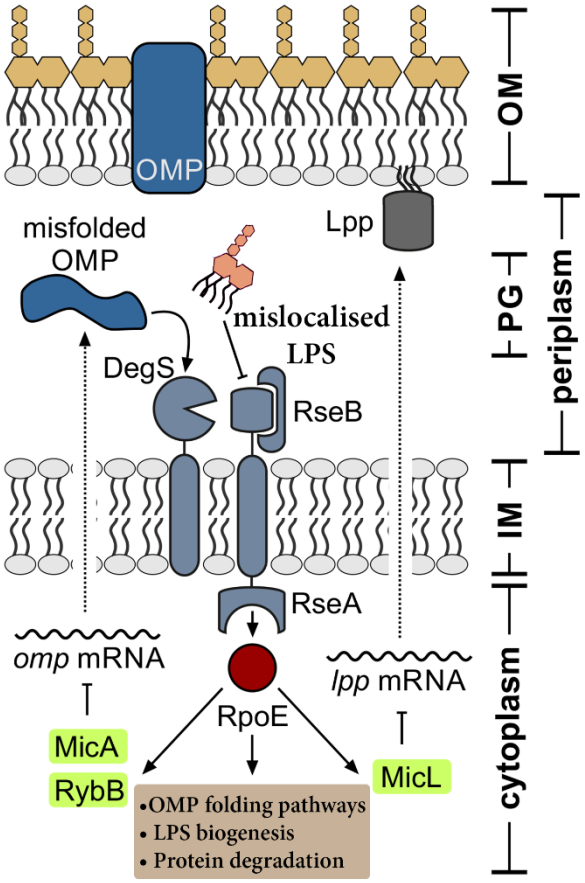

Figure 16. The extracytoplasmic sigma factor σ^E (RpoE). Misfolded OMP and mislocalised LPS lead to the cleavage and disengagement of the anti-sigma proteins RseA and RseB respectively, thus releasing the sigma factor σ^E (RpoE). The σ^E ESRs modulates the expression of more than 100 genes involved in OMP maturation and LPS synthesis. Furthermore, among the σ^E regulon there are several sRNA (highlighted in green) that repress the translation of Braun lipoprotein Lpp (MicL), and of OMPs (RybB and MicA) (Modified from Fröhlich and Gottesman, 2018).

The σ^E ESRs response is driven by the periplasmic accumulation of misfolded OMPs and mislocalised LPS, including defective LPS molecules. The core component of the pathway relies on the alternative RNA polymerase factor sigmaE (RpoE, σ^E) whose activation occurs through a regulated proteolytic cascade **(Fig. 16)** (Hews et al., 2019). Under normal conditions σ^E is trapped by the IMP anti-sigma factor RseA, thus impeding its interaction with the RNA polymerase. RseA is an IM single pass protein whose periplasmic domain is bound by the RseB protein. Two signals are needed for full activation of σ^E: misfolded OMPs activate the IM protease DegS whereas mislocalised LPS in the periplasm allows RseB to dissociate from RseA thus facilitating RseA

cleavage by DegS. (Kim, 2015; Lima et al., 2013). Following cleavage by DegS, the cytoplasmic domain of RseA is cleaved by the RseP protease, hence dropping a soluble portion of RseA containing σ^E in the cytoplasm. In the cytoplasm, free σ^E binds the RNA polymerase and induces the expression of its regulon. The σ^E regulon comprises genes related to maintain OMP and LPS homeostasis, such as periplasmic chaperones and proteases, components of the BAM machinery, LPS synthesis and transport proteins, and several sRNAs that downregulate OMP synthesis (Barchinger and Ades, 2013; Ades, 2008).

1.6.3 Rcs phosphorelay

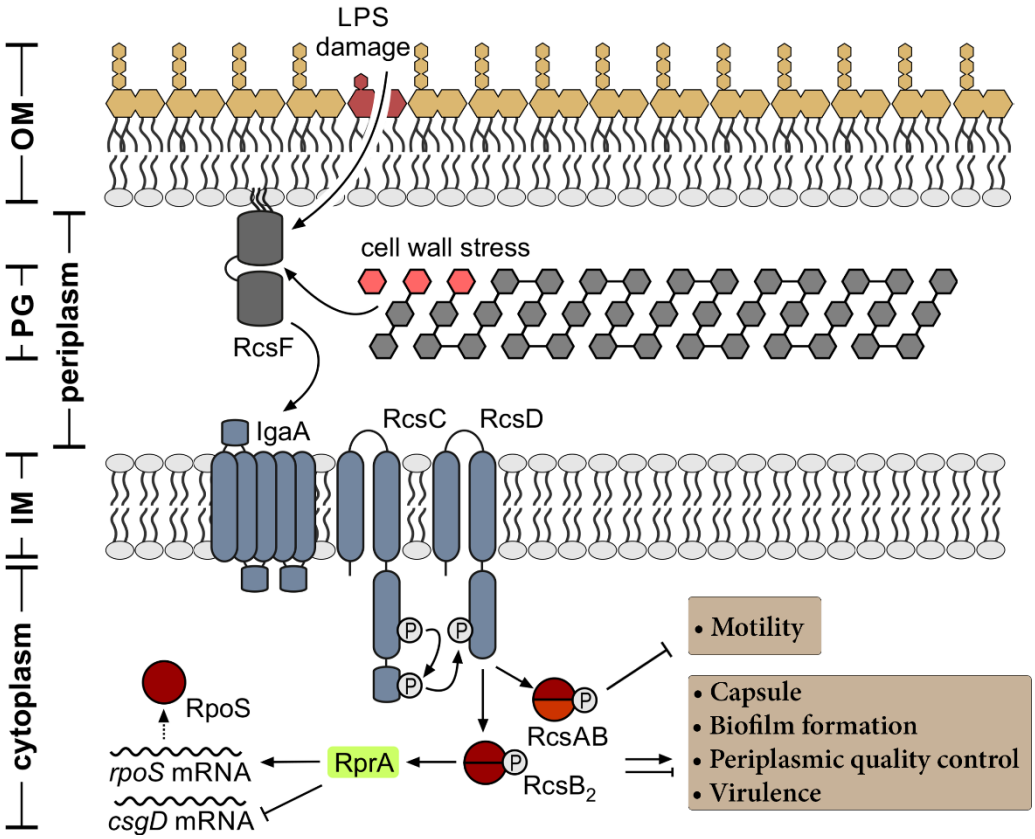

Figure 17. The Rcs pathway. The components of the Rcs ESRs are distributed in all the compartments of the cell envelope. Stress cues as perturbations in LPS or PG activates RcsF that binds to the inhibitor of the pathway, IgaA. The association of RcsF with IgaA allows activation of the downstream components: the IM proteins RcsC and RcsD, and the cytoplasmic effectors. RcsB controls the transcription of sRNA (highlighted in green), and expression of many genes adopting a homodimer or heterodimer conformation (Modified from Fröhlich and Gottesman, 2018).

The Rcs phosphorelay is a complex variant of the two-component system paradigm. Rcs is activated upon modifications in the LPS, disruptions in PG biosynthesis, and impaired

lipoprotein trafficking (Mitchell and Silhavy, 2019; Wall et al., 2018). The Rcs is composed of the sensor OM lipoprotein RcsF, the IgaA IM protein inhibitor of the phosphorelay system, the IM sensor kinases RcsC and RcsD, and the RcsB response regulator which can act alone or in complex with the accessory regulator RcsA. **(Fig. 17)**.

In the off state (non-stress conditions) the IgaA proteins inhibits the phosphorelay signalling to the downstream components. In absence of stress the IM protein IgaA interacts with the IMPs RcsC or RcsD, thus avoiding the phosphorylation of the response regulator RcsB. Most of the inducing signals are sensed by the OM lipoprotein RcsF, which is funnelled to β-barrels protein at the OM via BamA in non-stressed conditions (Cho et al., 2014b). Currently, two different mechanisms of activating the Rcs pathway via RcsF have been proposed (Laloux and Collet, 2017). According to one model, stressing cells with polymyxin B or an inhibitor of PBP2 impairs the ability of RcsF to interact with BamA, thus allowing untethered RcsF in the periplasm to activate the Rcs cascade (Cho et al., 2014b). An alternative model postulates that RcsF bound to β-barrels is able to directly sense alterations in LPS layer via its positively charged residues. According to the latter model no RcsF synthesis is needed in stressed cells to activate the Rcs sytem (Konovalova et al., 2016). Independently of the activation model, activated RcsF associates with IgaA, relieving the blockade of the system imposed by IgaA. Therefore, the histidine kinase RcsC autophosphorylates and phosphorylates RcsD, which in turn plays a role as phosphorelay by transferring the phosphate group to the receiver domain of the cytoplasmic protein RcsB. Phosphorylated RcsB then activates the transcriptional regulation of several genes (Filippova et al., 2018). Interestingly, RcsB can work as homodimer or as a heterodimer along with the auxiliary regulator RcsA. The RcsB homodimer, or as heterodimer with RcsA, are dependent on the RcsB phosphorylation for activity. Interestingly, RcsB can work as a transcriptional regulation with other proteins such as BglJ, GadE, and MatA in its non-phosphorylated state (Pannen et al., 2016). The Rcs ESRs induce the transcription of genes involved in colanic acid capsule and biofilm formation, flagellum and fimbria synthesis, lipoproteins sorting, environmental-stress response and virulence, among others (Farris et al., 2010; Guo and Sun, 2017; Tao et al., 2012). Moreover, it should be noted that the Rcs ESRs also upregulates the transcription of the sRNA RprA which in addition of modulating Cpx system response, downregulates the expression of the biofilm regulator CsgD, and also promotes the translation of *rpoS* which encodes the stationary-phase sigma factor σ^S that

mediates the response to numerous cell-damaging stresses (Fröhlich and Gottesman, 2018; Mika et al., 2012).

1.7 References

1. Ades, S.E. (2008). Regulation by destruction: design of the sigmaE envelope stress response. Curr. Opin. Microbiol. 11, 535–540.
2. Ago, R., and Shiomi, D. (2019). RodZ: a key-player in cell elongation and cell division in *Escherichia coli*. AIMS Microbiol. 5, 358–367.
3. Allen, W.J., Phan, G., and Waksman, G. (2009). Structural biology of periplasmic chaperones. Adv. Protein. Chem. Struct. Biol. 78, 51–97.
4. Anderson MS, Bull HG, Galloway SM, Kelly TM, Mohan S, Radika K, Raetz CR. (1993). UDP-N-acetylglucosamine acyltransferase of *Escherichia coli*. The first step of endotoxin biosynthesis is thermodynamically unfavorable. J Biol Chem. 268:19858–19865.
5. Anderson, M.S., and Raetz, C.R. (1987). Biosynthesis of lipid A precursors in *Escherichia coli*. A cytoplasmic acyltransferase that converts UDP-N-acetylglucosamine to UDP-3-O-(R-3 hydroxymyristoyl)-N- acetylglucosamine. J. Biol. Chem. 262, 5159–5169.
6. Babinski, K.J., Ribeiro, A.A., and Raetz, C.R.H. (2002). The *Escherichia coli* gene encoding the UDP-2,3-diacylglucosamine pyrophosphatase of lipid A biosynthesis. J. Biol. Chem. 277, 25937–25946.
7. Bakelar, J., Buchanan, S.K., and Noinaj, N. (2017). Structural snapshots of the β-barrel assembly machinery. FEBS J. 284, 1778–1786.
8. Banzhaf, M., van den Berg van Saparoea, B., Terrak, M., Fraipont, C., Egan, A., Philippe, J., Zapun, A., Breukink, E., Nguyen-Distèche, M., den Blaauwen, T., et al. (2012). Cooperativity of peptidoglycan synthases active in bacterial cell elongation. Mol. Microbiol. 85, 179–194.
9. Barchinger, S.E., and Ades, S.E. (2013). Regulated proteolysis: control of the *Escherichia coli* σ(E)-dependent cell envelope stress response. Subcell. Biochem. 66, 129–160.
10. Barreteau, H., Kovač, A., Boniface, A., Sova, M., Gobec, S., and Blanot, D. (2008). Cytoplasmic steps of peptidoglycan biosynthesis. FEMS Microbiol. Rev. 32, 168–207.
11. Barrett D, Leimkuhler C, Chen L, Walker D, Kahne D & Walker S. (2005) Kinetic characterization of the glycosyltransferase module of Staphylococcus aureus PBP2. J. Bacteriol. 187: 2215–2217.
12. Benedet, M., Falchi, F.A., Puccio, S., Di Benedetto, C., Peano, C., Polissi, A., and Dehò, G. (2016). The Lack of the Essential LptC Protein in the Trans-Envelope Lipopolysaccharide Transport Machine Is Circumvented by Suppressor Mutations in LptF, an Inner Membrane Component of the *Escherichia coli* Transporter. PLoS ONE 11, e0161354.
13. Benson, T.E., Walsh, C.T., and Hogle, J.M. (1996). The structure of the substrate-free form of MurB, an essential enzyme for the synthesis of bacterial cell walls. Structure 4, 47–54.
14. Bernal-Cabas, M., Ayala, J.A., and Raivio, T.L. (2015). The Cpx Envelope Stress Response Modifies Peptidoglycan Cross-Linking via the L,D-Transpeptidase LdtD and the Novel Protein YgaU. J. Bacteriol. 197, 603–614.

15. Bernhardt, T.G., and de Boer, P.A.J. (2003). The *Escherichia coli* amidase AmiC is a periplasmic septal ring component exported via the twin-arginine transport pathway. Mol. Microbiol. 48, 1171–1182.
16. Bertani, B., and Ruiz, N. (2018). Function and biogenesis of lipopolysaccharides. EcoSal Plus 8, 10.1128.
17. Bertsche, U., Kast, T., Wolf, B., Fraipont, C., Aarsman, M.E.G., Kannenberg, K., Rechenberg, M.V., Nguyen-Distèche, M., Blaauwen, T.D., Höltje, J.-V., et al. (2006). Interaction between two murein (peptidoglycan) synthases, PBP3 and PBP1B, in *Escherichia coli*. Mol. Microbiol. 61, 675–690.
18. Besprozvannaya, M., and Burton, B.M. (2014). Do the same traffic rules apply? Directional chromosome segregation by SpoIIIE and FtsK. Mol. Microbiol. 93, 599–608.
19. Biarrotte-Sorin, S., Hugonnet, J.-E., Delfosse, V., Mainardi, J.-L., Gutmann, L., Arthur, M., and Mayer, C. (2006). Crystal Structure of a Novel β-Lactam-insensitive Peptidoglycan Transpeptidase. J. Mol. Biol. 359, 533–538.
20. Blaauwen, T. den, and Luirink, J. (2019). Checks and Balances in Bacterial Cell Division. MBio 10, e00149-19.
21. Boes, A., Olatunji, S., Breukink, E., and Terrak, M. (2019). Regulation of the Peptidoglycan Polymerase Activity of PBP1b by Antagonist Actions of the Core Divisome Proteins FtsBLQ and FtsN. MBio 10, e01912-18.
22. Borbat, P.P., Surendhran, K., Bortolus, M., Zou, P., Freed, J.H., and Mchaourab, H.S. (2007). Conformational Motion of the ABC Transporter MsbA Induced by ATP Hydrolysis. PLoS Biol. 5, e271.
23. Bouhss, A., Trunkfield, A.E., Bugg, T.D.H., and Mengin-Lecreulx, D. (2008). The biosynthesis of peptidoglycan lipid-linked intermediates. FEMS Microbiol. Rev. 32, 208–233.
24. Budd, A., Blandin, S., Levashina, E.A., and Gibson, T.J. (2004). Bacterial α2-macroglobulins: colonization factors acquired by horizontal gene transfer from the metazoan genome? Genome Biol. 5, R38.
25. Carty, S.M., Sreekumar, K.R., and Raetz, C.R.H. (1999). Effect of Cold Shock on Lipid A Biosynthesis in *Escherichia coli*. Induction at 12 °c of an acyltransferase specific for palmitoleoyl-acyl carrier protein. J. Biol. Chem. 274, 9677–9685.
26. Cayley, D.S., Guttman, H.J., and Record, M.T. (2000). Biophysical characterization of changes in amounts and activity of *Escherichia coli* cell and compartment water and turgor pressure in response to osmotic stress. Biophys. J. 78, 1748–1764.
27. Chimalakonda, G., Ruiz, N., Chng, S.-S., Garner, R.A., Kahne, D., and Silhavy, T.J. (2011). Lipoprotein LptE is required for the assembly of LptD by the β-barrel assembly machine in the outer membrane of *Escherichia coli*. Proc. Natl. Acad. Sci. USA 108, 2492–2497.
28. Cho, H., Uehara, T., and Bernhardt, T.G. (2014a). Beta-Lactam Antibiotics Induce a Lethal Malfunctioning of the Bacterial Cell Wall Synthesis Machinery. Cell 159, 1300–1311.

29. Cho, H., Wivagg, C.N., Kapoor, M., Barry, Z., Rohs, P.D.A., Suh, H., Marto, J.A., Garner, E.C., and Bernhardt, T.G. (2016). Bacterial cell wall biogenesis is mediated by SEDS and PBP polymerase families functioning semi-autonomously. Nat. Microbiol. 1, 16172.
30. Cho, S.-H., Szewczyk, J., Pesavento, C., Zietek, M., Banzhaf, M., Roszczenko, P., Asmar, A., Laloux, G., Hov, A.-K., Leverrier, P., et al. (2014b). Detecting envelope stress by monitoring β-barrel assembly. Cell 159, 1652–1664.
31. Chodisetti, P.K., and Reddy, M. (2019). Peptidoglycan hydrolase of an unusual cross-link cleavage specificity contributes to bacterial cell wall synthesis. Proc. Natl. Acad. Sci. USA 116, 7825–7830.
32. Costello, S.M., Plummer, A.M., Fleming, P.J., and Fleming, K.G. (2016). Dynamic periplasmic chaperone reservoir facilitates biogenesis of outer membrane proteins. Proc. Natl. Acad. Sci. USA 113, E4794-4800.
33. Cymer, F., von Heijne, G., and White, S.H. (2015). Mechanisms of integral membrane protein insertion and folding. J. Mol. Biol. 427, 999–1022.
34. Dalbey, R.E., Wang, P., and Kuhn, A. (2011). Assembly of bacterial inner membrane proteins. Annu. Rev. Biochem. 80, 161–187.
35. Davidson, A.L., Dassa, E., Orelle, C., and Chen, J. (2008). Structure, Function, and Evolution of Bacterial ATP-Binding Cassette Systems. Microbiol. Mol. Biol. Rev. 72, 317–364.
36. DebRoy, C., Fratamico, P.M., Yan, X., Baranzoni, G., Liu, Y., Needleman, D.S., Tebbs, R., O'Connell, C.D., Allred, A., Swimley, M., et al. (2016). Comparison of O-Antigen Gene Clusters of All O-Serogroups of *Escherichia coli* and Proposal for Adopting a New Nomenclature for O-Typing. PLoS One 11, e.0147434.
37. Delhaye, A., Collet, J.-F., and Laloux, G. (2016). Fine-Tuning of the Cpx Envelope Stress Response Is Required for Cell Wall Homeostasis in *Escherichia coli*. MBio 7, e00047-00016.
38. Delhaye, A., Laloux, G., and Collet, J.-F. (2019). The Lipoprotein NlpE Is a Cpx Sensor That Serves as a Sentinel for Protein Sorting and Folding Defects in the *Escherichia coli* Envelope. J. Bacteriol. 201, e00611-18.
39. Den Blaauwen, T., de Pedro, M.A., Nguyen-Distèche, M., and Ayala, J.A. (2008). Morphogenesis of rod-shaped sacculi. FEMS Microbiol. Rev. 32, 321–344.
40. Denome, S.A., Elf, P.K., Henderson, T.A., Nelson, D.E., and Young, K.D. (1999). *Escherichia coli* mutants lacking all possible combinations of eight penicillin binding proteins: viability, characteristics, and implications for peptidoglycan synthesis. J. Bacteriol. 181, 3981–3993.
41. Derouaux, A., Wolf, B., Fraipont, C., Breukink, E., Nguyen-Distèche, M., and Terrak, M. (2008). The monofunctional glycosyltransferase of *Escherichia coli* localizes to the cell division site and interacts with penicillin-binding protein 3, FtsW, and FtsN. J. Bacteriol. 190, 1831–1834.
42. Dik, D.A., Fisher, J.F., and Mobashery, S. (2018). Cell-Wall Recycling of the Gram-Negative Bacteria and the Nexus to Antibiotic Resistance. Chem. Rev. 118, 5952–5984.
43. Dong, H., Xiang, Q., Gu, Y., Wang, Z., Paterson, N.G., Stansfeld, P.J., He, C., Zhang, Y., Wang, W., and Dong, C. (2014). Structural basis for outer membrane lipopolysaccharide insertion. Nature 511, 52–56.

44. Drawz, S.M., and Bonomo, R.A. (2010). Three Decades of β-Lactamase Inhibitors. Clin. Microbiol. Rev 23, 160–201.
45. Du, S., and Lutkenhaus, J. (2017). Assembly and Activation of the *Escherichia coli* Divisome. Mol. Microbiol. 105, 177–187.
46. Du, S., Pichoff, S., and Lutkenhaus, J. (2016). FtsEX acts on FtsA to regulate divisome assembly and activity. PNAS 113, E5052–E5061.
47. Edwards, D.H., and Donachie, W.D. (1993). Construction of a Triple Deletion of Penicillin-Binding Proteins 4, 5, and 6 in *Escherichia coli*. In Bacterial Growth and Lysis: Metabolism and Structure of the Bacterial Sacculus, M.A. de Pedro, J.-V. Höltje, and W. Löffelhardt, eds. (Boston, MA: Springer US), pp. 369–374.
48. Egan, A.J.F., Cleverley, R.M., Peters, K., Lewis, R.J., and Vollmer, W. (2017). Regulation of bacterial cell wall growth. FEBS J. 284, 851–867.
49. Evans, K.L., Kannan, S., Li, G., de Pedro, M.A., and Young, K.D. (2013). Eliminating a set of four penicillin binding proteins triggers the Rcs phosphorelay and Cpx stress responses in *Escherichia coli*. J. Bacteriol. 195, 4415–4424.
50. Fairman, J.W., Noinaj, N., and Buchanan, S.K. (2011). The structural biology of β-barrel membrane proteins: a summary of recent reports. Curr. Opin. Struct. Biol. 21, 523–531.
51. Farris, C., Sanowar, S., Bader, M.W., Pfuetzner, R., and Miller, S.I. (2010). Antimicrobial peptides activate the Rcs regulon through the outer membrane lipoprotein RcsF. J. Bacteriol. 192, 4894–4903.
52. Fenton, A.K., and Gerdes, K. (2013). Direct interaction of FtsZ and MreB is required for septum synthesis and cell division in *Escherichia coli*. EMBO J. 32, 1953–1965.
53. Filippova, E.V., Zemaitaitis, B., Aung, T., Wolfe, A.J., and Anderson, W.F. (2018). Structural Basis for DNA Recognition by the Two-Component Response Regulator RcsB. MBio 9, e01993-17.
54. Fleischer, R., Heermann, R., Jung, K., and Hunke, S. (2007). Purification, Reconstitution, and Characterization of the CpxRAP Envelope Stress System of *Escherichia coli*. J. Biol. Chem. 282, 8583–8593.
55. Freinkman, E., Chng, S.-S., and Kahne, D. (2011). The complex that inserts lipopolysaccharide into the bacterial outer membrane forms a two-protein plug-and-barrel. Proc. Natl. Acad. Sci. U.S.A. 108, 2486–2491.
56. Freinkman, E., Okuda, S., Ruiz, N., and Kahne, D. (2012). Regulated assembly of the transenvelope protein complex required for lipopolysaccharide export. Biochem. 51, 4800–4806.
57. Frère, J.-M., and Page, M.G. (2014). Penicillin-binding proteins: evergreen drug targets. Cur. Op. Pharma. 18, 112–119.
58. Frirdich, E., and Whitfield, C. (2005). Lipopolysaccharide inner core oligosaccharide structure and outer membrane stability in human pathogens belonging to the Enterobacteriaceae. J. Endotoxin Res. 11, 133–144.
59. Fröhlich, K.S., and Gottesman, S. (2018). Small Regulatory RNAs in the Enterobacterial Response to Envelope Damage and Oxidative Stress. Microbiol. Spectr. 6 (4).

60. Galley, N.F., O'Reilly, A.M., and Roper, D.I. (2014). Prospects for novel inhibitors of peptidoglycan transglycosylases. Bioorg. Chem. 55, 16–26.
61. Gerding, M.A., Liu, B., Bendezú, F.O., Hale, C.A., Bernhardt, T.G., and de Boer, P.A.J. (2009). Self-enhanced accumulation of FtsN at Division Sites and Roles for Other Proteins with a SPOR domain (DamX, DedD, and RlpA) in *Escherichia coli* cell constriction. J. Bacteriol. 191, 7383–7401.
62. Gerding, M.A., Ogata, Y., Pecora, N.D., Niki, H., and de Boer, P.A.J. (2007). The trans-envelope Tol-Pal complex is part of the cell division machinery and required for proper outer-membrane invagination during cell constriction in *E. coli*. Mol. Microbiol. 63, 1008–1025.
63. Ghosh, A.S., Chowdhury, C., and Nelson, D.E. (2008). Physiological functions of D-alanine carboxypeptidases in *Escherichia coli*. Trends. Microbiol. 16, 309–317.
64. Glauner, B., Höltje, J.V., and Schwarz, U. (1988). The composition of the murein of *Escherichia coli*. J. Biol. Chem. 263, 10088–10095.
65. Goffin, C., and Ghuysen, J.M. (1998). Multimodular penicillin-binding proteins: an enigmatic family of orthologs and paralogs. Microbiol. Mol. Biol. Rev. 62, 1079–1093.
66. González-Leiza, S.M., de Pedro, M.A., and Ayala, J.A. (2011). AmpH, a bifunctional DD-endopeptidase and DD-carboxypeptidase of *Escherichia coli*. J. Bacteriol. 193, 6887–6894.
67. Grabowicz, M., and Silhavy, T.J. (2017). Envelope Stress Responses: An Interconnected Safety Net. Trends Biochem. Sci. 42, 232–242.
68. Grabowicz, M., Koren, D., and Silhavy, T.J. (2016). The CpxQ sRNA Negatively Regulates Skp To Prevent Mistargeting of β-Barrel Outer Membrane Proteins into the Cytoplasmic Membrane. MBio 7, e00312-16.
69. Gray, A.N., Egan, A.J., van't Veer, I.L., Verheul, J., Colavin, A., Koumoutsi, A., Biboy, J., Altelaar, A.F.M., Damen, M.J., Huang, K.C., et al. (2015). Coordination of peptidoglycan synthesis and outer membrane constriction during *Escherichia coli* cell division. ELife 4, e07118.
70. Greenfield, L.K., and Whitfield, C. (2012). Synthesis of lipopolysaccharide O-antigens by ABC transporter-dependent pathways. Carbohydr. Res. 356, 12–24.
71. Griffin, M.E., Hespen, C.W., Wang, Y.-C., and Hang, H.C. (2019). Translation of peptidoglycan metabolites into immunotherapeutics. Clin. Transl. Imm. 8, e1095.
72. Gu, Y., Stansfeld, P.J., Zeng, Y., Dong, H., Wang, W., and Dong, C. (2015). Lipopolysaccharide is Inserted into the Outer Membrane through An Intramembrane Hole, A Lumen Gate, and the Lateral Opening of LptD. Structure 23, 496–504.
73. Guo, X.-P., and Sun, Y.-C. (2017). New Insights into the Non-orthodox Two Component Rcs Phosphorelay System. Front. Microbiol. 8, 2014.
74. Haenni, M., Majcherczyk, P.A., Barblan, J.-L., and Moreillon, P. (2006). Mutational Analysis of Class A and Class B Penicillin-Binding Proteins in Streptococcus gordonii. Antimicrob. Agents. Chemother. 50, 4062–4069.
75. Hagan, C.L., Silhavy, T.J., and Kahne, D. (2011). β-Barrel Membrane Protein Assembly by the Bam Complex. Annu. Rev. Biochem. 80, 189–210.

76. Hagan, C.L., Wzorek, J.S., and Kahne, D. (2015). Inhibition of the β-barrel assembly machine by a peptide that binds BamD. Proc. Natl. Acad. Sci. USA 112, 2011–2016.
77. Han, W., Wu, B., Li, L., Zhao, G., Woodward, R., Pettit, N., Cai, L., Thon, V., and Wang, P.G. (2012). Defining function of lipopolysaccharide O-antigen ligase WaaL using chemoenzymatically synthesized substrates. J. Biol. Chem. 287, 5357–5365.
78. Hantke, K., and Braun, V. (1973). Covalent binding of lipid to protein. Diglyceride and amide-linked fatty acid at the N-terminal end of the murein-lipoprotein of the *Escherichia coli* outer membrane. Eur. J. Biochem. 34, 284–296.
79. Hara, T., Matsuyama, S., and Tokuda, H. (2003). Mechanism Underlying the Inner Membrane Retention of *Escherichia coli* Lipoproteins Caused by Lol Avoidance Signals. J. Biol. Chem. 278, 40408–40414.
80. Heidrich, C., Templin, M.F., Ursinus, A., Merdanovic, M., Berger, J., Schwarz, H., De Pedro, M.A., and Höltje, J.-V. (2001). Involvement of N-acetylmuramyl-l-alanine amidases in cell separation and antibiotic-induced autolysis of *Escherichia coli*. Mol. Microbiol. 41, 167–178.
81. Hesek, D., Lee, M., Zhang, W., Noll, B.C., and Mobashery, S. (2009). Total synthesis of N-acetylglucosamine-1,6-anhydro-N-acetylmuramylpentapeptide and evaluation of its turnover by AmpD from *Escherichia coli*. J. Am. Chem. Soc. 131, 5187–5193.
82. Hews, C.L., Cho, T., Rowley, G., and Raivio, T.L. (2019). Maintaining Integrity Under Stress: Envelope Stress Response Regulation of Pathogenesis in Gram-Negative Bacteria. Front. Cell. Infect. Microbiol. 9, 313.
83. Hicks, G., and Jia, Z. (2018). Structural Basis for the Lipopolysaccharide Export Activity of the Bacterial Lipopolysaccharide Transport System. Int. J. Mol. Sci. 19, 2680.
84. Höltje, J.V. (1998). Growth of the stress-bearing and shape-maintaining murein sacculus of *Escherichia coli*. Microbiol. Mol. Biol. Rev. 62, 181–203.
85. Hugonnet, J.-E., Mengin-Lecreulx, D., Monton, A., den Blaauwen, T., Carbonnelle, E., Veckerlé, C., Brun, Y., V., van Nieuwenhze, M., Bouchier, C., Tu, K., et al (2016). Factors essential for L,D-transpeptidase-mediated peptidoglycan cross-linking and β-lactam resistance in *Escherichia coli*. ELife 5, e19469.
86. Jackman, J.E., Raetz, C.R., and Fierke, C.A. (1999). UDP-3-O-(R-3-hydroxymyristoyl)-N-acetylglucosamine deacetylase of *Escherichia coli* is a zinc metalloenzyme. Biochem. 38, 1902–1911.
87. Jean, N.L., Bougault, C.M., Lodge, A., Derouaux, A., Callens, G., Egan, A.J.F., Ayala, I., Lewis, R.J., Vollmer, W., and Simorre, J.-P. (2014). Elongated Structure of the Outer-Membrane Activator of Peptidoglycan Synthesis LpoA: Implications for PBP1A Stimulation. Structure 22, 1047–1054.
88. Jorgenson, M.A., and Young, K.D. (2016). Interrupting Biosynthesis of O Antigen or the Lipopolysaccharide Core Produces Morphological Defects in *Escherichia coli* by Sequestering Undecaprenyl Phosphate. J. Bacteriol. 198, 3070–3079.
89. Kalynych, S., Morona, R., and Cygler, M. (2014). Progress in understanding the assembly process of bacterial O-antigen. FEMS. Microbiol. Rev. 38, 1048–1065.

90. Kim, D.Y. (2015). Two stress sensor proteins for the expression of sigmaE regulon: DegS and RseB. J. Microbiol. 53, 306–310.
91. Kim, K.H., Aulakh, S., and Paetzel, M. (2012). The bacterial outer membrane β-barrel assembly machinery. Prot. Sci. 21, 751–768.
92. Kimkes, T.E.P., and Heinemann, M. (2018). Reassessing the role of the *Escherichia coli* CpxAR system in sensing surface contact. PLoS ONE 13, e0207181.
93. Knowles, T.J., Scott-Tucker, A., Overduin, M., and Henderson, I.R. (2009). Membrane protein architects: the role of the BAM complex in outer membrane protein assembly. Nature. Rev. Microbiol 7, 206–214.
94. Konovalova, A., Mitchell, A.M., and Silhavy, T.J. (2016). A lipoprotein/β-barrel complex monitors lipopolysaccharide integrity transducing information across the outer membrane. ELife 5, e15276.
95. Kouidmi, I., Levesque, R.C., and Paradis-Bleau, C. (2014). The biology of Mur ligases as an antibacterial target. Mol. Microbiol. 94, 242–253.
96. Kruse, T., Møller-Jensen, J., Løbner-Olesen, A., and Gerdes, K. (2003). Dysfunctional MreB inhibits chromosome segregation in *Escherichia coli*. EMBO J 22, 5283–5292.
97. Kumar, S., Rubino, F.A., Mendoza, A.G., and Ruiz, N. (2018). The bacterial lipid II flippase MurJ functions by an alternating-access mechanism. J. Biol. Chem. jbc. RA118.006099.
98. Laguri, C., Sperandeo, P., Pounot, K., Ayala, I., Silipo, A., Bougault, C.M., Molinaro, A., Polissi, A., and Simorre, J.-P. (2017). Interaction of lipopolysaccharides at intermolecular sites of the periplasmic Lpt transport assembly. Sci Rep. 7, 9715.
99. Laloux, G., and Collet, J.-F. (2017). Major Tom to Ground Control: How Lipoproteins Communicate Extracytoplasmic Stress to the Decision Center of the Cell. J. Bacteriol. 199, e00216-17.
100. Lavollay, M., Arthur, M., Fourgeaud, M., Dubost, L., Marie, A., Veziris, N., Blanot, D., Gutmann, L., and Mainardi, J.-L. (2008). The peptidoglycan of stationary-phase Mycobacterium tuberculosis predominantly contains cross-links generated by L,D-transpeptidation. J. Bacteriol. 190, 4360–4366.
101. Lee, J., Sutterlin, H.A., Wzorek, J.S., Mandler, M.D., Hagan, C.L., Grabowicz, M., Tomasek, D., May, M.D., Hart, E.M., Silhavy, T.J., et al. (2018). Substrate binding to BamD triggers a conformational change in BamA to control membrane insertion. Proc. Natl. Acad. Sci. USA 115, 2359–2364.
102. Lee, J., Xue, M., Wzorek, J.S., Wu, T., Grabowicz, M., Gronenberg, L.S., Sutterlin, H.A., Davis, R.M., Ruiz, N., Silhavy, T.J., et al. (2016). Characterization of a stalled complex on the β-barrel assembly machine. Proc. Natl. Acad. Sci. USA 113, 8717–8722.
103. Lerouge, I., and Vanderleyden, J. (2002). O-antigen structural variation: mechanisms and possible roles in animal/plant–microbe interactions. FEMS. Microbiol. Rev. 26, 17–47.
104. Li, Y., Orlando, B.J., and Liao, M. (2019). Structural basis of lipopolysaccharide extraction by the LptB2FGC complex. Nature 567, 486–490.

105. Lima, S., Guo, M.S., Chaba, R., Gross, C.A., and Sauer, R.T. (2013). Dual molecular signals mediate the bacterial response to outer-membrane stress. Science 340, 837–841.
106. Liu, B., Persons, L., Lee, L., and de Boer, P.A.J. (2015). Roles for both FtsA and the FtsBLQ subcomplex in FtsN-stimulated cell constriction in *Escherichia coli*. Mol. Microbiol. 95, 945–970.
107. Liu, X., Meiresonne, N.Y., Bouhss, A., and den Blaauwen, T. (2018). FtsW activity and lipid II synthesis are required for recruitment of MurJ to midcell during cell division in *Escherichia coli*. Mol. Microbiol. 109, 855–884.
108. Liu, Y., Rodrigues, J.P.G.L.M., Bonvin, A.M.J.J., Zaal, E.A., Berkers, C.R., Heger, M., Gawarecka, K., Swiezewska, E., Breukink, E., and Egmond, M.R. (2016). New Insight into the Catalytic Mechanism of Bacterial MraY from Enzyme Kinetics and Docking Studies. J. Biol. Chem. 291, 15057–15068.
109. Luirink, J., Yu, Z., Wagner, S., and de Gier, J.-W. (2012). Biogenesis of inner membrane proteins in *Escherichia coli*. BBA - Bioenergetics 1817, 965–976.
110. Lutkenhaus, J., Pichoff, S., and Du, S. (2012). Bacterial cytokinesis: From Z ring to divisome. Cytoskeleton 69, 778–790.
111. Madigan, Michael T., Kelly S. Bender, Daniel H. Buckley, W. Matthew Sattley, and David Allan Stahl. (2018). Brock Biology of Microorganisms Global Edition (Pearson).
112. Magnet, S., Bellais, S., Dubost, L., Fourgeaud, M., Mainardi, J.-L., Petit-Frère, S., Marie, A., Mengin-Lecreulx, D., Arthur, M., and Gutmann, L. (2007). Identification of the l,d-Transpeptidases Responsible for Attachment of the Braun Lipoprotein to *Escherichia coli* Peptidoglycan. J. Bacteriol. 189, 3927–3931.
113. Magnet, S., Dubost, L., Marie, A., Arthur, M., and Gutmann, L. (2008). Identification of the l,d-Transpeptidases for Peptidoglycan Cross-Linking in *Escherichia coli*. J. Bacteriol. 190, 4782–4785.
114. Mainardi, J.-L., Hugonnet, J.-E., Rusconi, F., Fourgeaud, M., Dubost, L., Moumi, A.N., Delfosse, V., Mayer, C., Gutmann, L., Rice, L.B., et al. (2007). Unexpected inhibition of peptidoglycan LD-transpeptidase from Enterococcus faecium by the beta-lactam imipenem. J. Biol. Chem. 282, 30414–30422.
115. Maldonado, R.F., Sá-Correia, I., and Valvano, M.A. (2016). Lipopolysaccharide modification in Gram-negative bacteria during chronic infection. FEMS Microbiol. Rev. 40, 480–493.
116. Malinverni, J.C., and Silhavy, T.J. (2011). Assembly of Outer Membrane β-Barrel Proteins: the Bam Complex. EcoSal Plus 2011.
117. Marcyjaniak, M., Odintsov, S.G., Sabala, I., and Bochtler, M. (2004). Peptidoglycan Amidase MepA Is a LAS Metallopeptidase. J. Biol. Chem. 279, 43982–43989.
118. Mathelié-Guinlet, M., Asmar, A.T., Collet, J.-F., and Dufrêne, Y.F. (2020). Lipoprotein Lpp regulates the mechanical properties of the *E. coli* cell envelope. Nat. Commun. 11, 1789.
119. May, K.L., Lehman, K.M., Mitchell, A.M., and Grabowicz, M. (2019). A Stress Response Monitoring Lipoprotein Trafficking to the Outer Membrane. MBio 10, e00618-19.

120. Meberg, B.M., Paulson, A.L., Priyadarshini, R., and Young, K.D. (2004). Endopeptidase penicillin-binding proteins 4 and 7 play auxiliary roles in determining uniform morphology of *Escherichia coli*. J. Bacteriol. 186, 8326–8336.
121. Meeske, A.J., Riley, E.P., Robins, W.P., Uehara, T., Mekelanos, J.J., Kahne, D., Walker, S., Kruse, A.C., Bernhardt, T.G., and Rudner, D.Z. (2016). SEDS proteins are a widespread family of bacterial cell wall polymerases. Nature 537, 634–638.
122. Meredith, T.C., Aggarwal, P., Mamat, U., Lindner, B., and Woodard, R.W. (2006). Redefining the Requisite Lipopolysaccharide Structure in *Escherichia coli*. ACS Chem. Biol. 1, 33–42.
123. Merten, J.A., Schultz, K.M., and Klug, C.S. (2012). Concentration-dependent oligomerization and oligomeric arrangement of LptA. Protein Sci. 21, 211–218.
124. Mika, F., Busse, S., Possling, A., Berkholz, J., Tschowri, N., Sommerfeldt, N., Pruteanu, M., and Hengge, R. (2012). Targeting of csgD by the small regulatory RNA RprA links stationary phase, biofilm formation and cell envelope stress in *Escherichia coli*. Mol. Microbiol. 84, 51–65.
125. Miller, S.I., and Salama, N.R. (2018). The gram-negative bacterial periplasm: Size matters. PLoS Biol. 16, e2004935.
126. Mitchell, A.M., and Silhavy, T.J. (2019). Envelope stress responses: balancing damage repair and toxicity. Nat. Rev. Microbiol. 17, 417–428.
127. Miyachiro, M.M., Contreras-Martel, C., and Dessen, A. (2019). Penicillin-Binding Proteins (PBPs) and Bacterial Cell Wall Elongation Complexes. In Macromolecular Protein Complexes II: Structure and Function, J.R. Harris, and J. Marles-Wright, eds. (Cham: Springer International Publishing), pp. 273–289.
128. Miyamoto, T., Katane, M., Saitoh, Y., Sekine, M., and Homma, H. (2020). Involvement of penicillin-binding proteins in the metabolism of a bacterial peptidoglycan containing a non-canonical d-amino acid. Amino Acids 52, 487–497.
129. Morè, N., Martorana, A.M., Biboy, J., Otten, C., Winkle, M., Serrano, C.K.G., Montón Silva, A., Atkinson, L., Yau, H., Breukink, E., et al. (2019). Peptidoglycan Remodeling Enables *Escherichia coli* To Survive Severe Outer Membrane Assembly Defect. MBio 10, e02729-18.
130. Morgenstein, R.M., Bratton, B.P., Nguyen, J.P., Ouzounov, N., Shaevitz, J.W., and Gitai, Z. (2015). RodZ links MreB to cell wall synthesis to mediate MreB rotation and robust morphogenesis. Proc. Natl. Acad. Sci. USA. 112, 12510–12515.
131. Moura, E.C.C.M., Baeta, T., Romanelli, A., Laguri, C., Martorana, A.M., Erba, E., Simorre, J.-P., Sperandeo, P., and Polissi, A. (2020). Thanatin Impairs Lipopolysaccharide Transport Complex Assembly by Targeting LptC-LptA Interaction and Decreasing LptA Stability. Front. Microbiol. 11, 909.
132. Narita, S., and Tokuda, H. (2009). Biochemical characterization of an ABC transporter LptBFGC complex required for the outer membrane sorting of lipopolysaccharides. FEBS Letters 583, 2160–2164.
133. Narita, S.-I., and Tokuda, H. (2017). Bacterial lipoproteins; biogenesis, sorting and quality control. BBA – Mol. Cell. Biol. Lipids. 1862, 1414–1423.

134. Nelson, D.E., and Young, K.D. (2001). Contributions of PBP 5 anddd-Carboxypeptidase Penicillin Binding Proteins to Maintenance of Cell Shape in *Escherichia coli*. J. Bacteriol. 183, 3055–3064.
135. Nikaido, H. (2003). Molecular Basis of Bacterial Outer Membrane Permeability Revisited. Microbiol. Mol. Biol. Rev. 67, 593–656.
136. Nilsen, T., Yan, A.W., Gale, G., and Goldberg, M.B. (2005). Presence of Multiple Sites Containing Polar Material in Spherical *Escherichia coli* Cells That Lack MreB. J. Bacteriol. 187, 6187–6196.
137. Ogura T, Inoue K, Tatsuta T, Suzaki T, Karata K, Young K, Su LH, Fierke CA, Jackman JE, Raetz CR, Coleman J, Tomoyasu T, Matsuzawa H. 1999. Balanced biosynthesis of major membrane components through regulated degradation of the committed enzyme of lipid A biosynthesis by the AAA protease FtsH (HflB) in *Escherichia coli*. Mol. Microbiol. 31:833–844.
138. Okuda, S., and Tokuda, H. (2011). Lipoprotein sorting in bacteria. Annu. Rev. Microbiol. 65, 239–259.
139. Okuda, S., Freinkman, E., and Kahne, D. (2012). Cytoplasmic ATP hydrolysis powers transport of lipopolysaccharide across the periplasm in *E. coli*. Science 338, 1214–1217.
140. Okuda, S., Sherman, D.J., Silhavy, T.J., Ruiz, N., and Kahne, D. (2016). Lipopolysaccharide transport and assembly at the outer membrane: the PEZ model. Nat. Rev. Microbiol. 14, 337–345.
141. Opiyo, S.O., Pardy, R.L., Moriyama, H., and Moriyama, E.N. (2010). Evolution of the Kdo2-lipid A biosynthesis in bacteria. BMC Evol. Biol. 10, 362.
142. Otten, C., Brilli, M., Vollmer, W., Viollier, P.H., and Salje, J. (2018). Peptidoglycan in obligate intracellular bacteria. Mol. Microbiol. 107, 142–163.
143. Owens, T.W., Taylor, R.J., Pahil, K.S., Bertani, B.R., Ruiz, N., Kruse, A.C., and Kahne, D. (2019). Structural basis of unidirectional export of lipopolysaccharide to the cell surface. Nature 567, 550–553.
144. Özbaykal, G., Wollrab, E., Simon, F., Vigouroux, A., Cordier, B., Aristov, A., Chaze, T., Matondo, M., and van Teeffelen, S. The transpeptidase PBP2 governs initial localization and activity of the major cell-wall synthesis machinery in *E. coli*. ELife 9, e50629.
145. Pannen, D., Fabisch, M., Gausling, L., and Schnetz, K. (2016). Interaction of the RcsB Response Regulator with Auxiliary Transcription Regulators in *Escherichia coli*. J. Biol. Chem. 291, 2357–2370.
146. Pazos, M., and Peters, K. (2019). Peptidoglycan. In Bacterial Cell Walls and Membranes, A. Kuhn, ed. (Cham: Springer International Publishing), pp. 127–168.
147. Peters, K., Kannan, S., Rao, V.A., Biboy, J., Vollmer, D., Erickson, S.W., Lewis, R.J., Young, K.D., and Vollmer, W. (2016). The Redundancy of Peptidoglycan Carboxypeptidases Ensures Robust Cell Shape Maintenance in *Escherichia coli*. MBio 7, e00819-16.
148. Peters, N.T., Morlot, C., Yang, D.C., Uehara, T., Vernet, T., and Bernhardt, T.G. (2013). Structure-function analysis of the LytM domain of EnvC, an activator of cell wall remodelling at the *Escherichia coli* division site. Mol. Microbiol. 89, 690–701.

149. Philippe, N., Pelosi, L., Lenski, R.E., and Schneider, D. (2009). Evolution of Penicillin-Binding Protein 2 Concentration and Cell Shape during a Long-Term Experiment with *Escherichia coli*. J Bacteriol 191, 909–921.
150. Pichoff, S., Du, S., and Lutkenhaus, J. (2018). Disruption of divisome assembly rescued by FtsN–FtsA interaction in *Escherichia coli*. PNAS 115, E6855–E6862.
151. Ploeg, R. van der, Verheul, J., Vischer, N.O.E., Alexeeva, S., Hoogendoorn, E., Postma, M., Banzhaf, M., Vollmer, W., and Blaauwen, T. den (2013). Colocalization and interaction between elongasome and divisome during a preparative cell division phase in *Escherichia coli*. Mol. Microbiol. 87, 1074–1087.
152. Polissi, A., and Georgopoulos, C. (1996). Mutational analysis and properties of the msbA gene of *Escherichia coli*, coding for an essential ABC family transporter. Mol. Microbiol. 20, 1221–1233.
153. Potluri, L., Karczmarek, A., Verheul, J., Piette, A., Wilkin, J.-M., Werth, N., Banzhaf, M., Vollmer, W., Young, K.D., Nguyen-Distèche, M., et al. (2010). Septal and lateral wall localization of PBP5, the major D, D-carboxypeptidase of *Escherichia coli*, requires substrate recognition and membrane attachment. Mol. Microbiol. 77, 300–323.
154. Potluri, L.-P., de Pedro, M.A., and Young, K.D. (2012). *Escherichia coli* low-molecular-weight penicillin-binding proteins help orient septal FtsZ, and their absence leads to asymmetric cell division and branching. Mol. Microbiol. 84, 203–224.
155. Priyadarshini, R., Pedro, M.A. de, and Young, K.D. (2007). Role of Peptidoglycan Amidases in the Development and Morphology of the Division Septum in *Escherichia coli*. J. Bacteriol. 189, 5334–5347.
156. Raetz, C.R., Guan, Z., Ingram, B.O., Six, D.A., Song, F., Wang, X., and Zhao, J. (2009). Discovery of new biosynthetic pathways: the lipid A story. J. Lipid Res. 50 (Suppl), S103-S108.
157. Raetz, C.R.H., and Whitfield, C. (2002). Lipopolysaccharide endotoxins. Annu. Rev. Biochem. 71, 635–700.
158. Raetz, C.R.H., Reynolds, C.M., Trent, M.S., and Bishop, R.E. (2007). Lipid a modification system in gram-negative bacteria. Annu. Rev. Biochem. 76, 295–329.
159. Raivio, T.L. (2005). Envelope stress responses and Gram-negative bacterial pathogenesis. Mol. Microbiol. 56, 1119–1128.
160. Reeves, P. (1995). Role of O-antigen variation in the immune response. Trends. Microbiol. 3, 381–386.
161. Ricci, D.P., and Silhavy, T.J. (2019). Outer membrane protein insertion by the β-barrel assembly machine. EcoSal Plus 2019.
162. Rohs, P.D.A., Buss, J., Sim, S.I., Squyres, G.R., Srisuknimit, V., Smith, M., Cho, H., Sjodt, M., Kruse, A.C., Garner, E.C., et al. (2018). A central role for PBP2 in the activation of peptidoglycan polymerization by the bacterial cell elongation machinery. PLoS Genetics 14, e1007726.
163. Romeis, T., and Höltje, J.V. (1994). Specific interaction of penicillin-binding proteins 3 and 7/8 with soluble lytic transglycosylase in *Escherichia coli*. J. Biol. Chem. 269, 21603–21607.
164. Ruiz, N. (2008). Bioinformatics identification of MurJ (MviN) as the peptidoglycan lipid II flippase in *Escherichia coli*. Proc. Natl. Acad. Sci. USA 105, 15553–15557.

165. Sabala, I., Jonsson, I.-M., Tarkowski, A., and Bochtler, M. (2012). Anti-staphylococcal activities of lysostaphin and LytM catalytic domain. BMC Microbiol. 12, 97.
166. Sanders, A.N., and Pavelka, M.S. (2013). Phenotypic analysis of *Escherichia coli* mutants lacking L, D-transpeptidases. Microbiology (Reading, Engl.) 159, 1842–1852.
167. Sankaran, K., and Wu, H.C. (1994). Lipid modification of bacterial prolipoprotein. Transfer of diacylglyceryl moiety from phosphatidylglycerol. J. Biol. Chem. 269, 19701–19706.
168. Santambrogio, C., Sperandeo, P., Villa, R., Sobott, F., Polissi, A., and Grandori, R. (2013). LptA assembles into rod-like oligomers involving disorder-to-order transitions. J. Am. Soc. Mass Spectrom. 24, 1593–1602.
169. Sarkar, S.K., Dutta, M., Chowdhury, C., Kumar, A., and Ghosh, A.S. (2011). PBP5, PBP6 and DacD play different roles in intrinsic β-lactam resistance of *Escherichia coli*. Microbiology, 157, 2702–2707.
170. Sauvage, E., and Terrak, M. (2016). Glycosyltransferases and Transpeptidases/Penicillin-Binding Proteins: Valuable Targets for New Antibacterials. Antibiotics (Basel) 5, 12.
171. Sauvage, E., Derouaux, A., Fraipont, C., Joris, M., Herman, R., Rocaboy, M., Schloesser, M., Dumas, J., Kerff, F., Nguyen-Distèche, M., et al. (2014). Crystal Structure of Penicillin-Binding Protein 3 (PBP3) from *Escherichia coli*. PLoS One 9, e98042.
172. Sauvage, E., Kerff, F., Terrak, M., Ayala, J.A., and Charlier, P. (2008). The penicillin-binding proteins: structure and role in peptidoglycan biosynthesis. FEMS Microbiol. Rev. 32, 234–258.
173. Schäkermann, M., Langklotz, S., and Narberhaus, F. (2013). FtsH-mediated coordination of lipopolysaccharide biosynthesis in *Escherichia coli* correlates with the growth rate and the alarmone (p)ppGpp. J. Bacteriol. 195, 1912–1919.
174. Scheffers, D.-J., and Pinho, M.G. (2005). Bacterial Cell Wall Synthesis: New Insights from Localization Studies. Microbiol. Mol. Biol. Rev. 69, 585–607.
175. Schiffer, G., and Höltje, J.-V. (1999). Cloning and Characterization of PBP 1C, a Third Member of the Multimodular Class A Penicillin-binding Proteins of *Escherichia coli*. J. Biol. Chem. 274, 32031–32039.
176. Schwalm, J., Mahoney, T.F., Soltes, G.R., and Silhavy, T.J. (2013). Role for Skp in LptD Assembly in *Escherichia coli*. J. Bacteriol. 195, 3734–3742.
177. Seydel, A., Gounon, P., and Pugsley, A.P. (1999). Testing the "+2 rule" for lipoprotein sorting in the *Escherichia coli* cell envelope with a new genetic selection. Mol. Microbiol. 34, 810–821.
178. Sham, L.-T., Butler, E.K., Lebar, M.D., Kahne, D., Bernhardt, T.G., and Ruiz, N. (2014). MurJ is the flippase of lipid-linked precursors for peptidoglycan biogenesis. Science 345, 220–222.
179. Silhavy, T.J., Kahne, D., and Walker, S. (2010). The Bacterial Cell Envelope. Cold Spring Harb Perspect Biol 2, a000414.
180. Singh, S.K., SaiSree, L., Amrutha, R.N., and Reddy, M. (2012). Three redundant murein endopeptidases catalyse an essential cleavage step in peptidoglycan synthesis of *Escherichia coli* K12. Mol. Microbiol. 86, 1036–1051.
181. Sklar, J.G., Wu, T., Kahne, D., and Silhavy, T.J. (2007). Defining the roles of the periplasmic chaperones SurA, Skp, and DegP in *Escherichia coli*. Genes. Dev. 21, 2473–2484.

182. Sperandeo, P., Lau, F.K., Carpentieri, A., De Castro, C., Molinaro, A., Dehò, G., Silhavy, T.J., and Polissi, A. (2008). Functional analysis of the protein machinery required for transport of lipopolysaccharide to the outer membrane of *Escherichia coli*. J. Bacteriol. 190, 4460–4469.
183. Sperandeo, P., Martorana, A.M., and Polissi, A. (2017a). The lipopolysaccharide transport (Lpt) machinery: A nonconventional transporter for lipopolysaccharide assembly at the outer membrane of Gram-negative bacteria. J. Biol. Chem. 292, 17981–17990.
184. Sperandeo, P., Martorana, A.M., and Polissi, A. (2017b). Lipopolysaccharide biogenesis and transport at the outer membrane of Gram-negative bacteria. BBA – Mol. Cell. Biol. Lipids 1862, 1451–1460.
185. Sperandeo, P., Martorana, A.M., and Polissi, A. (2019a). Lipopolysaccharide Biosynthesis and Transport to the Outer Membrane of Gram-Negative Bacteria. In Bacterial Cell Walls and Membranes, A. Kuhn, ed. (Cham: Springer International Publishing), pp. 9–37.
186. Sperandeo, P., Martorana, A.M., and Polissi, A. (2019b). The Lpt ABC transporter for lipopolysaccharide export to the cell surface. Res Microbiol. 170, 366–373.
187. Sperandeo, P., Villa, R., Martorana, A.M., Samalikova, M., Grandori, R., Dehò, G., and Polissi, A. (2011). New insights into the Lpt machinery for lipopolysaccharide transport to the cell surface: LptA-LptC interaction and LptA stability as sensors of a properly assembled transenvelope complex. J. Bacteriol. 193, 1042–1053.
188. Spratt, B.G. (1975) Distinct penicillin binding proteins involved in the division, elongation, and shape of *Escherichia coli* K12. Proc. Nat. Acad. Sci. USA 72: 2999–3003.
189. Stevenson, G., Neal, B., Liu, D., Hobbs, M., Packer, N.H., Batley, M., Redmond, J.W., Lindquist, L., and Reeves, P. (1994). Structure of the O antigen of *Escherichia coli* K-12 and the sequence of its rfb gene cluster. J. Bacteriol. 176, 4144–4156.
190. Suits, M.D.L., Sperandeo, P., Dehò, G., Polissi, A., and Jia, Z. (2008). Novel structure of the conserved gram-negative lipopolysaccharide transport protein A and mutagenesis analysis. J. Mol. Biol. 380, 476–488.
191. Szwedziak, P., and Löwe, J. (2013). Do the divisome and elongasome share a common evolutionary past? Curr. Opin. Microbiol. 16, 745–751.
192. Taguchi, A., Welsh, M.A., Marmont, L.S., Lee, W., Sjodt, M., Kruse, A.C., Kahne, D., Bernhardt, T.G., and Walker, S. (2019). FtsW is a peptidoglycan polymerase that is functional only in complex with its cognate penicillin-binding protein. Nat. Microbiol. 4, 587–594.
193. Tang, X., Chang, S., Luo, Q., Zhang, Z., Qiao, W., Xu, C., Zhang, C., Niu, Y., Yang, W., Wang, T., et al. (2019). Cryo-EM structures of lipopolysaccharide transporter LptB2FGC in lipopolysaccharide or AMP-PNP-bound states reveal its transport mechanism. Nat. Commun. 10, 4175.
194. Tao, K., Narita, S., and Tokuda, H. (2012). Defective Lipoprotein Sorting Induces lolA Expression through the Rcs Stress Response Phosphorelay System. J. Bacteriol. 194, 3643–3650.
195. Templin, M.F., Edwards, D.H., and Höltje, J.V. (1992). A murein hydrolase is the specific target of bulgecin in *Escherichia coli*. J. Biol. Chem. 267, 20039–20043.

196. Templin, M.F., Ursinus, A., and Höltje, J.V. (1999). A defect in cell wall recycling triggers autolysis during the stationary growth phase of *Escherichia coli*. EMBO J. 18, 4108–4117.
197. Tenaillon, O., Skurnik, D., Picard, B. et al. The population genetics of commensal *Escherichia coli*. Nat Rev Microbiol. 8, 207–217 (2010).
198. Tokuda, H. (2009). Biogenesis of Outer Membranes in Gram-Negative Bacteria. BBB 73, 465–473
199. Tokuda, H., and Matsuyama, S. (2004). Sorting of lipoproteins to the outer membrane in *E. coli*. Biochimica et Biophysica Acta (BBA) – Mol. Cell. Res. 1693, 5–13.
200. Tokuda, H., Matsuyama, S., and Tanaka-Masuda, K. (2007). Structure, Function, and Transport of Lipoproteins in *Escherichia coli*. In The Periplasm, E. Michael, ed. (Cham: ASM press) pp. 67–79.
201. Tommassen, J. (2010). Assembly of outer-membrane proteins in bacteria and mitochondria. Microbiology, 156, 2587–2596.
202. Tsang, M.-J., Yakhnina, A.A., and Bernhardt, T.G. (2017). NlpD links cell wall remodeling and outer membrane invagination during cytokinesis in *Escherichia coli*. PLoS Genet. 13, e1006888.
203. Tschauner, K., Hörnschemeyer, P., Müller, V.S., and Hunke, S. (2014). Dynamic interaction between the CpxA sensor kinase and the periplasmic accessory protein CpxP mediates signal recognition in *E. coli*. PLoS ONE 9, e107383.
204. Typas, A., Banzhaf, M., Gross, C.A., and Vollmer, W. (2011). From the regulation of peptidoglycan synthesis to bacterial growth and morphology. Nat. Rev. Microbiol. 10, 123–136.
205. Typas, A., Banzhaf, M., van den Berg van Saparoea, B., Verheul, J., Biboy, J., Nichols, R.J., Zietek, M., Beilharz, K., Kannenberg, K., von Rechenberg, M., et al. (2010). Regulation of peptidoglycan synthesis by outer-membrane proteins. Cell 143, 1097–1109.
206. Uehara, T., and Park, J.T. (2007). An Anhydro-N-Acetylmuramyl-l-Alanine Amidase with Broad Specificity Tethered to the Outer Membrane of *Escherichia coli*. J of Bacteriol. 189, 5634–5641.
207. Uehara, T., Dinh, T., and Bernhardt, T.G. (2009). LytM-domain factors are required for daughter cell separation and rapid ampicillin-induced lysis in *Escherichia coli*. J. Bacteriol. 191, 5094–5107.
208. Uehara, T., Parzych, K.R., Dinh, T., and Bernhardt, T.G. (2010). Daughter cell separation is controlled by cytokinetic ring-activated cell wall hydrolysis. EMBO J. 29, 1412–1422.
209. Van den Ent, F., Johnson, C.M., Persons, L., de Boer, P., and Löwe, J. (2010). Bacterial actin MreB assembles in complex with cell shape protein RodZ. EMBO J. 29, 1081–1090.
210. Vega, D., and Ayala, J.A. (2006). The DD-carboxypeptidase activity encoded by pbp4B is not essential for the cell growth of *Escherichia coli*. Arch Microbiol. 185, 23–27.
211. Vermassen, A., Talon, R., Andant, C., Provot, C., Desvaux, M., and Leroy, S. (2019). Cell-Wall Hydrolases as Antimicrobials against Staphylococcus Species: Focus on Sle1. Microorganisms 7, 559.
212. Villa, R., Martorana, A.M., Okuda, S., Gourlay, L.J., Nardini, M., Sperandeo, P., Dehò, G., Bolognesi, M., Kahne, D., and Polissi, A. (2013). The *Escherichia coli* Lpt Transenvelope Protein

Complex for Lipopolysaccharide Export Is Assembled via Conserved Structurally Homologous Domains. J. Bacteriol. 195, 1100–1108.

213. Vogt, S.L., Evans, A.D., Guest, R.L., and Raivio, T.L. (2014). The Cpx Envelope Stress Response Regulates and Is Regulated by Small Noncoding RNAs. J. Bacteriol. 196, 4229–4238.

214. Vollmer, W., Blanot, D., and de Pedro, M.A. (2008a). Peptidoglycan structure and architecture. FEMS Microbiol. Rev. 32, 149–167.

215. Vollmer, W., Joris, B., Charlier, P., and Foster, S. (2008b). Bacterial peptidoglycan (murein) hydrolases. FEMS Microbiol. Rev. 32, 259–286.

216. Wall, E., Majdalani, N., and Gottesman, S. (2018). The Complex Rcs Regulatory Cascade. Annu. Rev. Microbiol. 72, 111–139.

217. Wang, Z., Wang, J., Ren, G., Li, Y., and Wang, X. (2015). Influence of Core Oligosaccharide of Lipopolysaccharide to Outer Membrane Behavior of *Escherichia coli*. Mar Drugs 13, 3325–3339.

218. Weiner, J.H., and Rothery, R.A. (2007). Bacterial Cytoplasmic Membrane. In Encyclopedia of Life Sciences, (Cham: American Cancer Society).

219. White, C.L., Kitich, A., and Gober, J.W. (2010). Positioning cell wall synthetic complexes by the bacterial morphogenetic proteins MreB and MreD. Mol. Microbiol. 76, 616–633.

220. Wyckoff, T.J., Lin, S., Cotter, R.J., Dotson, G.D., and Raetz, C.R. (1998). Hydrocarbon rulers in UDP-N- acetylglucosamine acyltransferases. J. Biol. Chem. 273, 32369–32372.

221. Xiao, J., and Goley, E.D. (2016). Redefining the roles of the FtsZ-ring in bacterial cytokinesis. Curr. Opin. Microbiol. 34, 90–96.

222. Xie, R., Taylor, R.J., and Kahne, D. (2018). Outer Membrane Translocon Communicates with Inner Membrane ATPase To Stop Lipopolysaccharide Transport. J. Am. Chem. Soc. 140, 12691–12694.

223. Yakhnina, A.A., and Bernhardt, T.G. (2020). The Tol-Pal system is required for peptidoglycan-cleaving enzymes to complete bacterial cell division. PNAS 117, 6777–6783.

224. Yamashita, S., and Buchanan, S.K. (2010). Solute and Ion Transport: Outer Membrane Pores and Receptors. EcoSal Plus 2010.

225. Yang, D.C., Peters, N.T., Parzych, K.R., Uehara, T., Markovski, M., and Bernhardt, T.G. (2011). An ATP-binding cassette transporter-like complex governs cell-wall hydrolysis at the bacterial cytokinetic ring. Proc. Natl. Acad. Sci. USA. 108, E1052-1060.

226. Yousif, S.Y., Broome-Smith, J.K., and Spratt, B.G. (1985). Lysis of *Escherichia coli* by.-Lactam Antibiotics: Deletion Analysis of the Role of Penicillin-binding Proteins 1A and 1B. Microbiology 131, 2839–2845.

227. Zapun, A., Contreras-Martel, C., and Vernet, T. (2008). Penicillin-binding proteins and β-lactam resistance. FEMS Microbiol. Rev. 32, 361–385.

228. Zhang, G., Meredith, T.C., and Kahne, D. (2013). On the Essentiality of Lipopolysaccharide to Gram-Negative Bacteria. Curr. Opin. Microbiol. 16, 779–785.

229. Zheng, S., Sham, L.-T., Rubino, F.A., Brock, K.P., Robins, W.P., Mekalanos, J.J., Marks, D.S., Bernhardt, T.G., and Kruse, A.C. (2018). Structure and mutagenic analysis of the lipid II flippase MurJ from *Escherichia coli*. PNAS 115, 6709–6714.

230. Zhou, Z., White, K.A., Polissi, A., Georgopoulos, C., and Raetz, C.R. (1998). Function of *Escherichia coli* MsbA, an essential ABC family transporter, in lipid A and phospholipid biosynthesis. J. Biol. Chem. 273, 12466–12475.
231. Zoeiby, A.E., Sanschagrin, F., and Levesque, R.C. (2003). Structure and function of the Mur enzymes: development of novel inhibitors. Mol. Microbiol. 47, 1–12.
232. Zückert, W.R. (2014). Secretion of Bacterial Lipoproteins: Through the Cytoplasmic Membrane, the Periplasm and Beyond. BBA 1843, 1509–1516.
233. Zuegg, J., Muldoon, C., Adamson, G., McKeveney, D., Le Thanh, G., Premraj, R., Becker, B., Cheng, M., Elliott, A.G., Huang, J.X., et al. (2015). Carbohydrate scaffolds as glycosyltransferase inhibitors with in vivo antibacterial activity. Nat. Commu. 6, 1–11.

2. Aim of the Project

As it was stated in the preceding introductory chapters, the Gram-negative cell envelope possess a great complexity. The substantial amount of proteins working on the different cell envelope layers along with the diverse multiprotein machineries embedded into them, highlight the high grade of coordination needed, in terms of molecular events, among the three compartments (OM, PG and IM) to keep a functional cell envelope. For instance, the PG synthesis is controlled by OM proteins, and a defective LPS transport to the OM modulates the levels of several proteins involved in PG biogenesis (Martorana et al., 2014; Typas et al., 2010).

Preliminary data from our lab indicate that block of the LPS transport is coupled with a rise of the non-canonical 3,3-crosslinks in the PG sacculus, as compared to wild type, thus suggesting a crosstalk between the OM and the PG layer. Moreover, we found that the deletion of the L, D-TPases that catalyse 3,3 crosslinks causes cell lysis when LPS transport is defective. During the analysis of the potential factors associated to these lysis phenotypes, we spot the lipoprotein ygeR (Uehara et al., 2009), whose functionality in the cell remains unknown.

The aim of the project is to elucidate the link between LPS biogenesis and PG remodeling to unveil mechanisms and pathways that bacterial cells employ to monitor cell envelope integrity, and to understand bacterial response when envelope integrity is compromised.

1. Martorana, A.M., Motta, S., Silvestre, D.D., Falchi, F., Dehò, G., Mauri, P., Sperandeo, P., and Polissi, A. (2014). Dissecting *Escherichia coli* Outer Membrane Biogenesis Using Differential Proteomics. PLoS ONE *9*, e100941.
2. Uehara, T., Dinh, T., and Bernhardt, T.G. (2009). LytM-Domain Factors Are Required for Daughter Cell Separation and Rapid Ampicillin-Induced Lysis in *Escherichia coli*. J. Bacteriol. 191, 5094.
3. Typas, A., Banzhaf, M., van den Berg van Saparoea, B., Verheul, J., Biboy, J., Nichols, R.J., Zietek, M., Beilharz, K., Kannenberg, K., von Rechenberg, M., et al. (2010). Regulation of Peptidoglycan Synthesis by Outer-Membrane Proteins. Cell 143, 1097–1109.

3. Results

3.1 Peptidoglycan Remodeling Enables *Escherichia coli* To Survive Severe Outer Membrane Assembly Defect

The following chapter contains peer reviewed original research, for which I was a contributing author, published in the mBio journal in February 2019.

As a contributing author I designed and constructed several mutant strains, and I also contributed to the experiment shown in Fig. 7.

PMID: 30723128

PMCID: PMC6428754

DOI: 10.1128/mBio.02729-1

AMERICAN SOCIETY FOR MICROBIOLOGY | mBio®

RESEARCH ARTICLE
Molecular Biology and Physiology

Peptidoglycan Remodeling Enables *Escherichia coli* To Survive Severe Outer Membrane Assembly Defect

Niccolò Morè,[a] Alessandra M. Martorana,[a] Jacob Biboy,[b] Christian Otten,[b]* Matthias Winkle,[b] Carlos K. Gurnani Serrano,[a] Alejandro Montón Silva,[c] Lisa Atkinson,[b] Hamish Yau,[b] Eefjan Breukink,[d] Tanneke den Blaauwen,[c] Waldemar Vollmer,[b] Alessandra Polissi[a]

[a]Dipartimento di Scienze Farmacologiche e Biomolecolari, Università degli Studi di Milano, Milan, Italy
[b]The Centre for Bacterial Cell Biology, Institute for Cell and Molecular Biosciences, Newcastle University, Newcastle upon Tyne, United Kingdom
[c]Bacterial Cell Biology & Physiology, Swammerdam Institute for Life Sciences, University of Amsterdam, Amsterdam, The Netherlands
[d]Membrane Biochemistry and Biophysics, Department of Chemistry, Faculty of Science, Utrecht University, Utrecht, The Netherlands

ABSTRACT Gram-negative bacteria have a tripartite cell envelope with the cytoplasmic membrane (CM), a stress-bearing peptidoglycan (PG) layer, and the asymmetric outer membrane (OM) containing lipopolysaccharide (LPS) in the outer leaflet. Cells must tightly coordinate the growth of their complex envelope to maintain cellular integrity and OM permeability barrier function. The biogenesis of PG and LPS relies on specialized macromolecular complexes that span the entire envelope. In this work, we show that *Escherichia coli* cells are capable of avoiding lysis when the transport of LPS to the OM is compromised, by utilizing LD-transpeptidases (LDTs) to generate 3-3 cross-links in the PG. This PG remodeling program relies mainly on the activities of the stress response LDT, LdtD, together with the major PG synthase PBP1B, its cognate activator LpoB, and the carboxypeptidase PBP6a. Our data support a model according to which these proteins cooperate to strengthen the PG in response to defective OM synthesis.

IMPORTANCE In Gram-negative bacteria, the outer membrane protects the cell against many toxic molecules, and the peptidoglycan layer provides protection against osmotic challenges, allowing bacterial cells to survive in changing environments. Maintaining cell envelope integrity is therefore a question of life or death for a bacterial cell. Here we show that *Escherichia coli* cells activate the LD-transpeptidase LdtD to introduce 3-3 cross-links in the peptidoglycan layer when the integrity of the outer membrane is compromised, and this response is required to avoid cell lysis. This peptidoglycan remodeling program is a strategy to increase the overall robustness of the bacterial cell envelope in response to defects in the outer membrane.

KEYWORDS *Escherichia coli*, cell envelope, lipopolysaccharide, peptidoglycan, stress response

The integrity of a diderm (Gram-negative) bacterial cell is maintained by a complex cell envelope composed of the cytoplasmic membrane (CM), the periplasm with a thin peptidoglycan (PG) sacculus, and the outer membrane (OM) (1, 2). The asymmetrical OM contains in the outer leaflet lipopolysaccharide (LPS) (3), which makes the cell envelope impermeable to many toxic compounds and antibiotics (4).

LPS is assembled at the outer leaflet of the CM (5–7) and then transported across the periplasm to reach its final destination at the outermost surface of the cell (8, 9). In *Escherichia coli*, LPS transport is facilitated by seven essential proteins, LptA to LptG (10–15) which form a transenvelope protein bridge through the periplasm and its PG sacculus (11, 16–18). This organization allows the coupling of ATP hydrolysis with LPS

Citation Morè N, Martorana AM, Biboy J, Otten C, Winkle M, Serrano CKG, Montón Silva A, Atkinson L, Yau H, Breukink E, den Blaauwen T, Vollmer W, Polissi A. 2019. Peptidoglycan remodeling enables *Escherichia coli* to survive severe outer membrane assembly defect. mBio 10:e02729-18. https://doi.org/10.1128/mBio.02729-18.

Editor Kimberly A. Kline, Nanyang Technological University

Address correspondence to Waldemar Vollmer, w.vollmer@ncl.ac.uk, or Alessandra Polissi, alessandra.polissi@unimi.it.

* Present address: Christian Otten, Institute for Pharmaceutical Microbiology, University of Bonn, Bonn, Germany.

A.M.M. and J.B. contributed equally to this work.

This article is a direct contribution from a Fellow of the American Academy of Microbiology. Solicited external reviewers: David Popham, Virginia Tech; Ivo Gomperts Boneca, Institut Pasteur; Miguel Valvano, Queen's University Belfast.

Received 8 December 2018
Accepted 13 December 2018
Published 5 February 2019

movement across the periplasm up to the cell surface, as proposed in the so-called PEZ model (19). Depletion of any of the Lpt components results in block of LPS transport and its accumulation at the periplasmic leaflet of the cytoplasmic membrane (CM) (12, 14).

LPS export to the OM is among the cell's main transport processes. Considering a generation time of 20 min for fast growing *E. coli*, LPS transport must occur at a rate of more than 10^3 molecules per second to ensure complete coverage of the cell surface during growth (20). Moreover, the supply of LPS must be optimally coupled to the synthesis and assembly of other cell envelope components, such as PG, to prevent loss of OM integrity due to LPS depletion or detrimental effects by excessive LPS production. How LPS synthesis and export is regulated remains largely unknown.

LPS is exported through the periplasmic PG sacculus that has a net-like structure composed of glycan strands connected by short, cross-linked peptides (2, 21). PBP1A and PBP1B are major and semiredundant PG synthases that polymerize glycan strands by their glycosyltransferase (GTase) activity and cross-link stem peptides by DD-transpeptidase (DD-TPase) activity, forming the abundant 4-3 cross-links in PG (see Fig. S1A in the supplemental material) (22–24). The CM-anchored PBPs require activation by their cognate, OM-anchored lipoprotein (LpoA and LpoB, respectively) (25–27). LpoA and LpoB span the periplasm to activate their cognate PBP (28–30), presumably responding to the size of pores in the PG layer to couple PG growth with cell growth (21).

DD-carboxypeptidases (DD-CPase) such as PBP5, PBP6a, and PBP6b trim the pentapeptides present in new PG to tetrapeptides (31–33). PBP5 is the major DD-CPase in the cell; its absence causes aberrant cell morphology in strains lacking other PBPs (33, 34). PBP6b contributes substantially to PG remodeling and cell shape maintenance in cells growing at acidic pH (35).

In *E. coli*, the majority (90% to 98%) of cross-links in PG are of the 4-3 (or DD) type (between D-Ala and *meso*-diaminopimelic acid [*meso*-Dap]) (36). However, there are 2 to 10% of the 3-3 (or LD) type of cross-links between two *meso*-Dap residues of adjacent stem peptides (Fig. S1A), and these increase to up to 16% in stationary-phase cells (36, 37). 3-3 cross-links are produced by LD-transpeptidases (LDTs) of the YkuD family of proteins (PF03734), which are structurally unrelated to PBPs. LDTs use tetrapeptide donors in the TPase reaction and are insensitive to most β-lactams (Fig. S1A) (38).

E. coli has five LDTs with two distinct functions. LdtD (formerly YcbB) and LdtE (YnhG) form 3-3 cross-links, whereas LdtA (ErfK), LdtB (YbiS), and LdtC (YcfS) attach the abundant OM-anchored Lpp (Braun's lipoprotein) to *meso*-Dap residues in PG, providing a tight connection between the PG and OM. Notably, *E. coli* mutants with multiple or all *ldt* genes deleted exhibit only minor phenotypes, suggesting that these functions are dispensable during growth under laboratory conditions (39–41).

Certain strains of *Enterococcus faecium* can grow in the presence of β-lactam antibiotics using a β-lactam-insensitive LDT, Ldt_{fm} to produce 3-3 cross-links instead of the β-lactam-sensitive PBP TPases (42–44). More recently, a DD-TPase-independent and LDT-dependent mutant strain of *E. coli* has been selected by its ability to grow at a high and otherwise lethal concentration of ampicillin, at which it produces exclusively 3-3 cross-links in its PG (45). This strain has an elevated level of the alarmone (p)ppGpp and needs LdtD, the DD-CPase PBP5, and the GTase domain of PBP1B together with its regulator, LpoB, to bypass PBPs and achieve broad-spectrum β-lactam resistance (45). However, *E. coli* strains do not readily acquire this mechanism of resistance, and it is possible that the 3-3 cross-linking activities of LdtD and LdtE have another, yet undiscovered function in *E. coli*.

In this work, we show that *E. coli* cells defective in the LPS export pathway require LDTs that produce an increased level of 3-3 cross-links in the PG to avoid cell lysis. Our data suggest that LdtD is specifically expressed in response to OM damage and participates in a PG remodeling program activated in response to the block of LPS transport. Notably, PG remodeling also involves the GTase activity of PBP1B and the DD-CPase of previously unknown function, PBP6a. We propose a model whereby

PBP1B, LdtD, and PBP6a cooperate in a dedicated PG machine which is needed when LPS transport is compromised.

RESULTS

Defective LPS export induces the formation of 3-3 cross-links in PG. We previously observed that several PG-synthesizing or PG-modifying enzymes are upregulated upon depletion of the essential LptC component of the LPS export machinery (46), prompting us to analyze the composition of PG isolated from cells with compromised LPS transport.

For this purpose, we cultured an *araB*p*lptC* conditional strain, in which *lptC* expression is under the control of the arabinose-inducible *araB*p promoter. As previously reported (13), LptC-depleted cells formed short chains and arrested growth (Fig. 1A and B). The sacculi purified from these cells showed a four- to sixfold increase in the relative amount of 3-3 cross-links between two *meso*-Dap residues compared to sacculi from cells grown in the presence of arabinose (Fig. 1E and Table 1; see also Table S3 in the supplemental material). 3-3 cross-links increased early in LptC-depleted cells, indicating a rapid cellular response to the LPS transport arrest. We also observed only a moderate decrease in the canonical 4-3 (*meso*-Dap to D-Ala) cross-links in LptC-depleted cells (Fig. 1E and Table S3).

3-3 cross-links are not essential under standard growth conditions. *E. coli* has five LDTs (LdtA to LdtE) (39–41). When inspecting the *E. coli* genome, we identified another hypothetical *ldt* gene, *yafK*. The predicted YafK shares 33% and 41% sequence identity to the catalytic YkuD (LDT) domain of LdtD and LdtE, respectively, but lacks a conserved arginine residue near the active site cysteine and might not be fully active (Fig. S1B). We included *yafK* (now termed *ldtF*) in our further studies on the roles of LDTs in the formation of 3-3 cross-links during defective LPS export.

To assess the roles of the LDTs in *E. coli*, we examined the growth phenotypes and levels of 3-3 cross-links in sacculi purified from all possible single and multiple deletion mutants. The deletion of *ldtD*, *ldtE*, and *ldtF* alone and in all possible combinations did not affect the growth of *E. coli* (Table 1 and Fig. S3A and B). Even the deletion of all six *ldt* genes did not result in any growth defect under standard laboratory conditions (data not shown). The muropeptide analysis revealed that only 3.0% of the PG muropeptides from strain BW25113 contained 3-3 cross-links (Table 1 and Table S3), consistent with earlier reports (36, 37). The Δ*ldtD* Δ*ldtE* mutant contained 2.2% muropeptides with 3-3 cross-links, and 3-3 cross-links were not detected in the PG from the Δ*ldtD* Δ*ldtE* Δ*ldtF* triple mutant, suggesting that *E. coli* has no other enzyme for 3-3 cross-link formation in the absence of LdtD, LdtE, and LdtF. The Δ*ldtD* Δ*ldtF* double mutant did not produce detectable levels of 3-3 cross-links, suggesting that LdtE is either not active as an LD-TPase or it requires LdtD and/or LdtF for activity. In all other *ldt* defective strains, the level of 3-3 cross-links was comparable to that of the BW25113 wild-type strain, suggesting that one or more LDTs is active in these mutants (Table 1 and Table S3).

We next ectopically expressed *ldtD*, *ldtE*, and/or *ldtF* (Table S1) in an *E. coli* BW25113Δ6LDT background, which lacks *ldtABCDEF* (*ldtA-F*) (47), and analyzed the PG composition (Fig. 2). Expression of LdtD alone, but not expression of LdtE or LdtF, resulted in the presence of 3-3 cross-links in PG. Coexpression of LdtF with LdtD or LdtE increased the level of 3-3 cross-links (compared to LdtD or LdtE alone), suggesting that LdtF might not be an active LD-TPase but stimulates the other two enzymes. In line with this hypothesis, we found that 3-3 cross-links were not detected in a Δ*ldtA-E* mutant that expressed *ldtF* as the sole *ykuD* homologue (Table S3).

LDTs prevent cell lysis upon defective OM assembly. Because the level of the 3-3 cross-links increased in LptC-depleted cells, we deleted every *ldt* gene alone and all possible combinations in the *araB*p*lptC* conditional mutant, and we examined the growth profile and level of 3-3 cross-links in the PG under permissive and nonpermissive conditions.

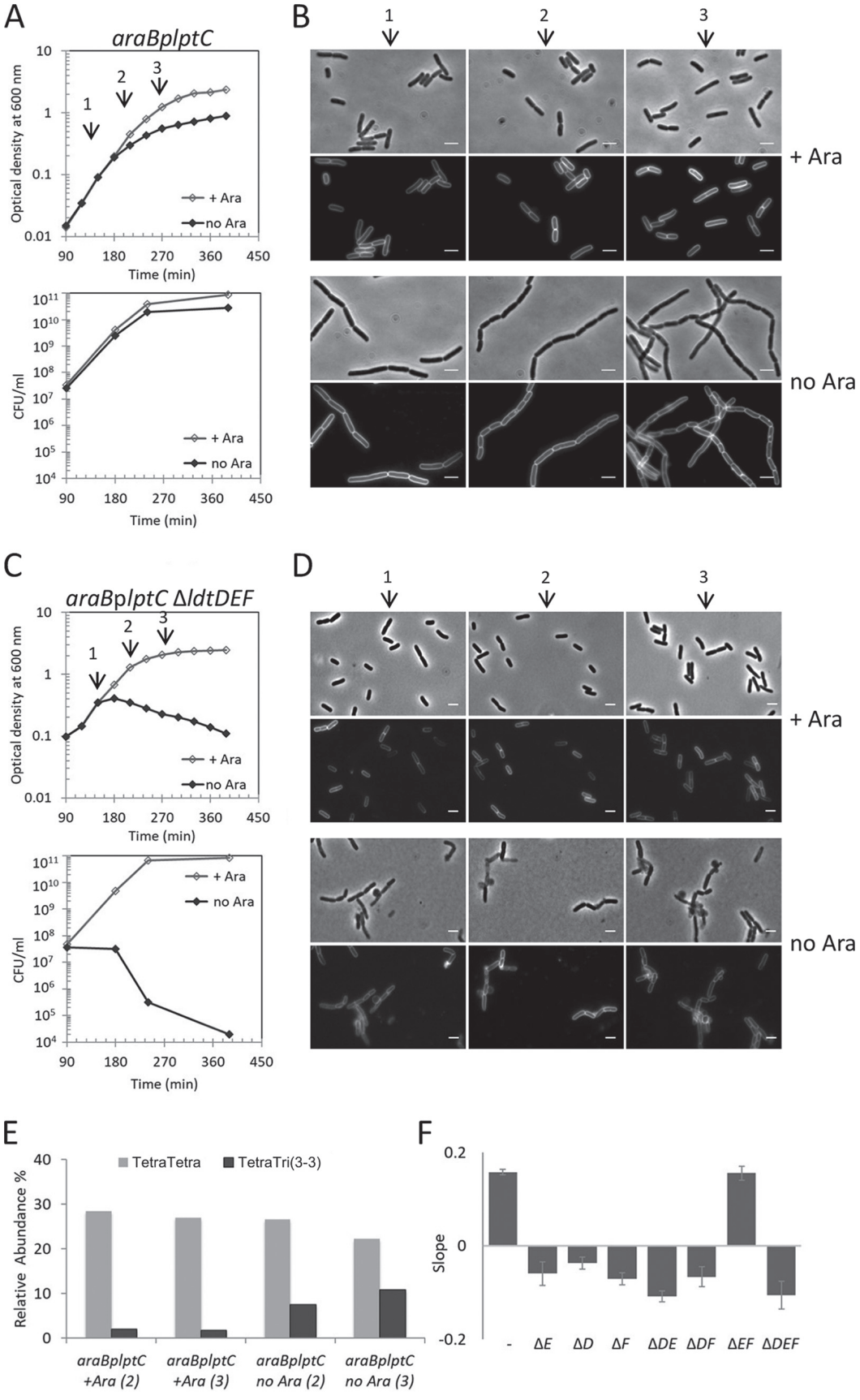

FIG 1 LDTs prevent cell lysis upon defective OM assembly. (A to D) Cells of the *araBplptC* conditional strain (A and B) and the isogenic mutants with *ldtD*, *ldtE*, and *ldtF* deleted (C and D) were grown in the presence of 0.2% arabinose to an OD_{600}

(Continued on next page)

TABLE 1 Summary of the level of 3-3 cross-links in PG and growth phenotype of single and multiple *ldt* mutant strains with or without depletion of LPS export[a]

Presence/absence of gene			3-3 cross-linkage or phenotype in:					
				*araB*p*lptC* strain				
				With arabinose		No arabinose		
ldtD	*ldtE*	*ldtF*	*lptC*$^+$ strain, 3-3 CL (area [%])[b]	Growth	3-3 CL (area [%])	Growth	3-3 CL (area [%])	Lysis rescue by p*ldtD*
+	+	+	3.0	Normal	1.7	Arrest	7.5	NT[e]
−	+	+	3.2	Normal	2.4	Lysis	6.1	+
+	−	+	2.9	Normal	1.9	Lysis	6.0	+
+	+	−	2.9	Normal	1.9	Lysis	8.4	+
−	−	+	2.2	Normal	1.9	Lysis	−[d]	+
−	+	−	ND[c]	Normal	ND[c]	Lysis	ND	+
+	−	−	2.4	Normal	8.2	Arrest	8.4	NT
−	−	−	ND	Normal	ND	Lysis	ND	+

[a]The table shows representative data of muropeptide analysis. The details of muropeptide profiles of repeats are shown in Table S3 in the supplemental material.
[b]Sum of the percentages of all muropeptides with 3-3 cross-links (CL) in the muropeptide profile. See Table S3 for complete data on muropeptide composition.
[c]ND, not detected. 3-3 cross-linked muropeptides were below the detection limit.
[d]−, not determined because the LptC-depleted cells lysed rapidly, preventing reliable peptidoglycan analysis.
[e]NT, not tested because cells do not lyse.

Upon shifting to the nonpermissive condition, LptC-depleted *ldt* mutant cultures (with the exception of Δ*ldtE* Δ*ldtF* mutant) decreased in optical density, and the cells lost viability as shown by their reduced ability to form colonies. Phase-contrast and fluorescence microscopy revealed bulges at variable positions on the cell surface, suggesting that the cellular integrity was compromised (Fig. 1C and F and Fig. S2 to S4). These effects were specific for the loss of LDTs forming 3-3 cross-links because the simultaneous removal of all Lpp attachment enzymes (*ldtA-C* deletion) did not result in lysis upon *lptC* depletion (Fig. S5A and B). In the lysis-prone *lptC*-depleted Δ*ldtD* or Δ*ldtE* mutants, the level of 3-3 cross-links was only slightly reduced compared to the *araB*p*lptC* parental strain (Table 1 and Table S3). The lysis phenotype of *araB*p*lptC* Δ*ldtD* cells was rescued by ectopic expression of native LdtD, but not LdtD^{C528A} in which the catalytic Cys residue is mutated to Ala (Fig. S5C), showing that the activity of LdtD is required to rescue cells from lysis upon OM defective assembly.

All strains with defective *ldt* genes lysed under nonpermissive conditions except the *araB*p*lptC* Δ*ldtE* Δ*ldtF* mutant which arrested growth like the *araB*p*lptC* parental strain (Fig. 1F and Fig. S4A and B). These cells displayed a high level (>8%) of 3-3 cross-links at all conditions (i.e., even without depletion of *lptC*) (Table 1). This suggests that LdtD is active and able to prevent lysis of these cells. In line with this finding, we indeed observed that ectopic expression of *ldtD* rescues all LptC-depleted single and multiple *ldt* mutant strains from lysis (Table 1 and Fig. S5D to H). Finally, the LptC-depleted Δ*ldtF* mutant produced 3-3 cross-links and lysed at nonpermissive conditions (Table 1 and Fig. S3C and D), but in sharp contrast to the other strains, *araB*p*lptC* Δ*ldtF* cells showed morphological defects even when grown at permissive conditions (Fig. S3D), and no

FIG 1 Legend (Continued)
of 0.2, harvested, washed three times, and resuspended in an arabinose-supplemented (+ Ara) or arabinose-free (no Ara) medium. (A and C) Growth was monitored by OD_{600} measurements (top panels) and by determining CFU (bottom panels). Growth curves shown are representative of at least three independent experiments. At $t = 120$, 210, and 270 min (arrows), samples were imaged (*araB*p*lptC* [B]; isogenic mutant deleted for *ldtD*, *ldtE*, and *ldtF* [D]). Phase-contrast images (top) and fluorescence images (bottom) are shown. Bars, 3 μm. (E) PG sacculi purified from *araB*p*lptC* cells grown in the presence of arabinose or after 210 min (2) or 270 min (3) growth in the absence of arabinose were digested with cellosyl, and the muropeptide composition was determined by HPLC. The graph shows the relative abundance of TetraTetra (with a 4-3 cross-link) and TetraTri(3-3) (with a 3-3 cross-link) muropeptides. The latter significantly increased upon depletion of LptC. (F) Cells of the *araB*p*lptC* conditional strain and isogenic mutants deleted for every *ldt* gene alone or in all possible combinations were grown in an arabinose-free medium as indicated above. Growth phenotypes are summarized as the slope of growth curves measured between 180 and 390 min. Positive and negative values indicate cell growth and cell lysis, respectively. Values are means plus standard deviations (SD) (error bars) from three independent experiments. The mean slope calculated from growth curves in arabinose-supplemented medium for the *araB*p*lptC* conditional strain and isogenic *ldt* mutants was 0.56 ± 0.03. The *ldt* genes are indicated by their loci shown by capital letters.

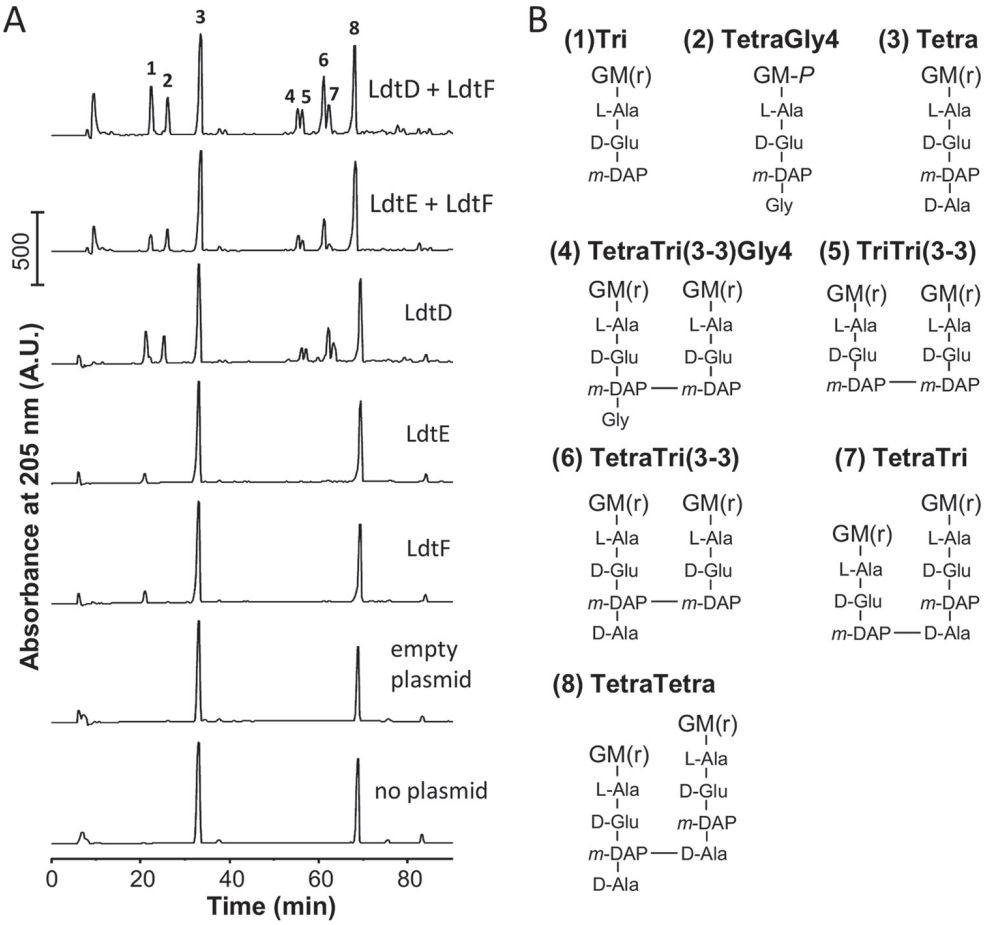

FIG 2 Ectopic expression of LdtD and LdtE-LdtF results in 3-3 cross-links. (A) Muropeptide profiles of *E. coli* BW25113Δ6LDT cells containing either no plasmid, empty plasmid (pJEH12), or plasmid with *ldtD* (pJEH12-*ldtD*), *ldtE* (pAMS01-*ldtE*), *ldtF* (pAMS02-*ldtF*), *ldtE-ldtF* (pAMS01-*ldtE* and pGS124), or *ldtD-ldtF* (pJEH12-*ldtD* and pGS124) grown in the presence of inducer. A.U., arbitrary units. (B) Structures of major peaks numbered in the top chromatogram in panel A. LDT products are muropeptides containing 3-3 cross-links (peaks 4 to 7), tripeptides (peaks 1, 5, and 7) and glycine at position 4 (Gly4, peaks 2 and 4). G, *N*-acetylglucosamine; M(r), *N*-acetylmuramitol; L-Ala, L-alanine; D-Glu, D-glutamic acid; D-Ala, D-alanine; *m*-DAP, *meso*-diaminopimelic acid. The detected muropeptides with tripeptides or glycine at position 4 (peaks 2 and 4) are typical products of side reactions in PG from cells with active LDTs (due to LD-CPase and Ala-Gly exchange reactions, respectively).

morphological defects were observed when *ldtF* was deleted in the *lptC*$^+$ background (Fig. S3B), suggesting that the deletion of *ldtF* caused additional problems to cells with depleted LptC levels.

Lysis of LptC-depleted cells could be caused by the accumulation of LPS at the outer leaflet of the CM (11, 14). We therefore assessed whether the LptC depletion-induced lysis occurs in cells with blocked LPS synthesis due to inhibition of LpxC by LPC-058 (48). We observed lysis in BW25113 Δ*ldtD* and *araB*p*lptC* Δ*ldtD* cells treated with LPC-058 but not in the corresponding parental strains (carrying a functional *ldtD* copy) treated with LPC-058 (Fig. 3A and B). These results suggest that lysis is not due to perturbation of the CM or periplasmic stress caused by depletion of a component of the Lpt machinery but is rather the consequence of lack of PG remodeling by LdtD.

The *ldtD* promoter is activated under envelope stress conditions. To assess how the *ldt* genes are regulated in the cell, we constructed transcriptional fusions of the promoter region of each *ldt* gene to *lacZ*, and the resulting plasmids with p*ldtD-lacZ*, p*ldtE-lacZ*, and p*ldtF-lacZ* were introduced into strain BW25113, the conditional *araB*-p*lptC* mutant, and their derivatives with deletion of *ldtD*, *ldtE*, and *ldtF* alone and in all possible combinations. β-Galactosidase activity was measured in extracts from cells collected at different time points during growth.

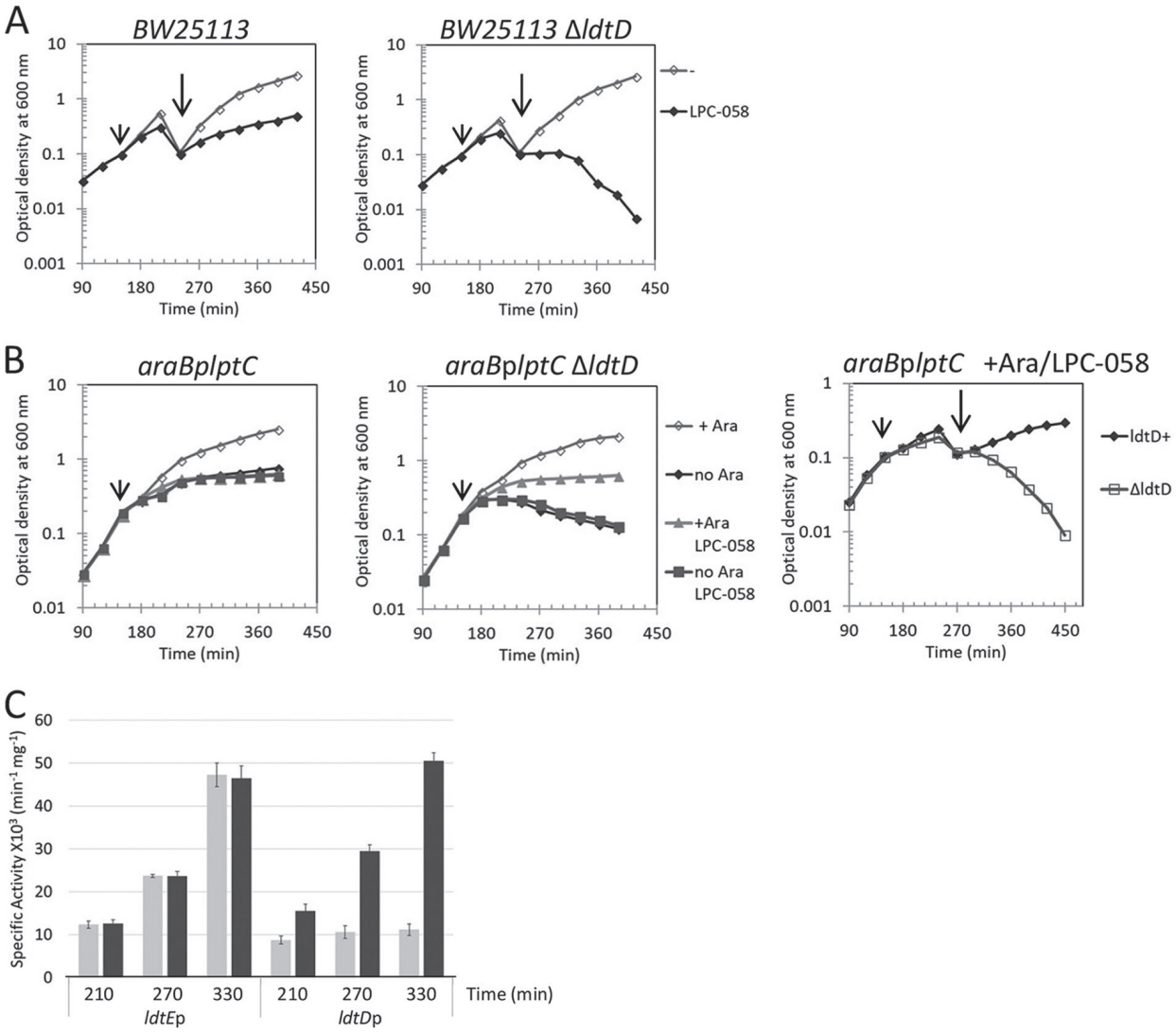

FIG 3 Inhibition of LPS synthesis causes lysis in *ldtD* deleted cells and activates the *ldtD* promoter. (A) *E. coli* BW25113 (left) and BW25113Δ*ldtD* (right) cells were grown in LB-Lennox medium. At $t = 150$ min, cells were treated with 0.031 μg/ml (1×MIC) of LPC-058 (short arrow) or not treated with LPC-058. Cell growth was monitored by OD_{600} measurements. When cells reached late exponential phase, cultures were diluted to an OD_{600} of 0.1 (long arrow), and growth was monitored by OD_{600} measurements. (B) Cells of *araBplptC* (left panel) and *araBplptC* Δ*ldtD* (middle and right panels) were grown in the presence of 0.2% arabinose to an OD_{600} of 0.2, harvested, washed three times, and resuspended in an arabinose-supplemented (+ Ara) or arabinose-free (no Ara) medium. Cell growth was then monitored by OD_{600} measurements. At $t = 150$ min, cells were treated with 0.006 μg/ml (0.75×MIC) of LPC-058 (short arrow) or not treated with LPC-057, and afterwards growth was monitored by OD_{600} measurements. When *araBplptC* and *araBplptC* Δ*ldtD* cells grown in the presence of arabinose and treated with LPC-058 (right panel) reached late exponential phase, the cultures were diluted to an OD_{600} of 0.1 (long arrow), and growth was monitored by OD_{600} measurements. Growth curves shown are representative of at least three independent experiments. (C) BW25113 cells carrying plasmids expressing *ldtD*p-*lacZ* and *ldtE*p-*lacZ* fusions were grown in LB Lennox broth. At $t = 150$ min cells were treated with 0.031 μg/ml (1×MIC) LPC-058 or not treated. β-Galactosidase specific activity was determined from cells collected at 210 min (OD_{600} of 0.5), 270 min (60 min after dilution), and 330 min (120 min after dilution). Light gray bars show strain BW25113, and gray bars show strain BW25113 treated with LPC-058. Note that *ldtE* expression is not affected by LPC-058.

The expression of *ldtE* and *ldtF* in the *lptC*$^+$ background was growth phase dependent. In the wild-type strain and the *araBplptC* conditional mutant grown under permissive and nonpermissive conditions, p*ldtE-lacZ* and p*ldtF-lacZ* were maximally expressed in stationary-phase cells (Fig. 4B and C). Consistent with their expression pattern, *ldtE* and *ldtF* were both regulated by RpoS, the alternative sigma factor for stationary-phase gene expression (49), and both genes lost their growth phase-dependent promoter activation in a BW25113Δ*rpoS* mutant (Fig. 4D).

The *ldtD* promoter was not activated in the wild-type *lptC*$^+$ strain and in *ldt* derivatives with the exception of the Δ*ldtE* Δ*ldtF* mutant and was up to eightfold

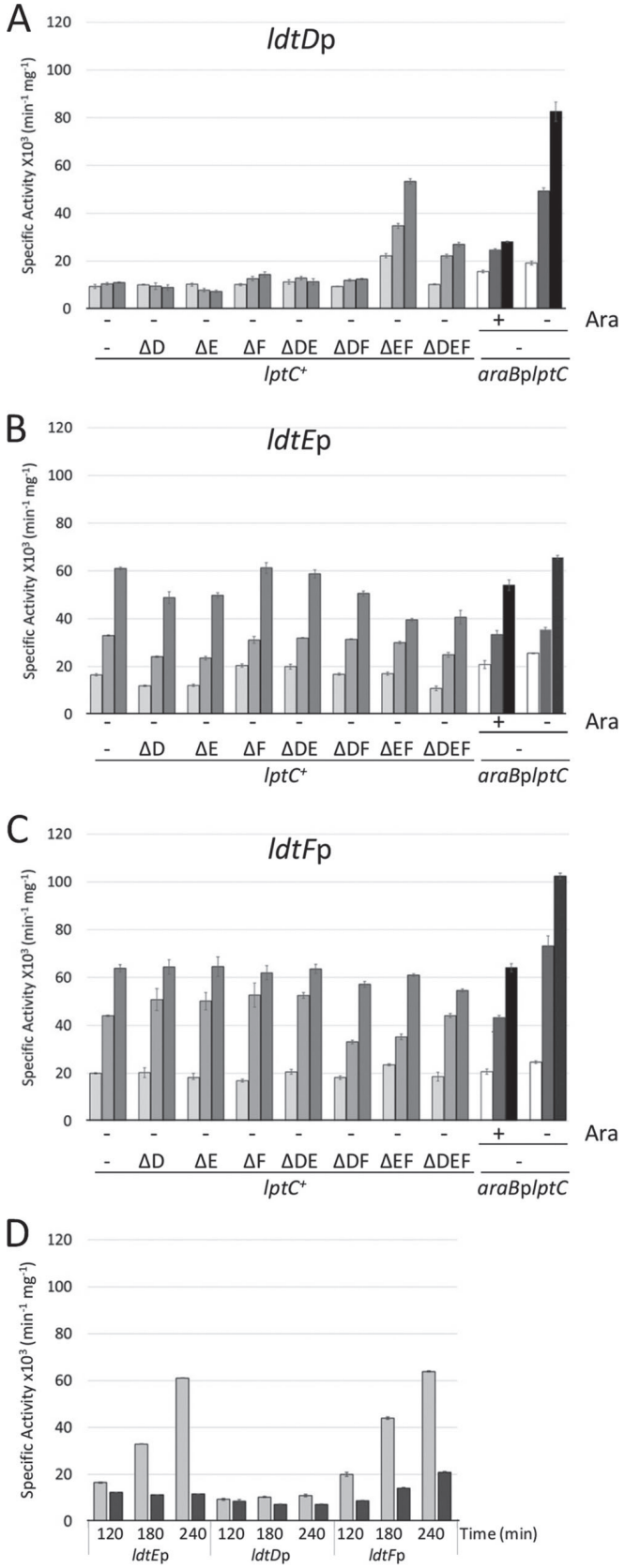

FIG 4 The *ldtD* promoter is activated under envelope stress conditions, and *ldtE* and *ldtF* are RpoS-regulated genes. Wild-type strain BW25113 (*lptC*⁺) and isogenic mutants with every *ldt* gene deleted alone and in all possible combinations were transformed with plasmids expressing *ldtD*p-*lacZ* (A), *ldtE*p-*lacZ* (B), or *ldtF*p-*lacZ* (C) fusions. Cells were grown in LD medium. β-Galactosidase specific activity

(Continued on next page)

activated by LptC depletion (Fig. 4A). We also observed *ldtD* but not *ldtE* activation in wild-type BW25113 cells carrying p*ldtD-lacZ* or p*ldtE-lacZ* and treated with LPC-058 (Fig. 3C).

In summary, *ldtE* and *ldtF* are housekeeping LDTs which share a growth phase-dependent activation profile under all conditions tested, and their expression was unaffected by the presence or absence of arabinose in the *araB*p*lptC* conditional strain. In contrast, *ldtD* was strongly expressed in the *lptC*$^+$ background in which both *ldtE* and *ldtF* were deleted, in LptC-depleted cells, and in cells with blocked LPS synthesis. Hence, LdtD is the stress LDT activated under cell envelope stress conditions or in the absence of the housekeeping LdtE/LtdF, consistent with the presence of increased levels of 3-3 cross-links under these conditions.

Growth arrest without lysis requires PG synthesis and maturation. Thus far, our data suggest that LDTs play a major role in PG remodeling in protecting cells from lysis upon LPS export pathway defects. LDTs can facilitate PG growth in certain β-lactam-resistant strains of *E. coli* and *E. faecium*, and in this situation, they function with a GTase domain of a bifunctional PG synthase, and a DD-CPase (42–45). LptC-depleted cells have been shown previously to have elevated levels of the bifunctional PBP1B and the DD-CPases PBP5 and PBP6a (46). PBP5 is the major DD-CPase active under standard laboratory conditions (32). PBP6a is an additional DD-CPase with an unknown physiological function, as it does not seem to be active under standard growth conditions (35).

We next asked whether bifunctional PBPs and DD-CPases are important to prevent lysis in LptC-depleted cells, as are the LDTs. PBP1B, but not PBP1A, was required to prevent lysis of LptC-depleted cells (Fig. 5A to D), and lysis could be prevented by ectopic expression of PBP1B (Fig. 5E). We next tested which of the two activities of PBP1B was needed to prevent lysis. The ectopic expression of PBP1B(S510A) with an active GTase and inactive TPase domain was fully functional in preventing lysis, showing that the TPase activity of PBP1B is not required (Fig. 5E). However, the ectopic expression of PBP1B(E233D) with inactive GTase function was unable to prevent lysis of LptC-depleted cells lacking wild-type PBP1B, suggesting that the GTase activity of PBP1B is crucial to prevent lysis (Fig. 5E). Consistent with this conclusion, lysis was also observed in cells lacking LpoB, a key activator of the GTase of PBP1B (26, 28, 50) (Fig. S4C and D). Another regulator of PBP1B, CpoB (27), was not required to prevent lysis upon LptC depletion (Fig. S4E), consistent with CpoB's exclusive regulation of the TPase function of PBP1B and our findings that TPase was not needed to prevent lysis.

Finally, survival of LptC-depleted cells required the DD-CPase gene *dacC*, encoding PBP6a, but not the *dacA* gene encoding PBP5 (Fig. 6). Therefore, preventing lysis upon severe LPS transport defect requires not only LDTs but also the GTase activity of PBP1B and the DD-CPase PBP6a, presumably to synthesize and to modify the nascent PG substrate for the LDTs.

LdtD interacts with PBP1B. Our data supported the hypothesis that LdtD may function with PBP1B to rescue sacculus integrity upon severe OM assembly defects. We then asked whether LdtD physically interacts with class A PBPs by mixing purified

FIG 4 Legend (Continued)
was calculated from cells collected at 120 min (OD_{600} of ~0.2) (light gray bars), 180 min (OD_{600} of ~0.8) (gray bars), and 210 min (OD_{600} of ~2.0) (dark gray bars) (left side). The *araB*p*lptC* conditional strain was transformed with plasmids expressing *ldtD*p-*lacZ* (A), *ldtE*p-*lacZ* (B), or *ldtF*p-*lacZ* (C). Cells were grown with 0.2% arabinose to an OD_{600} of 0.2, harvested, washed three times, and resuspended in an arabinose-supplemented (+ Ara) or arabinose-free (− Ara) medium. Samples for determination of β-galactosidase specific activity were collected at the time point at which the strains cultivated under nonpermissive conditions arrested growth (white bars) and 30 min (gray bars) and 60 min (black bars) afterwards (+Ara and no Ara conditions, right side). (D) BW25113 Δ*rpoS* cells carrying plasmids expressing *ldtD*p-*lacZ*, *ldtE*p-*lacZ*, or *ldtF*p-*lacZ* fusions were grown in LD broth. β-Galactosidase specific activity was determined from cells collected at 120 min (OD_{600} of 0.2), 180 min (OD_{600} of 0.8), and 210 min (OD_{600} of 2.0). Strains BW25113 (light gray bars) and BW25113Δ*rpoS* (gray bars) are shown. Note that *ldtD* expression is not affected in a Δ*rpoS* background. The values are the means ± SD from at least three independent experiments. All mutants were also transformed with the empty plasmid, and the mean of β-galactosidase specific activity calculated from cells grown in any condition was 249 ± 30 ($min^{-1}\,mg^{-1}$). In panels A to C, the *ldt* genes are indicated by their loci shown in capital letters.

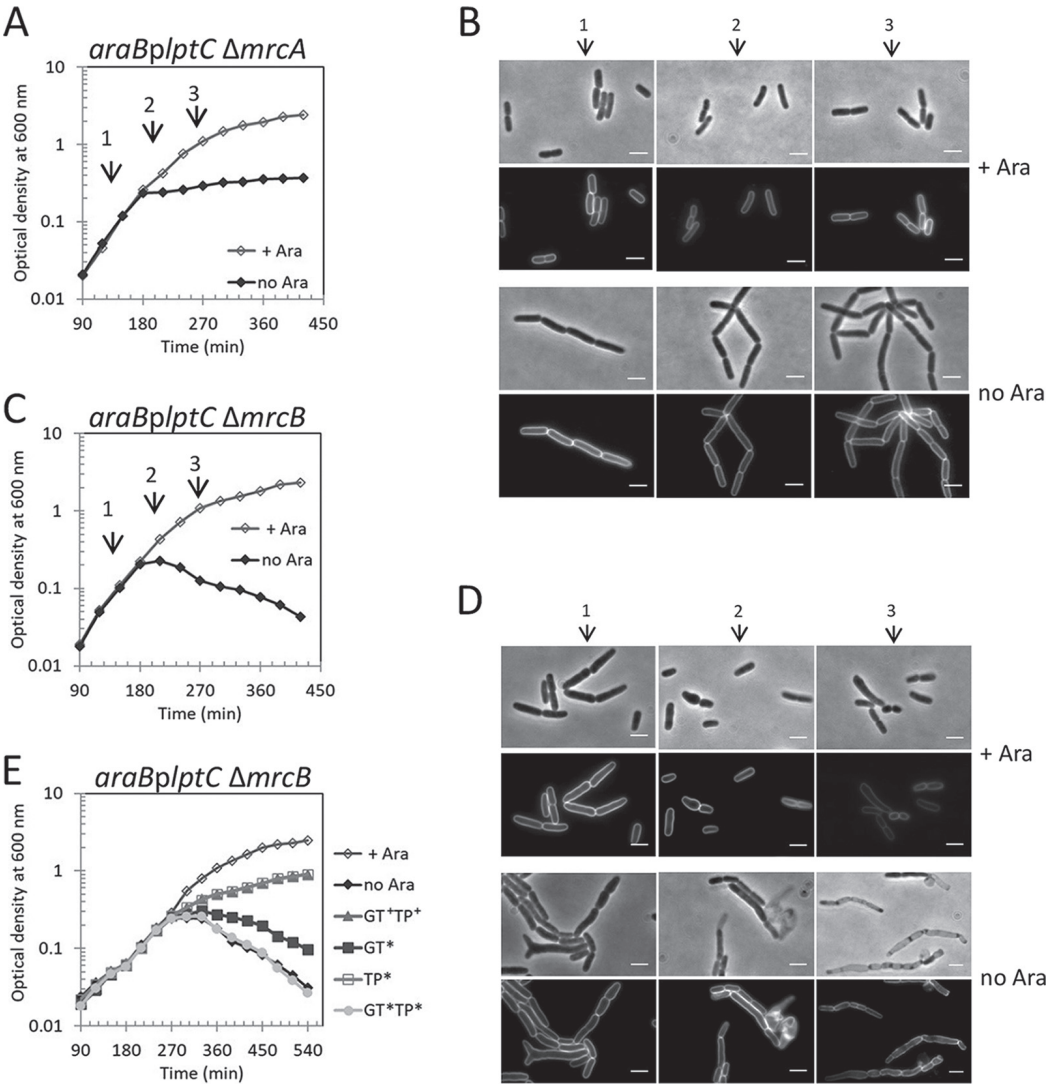

FIG 5 The GTase activity of PBP1B is required to prevent cell lysis upon defective OM assembly. Cultures of *araB*p*lptC* Δ*mrcA* (A) or *araB*p*lptC* Δ*mrcB* (C) strains lacking PBP1A and PBP1B, respectively, were grown with 0.2% arabinose to an OD_{600} of 0.2, harvested, washed three times, and resuspended in an arabinose-supplemented (+ Ara) or arabinose-free (no Ara) medium. Cell growth was then monitored by OD_{600} measurements. At $t = 120$ min, 210 min, and 270 min (arrows 1, 2, and 3, respectively), samples from *araB*p*lptC* Δ*mrc*A (B) and *araB*p*lptC* Δ*mrc*B (D) strains were collected for imaging. Phase-contrast images (top) and fluorescence images (bottom) are shown. Bars, 3 μm. (E) Complementation of the *araB*p*lptC* Δ*mrcB* lysis phenotype by ectopic expression of wild-type *mrcB* (GT^+TP^+), *mrcB* with mutated GTase (GT*), TPase (TP*), or both (TP*GT*). All mutants were grown in the presence of 0.2% arabinose at 30°C to an OD_{600} of 0.2, harvested, washed three times, and resuspended in an arabinose-free medium. The growth of the *araB*p*lptC* Δ*mrcB* strain in arabinose-supplemented medium is shown as a control. Cell growth was monitored by OD_{600} measurements. Growth curves shown are representative of at least three independent experiments.

oligohistidine-tagged PBP1A or PBP1B with untagged LdtD and assaying binding to Ni^{2+}-NTA beads. LdtD was pulled down by oligohistidine-tagged PBP1B, not by oligohistidine-tagged PBP1A or LpoB, or in the absence of tagged protein (Fig. 7A), suggesting a direct interaction with oligohistidine-tagged PBP1B. The pulldown was confirmed and extended by microscale thermophoresis, which revealed an interaction between LdtD and PBP1B, but not between LdtD and PBP1A. The K_D value of the LdtD-PBP1B interaction was 112 ± 33 nM (Fig. 7B). Moreover, PBP1B was pulled down by oligohistidine-tagged LdtD, expressed from the chromosome from its native promoter, only upon LptC depletion (Fig. 7C), and LdtD and PBP1B interacted in LptC-depleted cells as shown by chemical cross-linking followed by immunoprecipitation (Fig. 7D). These data suggest that a PBP1B-LdtD complex is formed in cells experiencing an OM assembly defect.

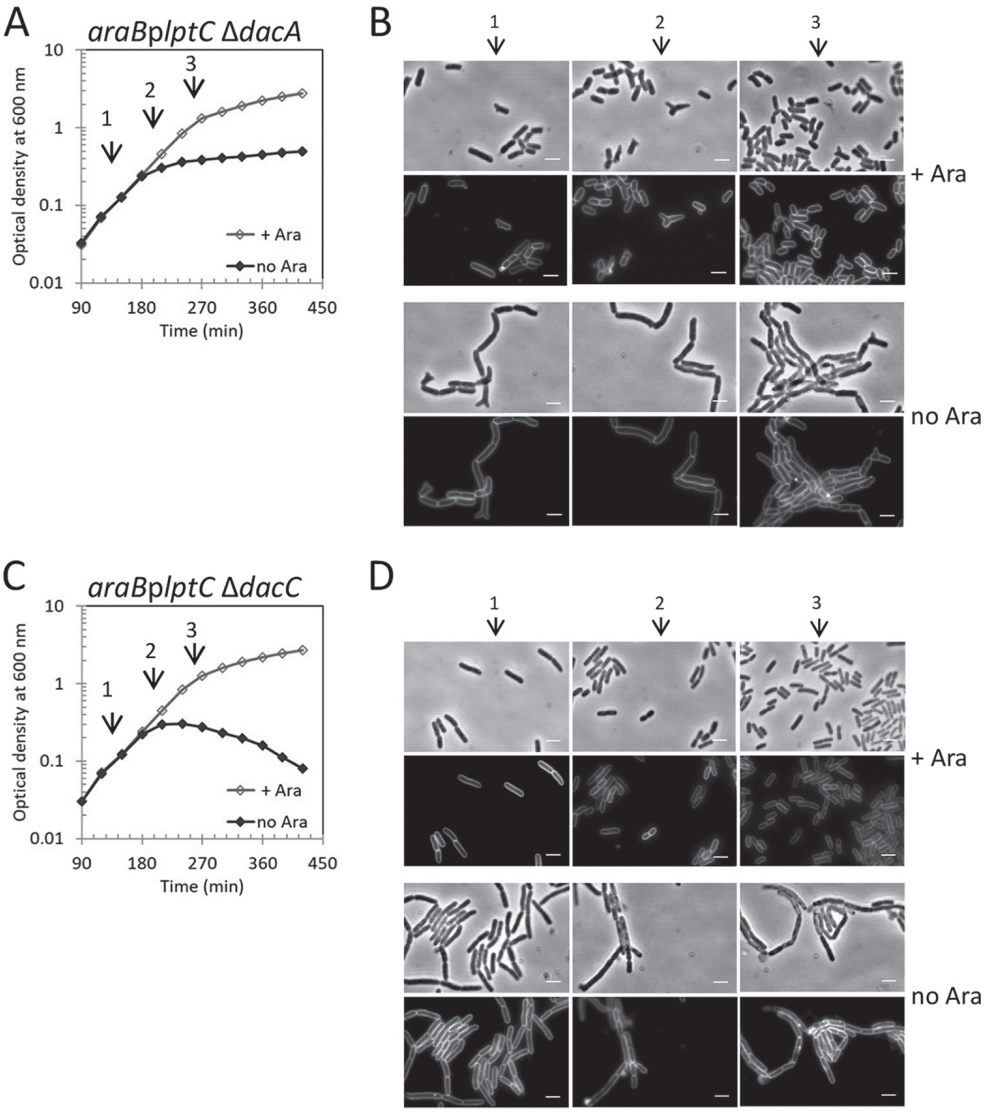

FIG 6 The DD-CPase PBP6a prevents cell lysis upon defective OM assembly. Cells of the *araB*p*lptC* Δ*dacA* (A) or *araB*p*lptC* Δ*dacC* (C) strain lacking PBP5 or PBP6a, respectively, were grown in the presence of 0.2% arabinose to an OD_{600} of 0.2, harvested, washed three times, and resuspended in an arabinose-supplemented (+ Ara) or arabinose-free (no Ara) medium. Cell growth was then monitored by OD_{600} measurements. Growth curves shown are representative of at least three independent experiments. At $t = 120$ min, 210 min, and 270 min (arrows 1, 2, and 3, respectively), samples from *araB*p*lptC* Δ*dacA* (B) and *araB*p*lptC* Δ*dacC* (D) strains were collected for imaging. Phase-contrast images (top) and fluorescence images (bottom) are shown. Bars, 3 μm.

LdtD forms 3-3 cross-links in mature and nascent PG. The LDT activity of LdtD has been demonstrated previously with a soluble disaccharide tetrapeptide substrate (45). Considering its role in PG remodeling and its interaction with PBP1B, we hypothesized that the enzyme must be active against larger PG fragments or even sacculi and/or nascent PG produced by PBP1B. We tested these possibilities by first incubating LdtD with either soluble glycan chains carrying non-cross-linked tetrapeptides (DS-tetra chains, the products of MepM [Fig. 8A]) and PG sacculi purified from strain BW25113Δ6LDT. LdtD was highly active against these substrates (Fig. 8A), utilizing almost all monomeric tetrapeptides to generate the 3-3 cross-linked dimer (disaccharide tetratripeptide, TetraTri). The high activity is particularly remarkable in the case of the sacculi, which after the reaction with LdtD contained an unusually high cross-linkage with ~84% of all muropeptides present in cross-links.

We next assayed the activity of LdtD during synthesis of PG *in vitro* using radiolabeled lipid II as the substrate in the presence of 10-fold excess of unlabeled PG sacculi.

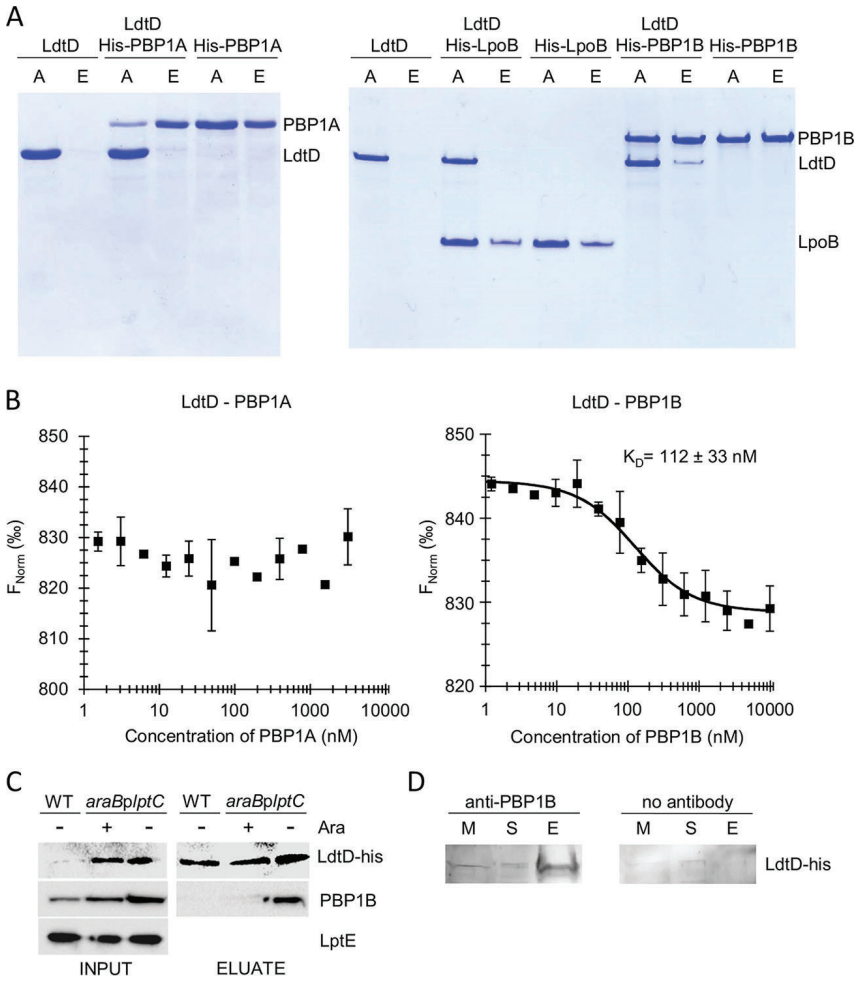

FIG 7 LdtD interacts with PBP1B *in vitro* and *in vivo*. (A) Coomassie blue-stained SDS-PAGE gel showing the pulldown of proteins to Ni^{2+}-NTA beads. LdtD bound to the beads and was present in the elution fraction (lanes E) only in the presence of oligohistidine-tagged PBP1B, and not in the presence of oligohistidine-tagged LpoB, oligohistidine-tagged PBP1A, or in the absence of another protein. A, applied sample. (B) Microscale thermophoresis curves showing that LdtD interacts with PBP1B and not with PBP1A. The K_D value for the LdtD-PBP1B interaction is indicated. Values are means ± SD from three independent experiments. (C). BW25113 *ldtD-his* and *araBpIptC ldtD-his* cells grown with and without arabinose (Ara) were treated with the DTSSP cross-linker. Cell-free extract was prepared, and LdtD-His was purified onto a Ni-NTA resin. PBP1B, LdtD-His, and LptE (as loading control) were immunodetected after SDS-PAGE and Western blotting. WT, wild type. (D) *In vivo* interaction between PBP1B and LdtD-His by cross-linking/coimmunoprecipitation assay. *araBpIptC ldtD-his* cells were treated with cross-linker DTSSP. The membrane fraction was prepared, and PBP1B was precipitated by specific antibody (the control sample received no antibody). LdtD-His was detected by Western blotting using specific anti-oligohistidine-tag antibody. M, membrane extract; S, supernatant; E, elution.

After the reaction, the products were digested with the muramidase cellosyl, and the resulting muropeptides were separated by HPLC using back-to-back UV and radioactivity detectors to monitor the products formed. LdtD produced a highly 3-3 cross-linked nascent PG, as seen by the abundant radiolabeled TetraTri(3-3) muropeptide present in the reaction with the TPase-inactive PBP1B(S510A) mutant, its activator LpoB, and the DD-CPase PBP6a (red trace in sample III [Fig. 8B]). In the absence of LdtD, PBP1B(S510A)/LpoB produced non-cross-linked glycan chains with pentapeptides of which most were trimmed by PBP6a to tetrapeptides (red traces in sample II [Fig. 8B]), and no 3-3 cross-links were observed in the UV traces (sample II [Fig. 8B]). Remarkably, LdtD preferentially acted on the nascent (radioactive) PG (red trace, sample III) despite the presence of an ~10-fold excess of unlabeled PG sacculi (black trace, sample III). The UV traces showed that ~52% of the unlabeled tetrapeptides were consumed by LdtD (comparing the black traces in samples II and III [Fig. 8B]), which was markedly less than

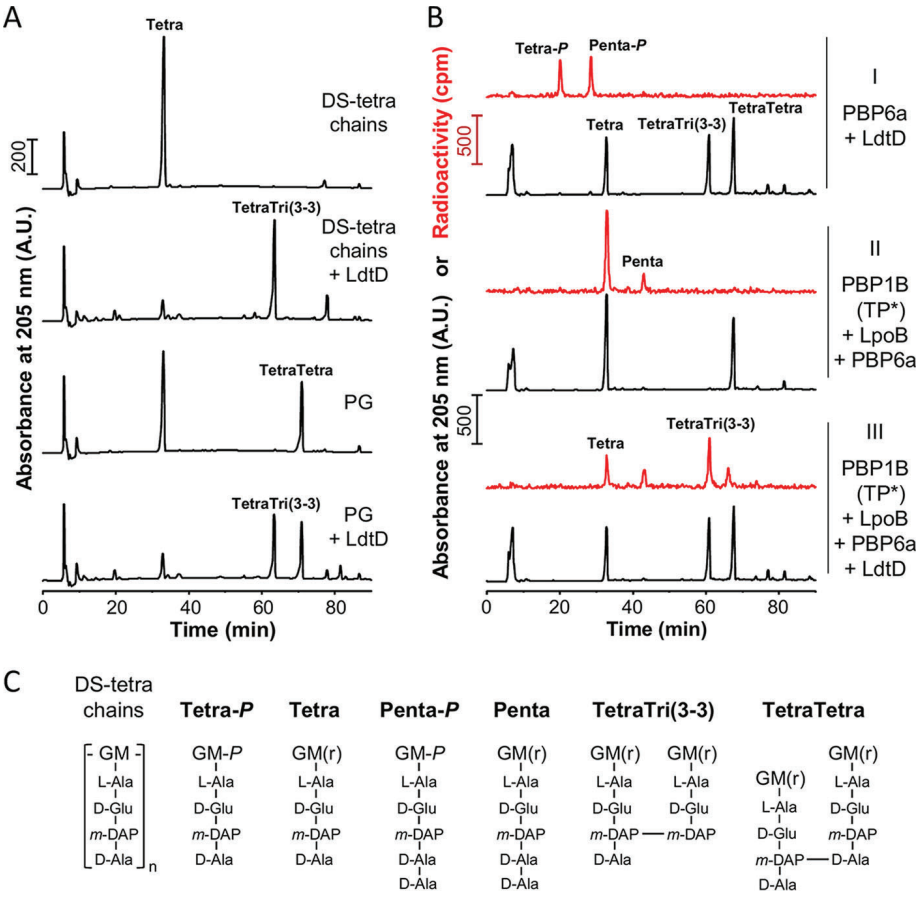

FIG 8 LdtD shows LD-TPase activity with different PG substrates. (A) HPLC chromatograms showing the formation of TetraTri(3–3) dimers by LdtD incubated with glycan chains harboring monomeric tetrapeptides (DS-tetra chains) or PG from BW25113Δ6LDT cells lacking all six *ldt* genes. Samples were digested with cellosyl and, reduced with sodium borohydride before HPLC analysis. (B) HPLC chromatograms obtained from samples upon incubating [^{14}C]Glc*N*Ac-labeled lipid II and PG from strain BW25113Δ6LDT and the proteins indicated to the right (I, II, and III indicate the different samples). Samples were digested with cellosyl, reduced with sodium borohydride, and subjected to HPLC analysis with detection of both UV signal (black traces) and radioactivity (red traces). PBP1B (TP*) is PBP1B with an inactive transpeptidase site due to the replacement of Ser-510 by Ala. Tetra-*P* and Penta-*P* originate from the hydrolysis of the respective pentapeptide and tetrapeptide versions of lipid II prior to HPLC analysis. (C) Proposed structures of muropeptides present in the fractions in panels A and B. G, *N*-acetylglucosamine; M, *N*-acetylmuramic acid; M(r), *N*-acetylmuramitol; M-*P*, N-acetylmuramic acid-1-phosphate; L-Ala, L-alanine; D-Glu, D-glutamic acid; D-Ala, D-alanine; *m*-DAP, *meso*-diaminopimelic acid.

the ~68% consumption of the radiolabeled tetrapeptides (comparing the red traces in samples II and III [Fig. 8B]). This suggests that LdtD prefers new PG, synthesized by PBP1B and trimmed by PBP6a, as the substrate. LdtD showed similar activity in reactions with PBP5 (instead of PBP6a), showing that both DD-CPases are capable of providing the tetrapeptide substrates (Fig. S6).

Together, the results of the activity assays support the phenotypic data and muropeptide analysis showing that LdtD is highly active in producing 3-3 cross-links in PG sacculi, and it is able to cooperate with the GTase activity of PBP1B and DD-CPases to utilize nascent PG as the substrate, consistent with a role in protective remodeling of PG during OM defective assembly.

DISCUSSION

LPS is essential in many Gram-negative bacteria with several notable exceptions, namely *Neisseria meningitidis* (51), *Moraxella catarrhalis* (52) and *Acinetobacter baumannii* (53), which can grow without LPS. *E. coli* requires LPS, and therefore, the depletion of LptC is not compatible with cell growth. However, although cells are unable to

continue growing, they do survive the block of LPS transport for several hours, and they resume growth once expression of LptC is restored.

In this work, we discovered a PG remodeling pathway involving LDTs that is essential for survival in cells with defective OM assembly, revealing a link between LPS export and a dedicated mode of PG synthesis. LDTs are not required in unstressed cells which, however, do remodel the PG to introduce a small number of 3-3 cross-links upon entry into stationary phase, perhaps to repair minor defects in PG. Expanding from previous work (39–41), we also show here that *E. coli* has an additional YkuD homologue, LdtF, which is not an active LD-TPase *per se* but might stimulate other LDTs.

Roles of the different LDTs. LdtE is the housekeeping LDT that is induced by RpoS when cells enter stationary phase (Fig. 4) consistent with the increase in 3-3 cross-links in stationary-phase cells (36, 54). LdtE seems to require LdtF for activity (Fig. 2) and the LdtE-LdtF couple forms most of the 3-3 cross-links in unstressed cells in which LdtD is poorly expressed (Table 1 and Fig. 4).

LDTs become essential to prevent cell lysis in LptC-depleted cells which upregulate *ldtD* and increase 3-3 cross-links (Fig. 4 and Table 1). Notably, LDTs are inhibited by sub-MIC copper ions which therefore reduce the robustness of the cell envelope to withstand LPS export stress (55). That LdtD plays a major role in PG remodeling during cell envelope stress is consistent with its induction by the Cpx-mediated stress response (56, 57). The single Δ*ldtE* or Δ*ldtF* mutants lysed upon LptC depletion despite the presence of a functional copy of *ldtD*; presumably, they are unable to accumulate sufficient LdtD activity to avoid lysis upon LptC depletion. In contrast, the Δ*ldtE* Δ*ldtF* double mutant is already stressed and has a high level of LdtD (and of 3-3 cross-links) before the depletion of LptC, preventing lysis once LptC is depleted (Table 1). This conclusion is further supported by the finding that ectopic expression of *ldtD* prevents lysis of all single and multiple *ldt* mutants depleted for LptC. For unknown reason, the *ldtF* mutant shows impaired cell morphology even before LptC depletion (see Fig. S3D in the supplemental material), suggesting that enhanced 3-3 cross-links are not always protective and that LdtF, which has been implicated in biofilm formation in enteroaggregative *E. coli* (58), has an additional role in the cell. Hence, our PG analysis highlights that an increased level of 3-3 cross-links cannot protect every *ldt* mutant cell from lysis, but importantly, the ability of cells to avoid lysis is always accompanied by an increase in 3-3 cross-links (Table 1).

LdtD is part of a "PG repair machine" with PBP1B/LpoB and PBP6a. LptC-depleted cells also required the GTase function of PBP1B, its activator LpoB, and the DD-CPase PBP6a (but not PBP1A or PBP5) to avoid lysis (Fig. 5 and 6). To our knowledge, this is the first condition where PBP6a becomes important. Our genetic evidence (Fig. 5C and D), the previously observed induction of the PBP1B and PBP6a genes in LptC-depleted cells (46), and the physical interaction of LdtD with PBP1B *in vitro* and in stressed cells (Fig. 7) all support a model in which PG remodeling machinery containing PBP1B/LpoB, LdtD, and PBP6a polymerizes PG strands (GTase of PBP1B), trims the pentapeptides (PBP6a), and utilizes the resulting tetrapeptides to form 3-3 cross-links (LdtD) (Fig. 9).

How does PG remodeling rescue cells from lysis? The PG layer is an elastic, net-like structure thought to be the major stress-bearing structure in the bacterial cell envelope allowing the cell to sustain large mechanical loads such as turgor pressure (37, 59). This prevailing dogma has been challenged by studies of phage lysis (60, 61) and more recently by Rojas and coworkers who showed that the OM and PG balance the mechanical loads during osmolality changes (62). Interestingly, a mutant defective in LPS export carrying the *imp4213* allele of *lptD* (63) produced an OM with an altered load-bearing capacity (62). Defects in the OM (i.e., perturbation of LPS layer and local loss of lipid asymmetry) may cause local mechanical stress on the PG structure, and hence, the LDT-mediated PG remodeling could strengthen the PG to rebalance the mechanical load between the OM and cell wall.

We also envision another possible reason why LDTs are essential upon defective LPS export. The size of pores in the PG net is too small for large transenvelope assemblies,

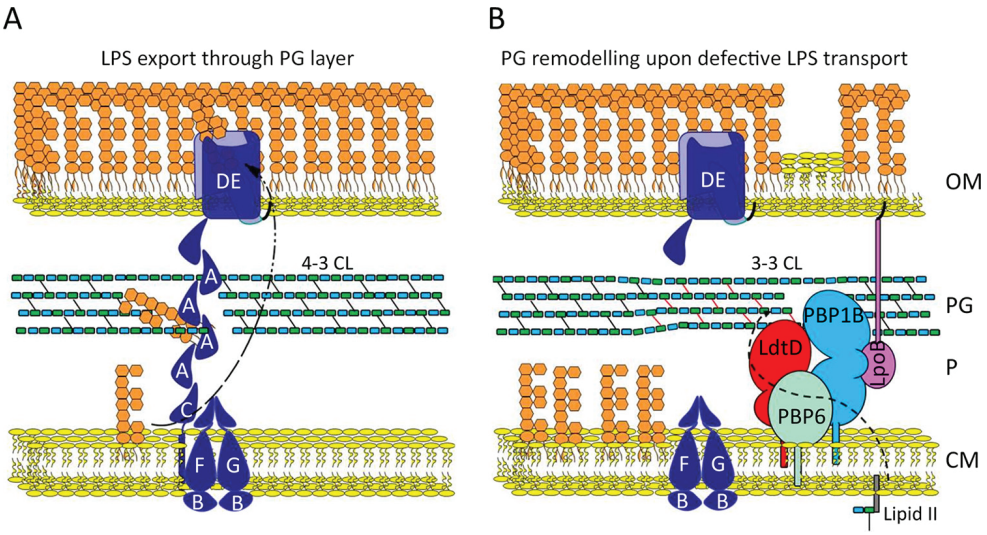

FIG 9 Role of a PG repair machine. (A) Nonperturbed LPS transport to the OM. (B) Upon LptC depletion, PBP1B-LpoB, LdtD, and PBP6a work in concert to repair the PG, synthesizing it locally with 3-3 cross-links (CL) (red line). Components of the Lpt machine are colored blue and indicated by capital letters.

such as the flagella and type II secretion systems, and hence, the assembly of these requires the local hydrolysis of the PG to increase the pore size (64, 65). The width of the periplasmic Lpt "bridge" together with its bulky LPS cargo (19, 66) is likely wider than the diameter of pores in PG (4.1 to 6.2 nm, depending on the turgor), necessitating the local hydrolysis of the PG, by an as yet unknown PG hydrolase, for the assembly of the Lpt machinery and rapid flux of LPS to the cell surface. The Lpt complex is known to disassemble when LPS transport is arrested due to depletion of LptC (14, 17, 18). Hence, it is possible that LDTs seal (repair) the PG locally after the disassembly of LPS export machines. We propose a dedicated PG repair machine, containing PBP1B/LpoB, LdtD, and PBP6a for this function (Fig. 9). The sequence of events that lead to cell lysis following the block of LPS biogenesis in the absence of LDTs are currently not known, but our data suggest that lysis is likely the consequence of the accumulation of defects in the PG that cannot be repaired and lead to unbalanced mechanical load between the OM and PG.

The GTase function of the PG repair machine is activated by the OM-anchored lipoprotein LpoB, which spans the periplasm to interact with the UB2H domain of PBP1B. Hence, apart from its role in the synthesis of "normal PG" (with 4-3 cross-links) during cell elongation and division, the PBP1B-LpoB system has another role in PG remodeling together with LdtD, producing PG with 3-3 cross-links. PBP1B/LpoB, LdtD, and the DD-CPase PBP5 enabled an *E. coli* mutant strain to grow in the presence of an otherwise lethal concentration of ampicillin (45), and PBP1B/LpoB (and not PBP1A/LpoA) promoted the recovery of PG-less L-form cells of *E. coli* to the walled state, generating a PG layer *de novo* (67). These observations and our own work highlight the versatility of the PBP1B/LpoB PG synthase/regulator pair, which is used by the cell in different processes and circumstances. PBP1A/LpoA are able to compensate for the loss of PBP1B/LpoB in normal growth, but they cannot compensate for the stress-related function of PBP1B/LpoB with LptD. Indeed, cells in which PG synthesis may be considered "weakened" by the lack of PBP1A or PBP5 do survive LPS transport defects just as well as wild-type cells. Hence, our combined data support a specific PG remodeling mechanism instead of nonspecific effects such as a general "weakening" of PG synthesis.

In summary, we discovered a role of 3-3 cross-links in the PG as a mean to fortify the sacculus in response to severe OM assembly defects. This functional connection between OM biogenesis and PG remodeling highlights an elegant and versatile mech-

anism bacteria employ to maintain the integrity of their essential cell envelope under a variety of growth and stress conditions.

MATERIALS AND METHODS

Bacterial strains, plasmids, and growth conditions. Bacterial strains and plasmids used in this work are listed in Table S1 in the supplemental material. Primers used are listed in Table S2. Cells were routinely grown aerobically at 37°C or 30°C in LB-Lennox medium (10 g/liter tryptone, 5 g/liter yeast extract, 5 g/liter NaCl) (Difco). When required, antibiotics or inducers were added: ampicillin (100 μg/ml), chloramphenicol (25 μg/ml), kanamycin (25 μg/ml), arabinose (0.2% [wt/vol]), IPTG (0.1 mM). For LptC depletion, bacteria were harvested from cultures with an OD_{600} of 0.2 by centrifugation, washed twice with LD, and diluted 100-fold in LD with or without arabinose. Cell growth was monitored by OD_{600} measurements, and viability was determined by quantifying the colony-forming units (CFU).

The phenotypes of *araB*p*lptC* and isogenic *ldt*s mutant derivatives were summarized as the slope of each growth curve between 180 and 390 minutes (Fig. 1F). Each slope was calculated as the regression line based on the data points identified by *y* values (expressed as absorbance at 600 nm) and *x* values (time expressed in hours) using Excel functions.

Other methods. The construction of plasmids and strains, microscopy of cells, protein purification and biochemical assays are described in detail in Text S1 in the supplemental material.

SUPPLEMENTAL MATERIAL

Supplemental material for this article may be found at https://doi.org/10.1128/mBio.02729-18.

TEXT S1, PDF file, 0.5 MB.
FIG S1, PDF file, 0.2 MB.
FIG S2, PDF file, 0.4 MB.
FIG S3, PDF file, 0.4 MB.
FIG S4, PDF file, 0.3 MB.
FIG S5, PDF file, 0.4 MB.
FIG S6, PDF file, 0.2 MB.
TABLE S1, DOCX file, 0.03 MB.
TABLE S2, DOCX file, 0.01 MB.
TABLE S3, XLSX file, 0.03 MB.

ACKNOWLEDGMENTS

We thank Alexander Egan and Katharina Peters (Newcastle University) for providing proteins, Daniel Kahne (Harvard University) for the kind gift of the anti-LptE antibody, Pei Zhou (Duke University) for the kind gift of LPC-058, Mohammed Terrak (University of Liège) for the expression plasmid for PBP1B(S510A), and Rick Lewis (Newcastle University) for critically reading the manuscript.

A.P., W.V., and T.D.B. were supported by the European Commission via the International Training Network Train2Target (721484). W.V. received support from the Wellcome Trust (101824/Z/13/Z). T.D.B. and W.V. received support from the NAPCLI project within the JPI AMR program (ZonMW project 60-60900-98-207; MR/N501840/1).

REFERENCES

1. Silhavy TJ, Kahne D, Walker S. 2010. The bacterial cell envelope. Cold Spring Harb Perspect Biol 2:a000414. https://doi.org/10.1101/cshperspect.a000414.
2. Vollmer W, Blanot D, de Pedro MA. 2008. Peptidoglycan structure and architecture. FEMS Microbiol Rev 32:149–167. https://doi.org/10.1111/j.1574-6976.2007.00094.x.
3. Kamio Y, Nikaido H. 1976. Outer membrane of *Salmonella typhimurium*: accessibility of phospholipid head groups to phospholipase c and cyanogen bromide activated dextran in the external medium. Biochemistry 15:2561–2570.
4. Nikaido H. 2003. Molecular basis of bacterial outer membrane permeability revisited. Microbiol Mol Biol Rev 67:593–656.
5. Raetz CR, Whitfield C. 2002. Lipopolysaccharide endotoxins. Annu Rev Biochem 71:635–700. https://doi.org/10.1146/annurev.biochem.71.110601.135414.
6. Polissi A, Georgopoulos C. 1996. Mutational analysis and properties of the *msbA* gene of *Escherichia coli*, coding for an essential ABC family transporter. Mol Microbiol 20:1221–1233.
7. Zhou Z, White KA, Polissi A, Georgopoulos C, Raetz CR. 1998. Function of *Escherichia coli* MsbA, an essential ABC family transporter, in lipid A and phospholipid biosynthesis. J Biol Chem 273:12466–12475.
8. Sperandeo P, Martorana AM, Polissi A. 2017. The lipopolysaccharide transport (Lpt) machinery: a nonconventional transporter for lipopolysaccharide assembly at the outer membrane of Gram-negative bacteria. J Biol Chem 292:17981–17990. https://doi.org/10.1074/jbc.R117.802512.
9. Sperandeo P, Martorana AM, Polissi A. 2017. Lipopolysaccharide biogenesis and transport at the outer membrane of Gram-negative bacteria. Biochim Biophys Acta 1862:1451–1460. https://doi.org/10.1016/j.bbalip.2016.10.006.
10. Braun M, Silhavy TJ. 2002. Imp/OstA is required for cell envelope biogenesis in *Escherichia coli*. Mol Microbiol 45:1289–1302.
11. Chng SS, Gronenberg LS, Kahne D. 2010. Proteins required for lipopolysaccharide assembly in *Escherichia coli* form a transenvelope complex. Biochemistry 49:4565–4567. https://doi.org/10.1021/bi100493e.
12. Ruiz N, Gronenberg LS, Kahne D, Silhavy TJ. 2008. Identification of two inner-membrane proteins required for the transport of lipopolysaccha-

ride to the outer membrane of *Escherichia coli*. Proc Natl Acad Sci U S A 105:5537–5542. https://doi.org/10.1073/pnas.0801196105.
13. Sperandeo P, Cescutti R, Villa R, Di Benedetto C, Candia D, Dehò G, Polissi A. 2007. Characterization of *lptA* and *lptB*, two essential genes implicated in lipopolysaccharide transport to the outer membrane of *Escherichia coli*. J Bacteriol 189:244–253. https://doi.org/10.1128/JB.01126-06.
14. Sperandeo P, Lau FK, Carpentieri A, De Castro C, Molinaro A, Dehò G, Silhavy TJ, Polissi A. 2008. Functional analysis of the protein machinery required for transport of lipopolysaccharide to the outer membrane of *Escherichia coli*. J Bacteriol 190:4460–4469. https://doi.org/10.1128/JB.00270-08.
15. Wu T, McCandlish AC, Gronenberg LS, Chng SS, Silhavy TJ, Kahne D. 2006. Identification of a protein complex that assembles lipopolysaccharide in the outer membrane of *Escherichia coli*. Proc Natl Acad Sci U S A 103:11754–11759. https://doi.org/10.1073/pnas.0604744103.
16. Freinkman E, Okuda S, Ruiz N, Kahne D. 2012. Regulated assembly of the transenvelope protein complex required for lipopolysaccharide export. Biochemistry 51:4800–4806. https://doi.org/10.1021/bi300592c.
17. Sperandeo P, Villa R, Martorana AM, Samalikova M, Grandori R, Dehò G, Polissi A. 2011. New insights into the Lpt machinery for lipopolysaccharide transport to the cell surface: LptA-LptC interaction and LptA stability as sensors of a properly assembled transenvelope complex. J Bacteriol 193:1042–1053. https://doi.org/10.1128/JB.01037-10.
18. Villa R, Martorana AM, Okuda S, Gourlay LJ, Nardini M, Sperandeo P, Dehò G, Bolognesi M, Kahne D, Polissi A. 2013. The *Escherichia coli* Lpt transenvelope protein complex for lipopolysaccharide export is assembled via conserved structurally homologous domains. J Bacteriol 195:1100–1108. https://doi.org/10.1128/JB.02057-12.
19. Okuda S, Sherman DJ, Silhavy TJ, Ruiz N, Kahne D. 2016. Lipopolysaccharide transport and assembly at the outer membrane: the PEZ model. Nat Rev Microbiol 14:337–345. https://doi.org/10.1038/nrmicro.2016.25.
20. Neidhardt FC, Umbarger HE. 1996. Chemical composition of *Escherichia coli*, p 1–13. *In* Neidhardt FC et al. (ed), Escherichia coli and Salmonella: cellular and molecular biology. ASM Press, Washington, DC.
21. Typas A, Banzhaf M, Gross CA, Vollmer W. 2011. From the regulation of peptidoglycan synthesis to bacterial growth and morphology. Nat Rev Microbiol 10:123–136. https://doi.org/10.1038/nrmicro2677.
22. Banzhaf M, van den Berg van Saparoea B, Terrak M, Fraipont C, Egan A, Philippe J, Zapun A, Breukink E, Nguyen-Distèche M, den Blaauwen T, Vollmer W. 2012. Cooperativity of peptidoglycan synthases active in bacterial cell elongation. Mol Microbiol 85:179–194. https://doi.org/10.1111/j.1365-2958.2012.08103.x.
23. Bertsche U, Breukink E, Kast T, Vollmer W. 2005. *In vitro* murein peptidoglycan synthesis by dimers of the bifunctional transglycosylase-transpeptidase PBP1B from *Escherichia coli*. J Biol Chem 280:38096–38101. https://doi.org/10.1074/jbc.M508646200.
24. Born P, Breukink E, Vollmer W. 2006. In vitro synthesis of cross-linked murein and its attachment to sacculi by PBP1A from *Escherichia coli*. J Biol Chem 281:26985–26993. https://doi.org/10.1074/jbc.M604083200.
25. Paradis-Bleau C, Markovski M, Uehara T, Lupoli TJ, Walker S, Kahne DE, Bernhardt TG. 2010. Lipoprotein cofactors located in the outer membrane activate bacterial cell wall polymerases. Cell 143:1110–1120. https://doi.org/10.1016/j.cell.2010.11.037.
26. Typas A, Banzhaf M, van den Berg van Saparoea B, Verheul J, Biboy J, Nichols RJ, Zietek M, Beilharz K, Kannenberg K, von Rechenberg M, Breukink E, den Blaauwen T, Gross CA, Vollmer W. 2010. Regulation of peptidoglycan synthesis by outer-membrane proteins. Cell 143:1097–1109. https://doi.org/10.1016/j.cell.2010.11.038.
27. Gray AN, Egan AJ, Van't Veer IL, Verheul J, Colavin A, Koumoutsi A, Biboy J, Altelaar AF, Damen MJ, Huang KC, Simorre JP, Breukink E, den Blaauwen T, Typas A, Gross CA, Vollmer W. 2015. Coordination of peptidoglycan synthesis and outer membrane constriction during Escherichia coli cell division. Elife 4:e07118. https://doi.org/10.7554/eLife.07118.
28. Egan AJ, Jean NL, Koumoutsi A, Bougault CM, Biboy J, Sassine J, Solovyova AS, Breukink E, Typas A, Vollmer W, Simorre JP. 2014. Outer-membrane lipoprotein LpoB spans the periplasm to stimulate the peptidoglycan synthase PBP1B. Proc Natl Acad Sci U S A 111:8197–8202. https://doi.org/10.1073/pnas.1400376111.
29. Jean NL, Bougault CM, Lodge A, Derouaux A, Callens G, Egan AJ, Ayala I, Lewis RJ, Vollmer W, Simorre JP. 2014. Elongated structure of the outer-membrane activator of peptidoglycan synthesis LpoA: implications for PBP1A stimulation. Structure 22:1047–1054. https://doi.org/10.1016/j.str.2014.04.017.
30. Sathiyamoorthy K, Vijayalakshmi J, Tirupati B, Fan L, Saper MA. 2017. Structural analyses of the *Haemophilus influenzae* peptidoglycan synthase activator LpoA suggest multiple conformations in solution. J Biol Chem 292:17626–17642. https://doi.org/10.1074/jbc.M117.804997.
31. Baquero MR, Bouzon M, Quintela JC, Ayala JA, Moreno F. 1996. *dacD*, an *Escherichia coli* gene encoding a novel penicillin-binding protein (PBP6b) with DD-carboxypeptidase activity. J Bacteriol 178:7106–7111.
32. Nelson DE, Young KD. 2001. Contributions of PBP 5 and DD-carboxypeptidase penicillin binding proteins to maintenance of cell shape in *Escherichia coli*. J Bacteriol 183:3055–3064. https://doi.org/10.1128/JB.183.10.3055-3064.2001.
33. Nelson DE, Young KD. 2000. Penicillin binding protein 5 affects cell diameter, contour, and morphology of *Escherichia coli*. J Bacteriol 182:1714–1721.
34. Ghosh AS, Young KD. 2003. Sequences near the active site in chimeric penicillin-binding proteins 5 and 6 affect uniform morphology of *Escherichia coli*. J Bacteriol 185:2178–2186.
35. Peters K, Kannan S, Rao VA, Biboy J, Vollmer D, Erickson SW, Lewis RJ, Young KD, Vollmer W. 2016. The redundancy of peptidoglycan carboxypeptidases ensures robust cell shape maintenance in *Escherichia coli*. mBio 7:e00819-16. https://doi.org/10.1128/mBio.00819-16.
36. Glauner B, Holtje JV, Schwarz U. 1988. The composition of the murein of *Escherichia coli*. J Biol Chem 263:10088–10095.
37. Holtje JV. 1998. Growth of the stress-bearing and shape-maintaining murein sacculus of *Escherichia coli*. Microbiol Mol Biol Rev 62:181–203.
38. Biarrotte-Sorin S, Hugonnet JE, Delfosse V, Mainardi JL, Gutmann L, Arthur M, Mayer C. 2006. Crystal structure of a novel beta-lactam-insensitive peptidoglycan transpeptidase. J Mol Biol 359:533–538. https://doi.org/10.1016/j.jmb.2006.03.014.
39. Magnet S, Bellais S, Dubost L, Fourgeaud M, Mainardi JL, Petit-Frere S, Marie A, Mengin-Lecreulx D, Arthur M, Gutmann L. 2007. Identification of the L,D-transpeptidases responsible for attachment of the Braun lipoprotein to *Escherichia coli* peptidoglycan. J Bacteriol 189:3927–3931. https://doi.org/10.1128/JB.00084-07.
40. Magnet S, Dubost L, Marie A, Arthur M, Gutmann L. 2008. Identification of the L,D-transpeptidases for peptidoglycan cross-linking in *Escherichia coli*. J Bacteriol 190:4782–4785. https://doi.org/10.1128/JB.00025-08.
41. Sanders AN, Pavelka MS. 2013. Phenotypic analysis of *Escherichia coli* mutants lacking L,D-transpeptidases. Microbiology 159:1842–1852. https://doi.org/10.1099/mic.0.069211-0.
42. Mainardi JL, Fourgeaud M, Hugonnet JE, Dubost L, Brouard JP, Ouazzani J, Rice LB, Gutmann L, Arthur M. 2005. A novel peptidoglycan cross-linking enzyme for a beta-lactam-resistant transpeptidation pathway. J Biol Chem 280:38146–38152. https://doi.org/10.1074/jbc.M507384200.
43. Mainardi JL, Legrand R, Arthur M, Schoot B, van Heijenoort J, Gutmann L. 2000. Novel mechanism of beta-lactam resistance due to bypass of DD-transpeptidation in *Enterococcus faecium*. J Biol Chem 275:16490–16496. https://doi.org/10.1074/jbc.M909877199.
44. Mainardi JL, Morel V, Fourgeaud M, Cremniter J, Blanot D, Legrand R, Frehel C, Arthur M, Van Heijenoort J, Gutmann L. 2002. Balance between two transpeptidation mechanisms determines the expression of beta-lactam resistance in *Enterococcus faecium*. J Biol Chem 277:35801–35807. https://doi.org/10.1074/jbc.M204319200.
45. Hugonnet JE, Mengin-Lecreulx D, Monton A, den Blaauwen T, Carbonnelle E, Veckerle C, Brun YV, van Nieuwenhze M, Bouchier C, Tu K, Rice LB, Arthur M. 2016. Factors essential for L,D-transpeptidase-mediated peptidoglycan cross-linking and beta-lactam resistance in *Escherichia coli*. Elife 5:e19469. https://doi.org/10.7554/eLife.19469.
46. Martorana AM, Motta S, Di Silvestre D, Falchi F, Dehò G, Mauri P, Sperandeo P, Polissi A. 2014. Dissecting *Escherichia coli* outer membrane biogenesis using differential proteomics. PLoS One 9:e100941. https://doi.org/10.1371/journal.pone.0100941.
47. Kuru E, Lambert C, Rittichier J, Till R, Ducret A, Derouaux A, Gray J, Biboy J, Vollmer W, VanNieuwenhze M, Brun YV, Sockett RE. 2017. Fluorescent D-amino-acids reveal bi-cellular cell wall modifications important for *Bdellovibrio bacteriovorus* predation. Nat Microbiol 2:1648–1657. https://doi.org/10.1038/s41564-017-0029-y.
48. Lee CJ, Liang X, Wu Q, Najeeb J, Zhao J, Gopalaswamy R, Titecat M, Sebbane F, Lemaitre N, Toone EJ, Zhou P. 2016. Drug design from the cryptic inhibitor envelope. Nat Commun 7:10638. https://doi.org/10.1038/ncomms10638.
49. Battesti A, Majdalani N, Gottesman S. 2011. The RpoS-mediated general stress response in *Escherichia coli*. Annu Rev Microbiol 65:189–213. https://doi.org/10.1146/annurev-micro-090110-102946.
50. Egan AJF, Maya-Martinez R, Ayala I, Bougault CM, Banzhaf M, Breukink E,

Vollmer W, Simorre JP. 2018. Induced conformational changes activate the peptidoglycan synthase PBP1B. Mol Microbiol 110:335–356. https://doi.org/10.1111/mmi.14082.
51. Steeghs L, den Hartog R, den Boer A, Zomer B, Roholl P, van der Ley P. 1998. Meningitis bacterium is viable without endotoxin. Nature 392:449–450. https://doi.org/10.1038/33046.
52. Peng D, Hong W, Choudhury BP, Carlson RW, Gu XX. 2005. Moraxella catarrhalis bacterium without endotoxin, a potential vaccine candidate. Infect Immun 73:7569–7577. https://doi.org/10.1128/IAI.73.11.7569-7577.2005.
53. Moffatt JH, Harper M, Harrison P, Hale JD, Vinogradov E, Seemann T, Henry R, Crane B, St Michael F, Cox AD, Adler B, Nation RL, Li J, Boyce JD. 2010. Colistin resistance in *Acinetobacter baumannii* is mediated by complete loss of lipopolysaccharide production. Antimicrob Agents Chemother 54:4971–4977. https://doi.org/10.1128/AAC.00834-10.
54. Pisabarro AG, de Pedro MA, Vázquez D. 1985. Structural modifications in the peptidoglycan of *Escherichia coli* associated with changes in the state of growth of the culture. J Bacteriol 161:238–242.
55. Peters K, Pazos M, Edoo Z, Hugonnet JE, Martorana A, Polissi A, VanNieuwenhze MS, Arthur M, Vollmer W. 2018. Copper inhibits peptidoglycan LD-transpeptidases suppressing β-lactam resistance due to by-pass of penicillin-binding proteins. Proc Natl Acad Sci U S A 115:10786–10791. https://doi.org/10.1073/pnas.1809285115.
56. Bernal-Cabas M, Ayala JA, Raivio TL. 2015. The Cpx envelope stress response modifies peptidoglycan cross-linking via the L,D-transpeptidase LdtD and the novel protein YgaU. J Bacteriol 197:603–614. https://doi.org/10.1128/JB.02449-14.
57. Delhaye A, Collet JF, Laloux G. 2016. Fine-tuning of the Cpx envelope stress response is required for cell wall homeostasis in *Escherichia coli*. mBio 7:e00047-16. https://doi.org/10.1128/mBio.00047-16.
58. Sheikh J, Hicks S, Dall'Agnol M, Phillips AD, Nataro JP. 2001. Roles for Fis and YafK in biofilm formation by enteroaggregative *Escherichia coli*. Mol Microbiol 41:983–997.
59. Deng Y, Sun M, Shaevitz JW. 2011. Direct measurement of cell wall stress stiffening and turgor pressure in live bacterial cells. Phys Rev Lett 107:158101. https://doi.org/10.1103/PhysRevLett.107.158101.
60. Berry J, Rajaure M, Pang T, Young R. 2012. The spanin complex is essential for lambda lysis. J Bacteriol 194:5667–5674. https://doi.org/10.1128/JB.01245-12.
61. Rajaure M, Berry J, Kongari R, Cahill J, Young R. 2015. Membrane fusion during phage lysis. Proc Natl Acad Sci U S A 112:5497–5502. https://doi.org/10.1073/pnas.1420588112.
62. Rojas ER, Billings G, Odermatt PD, Auer GK, Zhu L, Miguel A, Chang F, Weibel DB, Theriot JA, Huang KC. 2018. The outer membrane is an essential load-bearing element in Gram-negative bacteria. Nature 559:617–621. https://doi.org/10.1038/s41586-018-0344-3.
63. Ruiz N, Falcone B, Kahne D, Silhavy TJ. 2005. Chemical conditionality: a genetic strategy to probe organelle assembly. Cell 121:307–317. https://doi.org/10.1016/j.cell.2005.02.014.
64. Herlihey FA, Moynihan PJ, Clarke AJ. 2014. The essential protein for bacterial flagella formation FlgJ functions as a beta-N-acetylglucosaminidase. J Biol Chem 289:31029–31042. https://doi.org/10.1074/jbc.M114.603944.
65. Vanderlinde EM, Strozen TG, Hernandez SB, Cava F, Howard SP. 2017. Alterations in peptidoglycan cross-linking suppress the secretin assembly defect caused by mutation of GspA in the type II secretion system. J Bacteriol 199:e00617-16. https://doi.org/10.1128/JB.00617-16.
66. Le Brun AP, Clifton LA, Halbert CE, Lin B, Meron M, Holden PJ, Lakey JH, Holt SA. 2013. Structural characterization of a model gram-negative bacterial surface using lipopolysaccharides from rough strains of *Escherichia coli*. Biomacromolecules 14:2014–2022. https://doi.org/10.1021/bm400356m.
67. Ranjit DK, Jorgenson MA, Young KD. 2017. PBP1B glycosyltransferase and transpeptidase activities play different essential roles during the de novo regeneration of rod morphology in *Escherichia coli*. J Bacteriol 199:e00612-16. https://doi.org/10.1128/JB.00612-16.

SUPPLEMENTAL MATERIAL

Figures S1: Peptidoglycan cross-linking reactions and sequence alignment of the LdtD, LdtE, and LdtF proteins.

Figure S2: Deletion of *ldtD*, *ldtE*, and *ldtD ldtE* in the *araB*p*lptC* conditional strain compromises cell viability under nonpermissive conditions.

Figure S3: Phenotypes of wild-type BW25113 (*lptC*$^{+}$) and *araB*p*lptC* conditional strains lacking *ldtF* or *ldtD ldtF*.

Figure S4: Growth profiles and cell imaging of *araB*p*lptC* Δ*ldtE* Δ*ldtF* and *araB*p*lptC* Δ*lpoB* strains and growth profile of the *araB*p*lptC* Δ*cpoB* strain.

Figure S5: Growth profiles of *araB*p*lptC* Δ*ldtA* Δ*ldtB* Δ*ldtC* and *araB*p*lptC* Δ*ldtA* Δ*ldtB* Δ*ldtC* Δ*ldtD* Δ*ldtE* Δ*ldtF* strains. The *araB*p*lptC* strain with different combinations of *ldt* genes deleted was complemented by ectopic expression of wild-type *ldtD*.

Figure S6: LdtD is active during in vitro PG synthesis in the presence of PBP1B(TP*), LpoB, and PBP5.

Text S1: Details of the methods of strain and plasmid construction, protein purification procedures, protein-protein interaction protocols, and activity assays.

Table S1: Bacterial strains and plasmids used in this study.

Table S2: Oligonucleotides used in this study.

Table S3: Muropeptide composition of *ldt* mutant strains with or without (separate file) depletion of *lptC*.

A

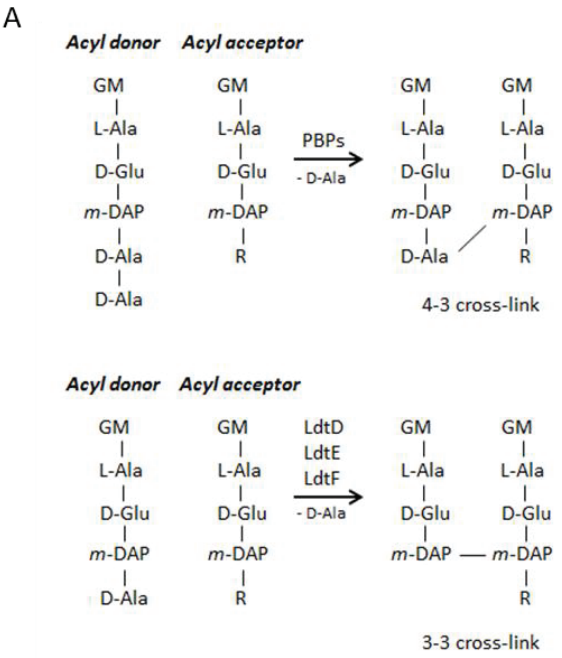

B

```
LdtD      GQLPTFVAGLAPQHPQYAAMHESLLALLCDTKPWPQLTGKATLRPGQWSNDVPALREILQ
LdtE      -------------------MKRASLL-T------LTLIGAFSAIQAAWAVDYPLPPTG--
LdtF      -------------------MRKIALILA------MLLIPCVSF-----------------
                             *:.  *          *    :

LdtD      RTGMLDGGPKITLPGDDTPTDAVVSPSAVTVETAETKPMDKQTTSRSKPAPAVRAAYDNE
LdtE      -SRLVGQNQTY-------------------TVQ-----------------------EGDKN
LdtF      -AGL-------------------------------------------------------
           : :

LdtD      LVEAVKRFQ--AWQGLGADGAIGPATRDWLNVTPAQRAGVLALNIQRLRLLPTELSTGIM
LdtE      LQAIARRFDTAAMLILEANNTIAPVPKPGT-----------TITIPSQLLLPDAPRQGII
LdtF      ---------------LGSSSSTTPVSKEYK-----------Q-----Q-LMGSPVYIQIF
                       * :..:  *. :                   *:       *:

LdtD      VNIPAYSLVYYQNGNQ--VLDS-RVIVGRPDRKTPMMSSALNNVVVNPPWNVPPTLAR--
LdtE      VNLAELRLYYYPPGEN--IVQVYPIGIGLQGLETPVMETRVGQKIPNPTWTPTAGIR---
LdtF      KEERTLDLY-VKMGEQYQLLDSYKICKYSGG---------LGPKQRQGDFKSPEGFYSVQ
           :    *    *::  :::   :     .         :.    :  :.    :

LdtD      -KDILPKVRNDPGYLESHGYTVMRGWNSREAIDPWQVDWSTITASNLPFRFQQAPGPRNS
LdtE      QRSLERG-----------------------------------------IKLPPVVPAGPNNP
LdtF      RNQLKPD-----------------------------------------SRYYKAINIGFPNA
           ..:                                                 *  *

LdtD      LGRYKFNMPSS-EAIYLHDTPNHNLFKRDTRALSSGCVRVNKASDLANMLLQDAGWNDKR
LdtE      LGRYALRLAHG-NGEYLIHGTS--APDSVGLRVSSGCIRMNAPDIKALFSSVRTGTPVKV
LdtF      -----YDRAHGYEGKYLMI---------HGDCVSIGCYAMTNQGIDEIFQFVTGALVFGQ
                    . :. **              :* **  :.  .    :     .

LdtD      ISD----ALKQGDTRYVNIRQSIPVNLY---------------YLTAFVG------AD--
LdtE      INEPVKYSVEPNGMRYVEVHRPLSAEEQQNVQTMPYTLPAGFTQFKDNKAVDQKL-----
LdtF      --PSVQVSIYPFRMTDANMKR----HKYSNFKDFWEQLKPGYDYFEQTRKPPTVSVVNGR
                ::       .::::    .                  :

LdtD      --------GRTQYRTDIYNYDLPARSSSQIVSKAE-------QLIR---
LdtE      --VDKALYRRAGYPVSVSSGATPAASNAPSVESAQNGEPEQGNMLRVTQ
LdtF      YVVSKPLSHEVVQPQLASNYTLPEAK----------------------
          ..   . * .
```

Figure S1. (**A**) Peptidoglycan cross-linking reactions catalyzed by the DD-transpeptidases (PBPs, top) and the LD-transpeptidases (LdtD, LdtE and LdtF, bottom) resulting in 4-3 and 3-3 cross-links, respectively. G, *N*-acetylglucosamine (G); M, *N*-acetylmuramic acid; R indicates H, D-Ala or D-Ala-D-Ala. (**B**) Sequence alignment of LdtD, LdtE and LdtF. LdtD sequence starts at amino acid 201 of the protein sequence. Residues flanking the Cys residue (**C**) of catalytic site are indicated in bold. Consensus symbols: (*) indicates fully conserved residues; (:) indicates residues with high degree of conservation; (.) indicates residues with low degree of conservation. Alignment was performed with ClustaOmega (https://www.ebi.ac.uk/Tools/msa/clustalo/).

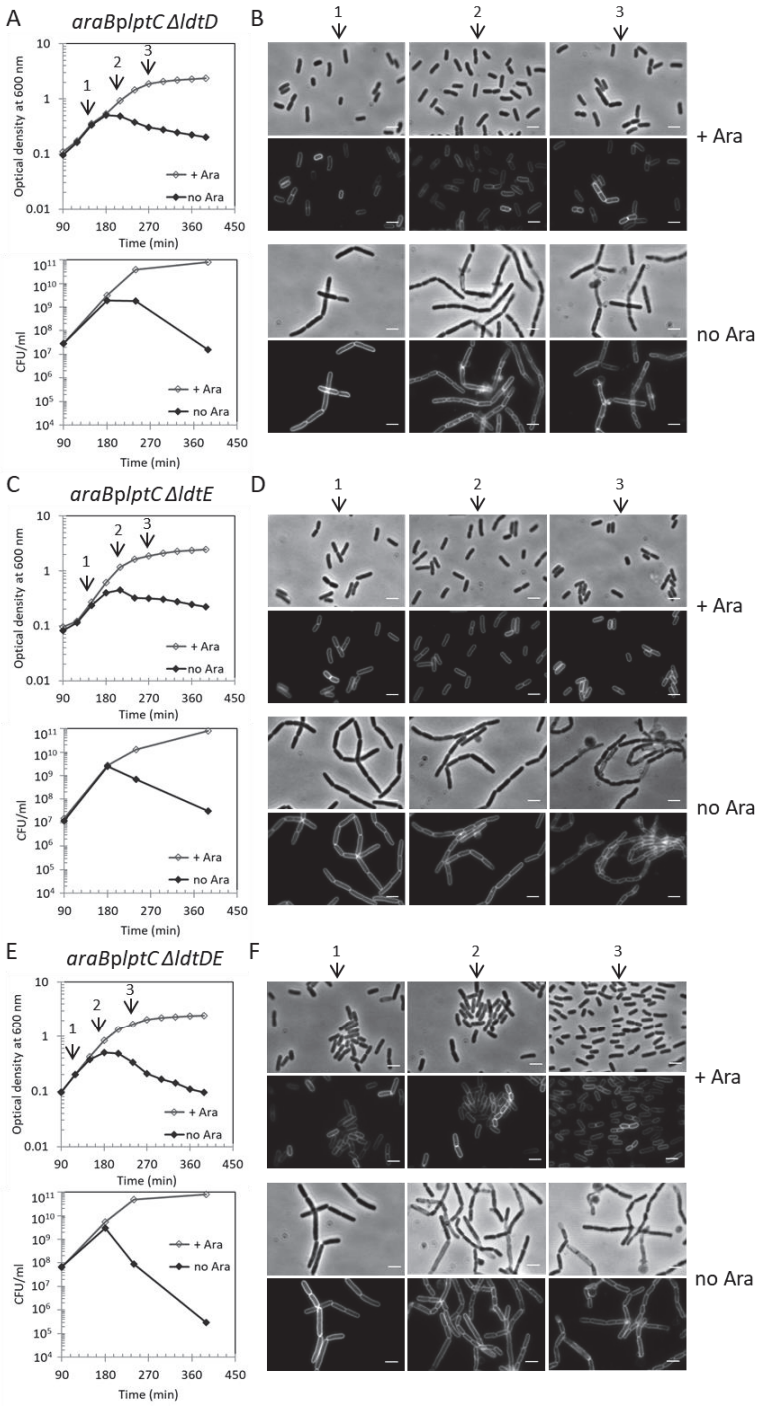

Figure S2. Deletion of *ldtD*, *ldtE* and *ldtD*-*ldtE* in the *araB*p*lptC* conditional strain compromises cell viability under non-permissive conditions. Cells of *araB*p*lptC* Δ*ldtD* (**A**), *araB*p*lptC* Δ*ldtE* (**C**) *araB*p*lptC* Δ*ldtD* Δ*ldtE* (**E**) were grown in the presence of 0.2% arabinose to an OD_{600} of 0.2, harvested, washed three times and resuspended in an arabinose-supplemented (+ Ara) or arabinose-free (no Ara) medium. Cell growth was monitored by OD_{600} measurements (upper panels) and viability was assessed by determining CFU (lower panels). Growth curves shown are representative of at least three independent experiments. At t = 120 min, 210 min and 270 min (arrows), a*raB*p*lptC* Δ*ldtD* (**B**), *araB*p*lptC* Δ*ldtE* (**D**) and *araB*p*lptC* Δ*ldtD* Δ*ldtE* (**F**) cells were collected for imaging. Phase contrast images are on the top and fluorescence images are on the bottom. Scale bars, 3 μm.

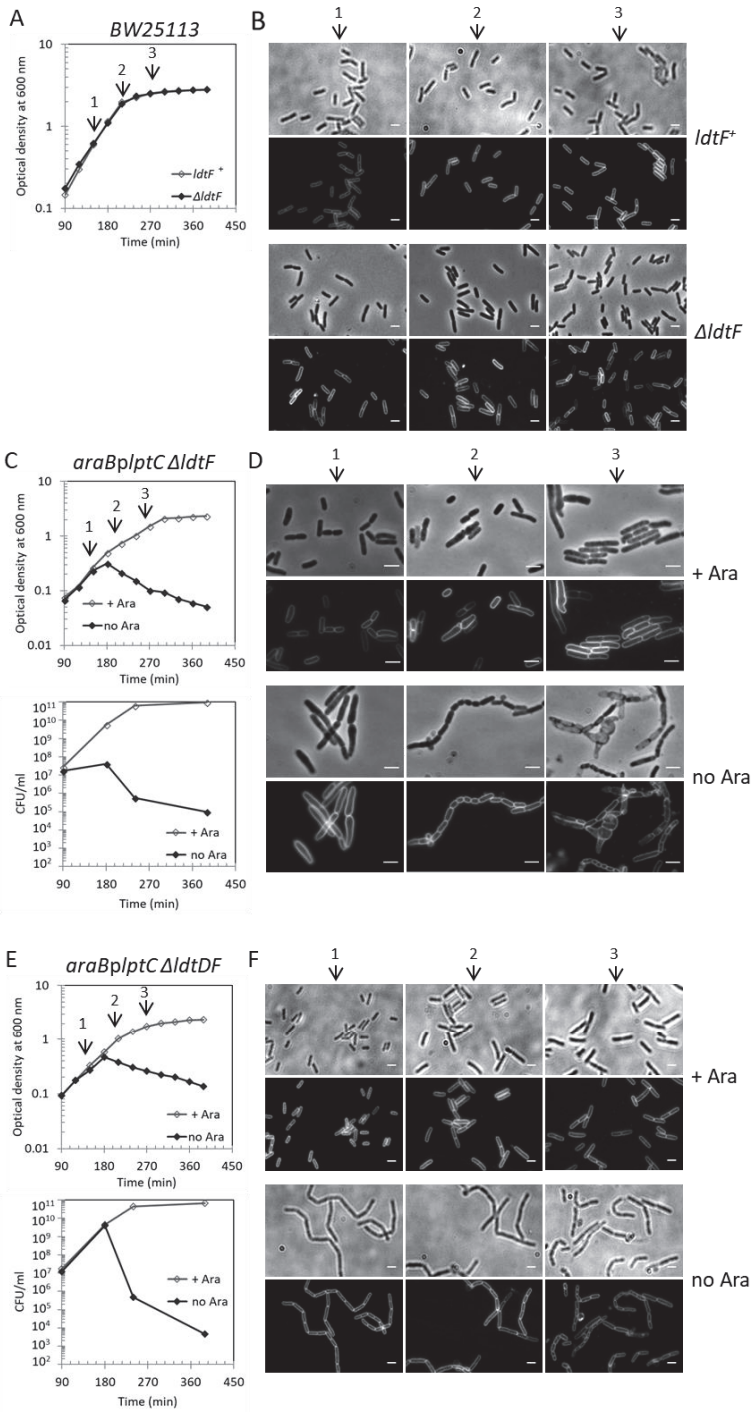

Figure S3. Phenotypes of wild type BW25113 (*lptC*$^{+}$) and *araB*p*lptC* conditional strains lacking *ldtF* and of *araB*p*lptC* lacking *ldtD-ldtF*. Cells of BW25113, the isogenic Δ*ldtF* mutant (**A**), the *araB*p*lptC* Δ*ldtF* mutant (**C**) and *araB*p*lptC* Δ*ldtD* Δ*ldtF* mutant (**E**) were grown and imaged as described in the legend of Figure S2. Growth curves shown are representative of at least three independent experiments. At t = 120 min, 210 min and 270 min (arrows), BW25113 and BW25113 Δ*ldtF* (**B**), *araB*p*lptC* Δ*ldtF* (**D**) *araB*p*lptC* Δ*ldtE* Δ*ldtF* mutant (**F**) cells were collected for imaging. Phase contrast images are on the top and fluorescence images are on the bottom. Scale bars 3 μm. *araB*p*lptC* Δ*ldtF* cells displayed morphological defects even when grown under permissive conditions.

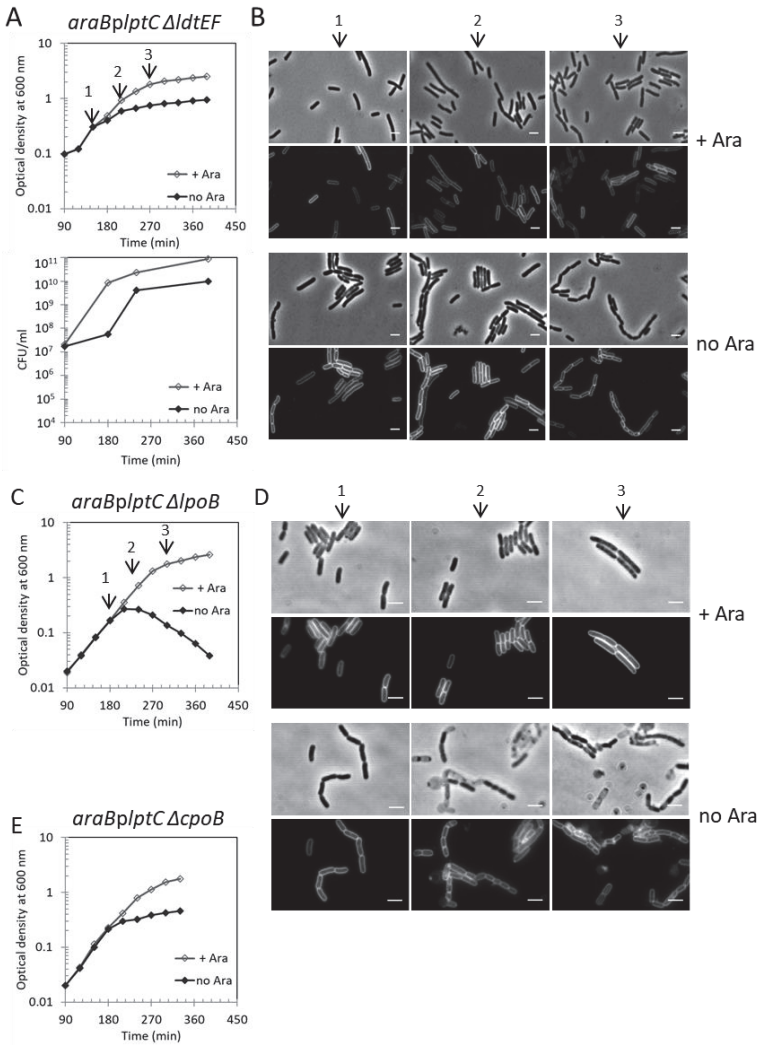

Figure S4. Growth profiles of *araB*p*lptC* conditional strain lacking *ldtE-ldtF* or *lpoB* or *cpoB*. Cells of *araB*p*lptC* Δ*ldtE* Δ*ldtF* (**A**, **B**), *araB*p*lptC* Δ*lpoB* (**C**, **D**) and *araB*p*lptC* Δ*cpoB* (**E**) were grown and imaged as described in the legend of Figure S2. Growth curves shown are representative of at least three independent experiments. *araB*p*lptC* Δ*ldtE* Δ*ldtF* cells did not lyse under non-permissive conditions (**A, B**). The PBP1B activator LpoB prevents lysis in *lptC*-depleted cells (**C, D**) whereas deletion of *cpoB* has no impact on cell viability (**E**).

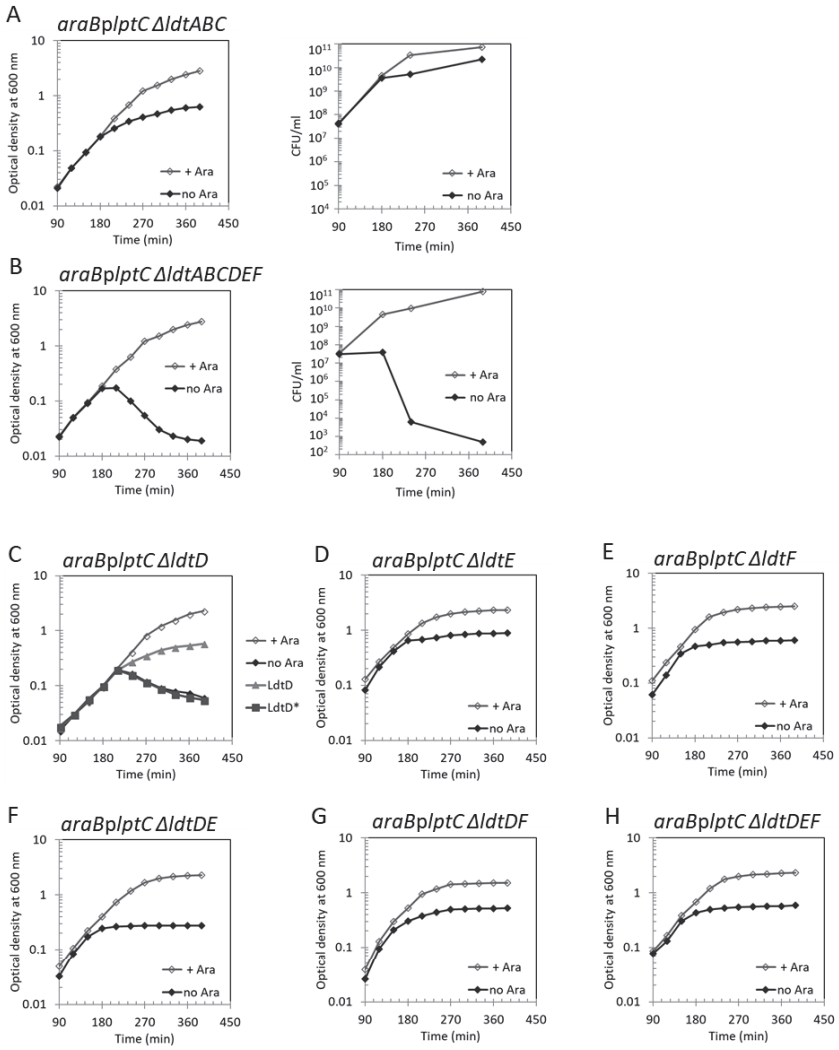

Figure S5. The simultaneous deletion of *ldtA*, *ldtB* and *ldtC* in the *araB*p*lptC* conditional strain has no impact on cell viability under non-permissive conditions and ectopic expression of LdtD rescues the lysis phenotype of single and multiple *araB*p*lptC ldt* mutants. Cells of the *araB*p*lptC* conditional strain with deletions of *ldtA*, *ldtB* and *ldtC* (**A**) and all six *ldt* genes (*ldtA*, *ldtB, ldtC*, *ldtD*, *ldtE* and *ldtF*) (**B**) were grown in the presence of 0.2% arabinose to an OD_{600} of 0.2, harvested, washed three times and resuspended in an arabinose-supplemented (+ Ara) or arabinose-free (no Ara) medium. Cell growth was then monitored by OD_{600} measurements and viability was assessed by determining the CFU. (**C**) Complementation of the *araB*p*lptC* Δ*ldtD* lysis phenotype by ectopic expression of wild type *ldtD* and *ldtD*^{C528A}. (**D-H**) Complementation of the *araB*p*lptC* Δ*ldtE, araB*p*lptC* Δ*ldtF, araB*p*lptC* Δ*ldtDE, araB*p*lptC* Δ*ldtDF, araB*p*lptC* Δ*ldtDEF* lysis phenotype by ectopic expression of wild type *ldtD.* Cells were grown in the presence of 0.2% arabinose to an OD_{600} of 0.2, harvested, washed three times and resuspended in an arabinose-free medium. The growth of *araB*p*lptC* Δ*ldtD* in arabinose-supplemented medium is shown as control. Cell growth was monitored by OD_{600} measurements. Growth curves shown are representative of at least three independent experiments. In panels A and B *ldt* genes are indicated by their capital letters.

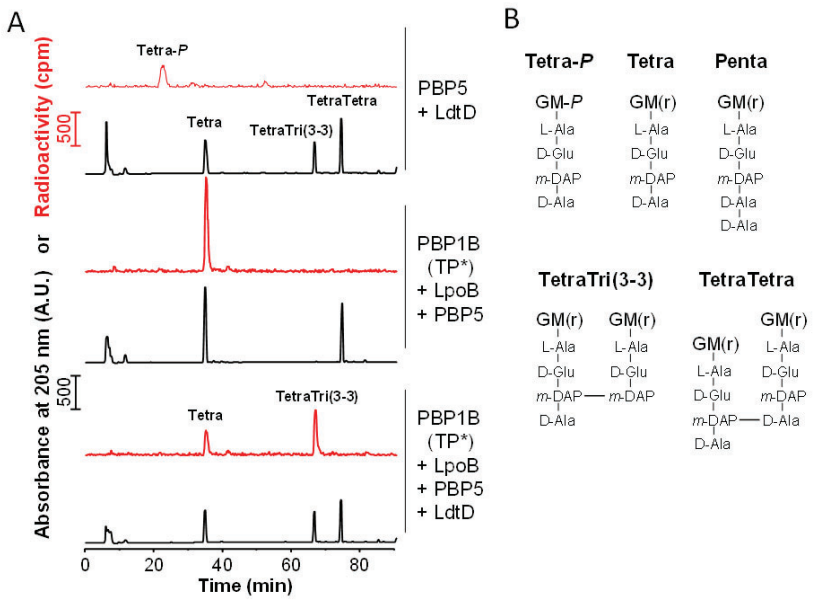

Figure S6. LdtD is active during *in vitro* PG synthesis in the presence of PBP1B(TP*), LpoB and PBP5. (**A**) HPLC chromatograms obtained from samples containing radioactive lipid II, PG from *E. coli* BW25113ΔLDT and the proteins indicated on the right side. (**B**) Proposed structures of muropeptides shown in panel A and B. G, *N*-acetylglucosamine; M, *N*-acetylmuramic acid; M(r), *N*-acetylmuramitol; M-*P*, N-acetylmuramic acid-1-phosphate; L-Ala, L-alanine; D-Glu, D-glutamic acid; D-Ala, D-alanine; *m*-DAP, *meso*-diaminopimelic acid.

Supplemental Methods

Construction of *E. coli* deletion or depletion strains

Deletion strains were obtained by moving *kan*-marked alleles from the Keio *E. coli* single-gene knockout library (1) by P1 phage transduction (2). Afterward, the *kan* cassette was removed by pCP20-encoded Flp recombinase to generate unmarked deletions with a FRT-site scar sequence (3). The removal of the *kan* gene was verified by colony PCR. Strains with multiple deletions were generated by sequential P1 transduction and *kan* cassette removal. *LptC* depletion strains were obtained by moving the *kan araC araB*p-*lptC* allele from BB-3 (4) into selected mutants by P1 transduction. Depletion strains were selected on media containing kanamycin and 0.2% arabinose. The insertion of the cassette was verified by PCR.

Construction of *ldtD*-his strains

The λ Red recombination system was used to fuse the His-tag coding sequence to chromosomally encoded *ldtD* to produce a *ldtD-his* C-terminal fusion. A linear PCR product encoding the *his*-tag and the *kan* cassette flanked by sequences for homologous recombination (Table S1) was obtained using primers AP565 and AP566 and as a template pKD4 (Table S2). and transformed into BW25113 strain harbouring the pKD46, a Red helper plasmid (3). The correct insertion of the *his-kan* cassette was confirmed by PCR. Afterward, the *kan* cassette was removed as described above. The *araB*p-*lptC ldtD-his* strain was obtained by moving the *kan araC araB*p-*lptC* allele from BB-3 (4) as described above.

Construction of plasmids

pGS121 and pGS124 were constructed by cloning *ldtE* and *ldtF* into the *Eco*RI/*Hind*III restriction sites of pGS100 (4). pGS123 was constructed by cloning *ldtD* into *Eco*RI/*Xba*I restriction sites of pGS100. Primers used for genes cloning are listed in Table S2. To assess transcriptional activity the promoter regions of *ldtE*, *ldtD* and *ldtF* genes were cloned into the *lacZ* vector pRS415 (5). For this, the promoter region of each *ldt* gene was amplified by PCR using primers listed in Table S2 and cloned into *EcoR*I/*Bam*HI (*ldtE*p and *ldtD*p) or *EcoR*I/*Sma*I (*ldtF*p) restriction sites of pRS415. Each cloned region contained at least 600 bp upstream and 150 bp downstream of the start codon of each gene to include putative regulatory elements.

For pET28a-His6-LdtF, *ldtF* was cloned starting from position 58 downstream the ATG codon, into *Nde*I/*Xho*I pET28a, eliminating the putative signal sequence. The correct nucleotide sequences of inserts were verified (Eurofins Genomics).

pAMS01(LdtE) and pAMS02(LdtF) were constructed using the Gibson assembly method (6) by cloning *ldtE* and *ldtF* into pJEH12(LdtD) (7), respectively. Primers used for gene cloning are listed in Table S2.

pGS123C528A was obtained by site-directed mutagenesis using the Q5® Site-Directed Mutagenesis Kit (New England BioLabs) on pGS123 following manufacturer instructions. Primers used for site directed mutagenesis are listed in Table S2.

Measurements of the minimum inhibitory concentration (MIC) of LPC-058.

The MIC assay protocol was adapted from (8) using 96-well plates. Bacterial were grown in LB-Lennox medium at 37°C in the presence of varying concentration of LPC-058 inhibitor and 5% of DMSO as control.

Overexpression plasmids and purification of proteins

Purification of PBP6a. DNA encoding for PBP6a (residues 28-400) from *E. coli* BW25113 was amplified by PCR and cloned into pET28a(+) using *Nde*I and *Xho*I. PBP6a was overexpressed in *E. coli* LOBSTR-BL21(DE3) (Kerafast) cells grown overnight at 37°C in 2 L of TB-autoinduction medium supplemented with 4 g lactose, 1 g glucose, 10 mM $MgCl_2$ and 10 mM $MgSO_4$ (9). Cells were harvested by centrifugation for 15 min at 4500 rpm and 14°C. The resulting cell pellet was resuspended in 50 ml buffer A (25 mM HEPES/NaOH pH 7.5, 100 mM NaCl) supplemented with 1 mM phenylmethyl sulfonyl fluoride (Sigma Aldrich), 1× protease inhibitor cocktail (Sigma Aldrich) and desoxyribonuclease I (Sigma Aldrich). Cells were broken by sonication and centrifuged for 1 h at 130,000×*g* and 4 °C. The resulting pellet was resuspended in buffer B (25 mM HEPES/NaOH pH 7.5, 1 M NaCl, 2 mM $MgCl_2$ 10% glycerol) supplemented with 1% CHAPS (Anatrace) and incubated under continuous stirring overnight at 4°C. Insoluble material was removed by centrifugation for 1 h at 130,000×*g* at 4°C. The supernatant was recovered, mixed with 1 ml Ni-NTA Superflow (Qiagen) preequilibrated in buffer B (supplemented with 0.5% CHAPS and 5 mM imidazole) and incubated under continuous gentle stirring for 3 h at 4°C. Ni-NTA agarose was poured in a gravity flow column, washed 5 times with 20 column volume (CV) buffer B (supplemented with 0.5% CHAPS and increasing concentrations of imidazole, 10-50 mM). PBP6a was eluted with buffer B supplemented with 0.5% CHAPS and 300 mM imidazole. Eluted protein was dialysed against 2 L dialysis buffer (25 mM HEPES/NaOH, 500 mM NaCl, 10% glycerol, 0.1% CHAPS, 10 mM EDTA). The protein was further purified by size exclusion chromatography on a HiLoad 16/60 Superdex 200 (GE Healthcare) column using size exclusion buffer (25 mM HEPES/NaOH, 300 mM NaCl, 10% glycerol, 0.1% CHAPS) and a flowrate of 1

ml/min. Purity was determined by SDS-PAGE and combined fractions were concentrated and stored in aliquots at -80°C.

Purification of LdtD. *E. coli* LOBSTR-BL21(DE3) (Kerafast) cells were transformed with pETMM82, a plasmid encoding for LdtD carrying an N-terminal DsbC-His6-tag followed by a TEV-protease cleavage site (7), and grown at 30°C in 1 L TB medium (10) (supplemented with 5 mM $MgCl_2$ and 5 mM $MgSO_4$) until OD600 0.3. LdtD overexpression was induced by adding IPTG (Generon) to a final concentration of 0.5 mM. The temperature was decreased to 16°C and cells were incubated for 19 h. Cells were harvested by centrifugation for 15 min at 4,500 rpm and 14°C. The resulting cell pellet was resuspended in 60 ml buffer A (20 mM Tris pH 8.0, 1 M NaCl, 10 mM imidazole) supplemented with 1 mM phenylmethyl sulfonyl fluoride (Sigma Aldrich), 1× protease inhibitor cocktail (Sigma Aldrich) and desoxyribonuclease I (Sigma Aldrich). Cells were broken by sonication and centrifuged for 1 h at 130,000×*g* at 4°C. The supernatant was recovered, mixed with 0.5 ml Ni-NTA Superflow (Qiagen) preequilibrated in buffer A (supplemented with 10 mM imidazole) and incubated under continuous gentle stirring at 4°C. After 1.5 h another 0.5 ml of Ni-NTA Superflow (Qiagen) was added and incubated for 1.5 h. The suspension was poured in a gravity flow column and washed 2 times with 20 CV buffer B (20 mM Tris/HCl pH 7.0, 150 mM NaCl) supplemented with 20 mM imidazole, 5 mM ATP and 1 mM $MgCl_2$ to remove tightly bound chaperone proteins. After 3 more washing steps with 20 CV of buffer B each (2× 40 mM imidazole, 1× 50 mM imidazole), the protein was eluted with buffer B supplemented with 300 mM imidazole and glycerol was added to the elution fractions to a final concentration of 10%. The protein was dialysed against 2× 2 L dialysis buffer 1 (25 mM Tris pH 7.0, 300 mM NaCl, 10% glycerol) for 1 h each at

4°C. The protein solution was supplemented with 5 mM β-mercaptoethanol (Sigma Aldrich), 10 U/ml TEV-protease (Promega) and dialysed against 1 L of dialysis buffer 2 (25 mM Tris pH 7.0, 300 mM NaCl, 5 mM β-mercaptoethanol, 10% glycerol) for 1 h and against an additional 1 L overnight at 4°C.

The sample was mixed with 1 ml of Ni-NTA-agarose preequilibrated in dialysis buffer 2 containing 50 mM of imidazole and incubated for 2-3 h at 4°C under gentle stirring. The suspension was poured in a gravity flow column and the DsbC-His-tag free protein present in the flow through was further purified by size exclusion chromatography on a HiLoad 26/60 Supedex 200 (GE Healthcare) column using size exclusion buffer (25 mM Tris/HCl pH 7.5, 300 mM NaCl, 10% glycerol) and a flowrate of 1 ml/min. Purity was determined by SDS-PAGE and combined fractions were concentrated and stored in aliquots at -80°C.

Purification of His-PBP1A and PBP1A. PBP1A was purified according to a published procedure (11) with modifications. *E. coli* LOBSTR-BL21(DE3) (Kerafast) cells carrying the plasmid pTK1Ahis were grown in 2 L of LB medium (12) at 30°C until an optical density (578 nm) of 0.5 was reached. IPTG (1 mM) was added and the cells were grown for 3 h, chilled on ice for 15 min, harvested by centrifugation for 20 min at 5,000 rpm and 4^0C. The cell pellet was resuspended in 140 ml of Buffer I (25 mM HEPES/NaOH pH 7.5, 1 M NaCl, 1 mM EGTA, 10% glycerol) supplemented with 1 mM phenylmethyl sulfonyl fluoride (Sigma Aldrich), 1× protease inhibitor cocktail (Sigma Aldrich) and desoxyribonuclease I (Sigma Aldrich). Cells were broken by sonication and the soluble fraction was removed after ultracentrifugation for 1 h at 130,000×*g* and 4°C. The membrane pellet was resuspended in extraction buffer (25 mM HEPES/NaOH pH 7.5, 5 mM $MgCl_2$, 1 M NaCl, 20% glycerol, 2% Triton X-100)

with continuous stirring overnight at 4°C. Insoluble material was removed by centrifugation for 1 h at 130,000×*g* at 4°C. The supernatant containing the solubilised membrane fraction was diluted with the same volume of IMAC dilution buffer (25 mM HEPES/NaOH pH 7.5, 1 M NaCl, 40 mM imidazole, 20% glycerol) and applied to a 5 mL HisTrap HP column using an ÄKTA PrimePlus. The column was washed with IMAC wash buffer (25 mM HEPES/NaOH pH 7.5, 500 mM NaCl, 50 mM imidazole, 20% glycerol, 0.2% reduced Triton X-100), and PBP1A was eluted with the elution buffer (25 mM HEPES/NaOH pH 7.5, 500 mM NaCl, 400 mM imidazole, 20% glycerol, 0.2% reduced Triton X-100). Fractions containing His-PBP1A were pooled. For the removal of the His-tag, 16 units of thrombin (restriction grade, Novagen) were added and the sample was dialysed in 3 × 1 l of cleavage buffer (20 mM HEPES/NaOH pH 7.5, 500 mM NaCl, 10% glycerol).

Purification of MepM. The protein was purified as described in (13) with modifications. Briefly, 2 L of LB medium (12) were inoculated with strain BL21(DE3) pET21b-*yebA* and protein expression was induced by addition of IPTG at a final concentration of 50 µM. Cells were incubated for 2 h at 25°C, harvested by centrifugation and resuspended in lysis buffer (25 mM Tris/HCl pH 7.5, 300 mM NaCl, 10% glycerol). The first purification step was performed on HisTrap HP column (GE healthcare) preequilibrated with wash buffer (25 mM Tris/HCl pH 7.5, 300 mM NaCl, 20 mM imidazole). Protein was eluted in the same buffer supplemented with 300 mM imidazole. Samples containing protein of interest were dialysed against 25 mM HEPES/NaOH pH 7.5, 300 mM NaCl, 10% glycerol overnight at 4°C. Dialysed samples were concentrated using Vivaspin 6 columns and applied to a HiLoad 16/60

Superdex 200 (GE healthcare) size exclusion column at a flowrate of 1 ml/min using the same buffer. The purified protein was stored in aliquots at -80 °C.

Other proteins. PBP1B and PBP1B(TP*) were purified as described in (14), LpoB was purified as described in (15), PBP5 was purified as described in (16).

Protein-protein interactions

Pull-down experiments were performed as described (17) using proteins at 2 μM concentration. Microscale thermophoresis (MST) experiments were carried out with a Monolith NT.115 instrument (NanoTemper GmbH, Germany). LdtD was labelled with the Monolith NT.115 Protein Labelling Kit RED-NHS according to the manufactory instructions. MST experiments were performed with serial dilution series of PBP1A or PBP1B and constant concentration of labelled LdtD in 20 mM HEPES/NaOH pH 7.5, 150 mM NaCl, 0.2 % Triton X-100, using premium capillaries, an LED-Power of 20% and an MST-Power of 40%. Changes in normalised fluorescence caused by the local temperature gradient were analysed by the MO.Affinity Analysis v2.1.2 software.

***In vivo* DTSSP cross-linking**

800 OD of BW25113 *ldtD*-his and *araB*p*lptC ldtD*-his cells were pelleted by centrifugation and resuspended in 25-mL ice-cold CL Buffer I (50 mM NaH_2PO_4, 20% [wt/vol] sucrose, pH 7.4) with 100 μg/mL DTSSP (freshly prepared as a 20 mg/ml stock in CL Buffer I). Cells were incubated at 4°C with mixing for 1 h, then pelleted and frozen at −80°C (17). Cells were then thawed, resuspended in 20 ml of 50 mM potassium phosphate buffer (pH 8.0), 150mM NaCl, 5mM $MgCl_2$, DNase I (50 μg/mL), and RNase I (50 μg/mL) and then lysed by sonication (3× 30 s at 20 mA). The lysate

was incubated with 1% ZW3-14 (*N*-tetradecyl-*N*,*N*-dimethyl-3-ammonio-1-propanesulfonate) for 20 min at room temperature with shaking to complete cell lysis. The mixture was then centrifuged at 10,000 *g* for 10 min to remove cell debris. To the cleared lysate (whole-cell extract) 20 mM imidazole (pH 8.0) was added, and the final mixture was loaded onto a 0.5-ml Ni-NTA column. Protein were eluted as described (18) and equal amount of proteins were used for Western blot analysis using Monoclonal Anti-polyHistidine antibody, anti-PBP1B (15) and anti-LptE (kind gift of D. Kahne) as loading control.

***In vivo* DTSSP cross-linking / co-immunoprecipitation assay**

The assay was performed as described in[17]. *araB*p*lptC ldtD-his* cells were grown overnight in LB Lennox media supplemented with 50 µg/mL kan and 0.2% L-arabinose, diluted 1:500 into 200 mL LB Lennox media with the same supplements. The cells were grown at 30°C to an OD_{578} of 0.2, washed 3 × with LB Lennox media (no supplements; centrifugation at 1500 × *g*, 10 min at RT), resuspended in 200 mL Lennox LB (supplemented with 50 µg/mL kan) until the cells arrested growth. Cells were pelleted by centrifugation (1500 × *g*, 4°C, 10 min) and resuspended in 6 mL of ice-cold CL Buffer I (50 mM NaH_2PO_4 20% (w/v) sucrose pH 7.4) with 100 µg/mL DTSSP (freshly prepared from a 20 mg/mL stock in CL Buffer I). Cells were incubated at 4°C with mixing for 1 h, then pelleted and resuspended to an OD_{578} of 4 in ice-cold CL Buffer II (100 mM Tris/HCl, 10 mM $MgCl_2$, 1 M NaCl, pH 7.5) with 100 µM PMSF, 50 µg/mL protease inhibitor cocktail (P8465, Sigma-Aldrich) and 50 µg/mL DNAse I. The cells were disrupted by sonication and membranes were sedimented by centrifugation (90,000 × *g*, 60 min, 4°C) and resuspended in CL buffer III (25 mM Tris/HCl, 10 mM $MgCl_2$, 1 M NaCl, 20% glycerol, 2% Triton X-100, pH 7.5).

Membrane proetins were extracted by stirring overnight at 6°C. After another centrifugation step (90,000 × g, 1 h, 4°C) the supernatant was taken and 3-fold diluted with CL buffer IV (75 mM Tris/HCl, 10 mM $MgCl_2$, 1 M NaCl, pH 7.5). Specific PBP1B antibodies were added and the sample was incubated for 5 h at 4°C. A control sample was incubated without antibody. Protein G-coupled agarose (120 µl suspension) was added to the membrane fraction and the sample was incubated overnight at 4°C. The beads were recovered by centrifugation and washed with 10 ml of CL wash buffer (42 mM Tris/HCl, 10 mM $MgCl_2$, 1 M NaCl, 0.7% Triton X-100, 13% glycerol, pH 7.5) and boiled for 10 min in 50 µl of sample buffer for SDS-PAGE. The supernatant was collected, proteins were separated by SDS-PAGE and transferred to nitrocellulose by Western Blot, and LdtD-his was detected with a monoclonal anti-polyhistidine antibody (Sigma No. H1029) and an anti-mouse IgA - peroxidase antibody (Sigma No. A4789).

MepM digest of sacculi from BW25113Δ6LDT

Sacculi from BW25113Δ6LDT were prepared as described in (19). MepM digest was carried out in a final volume of 200 µl containing 25 mM HEPES/NaOH pH 7.5, 150 mM NaCl, 0.05% Triton X-100, 750 µg sacculi using a final concentration of MepM of 2 µM. The sample was incubated overnight at 37°C. Then the reaction mixture was heated for 10 min at 100°C and centrifuged for 20 min. The supernatant containing disaccharide-tetrapeptide chains was collected and stored at 2-8°C.

LdtD activity assay with disaccharide-tetrapeptide chains or PG sacculi

Assays were carried out in a final volume of 50 µl containing 25 mM Tris/HCl pH 7.5, 100 mM NaCl, 10 mM $MgCl_2$, 0.1% Triton X-100, and 2 µM LdtD. Fifteen µl of

peptidoglycan or 20 µl of disaccharide-tetrapeptide chains were added and the reaction mixture was incubated at 37°C overnight. The reaction was stopped by boiling the samples for 10 min.

Coupled PG synthesis - LDT assay

Coupled assays were carried out in a final volume of 50 µl containing 25 mM HEPES/NaOH pH 7.5, 175 mM NaCl, 10 mM $MgCl_2$, 0.1% Triton X-100, [^{14}C]Glc*N*Ac-labelled lipid II [10,000 dpm; (21)], 15 µl of PG from BW25113Δ6LDT and 2 µM of each protein as needed (LdtD, PBP1B-TP*, LpoB, PBP6 and/or PBP5). The reaction mixture was incubated for 4 h at 37°C. The reaction was stopped by boiling the samples for 10 min.

LDTs expression for HPLC analysis

BW25113Δ6LDT strain was transformed with pJEH12(LdtD), pAMS01(LdtE), pAMS02(LdtF) or an empty plasmid (pSAV057;[20) . Empty BW25113Δ6LDT was used as control. The same strain was also co-transformed with pJEH12(LdtD) and pGS124 or pAMS02(LdtF) and pGS121. A single transformant was used to inoculate 5 mL of Antibiotic Broth (AB) (Sigma Aldrich) overnight at 37°C. A 1:1000 dilution was performed in fresh AB cultures (400 mL each, in duplicate) from the overnight cultures. Samples were grown at 37°C and expression of LDTs was carried out with 50 µM IPTG when OD_{600} was 0.2. After reaching the late exponential phase (OD_{600} 0.8), samples were cooled in ice and harvested by centrifugation at 4°C. The cell pellet was resuspended in 6 ml ice-cold water and dropped slowly into 6 ml boiling 8% SDS water solution. Samples were boiled for 60 minutes.

HPLC analysis

Samples were centrifuged for 20 minutes and the supernatant recovered and adjusted to pH 4 with 20% phosphoric acid. HPLC analysis was carried out as described in (21). Muropeptides were detected by online radioactivity detector and absorbance at 205 nm.

Imaging and image analysis

Microscopy images were obtained with a Nikon Eclipse Ti microscope through a 100× 1.45 oil objective and photometric/Cool-SNAP-HQ2 camera or with a Zeiss Axiovert 200M microscope through a 63× 1.45 oil objective coupled to a AxioCam Mrm device 290 camera (Zeiss). Cells at different time points, as indicated by arrows in the figures, were collected from a total amount corresponding to an OD of 4, and a 1:10 ratio of fixation solution (fixation solution: formaldehyde 37% - glutaraldehyde 25% in PBS) was added. Cells were incubated for 30 min at 37°C with shaking, washed with PBS and resuspended in 500 µl of PBS. A cell suspension (5 µl) was spotted onto an agarose-coated glass slide (1% agarose), the sample was covered with a glass coverslip. To stain cell membranes, SynaptoRed C2M or FM5-95 was added to agarose solution to a final concentration of 2 µg/ml.

β-galactosidase assay

β-galactosidase specific activity was measured from a total number of cells corresponding to an OD_{600} of 8 as previously described (22).

References

1. Baba T, Ara T, Hasegawa M, Takai Y, Okumura Y, Baba M, Datsenko, KA, Tomita M, Wanner BL, and Mori H. 2006. Construction of *Escherichia coli* K-12 in-frame, single-gene knockout mutants: the Keio collection. Mol Syst Biol *2*, 2006 0008

2. Silhavy TJ, Berman ML, and Enquist LW. 1984. Experiments with gene fusions., C.S.H. ColdSpringHarborLaboratory N.Y. , Editor.

3. Datsenko KA, and Wanner, BL. 2000. One-step inactivation of chromosomal genes in *Escherichia coli* K-12 using PCR products. Proc Natl Acad Sci U S A *97*, 6640-6645

4. Sperandeo P, Pozzi C, Dehò G, and Polissi A. 2006. Non-essential KDO biosynthesis and new essential cell envelope biogenesis genes in the *Escherichia coli yrbG-yhbG* locus. Res Microbiol *157*, 547-558.

5. Simons RW, Houman F, and Kleckner N. 1987. Improved single and multicopy *lac*-based cloning vectors for protein and operon fusions. Gene *53*, 85-96.

6. Gibson DG, Young L, Chuang RY, Venter JC, Hutchison CA 3rd, and Smith HO. 2009. Enzymatic assembly of DNA molecules up to several hundred kilobases. Nat Methods *6*, 343-345.

7. Hugonnet JE, Mengin-Lecreulx D, Monton A, den Blaauwen T, Carbonnelle E, Veckerle C, Brun YV, van Nieuwenhze M, Bouchier C, Tu K, Rice LB, Arthur M. 2016. Factors essential for L,D-transpeptidase-mediated peptidoglycan cross-linking and beta-lactam resistance in *Escherichia coli*. Elife 5:pii: e19469

8. Wiegand I, Hilpert K, Hancock RE. 2008. Agar and broth dilution methods to determine the minimal inhibitory concentration (MIC) of antimicrobial substances Nat Protoc. *3*,163-75. doi: 10.1038/nprot.2007.521

9. Studier FW. 2005. Protein production by auto-induction in high density shaking cultures. Protein Expr Purif *41*, 207-234.

10. Tartof KDH, CA. 1987. Improved media for growing plasmid and cosmid clones. Bethesda Res Lab Focus 9.

11. Born P, Breukink E, Vollmer W. 2006. In vitro synthesis of cross-linked murein and its attachment to sacculi by PBP1A from *Escherichia coli*. J Biol Chem 281:26985-93.

12. Miller JH. 1972. Experiments in molecular genetics. Cold Spring Harbor Laboratory, Cold Spring Harbor, New York.

13. Singh SK, SaiSree L, Amrutha RN, and Reddy M. 2012. Three redundant murein endopeptidases catalyse an essential cleavage step in peptidoglycan synthesis of *Escherichia coli* K12. Mol Microbiol 86, 1036-1051.

14. Typas A, Banzhaf M, van den Berg van Saparoea B, Verheul J, Biboy J, Nichols RJ, Zietek M, Beilharz K, Kannenberg K, von Rechenberg M, Breukink E, den Blaauwen T, Gross CA, Vollmer W. 2010. Regulation of peptidoglycan synthesis by outer-membrane proteins. Cell 143:1097-109.

15. Egan AJ, Jean NL, Koumoutsi A, Bougault CM, Biboy J, Sassine J, Solovyova AS, Breukink E, Typas A, Vollmer W, Simorre JP. 2014. Outer-membrane lipoprotein LpoB spans the periplasm to stimulate the peptidoglycan synthase PBP1B. Proc Natl Acad Sci U S A 111:8197-202.

16. Peters K, Kannan S, Rao VA, Biboy J, Vollmer D, Erickson SW, Lewis RJ, Young KD, Vollmer W. 2016. The Redundancy of Peptidoglycan Carboxypeptidases Ensures Robust Cell Shape Maintenance in *Escherichia coli*. MBio 7 e00819-16.
17. Gray AN, Egan AJ, Van't Veer IL, Verheul J, Colavin A, Koumoutsi A, Biboy J, Altelaar AF, Damen MJ, Huang KC, Simorre JP, Breukink E, den Blaauwen T, Typas A, Gross CA, Vollmer W. 2015. Coordination of peptidoglycan synthesis and outer membrane constriction during *Escherichia coli* cell division. Elife 4 e07118
18. Sperandeo P, Villa R, Martorana AM, Samalikova M, Grandori R, Dehò G, Polissi A. 2011. New insights into the Lpt machinery for lipopolysaccharide transport to the cell surface: LptA-LptC interaction and LptA stability as sensors of a properly assembled transenvelope complex. J Bacteriol 193:1042-53.
19. Glauner B, Holtje JV, Schwarz U. 1988. The composition of the murein of *Escherichia coli*. J Biol Chem 263:10088-95.
20. Alexeeva S, Gadella TW Jr., Verheul J, Verhoeven GS, and den Blaauwen T. 2010. Direct interactions of early and late assembling division proteins in *Escherichia coli* cells resolved by FRET. Mol Microbiol 77, 384-398.
21. Bertsche U, Breukink E, Kast T, Vollmer W. 2005. *In vitro* murein peptidoglycan synthesis by dimers of the bifunctional transglycosylase-transpeptidase PBP1B from *Escherichia coli.* J Biol Chem 280:38096-101.
22. Martorana AM, Sperandeo P, Polissi A, and Deho G. 2011. Complex transcriptional organization regulates an *Escherichia coli* locus implicated in lipopolysaccharide biogenesis. Res Microbiol 16*2*, 470-482.

Supplementary Table 1. Bacterial Strains and Plasmids.

Strain or Plasmid	Relevant Genotype, Features or Characteristics	Source or Reference
Strain		
AMM05	BW25113 Δ*ldtD*::frt	This work
AMM06	BW25113 Δ*ldtE*::frt	This work
AMM07	BW25113 Δ*ldtE*::frt Δl*dtD*::frt	This work
AMM10	BB-3 Δ*ldtD*::frt	This work
AMM11	BB-3 Δ*ldtE*::frt	This work
AMM12	BB-3 Δ*ldtD*::frt Δ*ldtE*::frt	This work
AMM14	BB-3 Δ*ldtA*::frt Δ*ldtB*::frt Δ*ldtC*::frt	This work
AMM24	BW25113 Δ*ldtF*::frt	This work
AMM25	BW25113 Δ*ldtD*::frt Δ*ldtF*::frt	This work
AMM26	BW25113 Δ*ldtE*::frt Δ*ldtF*::frt	This work
AMM28	BW25113 Δ*ldtD*::frt Δ*ldtE*::frt Δ*ldtF*::frt	This work
AMM30	BB-3 Δ*ldtF*::frt	This work
AMM31	BB-3 Δ*ldtD*::frt Δ*ldtF*::frt	This work
AMM32	BB-3 Δ*ldtE*::frt Δ*ldtF*::frt	This work
AMM33	BB-3 Δ*ldtA*::frt Δ*ldtB*::frt Δ*ldtC*::frt Δ*ldtD*::frt Δ*ldtE*::frt Δ*ldtF*::frt	This work
AMM34	BB-3 Δ*ldtD*::frt Δ*ldtE*::frt Δ*ldtF*::frt	This work
AMM36	BW25113 Δ*rpoS*:: frt	This work
AMM51	BW25113 Δ*mrcA*::frt	This work
AMM52	BW25113 Δ*mrcB*::frt	This work
AMM53	BW25113 Δ*dacA*::frt	This work
AMM54	BW25113 Δ*dacC*::frt	This work
AMM55	BW25113 Δ*lpoB*::frt	This work
AMM56	BW25113 Δ*cpoB*::frt	This work
AMM60	BB-3 Δ*mrcA*::frt	This work
AMM61	BB-3 Δ*mrcB*::frt	This work
AMM62	BB-3 Δ*dacA*::frt	This work
AMM63	BB-3 Δ*dacC*::frt	This work
AMM64	BB-3 Δ*lpoB*::frt	This work
AMM65	BB-3 Δ*cpoB*::frt	This work
AMM83	BW25113 *ldtD-his*::frt	This work
AMM84	BB-3 *ldtD-his*	This work
BB-3	BW25113 Φ(*kan araC araB*p*lptC*)1	(Sperandeo *et al*., 2006)
BL21(DE3)	F– *ompT hsdS*B(rB– mB–) *gal dcm* (DE3)	Novagen
BW25113	*lacI*^{q} *rrnB*$_{T14}$ Δ*lacZ*$_{WJ16}$ *hsdR514* Δ*araBAD*$_{AH33}$ Δ*rhaBAD*$_{LD78}$	(Datsenko and Wanner, 2000)
BW25113Δ6LDT	*lacI*^{q} *rrnB*$_{T14}$ Δ*lacZ*$_{WJ16}$ *hsdR514* Δ*araBAD*$_{AH33}$ Δ*rhaBAD*$_{LD78}$ *ΔycbB ΔerfK ΔycfS ΔybiS ΔynhG ΔyafK*	(Kuru *et al*., 2017)
DH5α	Δ(*argF-lac169*) ϕ80 *dlacZ58*(M15) *glnV44*(AS) λ^{-} *rfbD1 gyrA96 recA1 endA1 spoT1 thi-1 hsdR17*	(Hanahan, 1983)
JW0732	BW25113 Δ*cpoB*::*kan*	(Baba *et al*., 2006)
JW0803	BW25113 Δ*ldtB*790::*kan*	(Baba *et al*., 2006)
JW0908	BW25113 Δ*ldtD*742::*kan*	(Baba *et al*., 2006)
JW1668	BW25113 Δ*ldtE*753::*kan*	(Baba *et al*., 2006)
JW1968	BW25113 Δ*ldtA*761::*kan*	(Baba *et al*., 2006)
JW5820	BW25113 Δ*ldtC*775::*kan*	(Baba *et al*., 2006)
JW3359	BW25113 Δ*mrcA*::*kan*	(Baba *et al*., 2006)
JW0145	BW25113 Δ*mrcB*::*kan*	(Baba *et al*., 2006)
JW5157	BW25113 Δ*lpoB*::*kan*	(Baba *et al*., 2006)

JW0627	BW25113 Δ*dacA*::*kan*	(Baba *et al*., 2006)
JW0823	BW25113 Δ*dacC*::*kan*	(Baba *et al*., 2006)
JW5437	BW25113 Δ*rpoS*::*kan*	(Baba *et al*., 2006)
LOBSTR-BL21(DE3)	F– *ompT hsdS*B(rB– mB–) *gal dcm* (DE3), carries genomically modified copies of *arnA* and *slyD*	Kerafast
Plasmid		
pDACAhis	pET28a(+)derivative, for overexpression of His-PBP5	(Potluri *et al*., 2010)
pET28a-dacC	pET28a-dacC$^{28-400}$	This work
pGS100	pGZ119EH derivative, contains TIR sequence downstream of p*tac*, Cam^{R}	(Sperandeo *et al*., 2006)
pMN86	pET21b-yebA$^{40-440}$	(Singh *et al*., 2012)
pMUCα	pJFK118EH derivative, for ectopic expression of PBP1B	U. Bertsche, W. Vollmer, unpublished
pMUCα(mut)	pJFK118EH derivative, for ectopic expression of PBP1B S510A	U. Bertsche, W. Vollmer, unpublished
pMUC TG(mut)α	pJFK118EH derivative, for ectopic expression of PBP1B E233Q	U. Bertsche, W. Vollmer, unpublished
pMUC TG(mut) α(mut)	pJFK118EH derivative, for ectopic expression of PBP1B S510A E233Q	U. Bertsche, W. Vollmer, unpublished
pKD4	oriR; Amp^{R} Kan^{R}; source of *kan* cassette	Datsenko and Wanner, 2000
pRS415	pBR322 derivative; harbors the entire *lac* operon without promoter; Amp^{R}	(Simons *et al*., 1987)
pRS415-p*ldtD*	pRS415 derivative; expresses LacZ from the *ldtD* promoter region	This work
pRS415-p*ldtE*	pRS415 derivative; expresses LacZ from the *ldtE* promoter region	This work
pRS415-p*ldtF*	pRS415 derivative; expresses LacZ from the *ldtF* promoter region	This work
pET28a His6-*ldtF*	pET28a derivative; expresses LdtF from the T7 promoter starting from amino acid 20 and fused at N-terminal with 6xHis tag	This work
pETMM82 *dsbC*-His6-*ldtD*	pETMM82 derivative; expresses LdtD fused at N-terminal with DsbC and a 6×His tag	(Hugonnet *et al*., 2016)
pJEH12(*ldtD*)	pACYC184 derivative; expresses LdtD under the IPTG-inducible *trc* promoter; Tet^{R}	(Hugonnet *et al*., 2016)
pAMS01(*ldtE*)	pACYC184 derivative; expresses LdtE under the IPTG-inducible trc promoter; Tet^{R}	This work
pAMS02(*ldtF*)	pACYC184 derivative; expresses LdtF under the IPTG-inducible *trc* promoter; Tet^{R}	This work
pSAV057	ptrc99A derivative; contains weakened -35 promotor region (TTGACA-TTTACA); p15 origin; Cam^{R}	(Alexeeva *et al*., 2010)
pGS121	pGZ119H derivative; expresses LdtE under the *tac* promoter; Cam^{R}	This work
pGS123	pGZ119H derivative; expresses LdtD under the *tac* promoter; Cam^{R}	This work
pGS123C528A	pGZ119H derivative; expresses LdtDC528A under the *tac* promoter; Cam^{R}	This work
pGS124	pGZ119H derivative, expresses LdtF under the *tac* promoter; Cam^{R}	This work

Supplementary Table 2. Oligonucleotides.

Primer	Sequence 5' -> 3'	Description	Used to make
AP405/39 *ldtE*-f	CCGGAATTCACCATGAAACGCGCGTCTTTCCACTC	[CCG]-[*Eco*RI]-[ACC]-[start *ldtE*; fwd]	pGS121 construction
AP407/34 *ldtE*-r	CCCAAGCTTTTACTGCGTCACGCGTAACATATTC	[CCC]-[*Hind*III]-[TTA]-[stop *ldtE*; rev]	pGS121 construction
AP413/35 *ldtD*-f	ccggaattcaccATGTTGCTTAATATGATGTGTGG	[CCG]-[*Eco*RI]-[ACC]-[start *ldtD* fwd]	pGS123 construction
AP414/31-*ldtD*-r	ctagtctagaTTACCTGATTAATTGTTCCGC	[CTA]-[*Xba*I]-[stop *ldtD* rev]	pGS123 construction
AP458/31 *ldtF*-f	CCGGAATTCATGCGTAAAATCGCATTAATTC	[CCG]-[*Eco*RI]-[start *ldtF*; fwd]	pGS124 construction
AP460/34 *ldtF*-r	CCCAAGCTTTTATTTTGCCTCGGGGAGCGTGTAG	[CCC]-[*Hind*III]-[TTA]-[stop *ldtF*; rev]	pGS124 construction
AP475/33 *ldtD*-f	CGAGAGGAATTCGTGGTACAAAGCTGGGAAGAT	[CGAGAG]-[*Eco*RI]-[579 bp upstream of ATG of *ldtD*; fwd]	*ldtD*p cloning in pRS416
AP476/28 ldtD-r	CGCGGATCCTTTGCGTGCGGGCTTTTTC	[CGC]-[*Bam*HI]-[232 bp downstream of ATG of *ldtD*; rev]	*ldtD*p cloning in pRS416
AP477/31 *ldtE*-f	CCGAGAGGAATTCGTATTCACCGTTTGCTGGG	[CCGAGAG]-[*Eco*RI]-[601 bp upsrteam of ATG of *ldtE*; fwd]	*ldtE*p cloning in pRS415
AP478/27 *ldtE*-r	CGCGGATCCGGCGATAGTGTTATTGGC	[CGC]-[*Bam*HI]-[219 bp downstream of ATG of *ldtE*; rev]	*ldtE*p cloning in pRS415
AP490/30 *ldtF*-f	GGAATTCCATATGGGTTTGCTGGGCAGCAG	[GGAATTC]-[*Nde*I]-[starting at 58bp downstream of ATG of *ldtF*; fwd]	pET28a His6-*ldtF* cloning
AP491/29 *ldt*F-r	CCGCTCGAGTTATTTTGCCTCGGGGAGCG	[CCG]-[*Xho*I]-[stop *ldtF*; rev]	pET28a His6-*ldtF* cloning
AP538/32 *ldtF*-f	CGAGAGGAATTCGAATCAGGCAGCGGACGTAC	[CGAGAG]-[*Eco*RI]-[614 bp upstream of ATG of *ldtF*; fwd]	*ldtF*p cloning in pRS415
AP539/29 *ldtF*-r	TCCCCCCGGGCTCGCCCATTTTGACGTAG	[TCCC]-[*Sma*I]-[161 bp downstream of ATG of *ldtF*; rev]	*ldtF*p cloning in pRS416
AP651/33-*ldtD*mut	GAGCTCAGGCgcaGTACGAGTGAATAAAGCTTC	[10 bp complement of *ldtD*]- [TGT>GCA substitution]-[20 bp complement to *ldtD*]	*ldtD* mutagenesis
AP652/18-*ldtD*r	AATGCGCGTGTATCACGC	[18 bp complement to *ldtD*]	*ldtD* mutagenesis
AP565/83-*ldtD*Chf	CCAGCTCGCAAATCGTATCGAAAGCGGAACAATT AATCAGGCATCATCATCATCATCATTAAgtgtaggctgg agctgcttcg	[41 bp complement to *ldtD*]-[His tag coding sequence]-[taa stop codon]-[21 bp complement to *kan* cassette of pKD4]	*ldtD-his::kan* cassette construction
AP566/63-*ldtD*CHhr	CATGCTAATTATTACGACAACTGATTTCCCCGAAC TACTTCATcatatgaatatcctccttag	[41 bp complement to downstream region of *ldtD*]-[20 bp complement to *kan* cassette of pKD4]	*ldtD-his::kan* cassette construction
Pbp6a-sp_for	GCGCGCCATATGGCGGAACAAACCGTTG	[GCGCGC]-[*Nde*I]-[starting at 82 bp downstream of ATG of *dacC*; fwd]	pET28a His6-*dacC* cloning
Pbp6a-sp_rev	GCGCGCCTCGAGTTAAGAGAACCAGCTGCC	[GCGCGC]-[*XhoI*]-[stop *dacC*; rev]	pET28a His6-*dacC* cloning
AMS-GA7h-F	ATTTCACACAGGAAACAGACCATGGATGAAACGC GCGTCTTTGCTTAC	[24 bp complement of pJEH12(*ldtD*)]-[start of *ldtE*; fwd]	pAMS01(*ldtE*) construction
AMS-GA7h-R	GCATGCCTGCAGGTCGACTCTAGACTACTGCGTCA CGCGTAACATATTC	[24 bp complement of pJEH12(*ldtD*)]-[stop of *ldtE*; fwd]	pAMS01(*ldtE*) construction
AMS-GA7a_F	ATTTCACACAGGAAACAGACCATGGATGCGTAAA ATCGCATTAATTC	[24 bp complement of pJEH12(*ldtD*)]-[start of *ldtF*; fwd]	pAMS02(*ldtF*) contruction
AMS-GA7a_R	GCATGCCTGCAGGTCGACTCTAGATTATTTTGCCT CGGGGAGCG	[24 bp complement of pJEH12(*ldtD*)]-[stop of *ldtF*; fwd]	pAMS02(*ldtF*) contruction
AMS-GA7_F	TCTAGAGTCGACCTGCAGGCATGC	pACYC plasmid linearization for Gibson; fwd	pAMS01(*ldtE*) and pAMS2(*ldtF*) contruction
AMS-GA7_R	CCATGGTCTGTTTCCTGTGTGAAATT	pACYC plasmid linearization for Gibson; rev	pAMS01(*ldtE*) and pAMS2(*ldtF*) contruction

Supplementary Table S3. Muropeptide composition of *ldt* mutant strains (lptC^{+})

	BW25113	Δ*ldtD*	Δ*ldtE*	Δ*ldtF*	Δ*ldtD* Δ*ldtE*	Δ*ldtD* Δ*ldtF*	Δ*ldt*E Δ*ldtF*	Δ*ldtD* Δ*ldtE* Δ*ldtF*	ΔldtA ΔldtB ΔldtC ΔldtD ΔldtE ΔldtF
	Sample 1	Sample 2	Sample 3	Sample 4	Sample 5	Sample 6	Sample 7	Sample 8	Sample 9
Muropeptide									
Tri	6,61	6,35	6,22	1,96	7,37	0,00	1,38	0,00	0,00
TetraGly 4	1,70	1,72	1,68	2,85	1,47	2,68	2,55	2,55	0,00
Tetra	40,09	39,71	39,90	45,32	41,47	47,91	44,60	46,60	58,89
Di	1,82	1,81	2,12	1,54	1,99	1,80	1,82	1,99	0,88
TetraTri(DAP)Gly4	0,00	0,00	0,00	0,00	0,32	0,00	0,00	0,00	0,00
TriTri(DAP)	0,00	0,00	0,00	0,00	0,00	0,00	0,00	0,00	0,00
TetraTri(DAP)	2,96	3,16	2,85	2,88	2,18	0,00	2,41	0,00	0,00
TetraTetraGly4	0,00	0,00	0,00	0,00	0,00	0,00	0,00	0,00	0,00
TetraTri	3,31	3,13	3,39	2,45	4,30	1,72	2,12	1,64	0,00
TetraTetra	30,06	29,28	29,57	31,53	30,24	34,43	31,42	34,31	35,36
TetraPenta	0,64	0,60	0,65	0,64	0,34	0,66	1,03	0,51	0,94
TetraTetraTri	0,40	0,72	0,81	0,00	0,00	0,00	0,00	0,00	0,00
TetraTetraTetra	2,93	2,83	2,89	2,88	2,82	3,07	2,89	3,71	2,03
TetraTriAnh I	0,00	0,00	0,00	0,00	0,00	0,40	0,00	0,00	0,00
TeraTriAnh II	0,00	0,00	0,00	0,00	0,00	0,00	0,00	0,00	0,00
TetraTetraAnh I	0,63	0,61	0,64	1,92	1,44	1,40	1,62	1,35	1,15
TeraTetraAnh II	0,93	0,92	0,96	0,68	0,65	0,75	0,71	0,83	0,75
TetraTetraTriAnh	0,48	0,51	0,38	0,00	0,00	0,00	0,00	0,00	0,00
TetraTetraTetra Anh	1,34	1,63	0,95	0,75	0,93	0,94	0,85	1,02	0,00
all known	93,90	92,98	93,01	95,40	95,52	95,76	93,40	94,51	100,00
Monomers (total)	53,48	53,33	53,67	54,16	54,75	54,71	53,91	54,11	59,77
Monomer di	1,94	1,95	2,28	1,61	2,08	1,88	1,95	2,11	0,88
Monomer tri	7,04	6,83	6,69	2,05	7,72	0,00	1,48	0,00	0,00
Monomer tetra	42,69	42,71	42,90	47,51	43,41	50,03	47,75	49,31	58,69
Monomer tetraGly4	1,81	1,85	1,81	2,99	1,54	2,80	2,73	2,70	0,00
Dimers (total)	41,03	40,55	40,92	42,03	40,99	41,10	42,09	40,88	38,20
Dimers(4-3)	37,88	37,15	37,86	39,01	38,70	41,10	39,51	40,88	38,20
Dimers(3-3)	3,15	3,40	3,06	3,02	2,62	0,00	2,58	0,00	0,00
Dimers anhydroMurNAc	1,66	1,65	1,72	2,73	2,19	2,66	2,49	2,31	1,90
Trimers (Total)	5,48	6,12	5,41	3,81	3,93	4,19	4,00	5,00	2,03
Trimer (anhydro)	1,94	2,30	1,43	0,79	0,97	0,98	0,91	1,08	0,00
Dipeptides (total)	1,94	1,95	2,28	1,61	2,08	1,88	1,95	2,11	0,88
Tripeptides (total)	10,05	9,92	9,75	4,63	10,77	1,06	3,65	0,82	0,00
Tetrapeptides (total)	85,79	85,71	85,71	92,70	86,08	97,19	93,17	97,47	99,23
Pentapeptides (total)	0,34	0,32	0,35	0,34	0,18	0,34	0,55	0,27	0,47
Degree of 3-3 linkage	1,58	1,70	1,53	1,51	1,31	0,00	1,29	0,00	0,00
Chain ends (anhydroMurNAc)	1,48	1,59	1,34	1,62	1,42	1,66	1,55	1,51	0,95
Degree of cross-linkage	24,17	24,35	24,07	23,55	23,11	23,34	23,71	23,78	20,45
% Peptides in cross-links	46,52	46,67	46,33	45,84	45,25	45,29	46,09	45,89	40,23

Supplementary Table S3. Muropeptide composition of *ldt* mutant strains with or without depletion of *lptC* (*araB*p*lptC*)

	BB-3 (*araB* p*lptC*)	BB-3 (*araB* p*lptC*)	BB-3 (*araB* p*lptC*)	BB-3 (*araB* p*lptC*)	BB-3 Δ*ldtD*	BB-3 Δ*ldtD*	BB-3 Δ*ldtD*	BB-3 Δ*ldtD*	BB-3 Δ*ldtE*	BB-3 Δ*ldtE*	BB-3 Δ*ldtE*	BB-3 Δ*ldtE*	BB-3 Δ*ldtF*	BB-3 Δ*ldtF*	BB-3 Δ*ldtF*	BB-3 Δ*ldtD* Δ*ldtE*	BB-3 Δ*ldtD* Δ*ldtE*	BB-3 Δ*ldtD* Δ*ldtF*	BB-3 Δ*ldtD* Δ*ldtF*	BB-3 Δ*ldtE* Δ*ldtF*	BB-3 Δ*ldtE* Δ*ldtF*	BB-3 Δ*ldtE* Δ*ldtF*	BB-3 Δ*ldtE* Δ*ldtF*	BB-3 Δ*ldtD* Δ*ldtE* Δ*ldtF*	BB-3 Δ*ldtD* Δ*ldtE* Δ*ldtF*
	+ Arabinose	+ Arabinose	No Arabinose, early depletion	No Arabinose, late depletion	+ Arabinose	+ Arabinose	No Arabinose, early depletion	No Arabinose, early depletion	+ Arabinose	+ Arabinose	No Arabinose, early depletion	No Arabinose, early depletion	+ Arabinose	+ Arabinose	No Arabinose, early depletion	No Arabinose, early depletion	+ Arabinose	+ Arabinose	+ Arabinose	No Arabinose, early depletion	+ Arabinose	+ Arabinose	No Arabinose, early depletion	No Arabinose, early depletion	+ Arabinose	No Arabinose, early depletion
	OD = 0.4 - 0.6	OD = 2.0																								
	Sample 1	Sample 2	Sample 3	Sample 4	Sample 5	Sample 5 repeat	Sample 6	Sample 6 repeat	Sample 7	Sample 7 repeat	Sample 8	Sample 8 repeat	Sample 9	Sample 9 repeat	Sample 10	Sample 10 repeat	Sample 11	Sample 11 repeat	Sample 12	Sample 13	Sample 14	Sample 14 repeat	Sample 15	Sample 15 repeat	Sample 16	Sample 17
Muropeptide	Relative peak area (%)																									
Tri	7,1	7,7	6,3	6,8	7,0	6,5	7,7	3,5	5,7	5,6	5,2	5,3	2,0	6,7	3,3	5,5	1,8	1,6	0,0	0,0	2,2	5,7	4,2	5,8	0,0	0,0
TetraGly 4	1,8	2,5	1,6	1,8	1,3	1,3	1,0	1,3	1,2	1,1	1,3	1,3	2,9	2,6	1,8	1,8	2,5	2,7	2,2	2,8	2,2	1,7	2,4	1,8	2,6	1,5
Tetra	38,7	37,4	43,5	31,9	43,9	41,9	40,3	44,4	38,9	40,5	40,7	42,7	40,0	40,8	29,7	37,1	41,7	42,0	49,7	45,6	40,9	35,5	35,9	37,0	47,6	50,9
Di	1,8	2,0	0,0	0,0	0,9	1,0	0,7	1,0	1,4	1,4	0,0	0,0	1,8	2,0	1,0	0,5	1,8	2,0	1,4	2,3	0,8	0,5	0,6	0,6	1,6	0,9
TetraTri(DAP)Gly4	0,0	0,0	0,0	0,0	0,0	0,0	0,0	0,0	0,0	0,0	0,0	0,0	0,0	0,0	0,4	0,4	0,0	0,0	0,0	0,0	0,0	0,5	0,5	0,4	0,0	0,0
TriTri(DAP)	0,0	0,0	0,0	0,0	0,0	0,0	0,0	0,0	0,0	0,0	0,0	0,0	0,0	0,4	0,7	1,1	0,0	0,0	0,0	0,0	0,0	1,2	1,1	1,1	0,0	0,0
TetraTri(DAP)	1,9	1,7	7,5	10,8	2,4	2,3	5,9	6,3	2,1	1,7	6,1	5,8	1,9	3,2	8,4	9,8	1,9	1,8	0,0	0,0	8,2	10,1	8,4	10,0	0,0	0,0
TetraTetraGly4	0,4	0,7	0,0	0,9	0,0	0,0	0,5	0,5	0,7	0,7	0,7	0,6	2,0	0,0	1,1	0,0	2,0	2,1	0,0	1,9	1,4	0,0	1,6	0,0	1,3	0,9
TetraTri	4,8	4,8	2,7	3,4	2,5	2,7	0,9	0,9	1,4	1,4	1,4	1,3	1,1	4,1	1,0	2,8	0,8	0,6	1,4	0,0	0,9	2,9	1,9	2,9	0,0	0,0
TetraTetra	28,4	27,0	26,5	22,2	27,7	28,7	27,4	27,1	28,4	29,1	27,8	27,6	29,3	29,4	25,3	25,0	31,4	31,1	32,2	34,3	25,9	24,4	24,3	24,4	29,8	30,7
TetraPenta	1,0	0,9	0,6	0,7	1,1	1,1	0,5	0,7	4,1	3,8	1,5	1,5	0,8	0,7	0,7	0,6	0,3	0,9	0,8	0,7	1,0	0,6	0,7	0,6	0,9	1,3
TetraTetraTri	1,0	2,4	0,0	2,4	2,7	3,0	2,3	2,3	0,6	0,9	1,0	1,0	1,6	0,0	1,3	0,8	1,6	1,3	0,0	1,4	1,1	0,9	1,0	0,9	1,3	1,1
TetraTetraTetra	0,0	1,1	0,0	0,6	1,7	1,3	1,5	1,5	2,4	2,3	2,7	2,5	3,0	2,5	3,2	2,4	3,0	2,9	3,3	2,7	2,6	2,5	2,5	2,4	2,7	2,9
TetraTriAnh I	1,2	0,0	1,0	0,9	0,0	0,0	0,5	0,6	1,4	1,5	1,3	1,0	0,0	0,0	1,2	0,8	2,2	1,7	0,0	1,9	0,6	0,9	0,7	0,9	0,0	0,0
TeraTriAnh II	0,0	0,0	0,0	0,8	0,0	0,0	0,5	0,6	0,0	0,0	0,0	0,0	0,0	0,0	1,0	0,8	0,0	0,0	0,0	0,0	0,7	0,9	0,9	0,8	0,0	0,0
TetraTetraAnh I	0,7	1,7	0,7	0,8	0,8	1,0	1,4	1,4	0,7	0,7	1,0	0,9	0,6	1,2	1,5	1,0	0,7	0,8	1,7	0,8	1,0	1,0	1,3	0,6	0,6	1,5
TeraTetraAnh II	1,5	0,0	0,8	0,9	1,2	1,3	1,3	1,4	0,9	0,9	1,2	1,1	1,2	0,4	2,1	0,4	1,1	1,1	0,8	1,2	1,5	0,5	1,8	0,6	1,1	1,8
TetraTetraTriAnh	0,0	0,0	0,0	1,4	0,0	0,0	0,0	0,0	0,4	0,9	0,0	0,0	0,0	0,0	0,0	0,0	0,0	0,0	0,5	0,0	0,0	0,0	0,0	0,0	0,0	0,0
TetraTetraTetra Anh	1,3	1,8	0,0	0,9	1,0	1,3	1,3	1,2	1,0	0,7	1,4	1,2	1,1	0,8	1,7	1,3	1,0	1,0	1,1	0,8	1,2	1,6	1,4	1,5	0,9	1,5
all known	91,5	91,9	91,3	87,1	94,3	93,4	93,7	94,7	91,3	93,0	93,3	93,6	89,4	94,8	85,2	92,1	93,8	93,7	95,0	96,2	92,2	91,4	91,3	92,2	90,3	95,0
Monomers (total)	53,9	54,1	56,4	46,6	56,4	54,3	53,1	53,0	51,9	52,2	50,7	52,6	52,3	55,0	42,0	48,7	50,9	51,6	56,0	52,6	49,9	47,5	47,2	48,9	57,4	56,0
Monomer di	1,9	2,2	0,0	0,0	1,0	1,1	0,8	1,0	1,6	1,5	0,0	0,0	2,0	2,1	1,2	0,5	1,9	2,1	1,4	2,4	0,9	0,5	0,7	0,6	1,8	0,9
Monomer tri	7,7	8,4	6,9	7,9	7,4	6,9	8,2	3,7	6,3	6,0	5,6	5,6	2,3	7,1	3,9	6,0	1,9	1,7	0,0	0,0	2,3	6,3	4,6	6,3	0,0	0,0
Monomer tetra	42,3	40,7	47,6	36,7	46,6	44,8	43,0	46,9	42,7	43,6	43,7	45,6	44,8	43,0	34,8	40,2	44,5	44,8	52,3	47,4	44,4	38,8	39,3	40,1	52,7	53,5
Monomer tetraGly4	2,0	2,7	1,8	2,0	1,4	1,4	1,0	1,4	1,3	1,2	1,4	1,3	3,3	2,7	2,1	2,0	2,7	2,9	2,3	2,9	2,4	1,8	2,7	1,9	2,8	1,6
Dimers (total)	43,6	40,1	43,6	47,4	37,9	39,7	41,6	41,7	43,3	42,6	43,9	42,5	41,3	41,6	49,6	46,3	43,2	42,8	38,8	42,4	44,7	47,0	45,8	45,9	37,2	38,2
Dimers(4-3)	41,5	38,2	35,4	35,1	35,3	37,2	35,2	35,0	41,1	40,8	37,4	36,3	39,2	37,8	39,8	34,0	41,2	40,9	38,8	42,4	35,8	34,1	36,5	33,4	37,2	38,2
Dimers(3-3)		1,9	8,2	12,4	2,6	2,5	6,3	6,7	2,3	1,8	6,5	6,2	2,1	3,8	11,0	12,3	2,0	1,9	0,0	0,0	8,9	12,9	11,0	12,5	0,0	0,0
Dimers anhydroMurNAc	3,7	1,9	2,8	3,9	2,1	2,5	3,9	4,2	3,2	3,2	3,8	3,2	2,0	1,7	6,8	3,2	4,3	3,9	2,6	4,0	4,2	3,5	5,2	3,1	1,8	3,5
		2,1																								
Trimers (Total)	2,4	5,8	0,0	6,0	5,8	6,0	5,4	5,3	4,8	5,2	5,5	4,9	6,4	3,5	7,2	5,0	5,9	5,6	5,2	5,0	5,4	5,5	5,4	5,1	5,4	5,8
Trimer (anhydro)	1,4	2,0	0,0	2,6	1,1	1,4	1,4	1,3	1,6	1,7	1,5	1,3	1,2	0,8	2,0	1,4	1,0	1,1	1,7	0,8	1,3	1,7	1,5	1,6	1,0	1,6
Dipeptides (total)	1,9	2,2	0,0	0,0	1,0	1,1	0,8	1,0	1,6	1,5	0,0	0,0	2,0	2,1	1,2	0,5	1,9	2,1	1,4	2,4	0,9	0,5	0,7	0,6	1,8	0,9
Tripeptides (total)	11,3	11,8	11,9	16,1	10,4	10,0	12,4	8,5	8,5	8,5	10,0	9,7	4,1	10,8	10,3	14,2	4,7	4,1	0,9	1,4	7,8	14,9	11,8	14,7	0,4	0,4
Tetrapeptides (total)	83,7	84,4	82,3	74,9	86,6	86,9	83,0	86,8	85,4	86,0	85,1	85,7	93,3	85,1	86,4	78,5	91,1	91,5	98,1	95,2	90,4	77,3	86,3	77,6	97,5	98,8
Pentapeptides (total)	0,6	0,5	0,3	0,4	0,6	0,6	0,3	0,4	2,2	2,0	0,8	0,8	0,4	0,4	0,4	0,3	0,2	0,5	0,4	0,3	0,5	0,3	0,4	0,3	0,5	0,7
Degree of 3-3 linkage	1,1	0,9	4,1	6,2	1,3	1,2	3,2	3,3	1,1	0,9	3,3	3,1	1,1	1,9	5,5	6,2	1,0	1,0	0,0	0,0	4,5	6,5	5,5	6,3	0,0	0,0
Chain ends (anhydroMurNAc)	2,3	1,6	1,4	2,8	1,4	1,7	2,4	2,5	2,1	2,2	2,4	2,0	1,4	1,1	4,1	2,1	2,5	2,3	1,9	2,2	2,5	2,3	3,1	2,1	1,2	2,3
Degree of cross-linkage	23,4	23,9	21,8	27,7	22,8	23,9	24,4	24,4	24,9	24,7	25,6	24,5	24,9	23,1	29,6	26,5	25,5	25,1	22,9	24,5	26,0	27,2	26,5	26,4	22,2	22,9
% Peptides in cross-links	46,1	45,9	43,6	53,4	43,6	45,7	46,9	47,0	48,1	47,8	49,3	47,4	47,7	45,1	58,0	51,3	49,1	48,4	44,0	47,4	50,1	52,5	52,8	51,1	42,6	44,0

3.2 Characterisation of YgeR, a novel amidase regulator in *Escherichia coli*

The following chapter contains unpublished original research, for which I was the main author, submitted for publication.

Characterisation of YgeR, a novel amidase regulator in *Escherichia coli*

Carlos K. Gurnani Serrano,[a] Matthias Winkle,[b] Alessandra M. Martorana,[a], Niccolo Morè,[c] Waldemar Vollmer,[b] Alessandra Polissi[a].

[a]Dipartimento di Scienze Farmacologiche e Biomolecolari, Università degli Studi di Milano, Milan, Italy;

[b]The Centre for Bacterial Cell Biology, Institute for Cell and Molecular Biosciences, Newcastle University, Newcastle upon Tyne, United Kingdom.

[c]Nikon Instruments Europe B.V., Amsterdam, North Holland, Netherlands.

ABSTRACT

The integrity of the cell envelope of *E. coli* relies on the concerted activity of dedicated multiprotein machinery that govern the biogenesis of the three envelope layers: the inner membrane (IM), the peptidoglycan (PG), and the outer membrane (OM) which is coated with lipopolysaccharide (LPS) in the outer leaflet. Defects in LPS export to the OM induce a PG remodeling programme orchestrated by LD-Transpeptidases (LDTs). Indeed, lack of LDTs when OM biogenesis is defective, results in cell lysis. Here we found that the lysis phenotype and morphological defects observed in cells with impaired LPS transport and defective in *ldtF*, are corrected by the loss of YgeR, a predicted OM lipoprotein. We also show that YgeR, a member of the LytM-domain factors, functions as an amidase activator. While *in vitro* YgeR is capable to activate the three periplasmic amidases produced by *E. coli* AmiA, AmiB and AmiC, *in vivo* it preferentially activates AmiC. Overall, YgeR is a novel amidase activator whose action seems required upon envelope stress.

KEYWORDS *Escherichia coli*, cell envelope, lipopolysaccharide, peptidoglycan, cell division.

INTRODUCTION

The cell envelope of Gram-negative bacteria is composed of the inner membrane (IM), the outer membrane (OM), and the aqueous space between them, the periplasm, in which a thin layer of peptidoglycan (PG) is embedded (Silhavy et al., 2010; Huang et al., 2008). The IM is a phospholipid bilayer, while the OM is asymmetric containing mainly lipopolysaccharide (LPS) in the outer leaflet (Henderson et al., 2016; Silhavy et al., 2010). The OM asymmetry is guaranteed by Lipopolysaccharide transport machinery (Lpt) that escorts LPS from the IM across the periplasm to its final destination at the OM outer layer. (Whitfield and Trent, 2014; Sperandeo et al., 2019). In *Escherichia coli* the Lpt machinery is composed by seven essential proteins (LptABCDEFG) located in every cellular compartment that assemble to form a transenvelope complex (Chng et al., 2010; Okuda et al., 2016; Sperandeo et al., 2019). The Lpt machinery works as a single device, indeed when any Lpt component is depleted transport of LPS is blocked, cells arrest growth and form chains (Sperandeo et al., 2008; Ruiz et al., 2008).

The PG layer, located in between the IM and OM, is an essential continuous mesh-like layer that coats the IM, and which is needed to confer osmotic and structure stability. The PG layer is composed of glycan chains of alternating N-acetylglucosamine and N-acetylmuramic acid residues connected by short peptides (Vollmer et al., 2008). The stem peptides are typically connected in a 4-3 (DD) configuration with cross-links occurring between D-alanine and meso-Diaminopimelic acid (mDAP) residues and these bonds are catalysed by the DD-TPase activity of the class A Penicillin Binding Proteins (PBPs) PBP1A and PBP1B and class B PBP2 and PBP3 (Typas et al., 2011; Sauvage et al., 2008). Stem peptides can also be connected in a 3-3 (LD) configuration, linking two mDAP residues, this type of cross-link is made by LD-transpeptidases, (LDTs) (Vollmer et al., 2008). The PG of *Escherichia coli* contains a very low proportion of 3-3 bonds (2-10%) compared to that of 4-3 bonds (90-98%) (Höltje, 1998). *E. coli* has six LDTs (LdtA-F) with two distinct functions. LdtA, LdtB and LdtC catalyse the attachment of the abundant OM lipoprotein Lpp to the PG (Magnet et al., 2007) whereas LdtD and LdtE catalyse the formation of 3-3 cross-links (Magnet et al., 2008). LdtF, which does not have LD-TPase activity, seems to stimulate the activity of LdtE and LdtD (Montón Silva et al., 2018; Morè et al., 2019). LDTs are not essential for growth under laboratory conditions since mutants deleted for single or multiple *ldts* display only minor phenotypes (Magnet et al., 2007, Magnet et al., 2008; Pavelka and Sanders 2013; Morè et al., 2019). Although *ldts*

are dispensable under non-stress conditions, they become essential for cell survival upon OM stress. Indeed, deletion of *ldtD*, *ldtE* or *ldtF*, but not deletion of *ldts* catalysing the attachment of Lpp to PG, causes cell lysis when LPS transport is compromised (Morè et al., 2019). Cell envelope integrity of these mutants is restored when *ldtD* is ectopically expressed, thus suggesting a protective role of LdtD to counteract OM assembly defects (Morè et al., 2019).

The PG sacculus is in a constant reshuffle, demanding a synergism among PG synthesis and hydrolysis. Indeed, PG hydrolases are critical to ensure cell wall elongation and division (Uehara and Bernhardt, 2011). In *E. coli* about 30 % of newly made septal PG is removed shortly after its synthesis by hydrolases (Uehara and Park, 2008), mostly lytic transglycosylases and amidases. N-acetylmuramyl-L-alanine amidases cleave the amide bond within the L-alanine residue of the stem peptide and the N-Acetylmuramic acid subunit of the glycan chain. In *E. coli* this enzymatic activity is carried out by the redundant AmiA, AmiB and AmiC amidases. AmiA appears to be dispersed in the periplasm during cell division in contrast to AmiB and AmiC, which localize at the septum (Yang et al., 2011; Bernhardt and de Boer, 2003; Peters et al., 2011). The lack of any single amidase has a minor impact on the cell. However, loss of the three amidases results in the formation of long strings of chained cells due to merged septal PG of daughter cells (Heidrich et al., 2001; Priyadarshini et al., 2007).

Amidases overexpression leads to cell lysis, hence their activity must be tightly regulated in the cell (Heidrich et al., 2001). Amidase activity is controlled by the divisome associated proteins EnvC and NlpD. AmiA and AmiB are activated by EnvC whereas AmiC is activated by NlpD (Uehara et al., 2010). Mutants lacking *envC* and *nlpD* exhibit a severe cell chaining phenotype that resembles that of the triple *amiABC* mutant (Uehara et al., 2010). Both, EnvC and NlpD belong to the LytM (lysostaphin/peptidase M23)-domain containing proteins (Uehara et al., 2009). Proteins containing a LytM domain are present in many bacteria, with most of them playing an important role in PG hydrolysis and cell division (Meisner and Moran, 2011; Sabala et al., 2012; Zielińska et al., 2017). Notably, EnvC and NlpD, which are not PG hydrolases, carry a degenerate LytM domain missing residues required for function (Uehara et al., 2010; Peters et al., 2013). In addition to EnvC and NlpD, *E. coli* encodes two more LytM-domain factors, MepM and YgeR. MepM is a metallo-endopeptidase that cleaves 4-3 crosslinks in PG (Singh et al., 2012), whereas YgeR is an uncharacterised lipoprotein with predicted OM localisation (Uehara

et al., 2009). Deletion of MepM and YgeR slightly exacerbates the cell chaining phenotype of the double *envC nlpD* mutant (Uehara et al., 2009).

In this work, we show that lack of YgeR rescues from lysis cells defective in LPS transport in which *ldtF* is deleted. Notably, recovery from lysis is not due to an increased level of 3-3 crosslinks in PG. We also show that YgeR, which does not have PG hydrolase activity per se, functions as an amidase regulator, consistent with the finding that it displays a degenerate LytM domain. Finally, we show that in *vivo* YgeR preferentially activates AmiC through its LytM domain.

RESULTS

Deletion of *ygeR* rescues *araB*p*lptC* Δ*ldtF* cells from lysis

Previous data showed that deletion of *ldtF* in mutants defective for LPS transport is lethal. Indeed, an *araB*p*lptC* conditional mutant in which in which *lptC* expression is under the control of the arabinose-inducible *araB*p promoter undergoes to rapid lysis when the *ldtF* gene is deleted (Morè et al., 2019). LdtF does not catalyse the formation of 3-3 crosslinks in PG, but instead stimulates LdtE and LdtD activity (Montón Silva et al., 2018; Morè et al., 2019). Notably, *araB*p*lptC* conditional mutant lacking *ldtF* shows morphological defects even when grown under permissive conditions (+ Ara). On the contrary no morphological defects are observed in *araB*p*lptC* mutants lacking *ldtE* or *ldtD*. These data suggested that LdtF might have an additional role in the cell (Morè et al., 2019, see also **Fig. S3** of **previous chapter 3.1**) and prompted us to identify possible functional partners of LdtF. For this purpose, we took advantage of the online tool https://ecoliwiki.org/tools/chemgen/ which carries the phenotypic signature of hundreds of mutants of the KEIO collection (Baba et al., 2006) tested under thousand conditions, thus creating a phenomic profile of *E. coli* (Nichols et al., 2011). Using this tool, we found that mutants deleted for *ldtF* (*yafK*) shared a good correlation (score 0.48) with the phenotypic profile of mutants deleted for *ygeR*. YgeR is a predicted OM lipoprotein of 251 aa (UniProtKB accession number Q46798), with unknown function that belongs to the LytM-domain family of proteins (Uehara et al., 2009). To probe a functional connection between YgeR and LdtF and, more in general, with LDTs, we combined the *ygeR* deletion with that of the *ldts*, in the wild type strain BW25113 (*lptC*$^{+}$) and in the

conditional *araB*p*lptC* mutant. Indeed, we found a specific link between *ygeR* and *ldtF* since the deletion of *ygeR* suppresses the lysis phenotype of *araB*p*lptC* cells deleted for *ldtF*, and the strain arrests growth under nonpermissive conditions (no Ara) (**Fig. 1**). No rescue from lysis is observed when the deletion of *ygeR* is combined to that of *ldtE* or *ldtD* in the *araB*p*lptC* conditional mutant (**Fig. S1**). Phase-contrast and fluorescence microscopy of *araB*p*lptC* Δ*ldtF* Δ*ygeR* cells clearly show that deletion of *ygeR* rescues not only the lysis phenotype upon LPS defective transport but also corrects the observed morphological defects of the a*raB*p*lptC* Δ*ldtF* mutant grown under permissive condition (Morè et al., 2019) **(Fig. 1)**. In contrast, we did not observe any defect on growth and morphology in *lptC*$^{+}$ mutants when *ygeR* was deleted alone (**Fig. S2**) or in combination with that of *ldD*, *ldtE* and *ldtF* (**Fig. S3**).

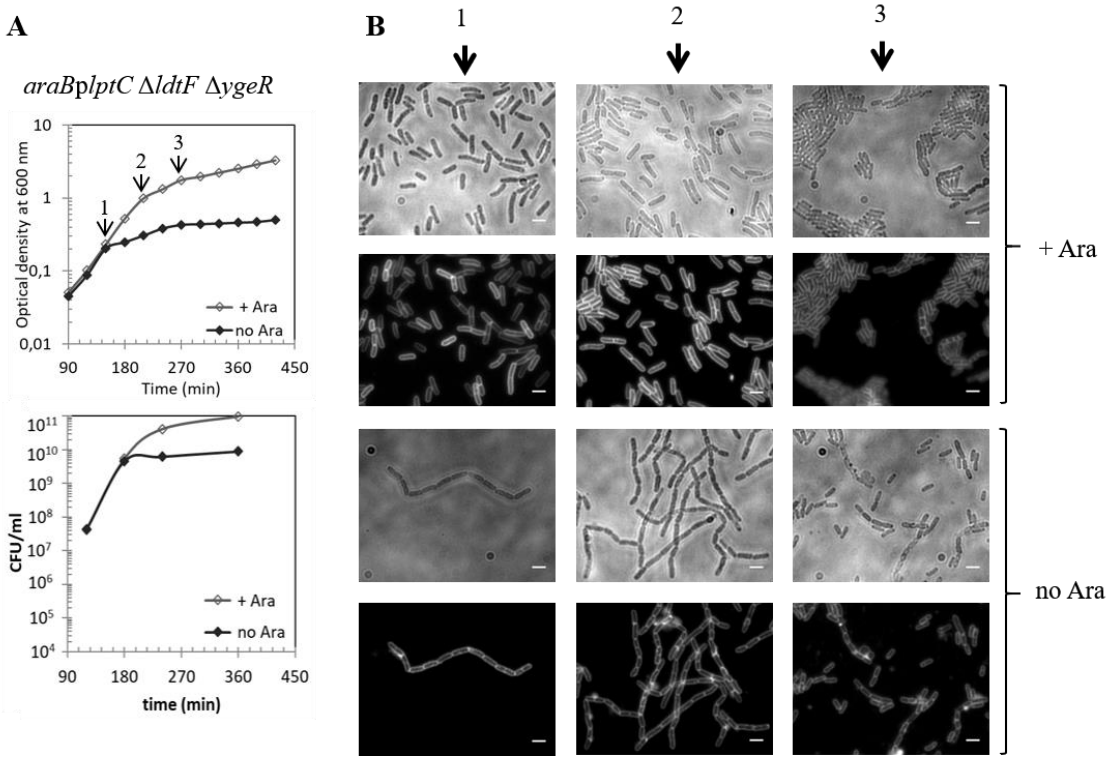

Figure 1. Deletion of *ygeR* rescues cell lysis and morphological defects of *araB*p*lptC* Δ*ldtF*. Cells of *araB*p*lptC* Δ*ldtF* Δ*ygeR* (**A**) were grown in the presence of 0.2% arabinose to an OD_{600} of 0.2, harvested, washed three times, and resuspended in an arabinose-supplemented (+ Ara) or arabinose-free (no Ara) medium. Growth was monitored by OD_{600} measurements (top panel) and by determining CFU (bottom panel). At t=150, 210, and 270 min (arrows), (**B**) cells were collected for imaging. Phase-contrast images (top) and fluorescence images (bottom) are shown. Bars, 3 μm.

We confirmed that the deletion of *ygeR* does rescue the cells from lysis as *araB*p*lptC* Δ*ldtF* Δ*ygeR* cells complemented with *ygeR* ectopically expressed from pGS100-*ygeR*

plasmid undergo lysis. (**Fig. 2 and Fig. S4)**. This result strongly suggests that is the loss of *ygeR* that suppresses the lysis phenotype

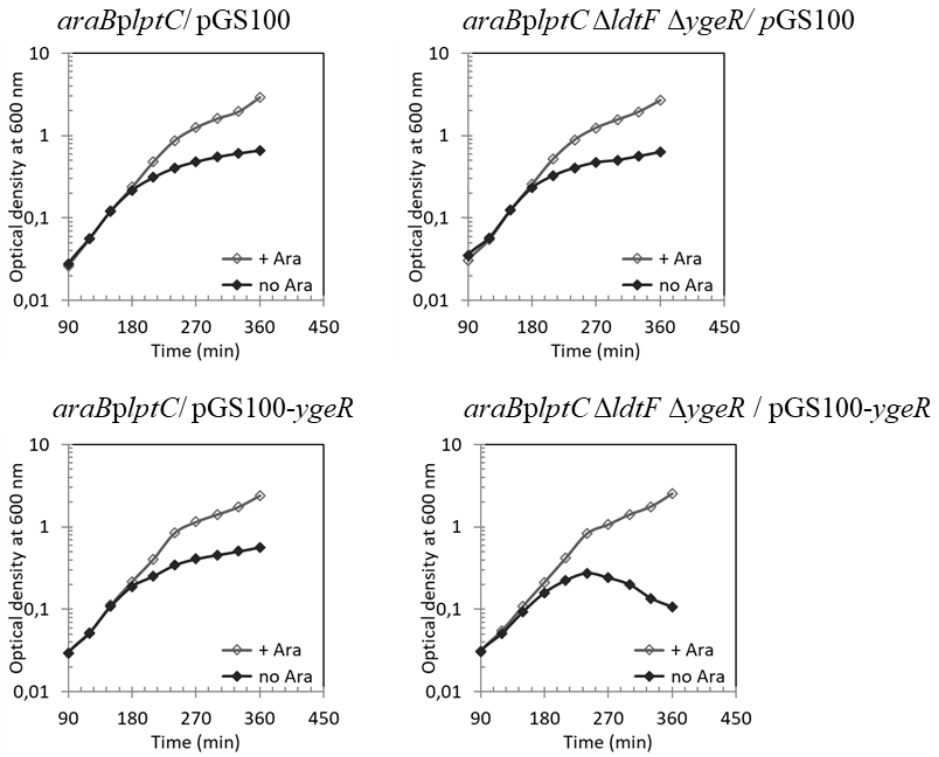

Figure 2. Ectopic expression of *ygeR* restores lysis phenotype in *araB*p*lptC* Δ*ldtF* Δ*ygeR*. Cells of *araB*p*lptC* and *araB*p*lptC* Δ*ldtF* Δ*ygeR* strains carrying pGS100 or pGS100-*ygeR* plasmids were grown in the presence of 0.2% arabinose to an OD_{600} of 0.2, harvested, washed three times, and resuspended in an arabinose-supplemented (+ Ara) or arabinose-free (no Ara) medium. Cell growth was monitored by OD_{600} measurements.

Recovery from lysis in *araB*p*lptC* Δ*ldtF* Δ*ygeR* strain is not related to the degree of 3-3 crosslinkage in PG

Previous work showed that LdtD is the stress LDT in *E. coli* cells. LdtD expression is strongly induced under LPS defective biogenesis and in the absence of LdtE and LdtF resulting in increased levels of 3-3 crosslinks in the PG. 3-3 crosslinks play a protective role of under these conditions as witnessed by the observation that *araB*p*lptC* mutant cells lacking *ldtE* and *ldtF* do not lyse and shows high level of 3-3 crosslinks even under permissive growth conditions (**Fig. 3B**) (Morè et al., 2019). We therefore analysed the PG composition of *araB*p*lptC* Δ*ldtF* Δ*ygeR* strain to assess whether suppression of lysis phenotype is due an increased level of the 3-3 crosslinks is the PG. The muropeptides analysis of the sacculi from *araB*p*lptC* Δ*ldtF* Δ*ygeR* cells show that the degree of 3-3

crosslinkage cannot account for the observed phenotype. (**Fig. 3**, see also **Table S4** and **S5** in the supplemental material**)**. Indeed, the level of 3-3 crosslinks in *araB*p*lptC* Δ*ldtF* Δ*ygeR* mutant was comparable to that of the *araB*p*lptC* conditional strain and its derivative deleted for *ygeR* both under permissive and non-permissive conditions (**Fig. 3B, Tables S4** and **S5)**. These data suggest that lack of YgeR does not impact on the level of 3-3 crosslinks in the PG and that the rescue from lysis phenotype observed is not due to protective PG remodeling.

A

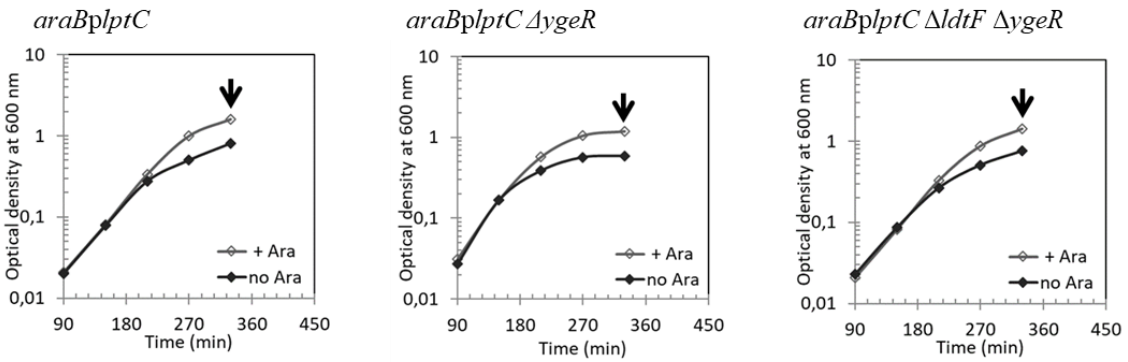

B

Presence/ absence of gene				*lptC*$^+$ strain	*araB* p*lptC* strain			
					With arabinose		No arabinose	
ldtF	*ldtD*	*ldtE*	*ygeR*	Growth	Growth	3-3 CL (area [%])	Growth	3-3 CL (area [%])
+	+	+	+	Normal	Normal	2,02	Arrest	6,72
+	+	+	-	Normal	Normal	2,5	Arrest	6,25
+	-	+	-	Normal	Normal	NT	Lysis	NT
+	+	-	-	Normal	Normal	NT	Lysis	NT
-	+	+	-	Normal	Normal	2,15	Arrest	7,33
-	+	+	+	Normal*	Normal*	1,9*	Lysis*	8,4*
-	+	-	+	Normal*	Normal*	8,2*	Arrest*	8,4*

Figure 3. The rescue from the lysis of the *araB*p*lptC* Δ*ldtF* Δ*ygeR* strain is not related to 3-3 crosslinks level. (A) Cells of the *araB*p*lptC* conditional strain and the isogenic mutants deleted for *ygeR* and *ldtF* were grown in the presence of 0.2% arabinose to an OD_{600} of 0.2, harvested, washed three times, and resuspended in an arabinose-supplemented (+ Ara) or arabinose-free (no Ara) medium, at 330 min (arrows) PG sacculi were extracted for analysis. (B) Summary of the level of 3-3 cross-links (CL) in PG and growth phenotype of *ldt* mutant strains, combined with *ygeR* deletion in *lptC* depleted or not depleted cells. NT, (not tested); *, Data from Morè et al., 2019.

YgeR has a degenerate LytM domain and is not active on PG *in vitro*

YgeR belongs to the family of the LytM-domain factors that in *E. coli* includes the DD-endopeptidase MepM and the amidases regulators EnvC and NlpD (Uehara et al., 2009). Deletion of *envC* and *nlpD* results in a severe chaining phenotype due to impaired cell separation. On the contrary, cells deleted for *ygeR* do not display a chaining phenotype, although the deletion of *ygeR* combined with the deletion of both *envC* and *nlpD* slightly exacerbates cell separation defects (Uehara et al., 2009). YgeR predicted structure reveals a LysM (Lysin Motif) domain that is typical of PG binding proteins (Buist et al., 2008) and a LytM (lysostaphin/peptidase M23) catalytic domain (Peters et al., 2013; Tsang et al., 2017). To gain insights into the role of YgeR, we inspected its LytM domain (Uehara et al., 2010; Tsang et al., 2017). Notably, the residues found to be essential for the hydrolase activity of LytM from *Staphylococcus aureus* (Peters et al., 2013) are conserved in the LytM domain of the *E. coli* MepM but not in EnvC and NlpD amidase regulators (**Fig. 4A**). Multiple sequence alignment revealed that the LytM domain of YgeR displays around 35 % and 65 % of sequence identity with those of EnvC and NlpD respectively, and 34 % to that of MepM (**Fig. 4A)**. Importantly, of the five residues required for activity in MepM (H314, D318, H362, H393 and H395), only three are conserved in YgeR (D149, H194 and H226) (**Fig. 4A)**, indicating that YgeR has a degenerated LytM domain as EnvC and NlpD. Indeed, neither EnvC nor NlpD show activity on PG *in vitro* unlike MepM (Uehara et al., 2010; Singh et al., 2012).

We next assayed the enzymatic activity of YgeR on PG *in vitro*. YgeR was incubated with PG sacculi purified from the strain BW25113Δ6LDT. The reaction was stopped, and the product was digested with the muramidase cellosyl, with the resulting muropeptides separated by HPLC and analysed. The assay confirmed that YgeR does not have enzymatic activity on PG *in vitro* (**Fig. 4B)**.

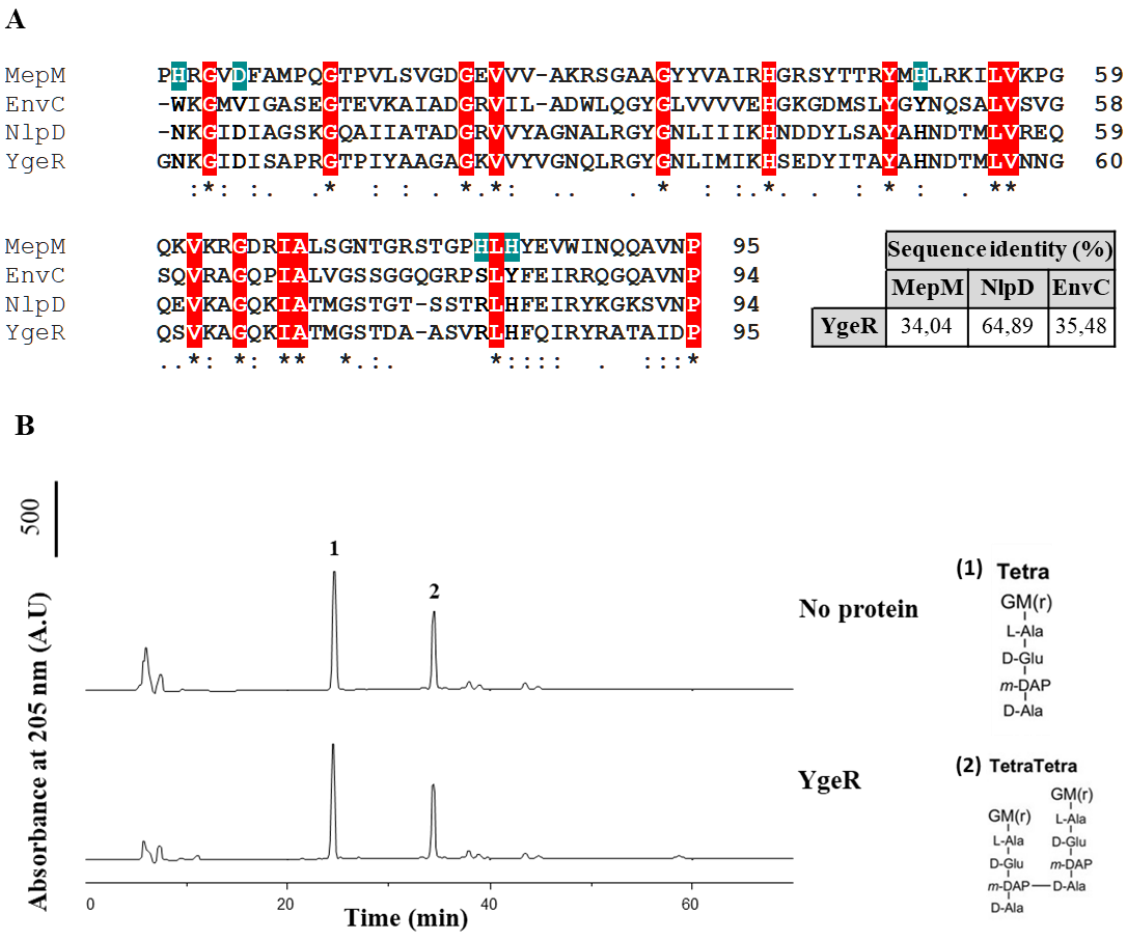

Figure 4. YgeR has a degenerate LytM domain and is not active on purified PG. (**A**) Sequence alignment of the LytM domains of MepM, EnvC, NlpD and YgeR. Residues required for activity are highlighted in blue. Positions that are absolutely conserved are boxed in red. Consensus symbols: (*) indicates fully conserved residues; (:) indicates residues with high degree of conservation; (.) indicates residues with low degree of conservation. Alignment was performed with ClustaOmega (https://www.ebi.ac.uk/Tools/msa/clustalo/). Sequence identity among the different LytM domains is shown in the table. UniProtKB accession numbers: EnvC (P37690), NlpD (P0ADA3), MepM (P0AFS9), and YgeR (Q46798). (**B**) YgeR activity *in vitro*. HPLC chromatograms showing lack of activity of YgeR on PG purified from cells lacking all six *ldt* genes (BW25113Δ6LDT). A.U., arbitrary units. Structures of major peaks numbered in the top chromatogram in panel (right). G, N-acetylglucosamine; M(r), N-acetylmuramitol; L-Ala, L-alanine; D-Glu, D-glutamic acid; D-Ala, D-alanine; mDAP, meso-Diaminopimelic acid.

YgeR is an amidase activator and binds PG *in vitro*

Altogether, our results indicate that YgeR might work as an amidase regulator as it shares some features with EnvC and NlpD such as the lack of activity on PG and the presence of a degenerate LytM domain. We tested this hypothesis by incubating YgeR along with AmiA, AmiB and AmiC, and with PG sacculi purified from BW25113Δ6LDT strain. The analysis of the obtained muropeptides profiles (**Fig. 5A** and **S5**) shows that the hydrolase activity of the amidases *in vitro* is significantly increased when YgeR was added to the mix, with AmiC displaying the most pronounced activity when mixed with YgeR (**Fig. 5A**). These results indicate that YgeR is capable to activate AmiA, AmiB and AmiC *in vitro*. Notably, neither EnvC nor NlpD are able to activate the three amidases *in vitro* (Uehara et al., 2010).

We then assayed whether YgeR physically interacts *in vitro* with amidases by mixing oligohistidine-tagged YgeR with AmiA, AmiB and AmiC and conducting a Ni^{2+}-NTA based pulldown. AmiC was pulled down by oligohistidine-tagged YgeR (**Fig. 5B**), indicating a direct interaction between YgeR and AmiC. We did not observe an interaction with AmiB although we cannot exclude that the conditions used in the assay hampered the formation of the protein complexes and we were unable to assess the interaction with AmiA because of technical problems (**data not shown**).

As stated above, YgeR carries a LysM domain, which is predicted to be involved in PG recognition and binding (Buist et al., 2008; Mesnage et al., 2014). We then assessed the ability of YgeR to bind PG by performing an *in vitro* PG pulldown binding assay. We found that YgeR is tightly retained in the PG fraction, suggesting that it does bind PG (**Fig. 5C**).

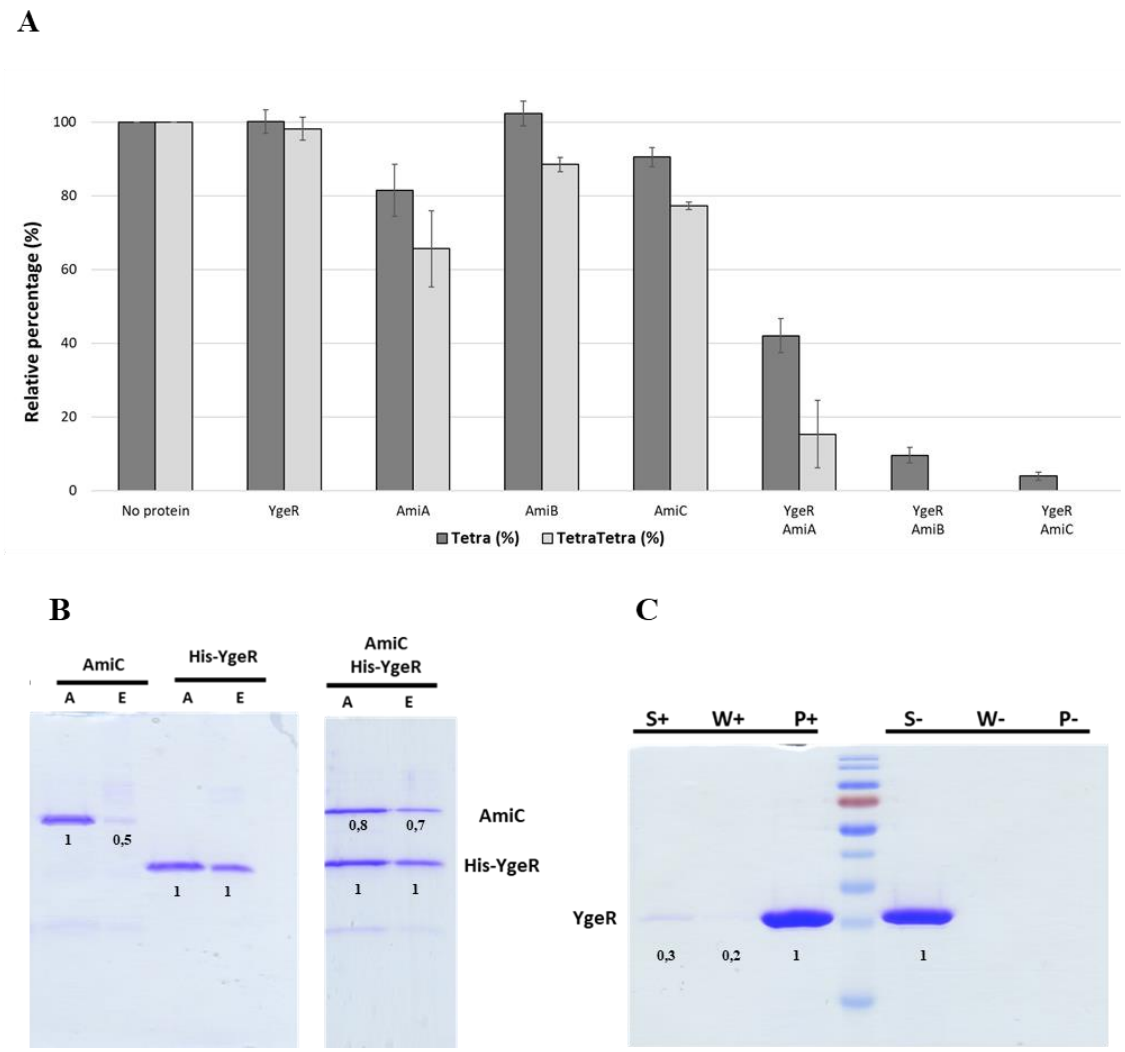

Figure 5. Evidence that YgeR modulates amidases activity *in vitro* and that binds PG. (**A**) Amidases (AmiA, AmiB and AmiC) are activated by YgeR. HPLC-based PG digestion assay representing endopeptidase activity. The graph shows the relative percentage of TetraTetra muropeptides present at the end of the respective incubation periods for each protein. Values are averages of at least three technical replicates from three independent experiments ± standard deviation. (**B**) AmiC is pulled down by His-YgeR**.** Coomassie blue-stained SDS-PAGE gel showing the pulldown of proteins to Ni^{2+}-NTA beads. AmiC is bound to the beads and was present in the elution fraction, E, in the presence of oligohistidine-tagged YgeR. A, applied sample; E, eluted sample. (**C**) YgeR is pulled down by PG. Coomassie blue-stained SDS-PAGE gel showing the pulldown of YgeR to PG (BW25113Δ6LDT). YgeR is bound to the PG (+) and was present in the pellet fraction (P). S, supernatant; W, wash. A control of YgeR in PG binding buffer without PG was set (-). Band intensities were quantified from the 16-bit digital image by densitometry in ImageJ and are shown normalized for each target.

Overexpression of YgeR restores cell separation in *envC nlpD* double mutant

Deletion of *envC* and *nlpD* genes, encoding for the canonical amidase regulators, leads to severe cell separation defects due to the abolishment of amidase activity (Uehara et al., 2010). However, our *in vitro* data supports the hypothesis that also YgeR is an amidase activator, suggesting that *ygeR* might be poorly expressed or not expressed at all in the Δ*nlpD* Δ*envC* mutant. Therefore, we sought to assess the effect of *ygeR* overexpression in this mutant. To this purpose, we introduced the plasmid pGS100-*ygeR*, in which *ygeR* expression is under the control of the IPTG-inducible p*tac* promoter, in the Δ*nlpD* Δ*envC* mutant. p*tac* is a leaky promoter and expression of downstream genes occurs even in the absence of inducer. Cells were grown overnight in the absence of IPTG and collected for imaging. As shown in **Fig. 6**, ectopic expression of *ygeR* restores cell separation in Δ*nlpD* Δ*envC* mutant but not in the Δ*amiABC* mutant, used as control, thus confirming that YgeR functions as an amidase activator *in vivo*.

In NlpD and EnvC the LytM domain is critical for amidase activation (Uehara et al., 2010; Peters et al., 2013; Tsang et al., 2017), we then asked whether the YgeR LytM domain was accountable for amidase activation as well. For this purpose, we generated two pGS100-*ygeR* derivative plasmids containing either the LysM (pGS100-$ygeR_{LysM}$) or the LytM (pGS100-$ygeR_{LytM}$) domains, which were introduced in the Δ*nlpD* Δ*envC* strain. The LytM domain of YgeR promoted cell separation in the double mutant (**Fig. 7**), though a mild chaining phenotype is observed when compared to cells overexpressing full-length YgeR (**Fig. 6**). On the contrary, Δ*nlpD* Δ*envC* cells expressing the LysM domain still display a severe chaining phenotype. Taken together, these results support the hypothesis that the LytM domain of YgeR does mediate amidase activation. However, we cannot exclude that the YgeR LysM domain might be required for a proper amidase activation as shown for NlpD (Tsang et al., 2017).

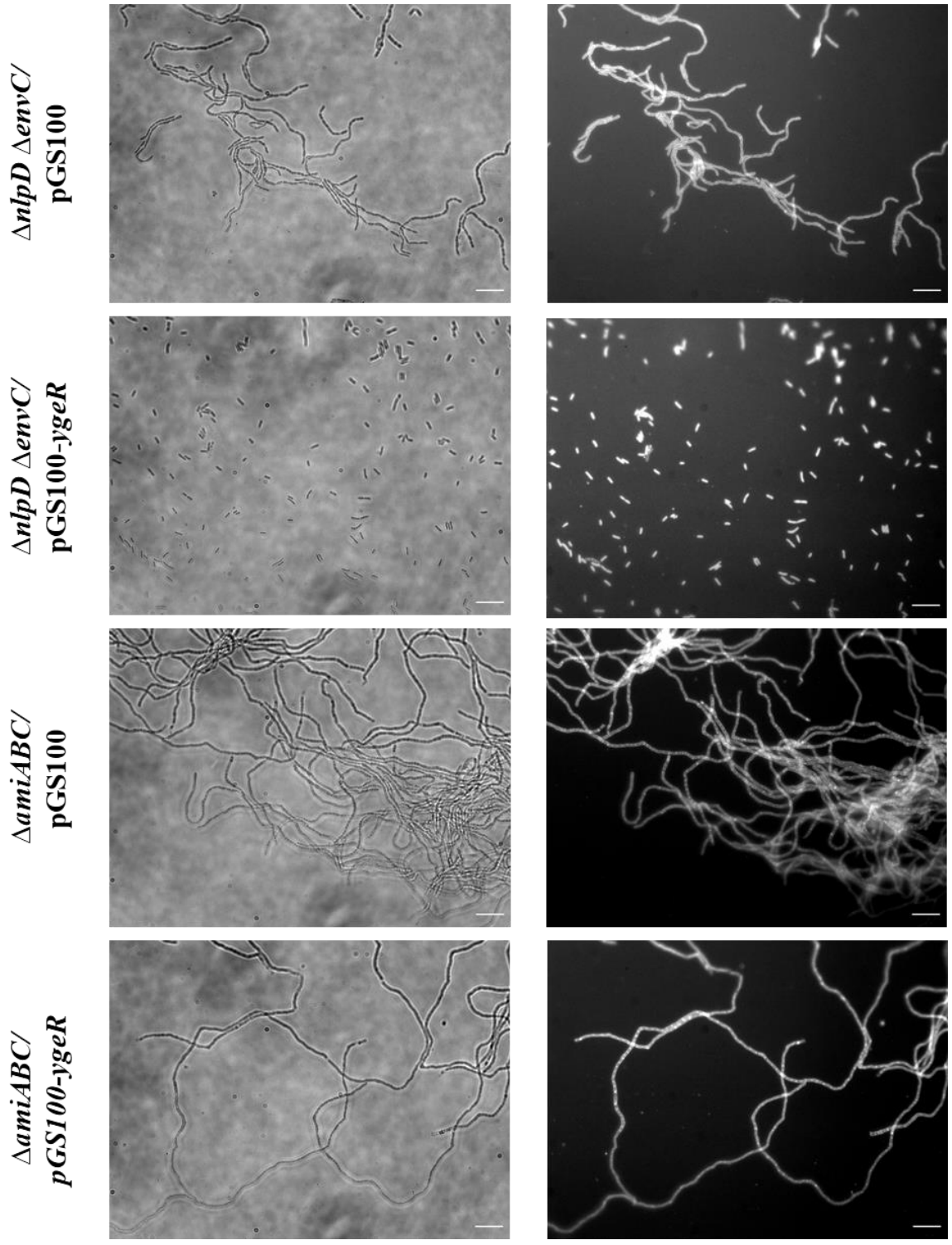

Figure 6. Overexpression of YgeR restores cell separation in Δ*nlpD* Δ*envC* mutants. BW25113Δ*nlpD*Δ*envC* or BW25113Δ*amiABC* cells containing empty plasmid (pGS100) or plasmid with *ygeR* (pGS100-*ygeR)* were grown overnight at 37ºC and collected for imaging. Phase-contrast images (left) and fluorescence images (right) are shown. Bars, 10 μm.

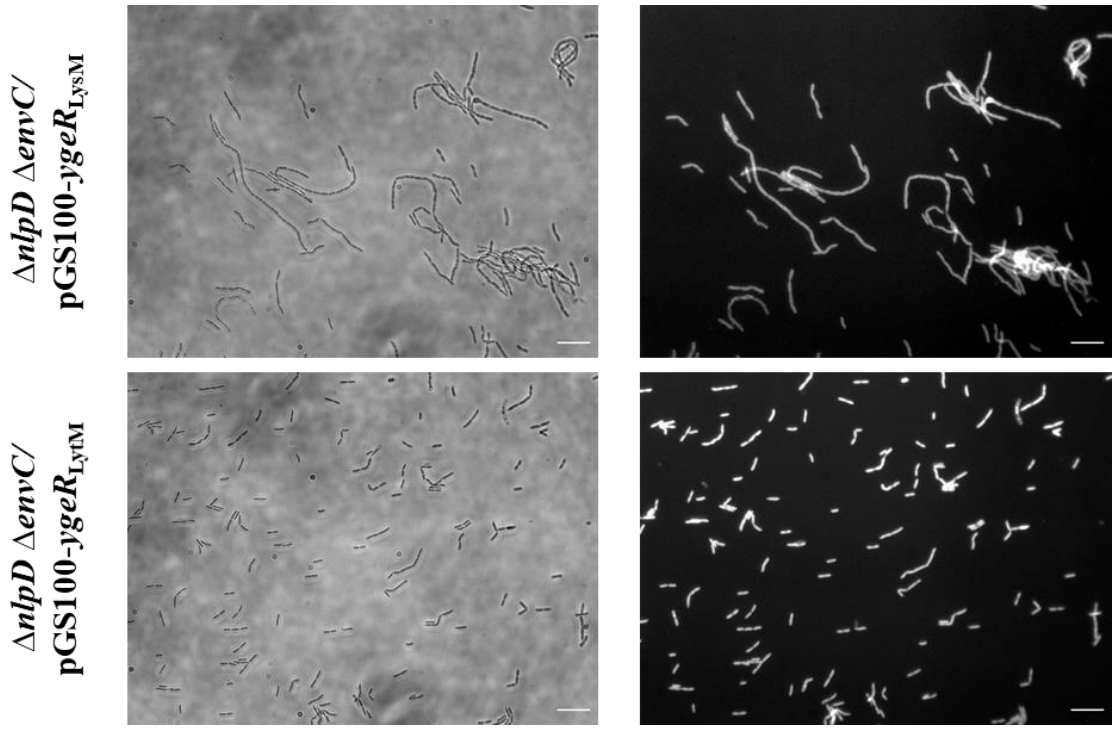

Figure 7. The LytM domain of YgeR promotes cell separation. BW25113Δ*nlpD*Δ*envC* cells carrying plasmid with the LysM domain of *ygeR* (pGS100-*ygeR*$_{LysM}$) or plasmid with the LytM domain of *ygeR* **(**pGS100-*ygeR*$_{LytM}$) were grown overnight at 37ºC and collected for imaging. Phase-contrast images (left) and fluorescence images (right) are shown. Bars, 10 μm.

YgeR preferentially activates AmiC *in vivo*

Our data support the hypothesis that YgeR is an additional amidase regulator in *E. coli*, capable of activating AmiA, AmiB and AmiC *in vitro*. As amidases are functionally redundant (Priyadarshini et al., 2006) we asked whether YgeR might preferentially activate one of them *in vivo*. Indeed, we observed that YgeR interacts with AmiC (**Fig. 5B**) and its LytM domain shares a high sequence identity with that of NlpD (**Fig. 4A**), suggesting that YgeR might have stronger affinity for AmiC. To test this hypothesis pGS100-*ygeR* plasmid was introduced in Δ*envC* Δ*amiC* and Δ*nlpD* Δ*amiAB* mutants to assess whether YgeR activates AmiA and AmiB or AmiC, respectively. Cells were grown overnight and collected for imaging. The ectopic expression of YgeR significantly reduced the cell chaining phenotype in the Δ*nlpD* Δ*amiAB* strain but not in the Δ*envC* Δ*amiC* strain (**Fig. 8**), thus suggesting that, *in vivo*, YgeR preferentially activates AmiC. Consistent with our previous observations, the LytM domain of YgeR is required for AmiC activation (**Fig. S6**).

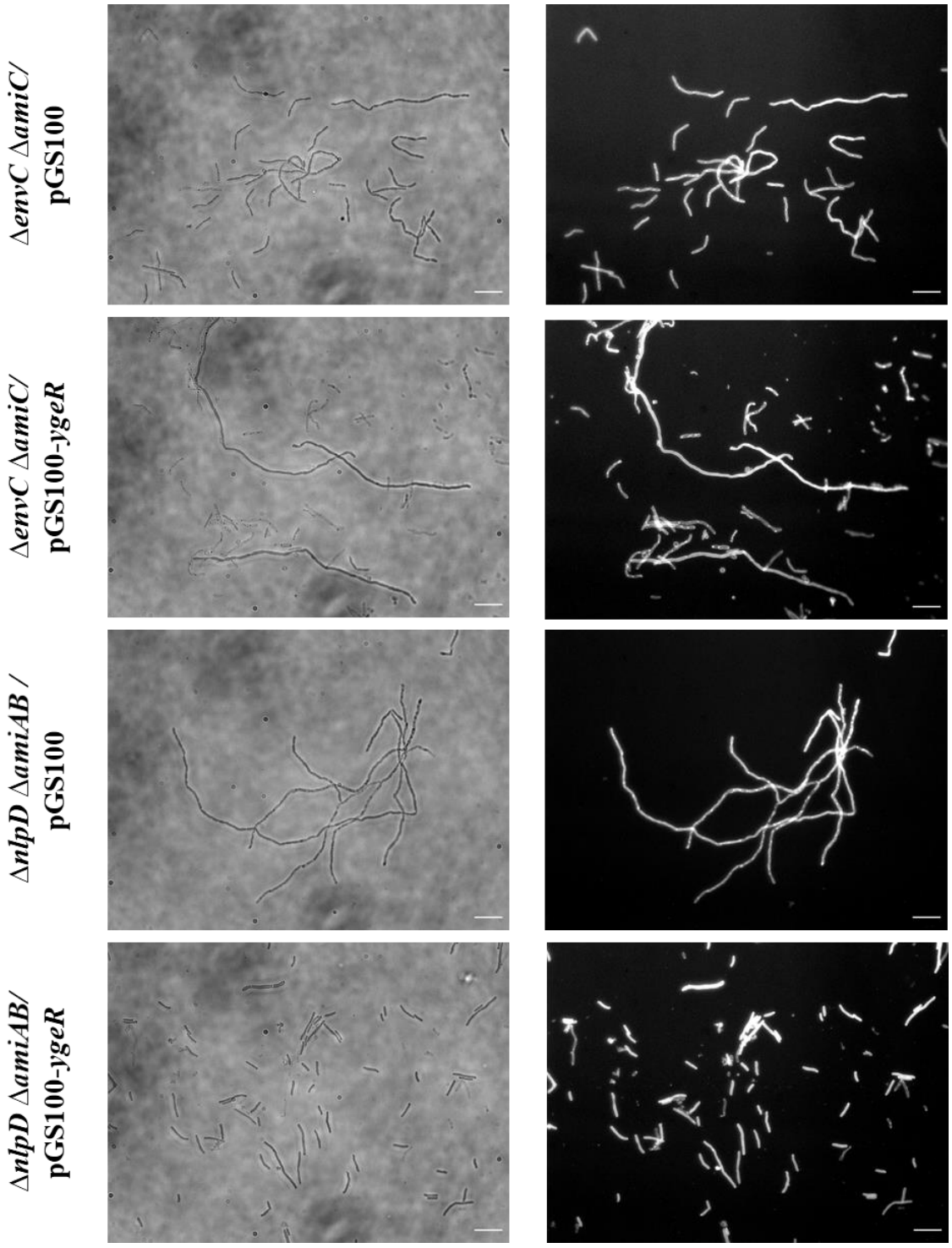

Figure 8. Overexpression of YgeR promotes cell separation by AmiC. BW25113Δ*envC*Δ*amiC* or BW25113Δ*nlpD*Δ*amiAB* cells containing empty plasmid (pGS100) or plasmid with *ygeR* (pGS100-*ygeR)* were grown overnight at 37ºC and collected for imaging. Phase-contrast images (left) and fluorescence images (right) are shown. Bars, 10 μm.

DISCUSSION

Bacterial cells must preserve the integrity of their sacculus at all times and under a variety of growth or stress conditions to prevent lysis and death (Egan et al., 2020). One such stress condition occurs when the biogenesis of the OM is disturbed. Under this condition robustness of PG is ensured by LDTs which introduce 3-3 crosslinks to reinforce the cell wall. Indeed, cells lacking LDTs are prone to lysis when LPS transport to the OM is defective (Peters et al., 2018; Morè et al., 2019). LdtD, whose expression increases upon OM stress, plays a major role in PG remodelling while LdtF stimulates LdtE and LdtD activity (Bernal-Cabas et al., 2015; Montón Silva et al., 2018; Morè et al., 2029). Here, we have shown that the deletion of the LytM-domain factor *ygeR* not only rescues from lysis *araB*p*lptC* cells lacking *ldtF* but also corrects the morphological defect observed in the conditional mutant grown under permissive conditions (**Fig. 1 and 2**). Notably, rescue-from-lysis phenotype cannot be explained by increased levels of 3-3 crosslinks in PG (**Fig. 3, Table S4** and **S5**). Interestingly, LdtF and YgeR appear to be relevant only under OM stress conditions, as these phenotypes were observed in LptC-depleted cells but not in a *lptC*$^{+}$ background (**Fig. S2 and S3**). The functional link between *ygeR* and *ldtF* appears to be specific as deletion of *ygeR* in LptC-depleted cells lacking either *ldtD* or *ldtE* does not mitigate the lysis phenotype (**Fig. 3B** and **S1)**. Overall, these data further support the hypothesis that LdtF has an additional but still unknown role in the cell.

Here we show that the predicted OM lipoprotein YgeR functions as amidase activator. Amidases are PG hydrolases that contribute most to septum cleavage during cell division (Priyadarshini et al., 2006; Priyadarshini et al., 2007). YgeR possesses a degenerate LytM domain (**Fig. 4A**) and does not exhibit any hydrolytic activity on PG similar to amidase regulators EnvC and NlpD (Uehara et al., 2010), (**Fig. 4B**). YgeR displays a LysM domain like the OM-anchored lipoprotein NlpD and it binds PG (**Fig. 5C**). Surprisingly, all three amidases AmiA, AmiB and AmiC are activated by YgeR *in vitro* (**Fig. 5A** and **S5**). Neither EnvC nor NlpD are able to activate all three amidases *in vitro* (Uehara et al., 2010), unveiling a novel pattern of amidase activation *in vitro* by YgeR. The *in vitro* biochemical data were here nicely complemented by *in vivo* results showing that ectopic expression of *ygeR* fully restores cell division in a double mutant deficient for *nlpD* and *envC* (**Fig. 6**). Furthermore, we showed that the LytM domain does mediate amidase activation as previously reported for EnvC and NlpD (Peters et al., 2013; Tsang et al., 2017) although splitting of septal PG appears less efficient when the sole LytM domain

was ectopically expressed in the double *nlpD envC* mutant. (**Fig. 7**). This observation is in line with the finding that the LysM domain of NlpD is required for septal recruitment and proper amidase activation during cytokinesis (Tsang et al., 2017). Finally, we showed that *in vivo* YgeR preferentially activates AmiC (**Fig. 8 and S6)** in line with the finding that YgeR physically interacts with AmiC *in vitro* (**Fig. 5B**). We still observed a low degree of cell chaining when overexpressing *ygeR* in Δ*nlpD* Δ*amiAB* mutant compared to the Δ*nlpD* Δ*envC* mutant (**Fig. 6** and **8**). It should be noted that the Δ*nlpD* Δ*amiAB* strain carries only *amiC* whereas in the Δ*nlpD* Δ*envC* strain all three amidases are present. While we show that YgeR preferentially activates AmiC, we cannot exclude a low level of cross activation of AmiA and AmiB as well, in line with our *in vitro* biochemical activity assays (**Fig. 5A**). To our knowledge AmiC is a first example of amidase whose activity is controlled by two distinct regulators.

YgeR function appears to be relevant under envelope stress conditions, indeed the Δ*nlpD* Δ*envC* double mutant displays a severe cell chaining phenotype despite carrying a functional copy of *ygeR*. Moreover, the single (*ygeR*) or double (*ygeR* and *ldtF*) deletion in wild type strain does not result in growth or morphological defects. Genetic analysis of the *ygeR* locus indicates that this gene is located in a monocistronic operon, and a putative σ^E-dependent promoter consensus sequence is observed 186 nucleotides upstream of the *ygeR* TTG start codon (https://ecocyc.org). The presence of this putative σ^E-dependent promoter places *ygeR* in the family of genes that responds to extra-cytoplasmic stress; notably several genes implicated in LPS transport or in counteracting damage provoked by defects in LPS transport belong to the σ^E regulon (Martorana et al., 2011; Martorana et al., 2014; Klein et al., 2016). Indeed, it has been proposed that upon OM stress, AmiC could be activated by other LytM-domain factors rather than NlpD, thus ensuring cell envelope integrity (Tsang et al., 2017).

It has been previously reported that the cleavage activities of amidases and other PG hydrolases play a crucial role in the bactericidal effect exerted by β-lactams antibiotics (Cho et al., 2014; Wivagg et al., 2014; Chung et al., 2009; Rice and Bayles, 2008). According to this model, the inhibition of PBPs activity by β-lactams disrupts the cycle of PG biogenesis (Vollmer, 2012): cell autolysis is promoted due to persistent activation of the PG turnover enzymes while those of PG synthesis are inhibited. Indeed, mutants lacking either two or all three amidases display a delayed response to β-lactams (Chung et al., 2009; Uehara et al., 2009). We believe that a similar mechanism might explain the

phenotypes observed in the *araB*p*lptC* Δ*ldtF* and *araB*p*lptC* Δ*ldtF* Δ*ygeR* strains. We speculate that the lack of LdtF triggers the overactivation of AmiC by YgeR upon block of LPS transport, thus causing cell lysis and the morphological defects seen under permissive conditions (Morè et al., 2019), therefore the deletion of *ygeR* in this mutant would suppress the detrimental effects produced by AmiC overactivation. We do not know what is the mechanism that leads to YgeR activation in the absence of LdtF nor what is the additional role of LdtF in the cell. Further work will be required to elucidate the functional link between LdtF and YgeR.

Overall, this work reports the characterization of the LytM-domain factor YgeR, as a novel activator of AmiC. The results shown in this work highlight a crosstalk between PG remodeling and amidase activity in response to impaired OM biogenesis.

MATERIALS AND METHODS

Bacterial strains, plasmids, and growth conditions.

Escherichia coli strains and plasmids used in this work are listed in **Table S1** and **Table S2**, respectively. Primers used are listed in **Table S3**. Cells were routinely grown aerobically at 37°C or 30°C in LB-Lennox medium (10 g/liter tryptone, 5 g/liter yeast extract, 5 g/liter NaCl) (Difco). When required, antibiotics or inducers were added: ampicillin (100 g/ml), chloramphenicol (25 g/ml), kanamycin (25 g/ml), arabinose (0.2% [wt/vol]), IPTG (0.1 mM). For LptC depletion, bacteria were harvested from cultures with an OD_{600} of 0.2 by centrifugation, washed twice with LD, and diluted 100-fold in LD with or without arabinose. Cell growth was monitored by OD_{600} measurements, and viability was determined by quantifying the colony-forming units (CFU).

Other methods. The construction of plasmids and strains, microscopy of cells, protein purification and biochemical assays are described in detail in **Text S1** in the supplemental material.

ACKNOWLEDGEMENTS

We thank Manuel Banzhaf (Birmingham University) for providing proteins. A.P. and W.V. are supported by the European Commission via the International Training Network Train2Target (721484).

REFERENCES

1. Baba, T., Ara, T., Hasegawa, M., Takai, Y., Okumura, Y., Baba, M., Datsenko, K.A., Tomita, M., Wanner, B.L., and Mori, H. (2006). Construction of *Escherichia coli* K-12 in-frame, single-gene knockout mutants: the Keio collection. Mol. Syst. Biol. 2, 2006.0008.
2. Bernal-Cabas, M., Ayala, J.A., and Raivio, T.L. (2015). The Cpx Envelope Stress Response Modifies Peptidoglycan Cross-Linking via the l,d-Transpeptidase LdtD and the Novel Protein YgaU. J Bacteriol. 197, 603–614.
3. Bernhardt, T.G., and de Boer, P.A.J. (2003). The Escherichia coli amidase AmiC is a periplasmic septal ring component exported via the twin-arginine transport pathway. Mol. Microbiol. 48, 1171–1182.
4. Bertsche U, Breukink E, Kast T, Vollmer W. (2005). In vitro murein peptidoglycan synthesis by dimers of the bifunctional transglycosylase-transpeptidase PBP1B from *Escherichia coli*. J. Biol. Chem. 280:38096-101.
5. Buist, G., Steen, A., Kok, J., and Kuipers, O.P. (2008). LysM, a widely distributed protein motif for binding to (peptido)glycans. Mol. Microbiol. 68, 838–847.
6. Chng, S.-S., Gronenberg, L.S., and Kahne, D. (2010). Proteins Required for Lipopolysaccharide Assembly in *Escherichia coli* Form a Transenvelope Complex. Biochem. 49, 4565–4567.
7. Cho, H., Uehara, T., and Bernhardt, T.G. (2014). Beta-Lactam Antibiotics Induce a Lethal Malfunctioning of the Bacterial Cell Wall Synthesis Machinery. Cell 159, 1300–1311.
8. Chung, H.S., Yao, Z., Goehring, N.W., Kishony, R., Beckwith, J., and Kahne, D. (2009). Rapid β-lactam-induced lysis requires successful assembly of the cell division machinery. PNAS 106, 21872–21877.
9. Egan, A.J.F., Errington, J., and Vollmer, W. (2020). Regulation of peptidoglycan synthesis and remodelling. Nat. Rev. Microbiol. 18, 446–460.
10. Gray AN, Egan AJ, Van't Veer IL, Verheul J, Colavin A, Koumoutsi A, Biboy J, Altelaar AF, Damen MJ, Huang KC, Simorre JP, Breukink E, den Blaauwen T, Typas A, Gross CA, Vollmer W. (2015). Coordination of peptidoglycan synthesis and outer membrane constriction during *Escherichia coli* cell division. Elife 4 e07118.
11. Heidrich, C., Templin, M.F., Ursinus, A., Merdanovic, M., Berger, J., Schwarz, H., De Pedro, M.A., and Höltje, J.-V. (2001). Involvement of N-acetylmuramyl-l-alanine amidases in cell separation and antibiotic-induced autolysis of *Escherichia coli*. Mol. Microbiol. 41, 167–178.
12. Henderson, J.C., Zimmerman, S.M., Crofts, A.A., Boll, J.M., Kuhns, L.G., Herrera, C.M., and Trent, M.S. (2016). The Power of Asymmetry: Architecture and Assembly of the Gram-Negative Outer Membrane Lipid Bilayer. Annu. Rev. Microbiol. 70, 255–278.
13. Höltje, J.V. (1998). Growth of the stress-bearing and shape-maintaining murein sacculus of *Escherichia coli*. Microbiol. Mol. Biol. Rev. 62, 181–203.
14. Huang, K.C., Mukhopadhyay, R., Wen, B., Gitai, Z., and Wingreen, N.S. (2008). Cell shape and cell-wall organization in Gram-negative bacteria. PNAS 105, 19282–19287.

15. Hugonnet, J.-E., Mengin-Lecreulx, D., Monton, A., den Blaauwen, T., Carbonnelle, E., Veckerlé, C., Brun, Y., V., van Nieuwenhze, M., Bouchier, C., Tu, K., et al. (2016). Factors essential for L, D-transpeptidase-mediated peptidoglycan cross-linking and β-lactam resistance in *Escherichia coli*. ELife 5, e19469.
16. Klein, G., Stupak, A., Biernacka, D., Wojtkiewicz, P., Lindner, B., and Raina, S. (2016). Multiple Transcriptional Factors Regulate Transcription of the rpoE Gene in *Escherichia coli* under Different Growth Conditions and When the Lipopolysaccharide Biosynthesis Is Defective. J. Biol. Chem. 291, 22999–23019.
17. Magnet, S., Bellais, S., Dubost, L., Fourgeaud, M., Mainardi, J.-L., Petit-Frère, S., Marie, A., Mengin-Lecreulx, D., Arthur, M., and Gutmann, L. (2007). Identification of the L, D-transpeptidases responsible for attachment of the Braun lipoprotein to *Escherichia coli* peptidoglycan. J. Bacteriol. 189, 3927–3931.
18. Magnet, S., Dubost, L., Marie, A., Arthur, M., and Gutmann, L. (2008). Identification of the l,d-Transpeptidases for Peptidoglycan Cross-Linking in *Escherichia coli*. J Bacteriol. 190, 4782–4785.
19. Mainardi, J.-L., Villet, R., Bugg, T.D., Mayer, C., and Arthur, M. (2008). Evolution of peptidoglycan biosynthesis under the selective pressure of antibiotics in Gram-positive bacteria. FEMS Microbiol. Rev. 32, 386–408.
20. Martorana, A.M., Motta, S., Silvestre, D.D., Falchi, F., Dehò, G., Mauri, P., Sperandeo, P., and Polissi, A. (2014). Dissecting *Escherichia coli* Outer Membrane Biogenesis Using Differential Proteomics. PLoS ONE 9, e100941.
21. Martorana, A.M., Sperandeo, P., Polissi, A., and Dehò, G. (2011). Complex transcriptional organization regulates an *Escherichia coli* locus implicated in lipopolysaccharide biogenesis. Res. Microbiol. 162, 470–482.
22. Meisner, J., and Moran, C.P. (2011). A LytM Domain Dictates the Localization of Proteins to the Mother Cell-Forespore Interface during Bacterial Endospore Formation. J. Bacteriol. 193, 591–598.
23. Mesnage, S., Dellarole, M., Baxter, N.J., Rouget, J.-B., Dimitrov, J.D., Wang, N., Fujimoto, Y., Hounslow, A.M., Lacroix-Desmazes, S., Fukase, K., et al. (2014). Molecular basis for bacterial peptidoglycan recognition by LysM domains. Nat Commun 5, 4269.
24. Montón Silva, A., Otten, C., Biboy, J., Breukink, E., VanNieuwenhze, M., Vollmer, W., and den Blaauwen, T. (2018). The Fluorescent D-Amino Acid NADA as a Tool to Study the Conditional Activity of Transpeptidases in *Escherichia coli*. Front Microbiol 9, 2101.
25. Morè, N., Martorana, A.M., Biboy, J., Otten, C., Winkle, M., Serrano, C.K.G., Montón Silva, A., Atkinson, L., Yau, H., Breukink, E., et al. (2019). Peptidoglycan Remodeling Enables Escherichia coli To Survive Severe Outer Membrane Assembly Defect. MBio 10, e02729-18.
26. Nichols, R.J., Sen, S., Choo, Y.J., Beltrao, P., Zietek, M., Chaba, R., Lee, S., Kazmierczak, K.M., Lee, K.J., Wong, A., et al. (2011). Phenotypic landscape of a bacterial cell. Cell 144, 143–156.
27. Okuda, S., Sherman, D.J., Silhavy, T.J., Ruiz, N., and Kahne, D. (2016). Lipopolysaccharide transport and assembly at the outer membrane: the PEZ model. Nat. Rev. Microbiol. 14, 337–345.

28. Peters, K., Pazos, M., Edoo, Z., Hugonnet, J.-E., Martorana, A.M., Polissi, A., VanNieuwenhze, M.S., Arthur, M., and Vollmer, W. (2018). Copper inhibits peptidoglycan LD-transpeptidases suppressing β-lactam resistance due to bypass of penicillin-binding proteins. Proc. Natl. Acad. Sci. U S A 115, 10786–10791.
29. Peters, N.T., Dinh, T., and Bernhardt, T.G. (2011). A Fail-Safe Mechanism in the Septal Ring Assembly Pathway Generated by the Sequential Recruitment of Cell Separation Amidases and Their Activators. J. Bacteriol. 193, 4973–4983.
30. Peters, N.T., Morlot, C., Yang, D.C., Uehara, T., Vernet, T., and Bernhardt, T.G. (2013). Structure-function analysis of the LytM domain of EnvC, an activator of cell wall remodeling at the Escherichia coli division site. Mol. Microbiol. 89, 690–701.
31. Priyadarshini, R., Pedro, M.A. de, and Young, K.D. (2007). Role of Peptidoglycan Amidases in the Development and Morphology of the Division Septum in *Escherichia coli*. J. Bacteriol. 189, 5334–5347.
32. Priyadarshini, R., Popham, D.L., and Young, K.D. (2006). Daughter Cell Separation by Penicillin-Binding Proteins and Peptidoglycan Amidases in *Escherichia coli*. J.Bacteriol. 188, 5345–5355.
33. Rice, K.C., and Bayles, K.W. (2008). Molecular Control of Bacterial Death and Lysis. Microbiol Mol. Biol. Rev. 72, 85–109.
34. Ruiz, N., Gronenberg, L.S., Kahne, D., and Silhavy, T.J. (2008). Identification of two inner-membrane proteins required for the transport of lipopolysaccharide to the outer membrane of *Escherichia coli*. PNAS 105, 5537–5542.
35. Sabala, I., Jonsson, I.-M., Tarkowski, A., and Bochtler, M. (2012). Anti-staphylococcal activities of lysostaphin and LytM catalytic domain. BMC Microbiology 12, 97.
36. Silhavy, T.J., Kahne, D., and Walker, S. (2010). The Bacterial Cell Envelope. Cold Spring Harb Perspect Biol 2.
37. Singh, S.K., SaiSree, L., Amrutha, R.N., and Reddy, M. (2012). Three redundant murein endopeptidases catalyse an essential cleavage step in peptidoglycan synthesis of *Escherichia coli* K12. Molecular Microbiology 86, 1036–1051.
38. Sperandeo, P., Lau, F.K., Carpentieri, A., De Castro, C., Molinaro, A., Dehò, G., Silhavy, T.J., and Polissi, A. (2008). Functional analysis of the protein machinery required for transport of lipopolysaccharide to the outer membrane of *Escherichia coli*. J. Bacteriol. 190, 4460–4469.
39. Sperandeo, P., Martorana, A.M., and Polissi, A. (2019). Lipopolysaccharide Biosynthesis and Transport to the Outer Membrane of Gram-Negative Bacteria. In Bacterial Cell Walls and Membranes, A. Kuhn, ed. (Cham: Springer International Publishing), pp. 9–37.
40. Stohl, E.A., Lenz, J.D., Dillard, J.P., and Seifert, H.S. (2015). The Gonococcal NlpD Protein Facilitates Cell Separation by Activating Peptidoglycan Cleavage by AmiC. J. Bacteriol. 198, 615–622.
41. Tsang, M.-J., Yakhnina, A.A., and Bernhardt, T.G. (2017). NlpD links cell wall remodeling and outer membrane invagination during cytokinesis in *Escherichia coli*. PLoS Genet. 13, e1006888.
42. Typas, A., Banzhaf, M., Gross, C.A., and Vollmer, W. (2011). From the regulation of peptidoglycan synthesis to bacterial growth and morphology. Nat. Rev. Microbiol. 10, 123–136.

43. Uehara, T., and Bernhardt, T.G. (2011). More than just lysins: peptidoglycan hydrolases tailor the cell wall. Curr. Opin. Microbiol. 14, 698–703.
44. Uehara, T., and Park, J.T. (2008). Growth of *Escherichia coli*: Significance of Peptidoglycan Degradation during Elongation and Septation. J. Bacteriol. 190, 3914–3922.
45. Uehara, T., Dinh, T., and Bernhardt, T.G. (2009). LytM-domain factors are required for daughter cell separation and rapid ampicillin-induced lysis in *Escherichia coli*. J. Bacteriol. 191, 5094–5107.
46. Uehara, T., Parzych, K.R., Dinh, T., and Bernhardt, T.G. (2010). Daughter cell separation is controlled by cytokinetic ring-activated cell wall hydrolysis. EMBO J. 29, 1412–1422.
47. Vollmer, W. (2012). Bacterial growth does require peptidoglycan hydrolases. Molecular Microbiology 86, 1031–1035.
48. Vollmer, W., Blanot, D., and de Pedro, M.A. (2008). Peptidoglycan structure and architecture. FEMS Microbiol. Rev. 32, 149–167.
49. Whitfield, C., and Trent, M.S. (2014). Biosynthesis and export of bacterial lipopolysaccharides. Annu. Rev. Biochem. 83, 99–128.
50. Wivagg, C.N., Bhattacharyya, R.P., and Hung, D.T. (2014). Mechanisms of β-lactam killing and resistance in the context of Mycobacterium tuberculosis. J. Antibiot. 67, 645–654.
51. Yang, D.C., Peters, N.T., Parzych, K.R., Uehara, T., Markovski, M., and Bernhardt, T.G. (2011). An ATP-binding cassette transporter-like complex governs cell-wall hydrolysis at the bacterial cytokinetic ring. Proc. Natl. Acad. Sci. U.S.A. 108, E1052-1060.
52. Zielińska, A., Billini, M., Möll, A., Kremer, K., Briegel, A., Martinez, A.I., Jensen, G.J., and Thanbichler, M. (2017). LytM factors affect the recruitment of autolysins to the cell division site in Caulobacter crescentus. Molecular Microbiology 106, 419–438.

SUPPLEMENTAL MATERIAL

Figure S1: Deletion of *ygeR* does not alter the morphology of *araB*p*lptC* Δ*ldtD* and *araB*p*lptC* Δ*ldtE* mutants under permissive conditions.

Figure S2: Deletion of *ygeR* does not affect growth and morphology of BW25113 (*lptC*$^{+}$) cells.

Figure S3: Deletion of *ygeR* along with that of *ldts* does not affect growth and morphology of BW25113 (*lptC*$^{+}$) cells.

Figure S4: Ectopic expression of *ygeR* restores lysis phenotype in *araB*p*lptC* Δ*ldtF* Δ*ygeR*.

Figure S5: *In vitro* amidases activation by YgeR.

Figure S6: YgeR activates AmiC via its LytM domain.

Text S1: Details of the methods of strain and plasmid construction, protein purification procedures, protein-protein interaction protocols, and activity assays.

Table S1: Bacterial Strains used in this study.

Table S2: Plasmids used in this study.

Table S3: Oligonucleotides used in this study.

Table S4: Muropeptide composition of *araB*p*lptC* and *araB*p*lptC* Δ*ygeR* mutant under permissive or nonpermissive conditions.

Table S5: Muropeptide composition of *araB*p*lptC* and *araB*p*lptC* Δ*ldtF ΔygeR* mutant under permissive or nonpermissive conditions.

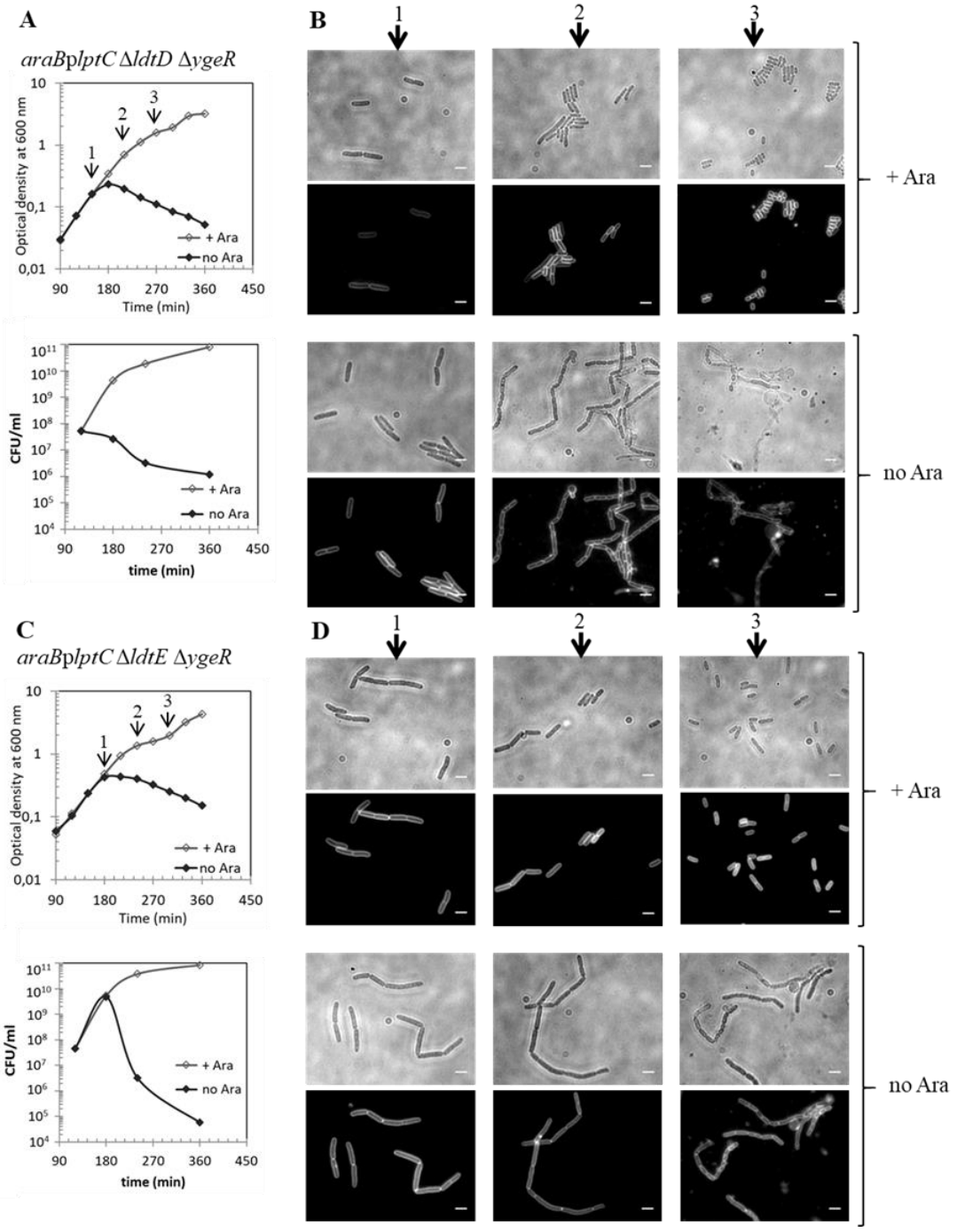

Figure S1. Deletion of *ygeR* does not alter the morphology of *araB*p*lptC* Δ*ldtD* and *araB*p*lptC* Δ*ldtE* mutants under permissive conditions. The strains *araB*p*lptC* Δ*ldtD* Δ*ygeR* (**A**) and *araB*p*lptC* Δ*ldtE* Δ*ygeR* (**C**) were grown in the presence of 0.2% arabinose to an OD_{600} of 0.2, harvested, washed three times, and resuspended in an arabinose-supplemented (+ Ara) or arabinose-free (no Ara) medium. Growth was monitored by OD_{600} measurements (top panel) and by determining CFU (bottom panel). At t=150, 210, and 270 min (arrows), *araB*p*lptC* Δ*ldtD* Δ*ygeR* (**B**) and *araB*p*lptC* Δ*ldtE* Δ*ygeR* (**D**) cells were imaged. Phase-contrast images (top) and fluorescence images (bottom) are shown. Bars, 3 μm.

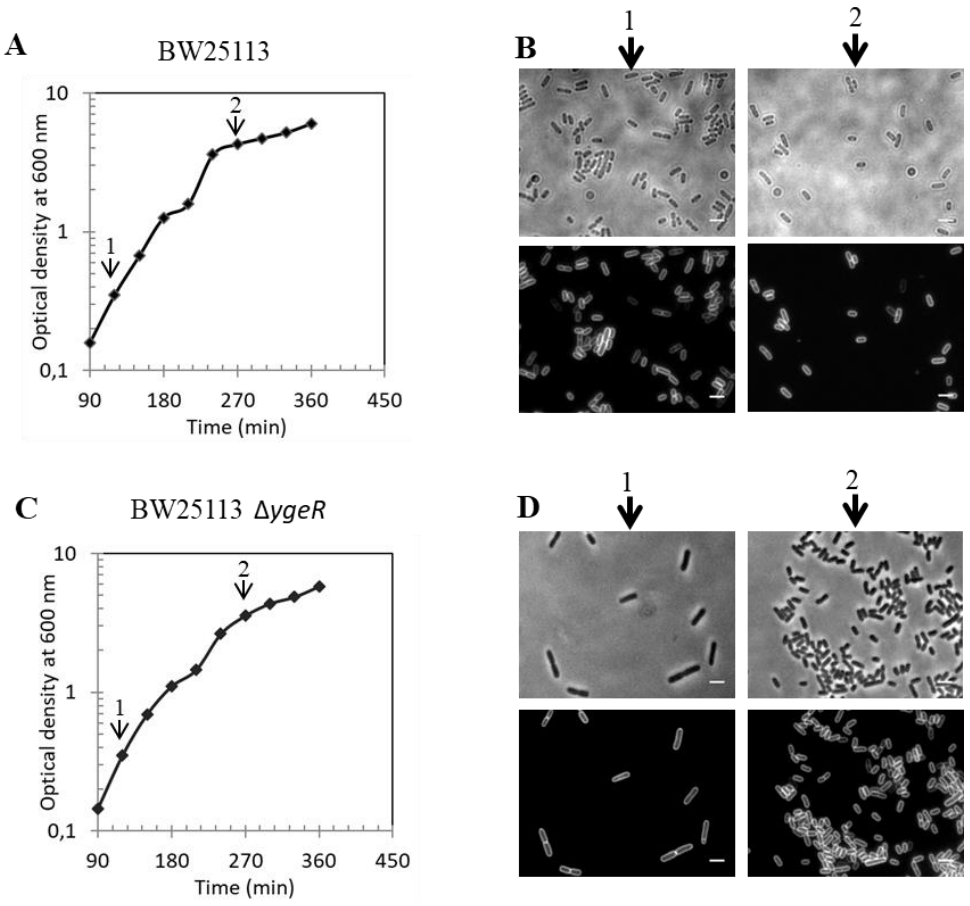

Figure S2. Deletion of *ygeR* does not affect growth and morphology of BW25113 (*lptC*$^{+}$) cells. BW25113 (**A**) and BW25113 Δ*ygeR* (**C**) were grown for 360 min. Growth was monitored by OD_{600} measurements. At t=120 and 270 min (arrows), BW25113 (**B**) and BW25113 Δ*ygeR* (**D**) cells were collecting for imaging. Phase-contrast images (top) and fluorescence images (bottom) are shown. Bars, 3 μm.

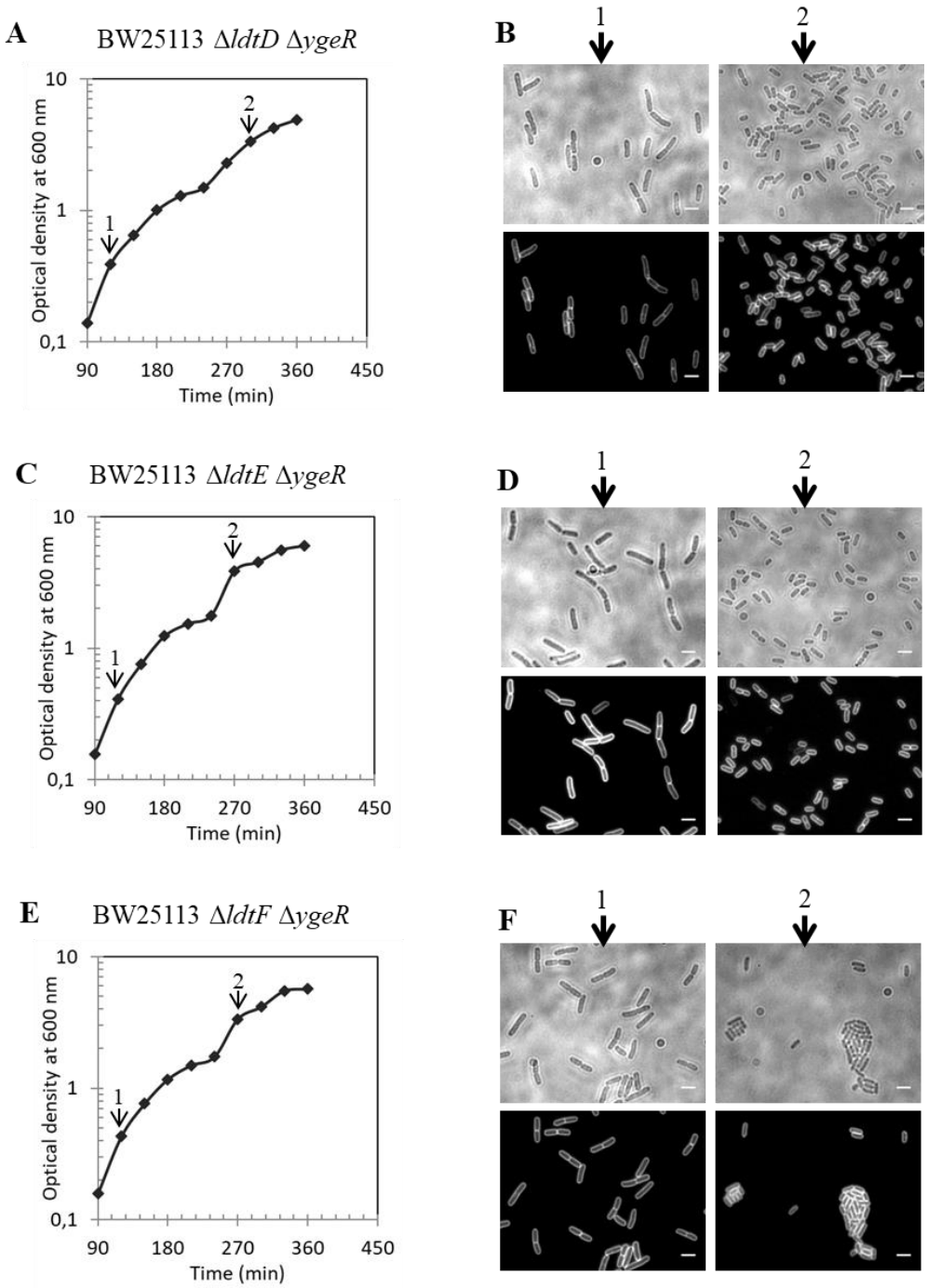

Figure S3. Deletion of *ygeR* along with that of *ldts* does not affect growth and morphology of BW25113 (*lptC*$^{+}$) cells. Cells of BW25113 Δ*ldtD* Δ*ygeR* (**A**), BW25113 Δ*ldtE* Δ*ygeR* (**C**) and BW25113 Δ*ldtF* Δ*ygeR* (**E**) were grown for 360 min. Growth was monitored by OD_{600} measurements. At t=120 and 270 min (arrows), BW25113 Δ*ldtD* Δ*ygeR* (**B**), BW25113 Δ*ldtE* Δ*ygeR* (**D**) and BW25113 Δ*ldtF* Δ*ygeR* (**F**) cells were collecting for imaging. Phase-contrast images (top) and fluorescence images (bottom) are shown. Bars, 3 μm.

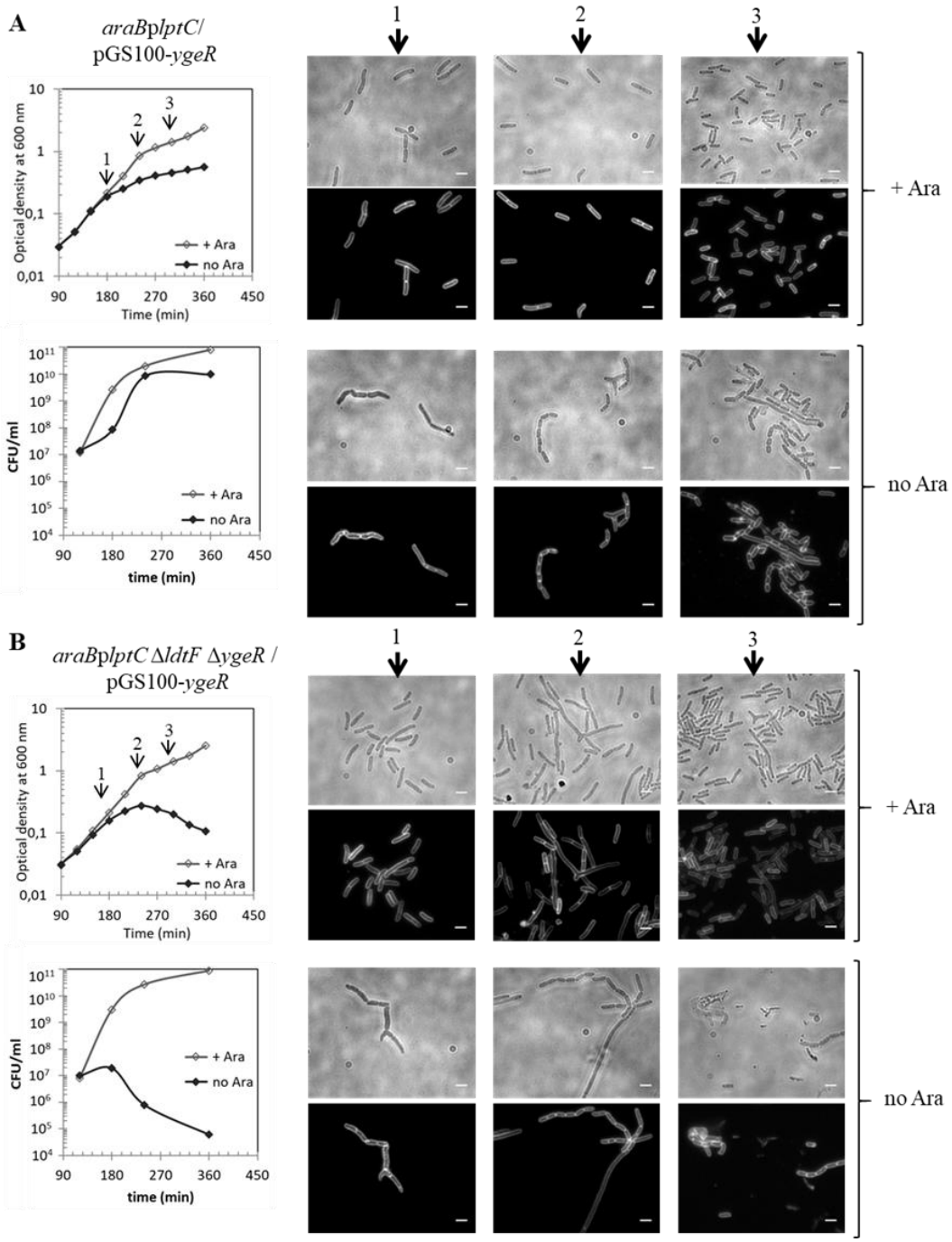

Figure S4. Ectopic expression of *ygeR* restores lysis phenotype in *araB*p*lptC* Δ*ldtF* Δ*ygeR*. Cells of *araB*p*lptC* (**A**) and *araB*p*lptC* Δ*ldtF* Δ*ygeR* (**B**) strains carrying pGS100-*ygeR* plasmids were grown in the presence of 0.2% arabinose to an OD_{600} of 0.2, harvested, washed three times, and resuspended in an arabinose-supplemented (+ Ara) or arabinose-free (no Ara) medium. Growth was monitored by OD_{600} measurements (top panel) and by determining CFU (bottom panel). At t=150, 210, and 270 min (arrows), samples were imaged. Phase-contrast images (top) and fluorescence images (bottom) are shown. Bars, 3 μm.

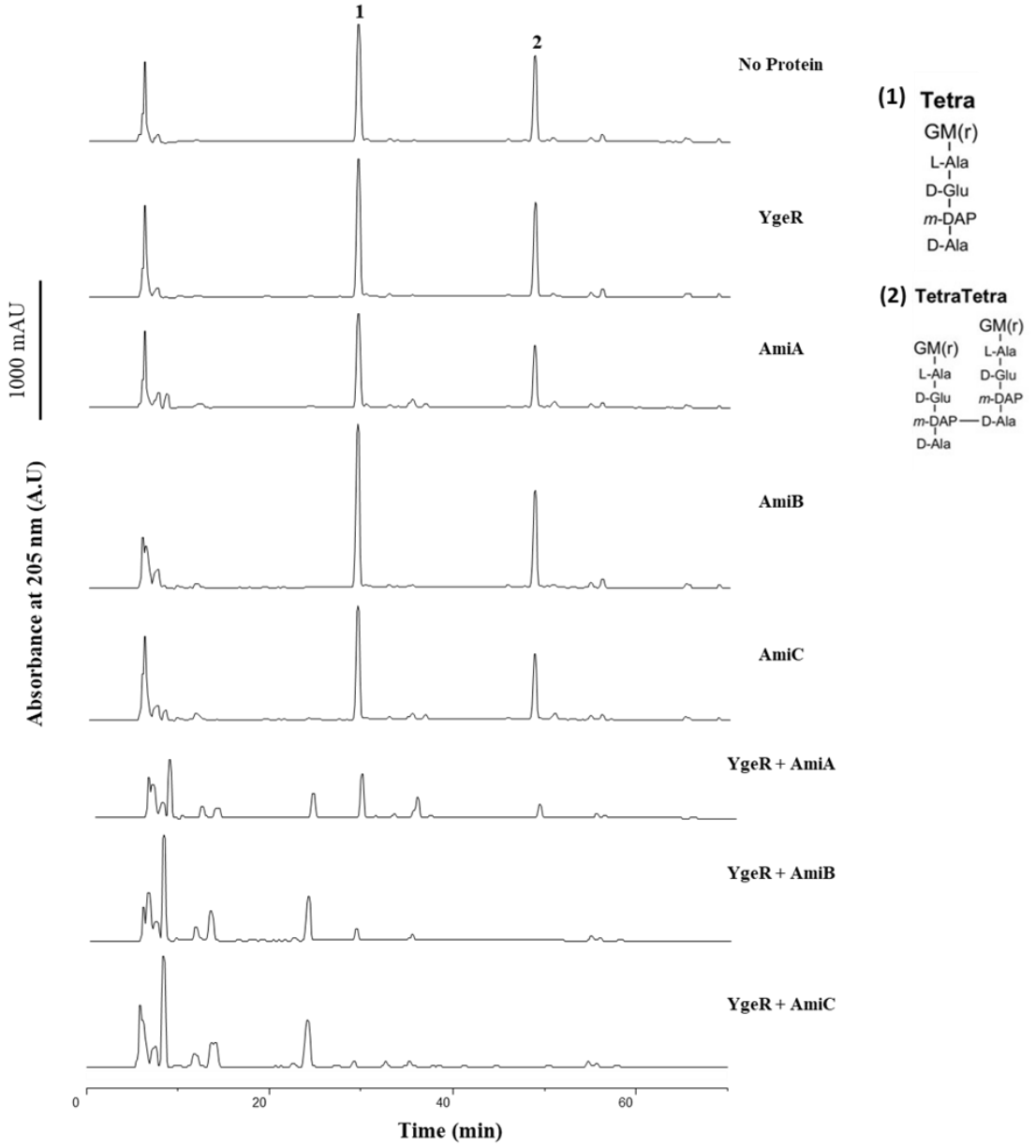

Figure S5. *In vitro* amidases activation by YgeR. HPLC chromatograms showing peptidoglycan hydrolase activity by AmiA, AmiB and AmiC in presence of YgeR in PG from cells lacking all six *ldt* genes (BW25113Δ6LDT). A.U., arbitrary units. Structures of major peaks numbered in the top chromatogram in panel (right). G, N-acetylglucosamine; M(r), N-acetylmuramitol; L-Ala, L-alanine; D-Glu, D-glutamic acid; D-Ala, D-alanine; mDAP, meso-Diaminopimelic acid.

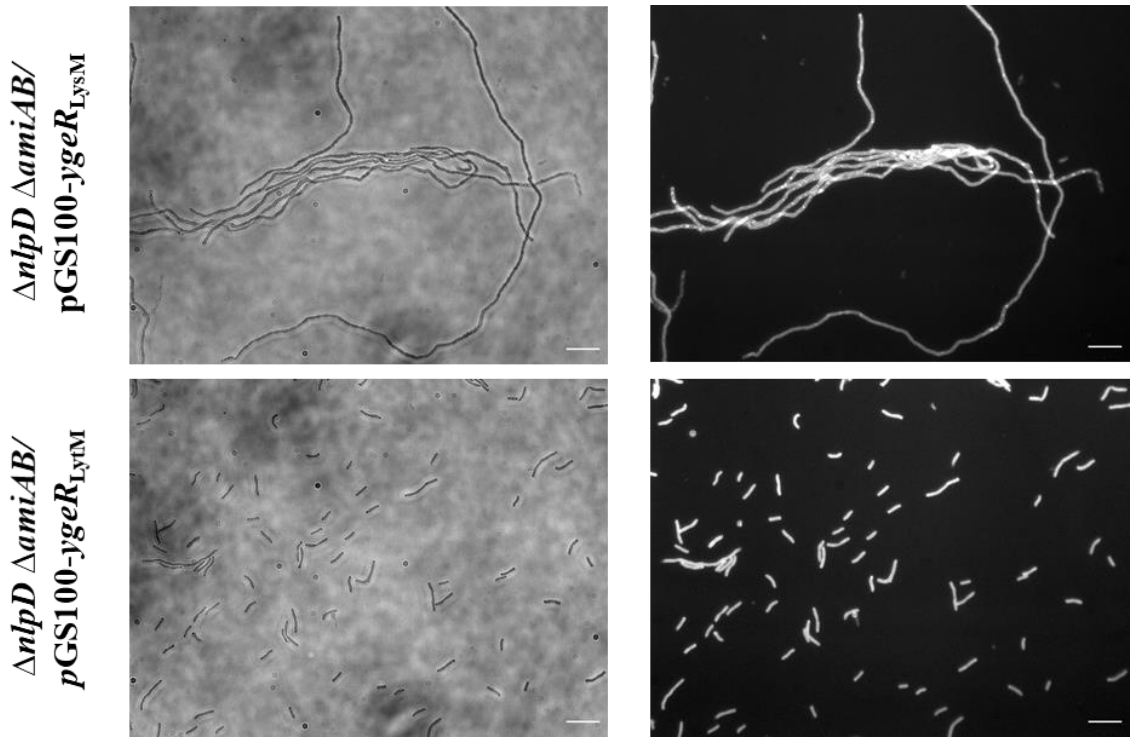

Figure S6. YgeR activates AmiC via its LytM domain. BW25113Δ*envC*Δ*amiC* or BW25113Δ*nlpD*Δ*amiAB* cells carrying plasmid with the LysM domain of *ygeR* (pGS100-*ygeR*$_{LysM}$) or plasmid with the LytM domain of *ygeR* **(**pGS100-*ygeR*$_{LytM}$**)** were grown overnight at 37ºC and collected for imaging. Phase-contrast images (left) and fluorescence images (right) are shown. Bars, 10 μm.

Text S1. Supplemental Methods

Construction of *E. coli* deletion or depletion strains

Deletion strains were obtained by moving *kan*-marked alleles from the Keio *E. coli* single-gene knockout library (Baba et al., 2006) by P1 phage transduction (Silhavy et al., 1984) or by inserting them through electroporation in the genome of strain carrying the λ_{RED} plasmid pKD46 (Datsenko and Wanner, 2000). The *kan* cassette was removed by pCP20-encoded Flp recombinase to generate unmarked deletions with a FRT-site scar sequence (Datsenko and Wanner, 2000). The removal of the *kan* gene was verified by PCR. Strains with multiple deletions were generated by sequential P1 transduction and *kan* cassette removal. LptC depletion strains were obtained by moving the *kan araC araB*p-*lptC* allele from BB-3 (Sperandeo et al., 2006) into selected mutants by P1 transduction. Depletion strains were selected on media containing kanamycin and 0.2% arabinose. The insertion of the cassette was verified by PCR. Strains used are listed in **Table S1**.

Construction of plasmids

pGS100-*ygeR* was constructed by cloning *ygeR* into the EcoRI/HindIII restriction sites of pGS100 plasmid (Sperandeo et al., 2006), using the primers AP618/AP619. pGS100-*ygeR*$_{LysM}$ was constructed by cloning *ygeR* from the TTG start codon to the position 318, using the primers AP618/AP703 into EcoRI/HindIII restriction sites of pGS100. pGS100-*ygeR*$_{LytM}$ was constructed by deleting the sequence coding for the LysM domain in pGS100-*ygeR*. Deletion was obtained by two-step PCR. Two fragments flaking the *ygeR* signal sequence were PCR amplified using pGS100-*ygeR* as template and the primer pairs AP618/ AP704, to generate Fragment SS (signal sequence), and AP705/ AP619 to generate Fragment LytM (LytM domain sequence). Fragments SS and LytM were used as template for a second round of PCR amplification using AP618 and AP619 primers. The resulting amplification product was cloned into EcoRI/HindIII restriction sites of pGS100. Primers used for genes cloning are listed in **Table S3**. The correct nucleotide sequences of inserts were verified by sequencing (Eurofins Genomics).

For pET28a-His-YgeR, *ygeR* was cloned starting from position 129 downstream the TTG start codon, into NdeI/XhoI pET28a, thus eliminating the putative signal sequence and the N-palmitoyl cysteine C26, using AP677 and AP621 primers. The correct nucleotide

sequences of inserts were verified by sequencing (Eurofins Genomics). Oligonucleotides used in this study are listed in **Table S3**. Plasmids used are listed in **Table S2**.

Imaging and image analysis

Cells grown overnight were collected to obtain a total amount corresponding to an OD of 3, and a 1:10 ratio of fixation solution (fixation solution: formaldehyde 37% - glutaraldehyde 25% in PBS) was added. Cells were incubated for 30 min at 37°C, with shaking, washed with PBS, and resuspended in 0.5 ml of PBS. A cell suspension (5 µl) was spotted onto a microscope slide coated with a thin layer of 1% agarose. Images were acquired with a Zeiss Axiovert 200M microscope coupled with an AxioCam Mrm device camera (Zeiss) and with Metamorph imaging software (Universal Imaging). For membrane staining, cells were mounted on a slide coated with 1% agarose supplemented with the membrane dye FM5-95 (ThermoFisher) to a final concentration of 2 µg/ml. Images were analysed with ImageJ (http://rsb.info.nih.gov/ij/).

Purification of His-YgeR and YgeR

E. coli LOBSTR-BL21(DE3) (Kerafast) cells carrying the plasmid pET28 His-YgeR were grown in 1 L of LB medium (12) at 37°C until an optical density (600 nm) of 0.5 was reached. IPTG (1 mM) was added and the cells were grown for 3 h, chilled on ice for 15 min, harvested by centrifugation for 15 min at 5.000 rpm and 4ºC. The cell pellet was resuspended in 60 ml of Buffer I (20 mM Tris/ HCl pH 7.5, 1 M NaCl, 10 mM MgCl2, 10% glycerol) supplemented with protease inhibitor cocktail (Sigma-Aldrich; 1/1000 dilution), small amount of DNase and 100 µM phenylmethyl sulfonyl fluoride (Sigma Aldrich). Cells were broken by sonication and the soluble fraction was removed after ultracentrifugation for 1 h at 130,000×g and 4°C. The supernatant was recovered, mixed with 4 mL of Buffer II (20 mM Tris/ HCl pH 7.5, 500 mM NaCl, 10 mM $MgCl_2$, 10% glycerol) containing 2.5 ml of preequilibrated Ni-NTA superflow beads (Qiagen) and incubated for 3h at 4°C. The suspension was poured in a gravity flow column and washed with 25 ml of Buffer II (supplemented with 30 mM imidazole). His-YgeR was eluted with Buffer III (20 mM Tris/ HCl pH 7.5, 500 mM NaCl, 10 mM $MgCl_2$, 10% glycerol, 400 mM imidazole). Elution fractions containing His-YgeR were pooled together and dialysed against 2 L dialyse buffer (20 mM HEPES/ NaOH pH 7.5, 300 mM NaCl, 10 mM $MgCl_2$, 10% glycerol) overnight. Dialysed proteins were concentrated and further

purified by size exclusion chromatography on a HiLoad 16/600 Superdex 200 pg (GE Healthcare) column using size exclusion buffer (20 mM HEPES/ NaOH pH 7.5, 300 mM NaCl, 10 mM $MgCl_2$, 10% glycerol). and a flowrate of 1 ml/min. Purity was determined by SDS-PAGE and combined fractions were concentrated and stored in aliquots at -80°C. For the removal of the His-tag, thrombin (1.32 U/ µl, Novagen) added and the sample was dialysed in 3 × 1 L of cleavage buffer (20 mM HEPES/NaOH pH 7.5, 300 mM NaCl, 10% glycerol).

***In vitro* cross-linking/ pulldown assays**

Proteins were mixed at appropriate concentrations in 200 µL of binding buffer (10 mM HEPES/NaOH pH 7.5, 150 mM NaCl, 10 mM $MgCl_2$, 0.05 % Triton X-100). His-YgeR at 3 µM was used, with 2.5 µM AmiC and 3 µM AmiB. His-AmiA at 3 µM was used, with 3 µM YgeR. Samples were incubated at room temperature for 15 min before addition of 0.2% wt/vol formaldehyde (Sigma-Aldrich) and further incubation at 37°C for 15 min. Excess cross-linking was blocked by addition of 1 M Tris/HCl, pH 7.5. Samples were applied to 110 µL of washed and equilibrated Ni-NTA superflow beads (Qiagen) and incubated for 2-3 h at 4°C, with gentle agitation. Beads were then washed 15 times with 0.5 mL wash buffer (10 mM HEPES/NaOH pH 7.5, 150 mM NaCl, 10 mM $MgCl_2$, 0.05% Triton X-100, 30 mM imidazole). Retained proteins were eluted by directly boiling beads in SDS-PAGE loading buffer; beads were then removed, and samples resolved by SDS-PAGE. Gels were stained with Coomassie brilliant blue (Roth).

***In vitro* peptidoglycan binding assay**

In this assay, 30 µg of purified YgeR protein were incubated for 30 min at 4°C either with or without PG (purified from BW25113Δ6LDT) in binding buffer (10 mM Tris/ maleate pH 6.8, 10 mM $MgCl_2$, 50 mM NaCl) in a total volume of 100 µl. The samples were centrifuged for 20 min at 13.000 g (4°C). The resulting pellets were washed in 200 µl of binding buffer, resuspended in 100 µl of 2% SDS, and incubated for 1 h at 4ºC with mixing. Supernatants of the binding step, washing steps and the resuspended pellets were analysed by SDS-PAGE.

PG sacculi preparation

The PG sacculi was prepared as previously described (Glauner et al., 1988). *E. coli araB*p*lptC* conditional strain and the isogenic mutants deleted for *ygeR* or for both *ldtF*, and *ygeR* were grown in the presence of 0.2% arabinose to an OD_{600} of 0.2, harvested, washed three times, and resuspended in 400 ml of an arabinose-supplemented (+ Ara) or arabinose-free (no Ara) medium and grown for 330 min. Cells were then rapidly chilled on ice and centrifugated for 15 min at 5000×g (4ºC). Cell pellet was resuspended in 5 mL of ice-cold deionized water and added drop wise into 5 mL of boiling 8% SDS with stirring using a magnetic stirrer. Samples were boiled for 30 min and cooled at room temperature. PG sacculi were collected by ultracentrifugation of the samples for 45 min at 90000×g (RT). The pellet was washed several times with deionized water to remove the SDS. Samples were treated with α-amylase (10mg /mL) and incubated 120 min at 37ºC to degrade high molecular weight glycogen, and treated with Pronase E (10mg /mL) and incubated 60 min at 60 ºC to release covalently bound lipoproteins. Enzymes reactions were stopped by boiling the mixtures with 4% SDS for 15 min. Pure PG sacculi were collected by ultracentrifugation (90000×g, 45 min, RT) and washed several times with deionized water until samples were free of SDS. The final pellet was resuspended in 400 µL of 0.02% NaN_3 and stored at 4°C.

HPLC analysis of muropeptides

HPLC analysis were carried out as previously described (Glauner et al., 1988). 100 µl of the PG sacculi were digested with 1 µM cellosyl overnight (Hoechst). Samples were dried by vacuum centrifugation at 1500 rpm, and subsequently reduced by resuspending them in 50 µl of MiliQ water and 50 µl of 0.5 M $NaBH_4$ buffer pH 9, followed by an adjustment to pH 4 by using 20% H3PO4. Muropeptides were then analysed by reverse -phase HPLC at 55ºC in a 180-min linear gradient from 50 mM NaPO4 pH 4.31 to 75 mM $NaPO_4$ pH 4.95, 15% methanol. Muropeptides were detected by absorbance at 205 using a radiochromatography software (Laura) for data acquisition and analysis.

***In vitro* YgeR activity assays**

Single or coupled assays were carried out in a final volume of 50 µl containing 20 mM HEPES/NaOH pH 7.5, 100 mM NaCl, 1 mM ZnCl2, 0.05% Triton X-100, 10 µl of PG sacculi from BW25113Δ6LDT and 2 µM of each protein as needed (YgeR, LdtF, AmiA,

AmiB, and AmiC). The reaction mixture was incubated overnight at 37°C with agitation. Following incubation, the reaction was stopped by boiling the samples for 10 min and incubated overnight at 37ºC with 1 µM cellosyl (Hoechst) to digest remaining PG. The samples were dried by vacuum centrifugation at 1500 rpm, and subsequently reduced by resuspending them in 50 µl of MiliQ water and 50 µl of 0.5 M $NaBH_4$ buffer pH 9, followed by an adjustment to pH 4 by using 20% H3PO4. Muropeptides were then analysed by reverse -phase HPLC (Glauner et al., 1988) at 55ºC in a 90-min linear gradient from 50 mM NaPO4 pH 4.31 to 75 mM $NaPO_4$ pH 4.95, 30% methanol. Muropeptides were detected by absorbance at 205 using a radiochromatography software (Laura) for data acquisition and analysis.

Supplemental References

1. Baba, T., Ara, T., Hasegawa, M., Takai, Y., Okumura, Y., Baba, M., Datsenko, K.A., Tomita, M., Wanner, B.L., and Mori, H. (2006). Construction of *Escherichia coli* K-12 in-frame, single-gene knockout mutants: the Keio collection. Mol. Syst. Biol. 2, 2006.0008.
2. Datsenko, K.A., and Wanner, B.L. (2000). One-step inactivation of chromosomal genes in *Escherichia coli* K-12 using PCR products. PNAS 97, 6640–6645.
3. Glauner B, Holtje JV, Schwarz U. 1988. The composition of the murein of *Escherichia coli*. J Biol Chem 263:10088-95.
4. Hanahan, D. (1983). Studies on transformation of *Escherichia coli* with plasmids. J. Mol. Biol. 166, 557–580.
5. Kuru, E., Lambert, C., Rittichier, J., Till, R., Ducret, A., Derouaux, A., Gray, J., Biboy, J., Vollmer, W., VanNieuwenhze, M., et al. (2017). Fluorescent D-amino-acids reveal bi-cellular cell wall modifications important for *Bdellovibrio bacteriovorus* predation. Nat Microbiol 2, 1648–1657.
6. Morè, N., Martorana, A.M., Biboy, J., Otten, C., Winkle, M., Serrano, C.K.G., Montón Silva, A., Atkinson, L., Yau, H., Breukink, E., et al. (2019). Peptidoglycan Remodeling Enables *Escherichia coli* To Survive Severe Outer Membrane Assembly Defect. MBio 10, e02729-18.
7. Silhavy TJ, Berman ML, and Enquist LW. (1984). Experiments with gene fusions., C.S.H. Cold Spring Harbor Laboratory N.Y.
8. Sperandeo P, Pozzi C, Dehò G, and Polissi A. (2006). Non-essential KDO biosynthesis and new essential cell envelope biogenesis genes in the *Escherichia coli* yrbG-yhbG locus. Res Microbiol 157, 547-558.

Table S1. Bacterial Strains

Strain	Relevant Genotype or Features	Source or Reference
AMM24	Δ*ldtF*::frt	Morè et al., 2019
AMM30	BB-3 Δ*ldtF*::frt	Morè et al., 2019
AMM39	BW25113 Δ*ygeR*::frt	This work
AMM43	BW25113 Δ*ygeR*::frt Δ*ldtD*::frt	This work
AMM44	BW25113 Δ*ygeR*::frtΔ*ldtE*::frt	This work
AMM45	BW25113 Δ*ygeR*::frt Δ*ldtF*::frt	This work
AMM46	BB-3 Δ*ygeR*::frt	This work
AMM47	BB-3 Δ*ldtD*::frt Δ*ygeR*::frt	This work
AMM48	BB-3 Δ*ldtE*::frt Δ*ygeR*::frt	This work
AMM49	BB-3 Δ*ldtF*::frt Δ*ygeR*::frt	This work
BB-3	BW25113 Φ(*kan araC araB*p*lptC*)1	Sperandeo et al., 2006
BL21(DE3)	F– *ompT hsdS*B(rB– mB–) *gal dcm* (DE3)	Novagen
BW25113	$lacI^q$ $rrnB_{T14}$ Δ$lacZ_{WJ16}$ *hsdR514* Δ$araBAD_{AH33}$ Δ$rhaBAD_{LD78}$	Datsenko and Wanner, 2000
BW25113	$lacI^q$ $rrnB_{T14}$ Δ$lacZ_{WJ16}$ *hsdR514* Δ$araBAD_{AH33}$ Δ$rhaBAD_{LD78}$	Datsenko and Wanner, 2000
BW25113Δ6LDT	$lacI^q$ $rrnB_{T14}$ Δ$lacZ_{WJ16}$ *hsdR514* Δ$araBAD_{AH33}$ Δ$rhaBAD_{LD78}$ *ΔycbB ΔerfK ΔycfS ΔybiS ΔynhG ΔyafK*	Kuru *et al*. 2017
CKG02	BW25113 Δ*nlpD*::frt	This work
CKG04	BW25113 Δ*envC*::frt	This work
CKG06	BW25113 Δ*amiA*::frt	This work

CKG08	BW25113 Δ*amiB*::frt	This work
CKG10	BW25113 Δ*amiC*::frt	This work
CKG12	BW25113 Δ*nlpD*::frt Δ*envC*::frt	This work
CKG14	BW25113 Δ*amiA*::frt Δ*amiC*::frt	This work
CKG16	BW25113 Δ*amiA*::frt Δ*amiB*::frt Δ*amiC*::frt	This work
CKG18	BW25113 Δ*envC*::frt Δ*amiC*::frt	This work
CKG20	BW25113 Δ*nlpD*::frt Δ*amiB*::frt	This work
CKG21	BW25113 Δ*nlpD*::frt Δ*amiA*::*kan* Δ*amiB*::frt	This work
DH5α	Δ(*argF-lac169*) ϕ80 *dlacZ58*(M15) *glnV44*(AS) λ^- *rfbD1 gyrA96 recA1 endA1 spoT1 thi-1 hsdR17*	Hanahan, 1983
JW2428	BW25113 Δ*amiA*764::*kan*	Baba et al., 2006
JW2712	BW25113 Δ*nlpD*747::*kan*	Baba et al., 2006
JW2833	BW25113 Δ*ygeR*787::*kan*	Baba et al., 2006
JW4127	BW25113 Δ*amiB*790::*kan*	Baba et al., 2006
JW5449	BW25113 Δ*amiC*742::*kan*	Baba et al., 2006
JW5646	BW25113 Δ*envC*725::*kan*	Baba et al., 2006
LOBSTR-BL21(DE3)	F– *ompT hsdS*B(rB– mB–) *gal dcm* (DE3), carries genomically modified copies of *arnA* and *slyD*	Kerafast

Table S2. Plasmids

Plasmids	Relevant characteristics	Source or Reference
pCP20	FLP expression, temperature sensitive replication; Cam^R and Amp^R.	Datsenko and Wanner, 2000
pET28a His-*ygeR*	pET28a derivative; expresses *ygeR* from the T7 promoter starting from amino acid 27 and fused at N-terminal with 6xHis tag.	This work
pGS100	pGZ119EH derivative, contains TIR sequence downstream of p*tac*, Cam^R.	Sperandeo et al., 2006
pGS100-*ygeR*	pGZ119H derivative; expresses full length $ygeR^{(1-251)}$ under the *tac* promoter; Cam^R.	This work
pGS100-$ygeR_{LysM}$	pGZ119H derivative; expresses *a ygeR* construct containing the signal sequence and the LysM domain (1-106 residues) under the *tac* promoter; Cam^R.	This work
pGS100-$ygeR_{LytM}$	pGZ119H derivative; expresses a chimeric version of *ygeR* containing the signal sequence (1-39 residues) fused to the LytM domain (84-251 residues) under the *tac* promoter; Cam^R.	This work
pKD46	λ-Red expression under the *araB*p promoter, temperature sensitive replication; Amp^R.	Datsenko and Wanner, 2000

Table S3. Oligonucleotides

Name	Sequence (5'-3')	Description	Used to make
AP618/30 *ygeR*-f	CAGGAATTCAACTTGAGTGCGGGACGCCTG	[CAG]-[EcoRI]-[AAC]-[start *ygeR*; fwd]	pGS100-*ygeR* construction pGS100-$ygeR_{LysM}$ construction pGS100-$ygeR_{LytM}$ construction
AP619/29 *ygeR*-r	TATCAAGCTTTCAGCATTTTGGCTTGCTG	[TATC]-[HindIII]-[stop *ygeR*; rev]	pGS100-*ygeR* construction pGS100-$ygeR_{LysM}$ construction pGS100-$ygeR_{LytM}$ construction
AP621/ 33 *ygeR*-r	CCGCTCGAGTCAGCATTTTGGCTTGCTGCCCTG	[CCG]-[XhoI]-[stop *ygeR*; rev]	pET28a-His-YgeR
AP677 28 *ygeR*26-f	AGCCATATGTCGGGTAGCAAATCATCCG	[AGC]-[NdeI]-[starting at 78 bp downstream of TTG of *ygeR*; fwd]	pET28a-His-YgeR
AP703/33 *ygeR*int-r	TATCAAGCTTTCATGCGGTTTTGGTCGTTGATT	[TATC]-[HindIII]-[TC]-[316 bp downstream of TTG of *ygeR*; rev]	pGS100-$ygeR_{LysM}$ construction
AP704/40 *ygeR*ssLytM-r	CTGCTACTTTTCGCCCCACCGCCGGAATACGTTCCTGTAT	[117 bp downstream of TTG of ygeR]-[252 bp downstream of TTG of *ygeR*; rev]	pGS100-$ygeR_{LytM}$ construction
AP705/ 20 *ygeR*LytM-f	GGTGGGGCGAAAAGTAGCAG	[252 bp downstream of TTG of ygeR; rev]	pGS100-$ygeR_{LytM}$ construction

Table S4. Muropeptide composition of *araB*p*lptC* and *araB*p*lptC* Δ*ygeR* mutant under permissive or nonpermissive conditions

Strain:	*araB* p*lptC*	*araB* p*lptC*	*araB* p*lptC*	*araB* p*lptC*	*araB* p*lptC* Δ*ygeR*	*araB* p*lptC* Δ*ygeR*	*araB* p*lptC* Δ*ygeR*	*araB* p*lptC* Δ*ygeR*
Harvest:	Late exponential	Late exponential	Late exponential	Late exponential	Late exponential	Late exponential	Late exponential	Late exponential
Arabinose:	+	-	+	-	+	-	+	-
Sample:	1	2	3	4	5	6	7	8
Muropeptide	% Area	% Area	% Area	% Area	% Area	% Area	% Area	% Area
Tri	7,3	7,4	7,2	8,1	8,3	5,5	8,1	5,2
TetraGly4	3,5	3,9	3,5	2,4	3,2	2,2	3,3	2,0
Tetra	31,6	28,2	31,4	29,5	29,4	30,0	28,2	30,7
Di	2,1	0,5	2,1	0,6	2,2	0,0	1,9	0,3
Tri-Lys-Arg	7,1	3,7	7,1	4,2	7,5	3,9	7,6	4,4
TriTri(DAP)	0,8	1,7	0,6	1,7	1,0	1,3	1,1	1,3
TetraTri(DAP)	3,4	9,8	3,0	8,3	3,7	9,7	3,9	9,8
TetraTetraGly4	2,7	1,7	2,7	1,9	2,6	1,5	2,6	1,4
TetraTri	2,6	1,9	2,5	2,3	2,6	1,5	2,7	1,2
TetraTetra	26,0	21,5	25,3	21,1	23,7	23,3	23,7	24,3
TetraAnh	1,0	0,9	0,9	1,1	1,6	1,3	1,8	1,2
TetraTetraTri(DAP)	0,0	0,0	0,0	1,1	0,0	1,2	0,0	1,2
TetraTetraTri	0,8	0,0	0,9	0,9	0,8	2,1	1,0	0,5
TetraTri-LysArg	3,3	8,5	4,3	2,3	5,0	2,4	5,4	3,8
TetraTetraTetra	2,8	2,1	2,6	2,6	2,3	2,7	2,5	2,6
TetraTriAnh I	0,0	0,9	0,5	0,7	0,6	1,0	0,6	0,9
TeraTriAnh II	0,0	0,5	0,4	0,4	0,5	0,6	0,0	0,5
TetraTetraAnh I	0,6	1,0	0,6	1,1	0,5	1,3	0,5	1,3
TetraTetraAnh II	1,0	1,4	1,0	1,3	0,7	1,7	0,8	1,8
TetraTetraTetra Anh	0,7	0,4	0,6	1,0	0,5	1,2	0,5	1,2
all known	97,2	95,8	97,1	92,5	96,6	94,3	96,2	95,4
monomers (total)	53,1	45,6	52,8	48,4	52,2	44,1	51,2	44,6
monomer di	2,1	0,5	2,2	0,6	2,2	0,0	2,0	0,3
monomer tri	7,5	7,8	7,4	8,8	8,5	5,9	8,5	5,4
monomer tetra	33,5	30,4	33,3	33,1	32,1	33,2	31,2	33,4
monomer tetraGly4	3,6	4,1	3,6	2,6	3,3	2,3	3,5	2,1
monomer Tri-LysArg	7,3	3,8	7,3	4,5	7,7	4,1	7,9	4,6
dimers (total)	41,6	50,9	42,1	45,6	42,4	48,2	42,8	49,6
dimers(DD)	33,8	30,0	33,9	31,1	32,3	32,7	32,1	32,8
dimers(LD)	4,4	12,0	3,7	10,9	4,9	11,7	5,2	11,6
dimers anhydro	1,6	4,2	3,1	4,9	3,0	6,0	2,5	5,9
Trimers (Total)	4,3	2,5	4,2	5,9	3,8	7,5	4,2	5,8
trimer (anhydro)	0,7	0,4	0,6	1,1	0,5	1,2	0,6	1,3
dipeptides (total)	2,1	0,5	2,2	0,6	2,2	0,0	2,0	0,3
tripeptides (total)	11,7	16,3	11,6	17,7	13,7	15,1	13,6	13,9
tetrapeptides (total)	76,2	74,3	75,8	75,2	72,9	78,9	72,7	78,8
pentapeptides (total)	0,0	1,0	4,0	5,0	2,0	3,0	6,0	7,0
Tri-LysArg (total)	9,1	8,3	9,5	5,7	10,3	5,4	10,7	6,5
3-3 linkage	2,2	6,0	1,9	5,8	2,4	6,3	2,6	6,2
chain ends (anhydros)	2,0	3,0	2,4	3,5	3,0	4,2	3,0	4,0
degree of cross-linkage	23,7	27,1	23,8	26,8	23,7	29,1	24,2	28,7
% peptides in cross-links	46,9	54,4	47,2	51,6	47,8	55,9	48,8	55,4
0.0 = NOT DETECTED								

Table S5. Muropeptide composition of *araB*p*lptC* and *araB*p*lptC* Δ*ldtF ΔygeR* mutant under permissive or nonpermissive conditions

Strain:	*araB*p*lptC*	*araB*p*lptC*	*araB*p*lptC*	*araB*p*lptC*	*araB*p*lptC ΔldtF ΔygeR*	*araB*p*lptC ΔldtF ΔygeR*	*araB*p*lptC ΔldtF ΔygeR*	*araB*p*lptC ΔldtF ΔygeR*
Harvest:	Late exponential	Late exponential	ate exponenti	Late exponential	Late exponential	Late exponential	Late exponential	Late exponential
Arabinose:	+ara	-ara	+ara	-ara	+ara	-ara	+ara	-ara
Sample:	1	2	3	4	5	6	7	8
Muropeptide	% Area	% Area	% Area	% Area	% Area	% Area	% Area	% Area
Tri	8,01	7,19	6,84	5,90	2,92	3,87	2,80	3,40
TetraGly 4	3,4	2,38	3,67	2,48	5,02	2,83	5,00	2,61
Tetra	38,42	36,40	33,55	30,26	41,97	36,51	35,27	31,11
Di	2,52	0,57	2,13	0,49	2,34	0,59	2,08	0,45
Penta/Tetratetra	0	0,00	0,00	0,00	0,00	0,00	0,00	0,00
Tri-Lys-Arg	0	0,00	4,09	2,07	0,00	0,00	8,54	2,20
TetraTri(DAP)Gly4	0	0,00	0,00	0,89	0,39	0,89	0,56	1,03
TriTri(DAP)	0	1,78	0,81	1,69	0,00	1,28	0,42	1,22
TetraTri(DAP)	2,87	11,55	3,81	11,83	3,21	10,25	3,57	11,95
TetraTetraGly4/TetraTri	6,03	4,00	5,47	3,50	0,00	3,36	5,00	3,10
TetraTetra	29,37	23,75	25,98	21,42	30,64	23,38	26,74	22,26
TetraPenta	0	0,00	0,00	0,00	0,00	0,93	0,54	1,03
TetraTetraTri	0,63	0,87	0,00	1,08	0,00	0,89	0,00	0,91
TetraTetraTetra	2,73	2,21	2,54	2,18	2,76	2,22	2,08	2,19
TetraTriAnh I	0	0,87	0,00	0,00	0,00	0,80	0,00	1,31
TeraTriAnh II	0	0,67	0,00	0,00	0,00	0,69	0,67	1,09
TetraTetraAnh I	0,55	0,98	0,45	1,37	0,54	1,04	0,47	1,57
TeraTetraAnh II	1,11	1,03	1,05	1,26	1,07	1,10	1,15	1,41
TetraTetraTriAnh	0	0,00	0,00	0,00	0,00	0,00	0,00	0,00
TetraTetraTetra Anh	0,9	0,83	0,77	1,26	0,99	0,83	0,50	1,34
TetraTriLysArg	0,00	0,00	1,45	1,25	0,00	0,00	1,74	0,00
all known	96,54	95,08	92,61	88,93	91,85	91,46	97,13	90,18
monomers (total)	54,23	48,95	49,88	44,00	56,89	47,89	46,48	41,66
monomer di	2,61	0,60	2,30	0,55	2,55	0,65	2,14	0,50
monomer tri	8,30	7,56	7,39	6,63	3,18	4,23	2,88	3,77
monomer tetra	39,80	38,28	36,23	34,03	45,69	39,92	36,31	34,50
monomer tetraGly4	3,52	2,50	3,96	2,79	5,47	3,09	5,15	2,89
dimers (total)	41,36	46,94	40,57	47,18	39,03	47,80	40,28	50,98
dimers(DD)	38,39	32,92	35,58	30,98	35,11	34,22	35,59	35,23
dimers(LD)	2,97	14,02	4,99	16,20	3,92	13,58	4,68	15,75
dimers anhydro	1,72	3,73	1,62	2,96	1,75	3,97	2,36	5,97
Trimers (Total)	4,41	4,11	5,14	6,49	4,08	4,31	4,45	4,92
trimer (anhydro)	0,93	0,87	0,83	1,42	1,08	0,91	0,51	1,49
dipeptides (total)	2,61	0,60	2,30	0,55	2,55	0,65	2,14	0,50
tripeptides (total)	9,66	15,81	10,08	14,78	4,72	11,76	6,22	12,61
tetrapeptides (total)	86,19	76,76	79,59	73,74	90,86	80,51	79,61	76,02
pentapeptides (total)	0,00	0,00	0,00	0,00	0,00	0,51	0,28	0,57
3-3 linkage	1,49	7,01	2,49	8,10	1,96	6,79	2,34	7,87
chain ends (anhydros)	1,17	2,16	1,09	1,95	1,24	2,29	1,35	3,48
degree of cross-linkage	23,62	26,21	23,71	27,92	22,24	26,77	23,10	28,77
% peptides in cross-links	45,77	51,05	50,12	56,00	43,11	52,11	53,52	58,34
0 = NOT DETECTED								

4. Conclusion

The growth and assembly of the tree-layered envelope of Gram-negative bacteria requires a close coordination of the synthetic machineries that orchestrate it. The robustness of the cell envelope depends on proper growth of these layers, and damage in of any of them has a significant impact in the cell fitness. Therefore, bacteria employ several mechanisms to overcome potential threats that challenge the cell envelope integrity.

In the first part of this thesis we have shown that bacteria remodel the PG sacculus by increasing the level of 3-3 crosslinks when the OM is compromised. Indeed, LDTs that introduce 3-3 crosslinks in PG become essential under OM stress to avoid cell lysis. Our work represents a notable example of coordinated growth and assembly of OM and PG as defects in biogenesis in the OM are counterbalanced by PG remodelling to maintain envelope integrity and prevent cell lysis. We characterized the putative *ldt* gene *ldtF*, as a LDT that stimulates the activity of LdtD and LdtE. We then determined that LDTs have a different expression profile: *ldtE* and *ldtF* are housekeeping *ldts* displaying a growth phase dependent activation whereas *ldtD* is the stress *ldt* highly expressed in the absence of *ldtE* and *ldtF* and when LPS biogenesis is defective. Notably, our data reveal a major role of LdtD in the protective PG remodelling programme, as the lysis phenotype of LptC-depleted *ldt* mutants was rescued by the ectopic expression of *ldtD*. Besides, our data supports a model in which LdtD works in concert with other PG biosynthetic machineries to reshape the PG. Thus, nascent PG strands are polymerised by the GTase activity of the pair PBP1B/ LpoB, trimmed by the DD-CPase PBP6a, and resulting tetrapeptides utilised by LdtD to produce 3-3 crosslinks. We then propose that this PG repair complex remodels the PG to counterbalance OM assembly defects.

In the second part of this thesis we explored the functional linkage among LdtF and the LytM-domain factor YgeR, which we characterised in this work for the first time. We found that loss of *ygeR* recovers viability of cells lacking *ldtF* upon *lptC* depletion. Notably, the level of 3-3 crosslinks in PG cannot be taken into account to explain the phenotype. Both, genetic and biochemical data support the hypothesis that YgeR functions as amidase activator. The catalytic domain of the protein, the LytM domain, lacks the required residues for function, which is consistent with the lack of activity of YgeR on PG *in vitro*. We showed that YgeR activates the three amidases AmiA, AmiB and AmiC *in vitro*, physically interacts with AmiC and is capable to bind PG. In line with these findings, we found that ectopic expression of *ygeR* restores cell separation in a mutant defective for amidase regulators *envC* and *nlpD*. The YgeR LytM but not the

LysM domain modulates amidase activity. Finally, we showed that *in vivo* YgeR facilitates cell separation through the activation of AmiC.

Nonetheless, several important questions are still open. We still do not know which additional role LdtF plays in the bacterial cell and which envelope stress systems control expression of YgeR whose activity seems specifically required under envelope stress. We believe that addressing these questions will give a better picture of the essential processes carried out in the cell envelope of Gram-negative bacteria.

The findings exposed in this thesis emphasise the close relationship between OM and PG biosynthetic machineries, showing the involvement of protein complexes dedicated to PG synthesis and degradation in response to disrupted LPS transport to the OM. Overall, the research discussed in this work unravels mechanism exerted by bacteria to tackle stress, and likewise unveils potential new targets for antimicrobial drug development.